Synthesis, characterization and antimicrobial activity of copper(II) complexes of some hydroxybenzaldimines and their derivatives

Submitted in fulfillment of the requirements for the degree of

Doctor of philosophy (science)

in the

Department of Chemistry

by

SOBOLA Abdullahi Owolabi

February 2012

Abstract

This study focuses on the antimicrobial activity of Cu(II) complexes of some ortho-hydroxybenzaldimines and its derivatives. Four different categories of Schiff base ligands were prepared by condensing salicylaldehyde, *o*-vanillin, *p*-vanillin and vanillin with *p*- and *o*-substituted anilines; 1-aminonaphthalene; 2- and 3-aminopyridine; 2- and 3-aminomethylpyridine as well as 2-aminobenzimidazole. The last category was prepared from *o*-phenylenediamine and *o*-vanillin. The Schiff base ligands have been characterized by a combination of elemental analysis and spectral (^{1}H- and ^{13}C-NMR, UV/Visible, infrared and Raman) data. The existence of strong intramolecular hydrogen bonding in the orthohydoxybenzaldimines was evident from the chemical shift values of the hydroxyl proton in the ^{1}H-NMR spectra of the Schiff base ligands. The hydroxyl proton resonates at high frequency and thus absorbed far downfield at 13.46-11.83 ppm, reflecting the presence of hydrogen bonding between the hydroxyl proton and the imine nitrogen. In the *p*-substituted aniline analogues of the Schiff base, a plot of the chemical shift values of the hydroxyl proton against the Hammett's substituent parameters gave a linear correlation between the electronegativities of the substituents and the chemical shift values. The nitro group with the highest electronegativity caused the least deshielding of the hydroxyl proton and thus absorbed upfield compared to the less electronegative substituents such as the CH_3 and OCH_3 analogues. Likewise, in the solid state infrared spectra of the ligands, the hydroxyl stretching band of the ortho-hydroxyl Schiff base ligands was observed as a very broad band and at much lower frequency, 3100-2100 cm^{-1}, indicating the existence of strong intramolecular hydrogen bonding.

In the same vein, ^{1}H- and ^{13}C-NMR spectral data for the Schiff base ligands indicated that the prepared compounds exist in the enol form in aprotic solvent, chloroform. The methine proton appeared as singlet and there was no carbonyl signal in the ^{13}C-NMR spectra of the Schiff base ligands. This was supported by the infrared data having no vibrational band attributable to the carbonyl stretching of the keto-form of the Schiff base ligands in solid state. However, the UV/Visible study of the Schiff base ligands in protic solvent, methanol, suggested the existence of some of the Schiff base ligands in keto-enol form. A band at greater than 400 nm was

observed in the UV/Visible spectra of the ligands and this has been attributed to the presence of the keto form of orthohydroxyl Schiff base ligands in solution. A plot of the molar absorptivity (ϵ) of the band at greater than 400 nm against Hammett substituent parameters revealed that the intensity of the bands increased with the electronegativity of the substituents.

The Cu(II) complexes of salicylaldehyde, *o*-vanillin and a few *p*-vanillin based Schiff base ligands are reported in this work. It was observed that introduction of Cu(II) ions into the ligand system resulted in the hydrolysis of the imine band in few cases. All the isolated complexes have been characterized by elemental analysis, conductivity measurement, infrared and UV/Visible spectral data. The structures of three of the Cu(II) complexes were further confirmed by X-ray single crystal diffraction. The Schiff base ligands either coordinated as neutral base through the imine nitrogen or via the imine nitrogen and the phenolic oxygen atoms. In addition, the benzimidazole-based and ovan-2-pico analogues equally coordinated through the imidazole N-3 nitrogen and the azine nitrogen respectively; thus acted as tridentate.

In general, the synthesized Cu(II) complexes fell into seven categories viz: $[Cu(LH)Cl(H_2O)]Cl$; $[Cu(LH)_2Cl_2].xH_2O$; $[CuL_2]$; $[Cu_2L_2]$; $[Cu(LH)Cl(H_2O)]Cl$; and [MLCl]. The Cu(II) complexes of the form, $M(LH)_2Cl_2.xH_2O$ were either 1:1 or non-electrolyte in methanol and DMF. The third category, CuL_2, was however, non-electrolyte existing as neutral four coordinate Cu(II) complexes. X-ray single crystal structure of Cu(II) complexes derived from the ammonia-based Schiff bases revealed a square planar geometry for the complexes and this agreed with the planar geometry that has been reported for Cu(II) complexes of N-arylsalicylaldimines of the type studied in this work. The complexes, $[Cu_2L_2]$, resulted from the ortho-hydroxyaniline analogues and were polymeric with the Schiff base ligands coordinating to the Cu(II) ions as tridentate dibasic via the imine nitrogen, phenolic oxygen and the aminophenolic oxygen atoms. Cu(II) complexes prepared from ovan-2-ampy and ovan-2-pico Schiff bases were of the forms $[Cu(LH)Cl(H_2O)]Cl$ and [CuLCl] respectively. The X-ray crystal structure of [Cu(ovan-2-pico)Cl] revealed a four-coordinate square planar geometry for the complex. In the same vein, the *o*-phenylenediamine complexes were of the form $[Cu(L)(H_2O)]$, with the X-ray crystal structure of $[Cu(bis\text{-}ovanphen)(H_2O)]$ revealing a square pyramidal geometry.

The Schiff base ligands and the isolated Cu(II) complexes have been evaluated for their antimicrobial activity against three bacterial strains (*Escherichia coli ATCC® 8739™*, Staphylococcus aureus subsp. aureus ATCC® 6538™** and *Bacillus subtilis* subsp. *spizizeni ATCC® 6633™*)* and one fungal strain, *Candida albicans ATCC® 2091™**, using agar disc diffusion and broth dilution techniques. It was observed that the presence of the methoxyl group at the ortho-position of the aldehyde moiety of the Schiff base ligands enhanced the activity of the ligand tremendously and thus the *o*-vanillin analogues showed the highest potency against the tested organisms. In addition, the hydroxyaniline analogues were equally the most promising of all the substituted aniline based Schiff bases. The *o*-vanillin analogues of the aminopyridines and aminomethylpyridines also exhibited significant activity against the tested organisms. All the 2-aminobenzimidazole series were active against the tested organisms. It should be noted that *E. coli* was the least susceptible of all the microorganisms while the highest potency was exhibited against the fungus of choice, *Candida albicans*.

Lastly, chelation of the Schiff base ligands with Cu(II) ions did not have significant influence on the activity of the free ligands.

Acknowledgements

I give thanks and adoration to almighty Allah for His benevolence, guidance and protection throughout the period of this study. I would also like to express my heartfelt gratitude to my mother, Mrs Kudirat Sobola, for her love and care, especially for providing the initial funding for this study. Perhaps, I would not have come without her encouragement and financial assistance. Thank you very much, my sweet mother.

I am highly indebted to my supervisor, Prof. G.M. Watkins, for his intellectual guidance and financial assistance throughout the course of this study. I am very grateful sir. Thanks also go to Dr Bernadus van Brecht of Nelson Mandela Metropolitan University, Port Elizabeth, for assisting with the x-rays single crystal diffraction of the complexes. It is also worthwhile to express my appreciation to Dr Zenixole Tshentu, Rhodes University, for his encouragement and assistance with the growing of the crystals. I would also like to thank the following people: Ms Tembisa Jauka, Ms Taryn Boden and Ms Tara Walmsley, all of Rhodes University, for assisting with the antimicrobial study of the compounds.

I am very grateful to all the academic and non-academic staff of the chemistry department, Rhodes University, for providing the enabling environment and the needed assistance for this research work. In the same vein, I'm highly indebted to the management of my home University, Lagos state University, Nigeria, for granted me the training leave that afforded my being at Rhodes University for this study. Special thanks go to Dr Isiaka Ogunwande, Dr Adebisi Kasali, Professor Adeleke Adeniyi and Mr Kamil Yusuf.

I am also seizing this opportunity to re-count my experience with my lab-mates for a wonderful time spent together during the course of this study. They include Ms Temitope Olalekan, Matthew Coombes and Hogdson Ivan. I equally had a nice time with other colleagues in labs F2 and F3; you are all appreciated. A big thank you also goes to my dear friend, Sam Chigome, for the smooth academic interactions that we had together throughout my stay at Rhodes University. It also behoves me to express my appreciation to Dr Sherif Adewuyi, Dr Kazeem Yusuf, Dr Mahboob Jimoh, Dr Idris Olasupo and Ms Bridget Moronkola for their financial assistance during the course of this study.

Finally, I cannot but express deep appreciation to my siblings and my dear hajia, Shakirat Babarinde, for their patience and prayers while the study lasted.

Table of contents

List of tables

List of figures

List of schemes

List of abbreviations

BM	Bohr Magneton
Cu^{2+}	copper(II) ions
cm^{-1}	per centimeter
dm^{-3}	per decimeter cube
DMF	dimethylformamide
DMSO	dimethylsulfoxide
Hr	hour
M	Molar
ml	milliliter
mol^{-1}	per mol
mmol	millimole
nm	nanometer
NMR	nuclear magnetic resonance
UV/Visible	ultraviolet/visible
viz:	includes

1.0.0 Introduction

Schiff bases have received overwhelming attention due to the ease of their preparation and their applications in several fields of chemistry and biochemistry. However, our interest is to use Schiff bases as a chelating agent and consequently evaluate their antimicrobial activity in the presence of copper(II) ions. Thus, this chapter describes the chemistry of Schiff bases, their metal complexes and various applications with emphasis on biological importance. The geometrical structure and biological applications of copper(II) ions are equally discussed.

1.1.0 Schiff bases

Schiff bases are unsaturated compounds that contain the azomethine functional group (HC=N). They are formed from the condensation reaction between a primary amine and active carbonyl, (a ketone or an aldehyde). The first Schiff base ligand was prepared in 1840 by Hugo Schiff [1].

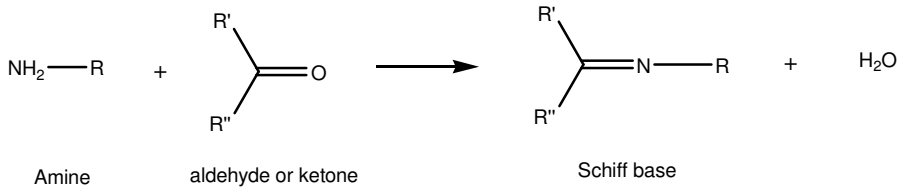

Scheme 1.1: Synthesis of Schiff bases

Schiff bases of aliphatic aldehydes are relatively unstable and readily polymerizable [2, 3]; while those of aromatic aldehydes having effective conjugation are more stable [4]. In general, aldehydes react faster than ketones in condensation reactions leading to the formation of Schiff bases, as the reaction centre of aldehyde are sterically less hindered than that of ketone [5]. Schiff bases can only act as coordinating ligands if they bear a functional group, usually the hydroxyl, sufficiently near the site of condensation in such a way that a five or six-membered chelate can be formed with a metal ion. It suffices to mention that ortho-hydroxysalicylaldimines have received the most attention of the Schiff base ligands reported so far.

The formation of a Schiff base from aldehydes or ketones is a reversible reaction and generally takes place under acid or base catalysis or upon heating. Mechanistically, the formation of Schiff base begins with the nucleophilic addition reaction of the amine nitrogen to the carbonyl carbon to form an unstable tetrahedral carbinolamine. This is followed by loss of water molecule via elimination reaction.

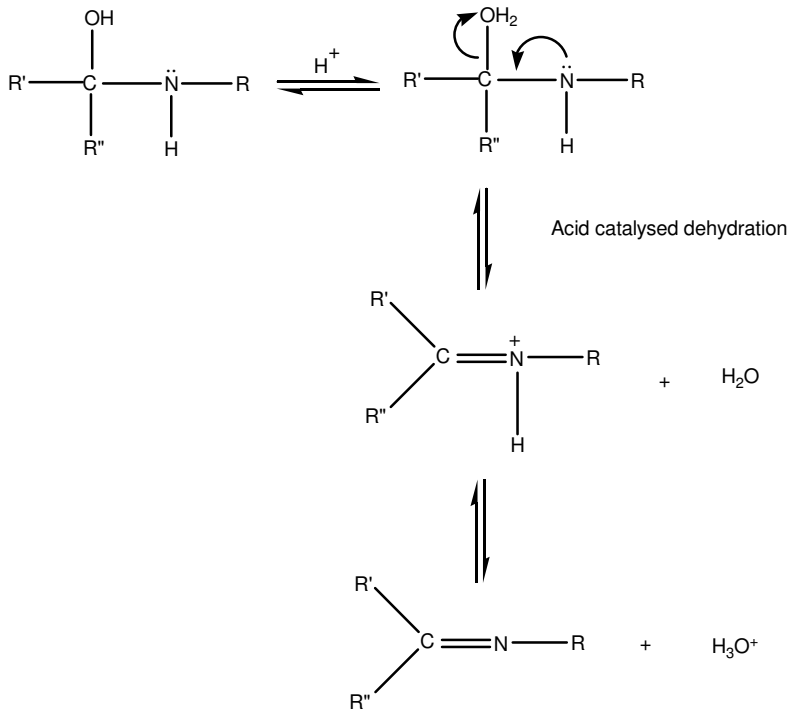

Scheme 1.2: Acid-dehydration of carbinolamine

Typically, the dehydration of the carbinolamine is the rate determining step of Schiff base formation and this is why the reaction is catalyzed by acids. However, the acid concentration cannot be too high because amines are basic compounds. If the amine is protonated and becomes non-nucleophilic, the equilibrium shifts to the left and carbinolamine formation cannot occur. Therefore, many Schiff base syntheses are best carried out at a mild pH of 4-5. The dehydration of carbinolamine is also catalysed by base. The reaction is somewhat analogous to the E2 elimination of alkyl halides except that it is not a concerted reaction. It proceeds in two steps through an anionic intermediate.

Aromatic aldehydes react smoothly under mild conditions and at low temperature in a suitable solvent or without it. If an electron-withdrawing substituent is in the para position of the amine the rate decreases, but increases when on the aldehyde [6]. The presence of dehydrating agents normally favours the formation of Schiff bases and $MgSO_4$ is commonly used as a dehydrating agent. The water produced in the reaction can also be removed from the equilibrium using a Dean Stark apparatus, when conducting the synthesis in toluene or benzene. Ethanol is also a suitable solvent for preparing Schiff bases at room temperature.

1.2.0 Spectroscopic studies of Schiff base ligands

The question of the exact structure of Schiff bases has long been controversial [7]. This is because the keto-amine / enol-imine tautomer is sensitive to the physical state, the nature of solvent, as well as the effects of substituents. In particular, some cases have been reported [7] where a ketimine form seems to have greater stability than the enol-imine tautomer. Spectroscopic techniques such as infrared, nuclear magnetic resonance and ultraviolet/visible spectroscopy have been used extensively to characterize Schiff base ligands. The $\nu_{C=N}$ and ν_{C-O} stretching frequencies are the main typical features used for the characterization of Schiff base ligands. While in the NMR study, the emphasis is always on the azomethine proton (HC=N).

All the C=N stretching frequency of Schiff base ligands occur in the region 1680-1603 cm^{-1} when H, alkyl or phenyl groups are bonded to carbon and nitrogen atoms [8]. The position of the stretching frequency in the range mentioned above is affected by the following factors: the physical state of the compound, the nature of the substituent, conjugation with either carbon or nitrogen, or both, and hydrogen bonding.

Fabian and Legrand [9] reported a frequency range of 1650-1638 cm^{-1} for Schiff bases of the type Ar-CH=N-R where Ar is an un-substituted phenyl group, while Suydam [10] reported a smaller range of 1650-1645 cm^{-1}. The range widens to 1657-1631 cm^{-1} if nitro or halogen is present in the phenyl ring [9]. A frequency region of 1631-1613 cm^{-1} were found for the compounds of the type Ar-CH=N-Ar [11]. The presence of an OH group at the 2-position of the

phenyl ring effects a red shift, with a frequency shift of about -8 cm^{-1} using N-benzylidene-aniline as a reference. In these compounds, the phenolic C-O stretching vibration occurs between 1288 cm^{-1} and 1265 cm^{-1}. A decrease of the C=N frequency is generally observed upon coordination to metal ions through both O and N atoms. Kovacic [12] assigned the $\nu_{C=N}$ stretching frequency in some substituted salicylaldiminatocopper(II) complexes in both the solid state and in solution. In unroll mull, the $\nu_{C=N}$ frquency was found at 1603-1616 cm^{-1}, while in methylenechloride solution, the band is shifted to 1601-1612 cm^{-1}. In the copper(II) complexes, the phenolic C-O appears in the region 1310-1330 cm^{-1}, as compared to 1265 -1288 cm^{-1} in the free anils.

It should be noted that the absorption due to the free O-H stretching vibration is not always observed in the infrared spectra of Schiff base ligands derived from 2-hydroxybenzaldehyde and aniline [12]. This is attributed to the formation of intra-molecular hydrogen bonding resulting in a stable six-membered chelate, as in figure 1. Instead, a broad, weak band having some fine structures is found in the region from 3100-2700cm^{-1}; most of the fine structure is due to the CH modes. However, Baker and Shulgin [13] as well as Kovacic [12] have assigned a weak band near 2730cm^{-1} to the internally hydrogen bonded O-H stretching vibration.

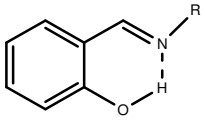

Fig. 1.1: Hydrogen bonding in salicylaldimines

NMR studies have been used to address the controversy about the exact structure of Schiff base ligands. For instance, Dudek and Holm [14-16] studied the keto-enol equilibra in a variety of Schiff bases obtained from ketones and concluded that the ketamine form predominates more than 80 percent. Their main evidence was the splitting of N-methyl or methylene signal by coupling with the N-H proton and the disappearance of the splitting upon deuteration. On the other hand, they reported a phenol-imine form for bases derived from 2-hydroxy-1-naphthone and salicylaldehyde. Other workers [17-20] have equally used the signals of the methine and

hydroxyl protons to determine whether a Schiff base is enol-imine or keto-amine tautomer. However, the existence of phenol-imine or keto-amine tautomer in solution depends on the intra-molecular hydrogen bonding. Salman and co-workers [21] claimed that keto-amine tautomerism is dominant in naphthaldimine, while phenol-imine is dominant in salicylaldimine Schiff bases, depending on the solvent.

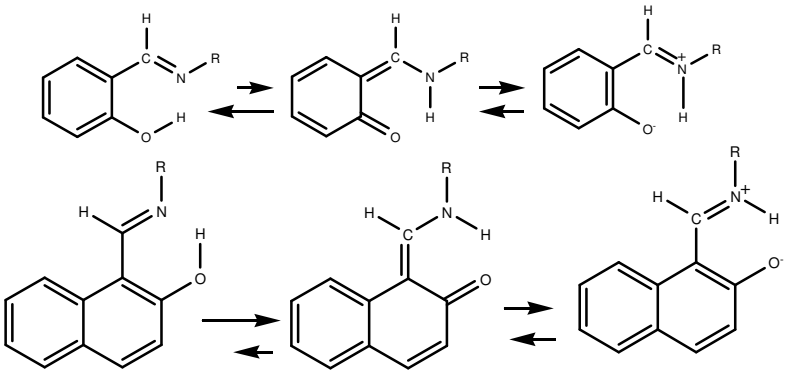

Scheme 1.3: Tautomerism in orthohydroxyl Schiff base ligands

Electronic spectroscopy has equally been used to study the existence of tautomerism between the enol-imine and the keto-enamine forms of ortho-hydroxyl Schiff bases as in scheme 1.3. [21-23]. Tautomerism is thought to occur via an intramolecular (or intermolecular in protonic solvents) hydrogen transfer to the imine nitrogen [22]; thus, the tautomerism should therefore, increase with increase in the imine basicity. On the other hand, it can take place through hydrogen transfer from the hydroxyl proton, in which case, it should increase with the hydroxyl acidity [22]. Tautomerism in ortho-hydroxyl Schiff bases has been studied in both polar and non-polar solvents [23-26].

A new band at greater than 400 nm has been observed in polar solvents and in acidic media in some solvents; but not in hydrocarbon solvents [27]. The absorption band at greater than 400 indicates a keto-imine form of the Schiff base; the enol form has no appreciable absorbance in this region [21, 22, 28].

UV/Visible studies have also been used to characterize the possible electronic transitions in Schiff base ligands. The Schiff base ligands synthesized by Abdu-Elzaher [29] exhibited three peaks at about 270 nm, 330 nm, and 372 nm and were characterized as follows: the first two peaks were attributed to benzene $\pi \rightarrow \pi^*$ and imino $\pi \rightarrow \pi^*$ transitions while 372 nm was assigned to $n \rightarrow \pi^*$ transition. Zhoa et al. [30] has also assigned the band at 334 nm to the azomethine chromophore $\pi \rightarrow \pi^*$ transition while the bands at higher energies (212 and 281 nm) were regarded as associated with the benzene $\pi \rightarrow \pi^*$. However, Ramesh and Maheswaran [31] assigned $\pi \rightarrow \pi^*$ and $n \rightarrow \pi^*$ of the imine bond to the bands at 295-249 nm and 330-346 nm respectively. On the other hand, the azomethine chromophore $\pi \rightarrow \pi^*$/ $n \rightarrow \pi^*$ transition always undergo either a red or blue shift in the complexes, depending on the nature of the Schiff base and the metal ion. This is constantly used as an indication that the imino nitrogen is involved in coordination to the metal ion. The bands assigned to benzene, $\pi \rightarrow \pi^*$, transitions are always only slightly affected.

1.3.0 Application of Schiff bases

Schiff bases have found applications in various fields of chemistry such as catalysis [32-34], electrochemistry [35, 36], organic syntheses [37, 38] and medicines [39-41].

Many Schiff base complexes show excellent catalytic activity in various reactions at high temperature (above 100 $^{\circ}$C) and in the presence of moisture [42]. The interest in polymerization of olefins has increased recently due to the observed catalytic activity of Schiff base complexes in the synthesis of commercially available branched [43, 44] and linear polyethylenes [45-48]. Also, Schiff bases have been employed in the oxidation of hydrocarbons to examine the catalytic ability of various metal complexes [49-53]. The chiral Schiff base complexes of salen [54] and binaphthyl were used as efficient catalysts in Michael addition reaction. Schiff base complexes showed catalytic activity in carbonylation of alcohols and alkenes at low pressure to produce α-arylpriopionic acid and their esters [55-58], which are used as non-steroidal anti-inflammatory drugs. The Heck reaction, an industrially useful process to synthesize fine chemicals and pharmaceuticals, was successfully catalyzed using Schiff base complexes [59-62]. Schiff base complexes also played a significant role in desymmetrization of meso compounds with

significant yield and enantiometric excess [63]. The homogeneous chiral lanthanum(III) Schiff base complexes showed catalytic activity in asymmetric Diels-Alder reaction [64].

Schiff bases play biological roles [65], for example, in vision and in determining the flexibility of the wall of the veins, etc. Schiff bases of aminoalkylpyridines are known to be structurally related to compounds participating in vitamin B6 chemistry [66]. They have equally been screened for their antimicrobial and antifungal [31, 67-73], anti-inflammatory [74], and anti-viral activity [75]. Schiff base ligands derived from indole-3-carboxaldehyde and some L-amino acids as well as some aminophenols were labelled with ^{99m}Tc with radiochemical purity above 97%. The ligands were stable for more than 24 hr under physiological conditions. They were equally evaluated for their antimicrobial activity against *Bacillus substilis*, *Pseudomonas fluorescence*, *Staphylococcus aureus*, *Aspergillus niger*, *Candida albicans* and *Trichophton rubrum* [73].

Salicylaldiminato Schiff bases have been used in DNA cleavage due to their intramolecular charge transfer [76, 77]. Schiff base products obtained from aminopyridines and *o*-hydroxyaromatic aldehydes have been demonstrated to serve as analytical agent [78-80] for metal analyses, hence encouraging investigations of the corresponding metal complexes.

Schiff bases are often used as ligands in coordination chemistry to form metal complexes owing to their metal binding ability [41, 70, 78, 79]. Ortho-hydroxyl Schiff base ligands, especially salicylaldimines, have received special attention because they form stable chelates readily with metal ions [77, 81-84]. It is known that activity of bioactive compounds may become enhanced in the presence of metal ions [78, 85].

1.4.0 Biological importance of Schiff bases

Schiff bases appear to be important intermediates in a number of enzymatic reactions involving interaction of the amino group of an enzyme, usually that of a lysine residue, with a carbonyl group of the substrate [86]. Schiff base formation in the biological environment is widely found in the chemistry of pyridoxal phosphate (PLP), a derivative of pyridoxine otherwise known as vitamin B_6. The role of this coenzyme is significant for living matter as far as the metabolism of amino acids is concerned [87]. In PLP-dependent enzymes, the coenzyme binds to the protein

through the formation of an imine with the E- amino group of a lysine residue [88]. Stereo-chemical investigations [89] carried out with the aid of molecular models showed that Schiff bases formed between methyl-glyoxal and the amino group of the lysine side chains of proteins can bend back towards the N atom of peptide groups in such a way that a charge transfer can occur between these groups and the oxygen atoms of the Schiff bases.

Schiff bases are involved as intermediates in the processes of non-enzymatic glycosylations. These processes are normal during aging but they are remarkably accelerated in pathogeneses caused by stress, excess of metal ions or diseases such as diabetes, Alzheimer's disease, and atherosclerosis [90]. Non-enzymatic glycosylation begins with an attack of sugar carbonyls or lipid peroxidation fragments on amino groups of proteins, aminophospholipids and nucleic acid, causing tissue damages by numerous oxidative rearrangements. One of the consequences is cataract of lens proteins.

Another important role of Schiff base structure is in transamination [91]. Transamination reactions are catalyzed by a class of enzymes called transaminases. Transaminases are found in mitochondria and cytosal of eukaryotic cells. All the transaminases appear to have the same prosthetic group, i.e., pyridoxal phosphate, which is covalently attached to them via an imino group. Schiff base formation is also involved in the chemistry of vision, where the reaction occurs between the aldehyde function of 11-*cis*-retinal and amino group of the protein (opsin) [92].

The biosynthesis of porphyrin, for which glycine is a precursor, is another important pathway, which involves the intermediate formation of Schiff base between keto group of one molecule of δ-aminolevulinic acid and ε- amino group of lysine residue of an enzyme. A comprehensive review on the biological activity of Schiff bases and their metal complexes has been written by Arulmurugan et al., [93].

1.5.0 Salicylaldimine Schiff base metal complexes

After the work of Jorgensen and Werner, metal complexes of Schiff bases have occupied a central place in the development of coordination chemistry [94]. However, there was no comprehensive, systematic study until the preparative work of Pfeifer and associates [95].

Structure and mechanism of the formation of Schiff base complexes and stereochemistry of four coordinate chelate complexes formed from Schiff bases and their analogues have been discussed in several reviews [96, 97]. Various methods are employed for determining the structure of the complexes. Those often used include determination of magnetic moment, electronic spectrum and nuclear magnetic resonance, in addition to elemental analysis and molecular weight determination [97]. The configuration of the chelate group in the four coordinate complexes may be square-planar, tetrahedral, distorted tetrahedral or distorted trigonal pyramidal with the metal atom at the apex. The configuration depends primarily on the nature of the metal atom and also on the magnitude and symmetry of the ligand field.

Many complexes of the Cu(sal*R) type have been prepared. Most of them are considered to be square-planar [98]. Some of them, however, consist of a bi-nuclear unit, in which there is a very weak copper-to-copper bond [99]. For Cu(sal*R), R being alkyl or aryl groups, the square-planar configurations is stable, but when there is considerable steric hindrance, the distortion from planarity may occur. Metal complexes have also been reported with other ligands mixed with Schiff bases [100].

The Schiff base complexes derived from salicylaldiimines have been the most thoroughly studied so far. The advantage of the salicylaldimine ligand systems is the considerable flexibility of the synthetic procedures which have resulted in the preparation of a wide variety of complexes with a given metal whose properties are often dependent on the ligand structure. The literature survey of some complexes of Schiff base ligands derived from salicylaldehyde, 3-methoxy-2-hydroxybenzaldehyde (*o*-vanillin), 4-methoxy-2-hydroxylbenzaldehyde (*p*-vanillin) and 3-methoxy-4-hydroxybenzaldehyde (vanillin) is presented below.

Percy and Thornton [101] prepared a series of N-aryl salicylaldimines (I) from substituted aniline with a focus on the infrared and NMR spectra study of the compounds.

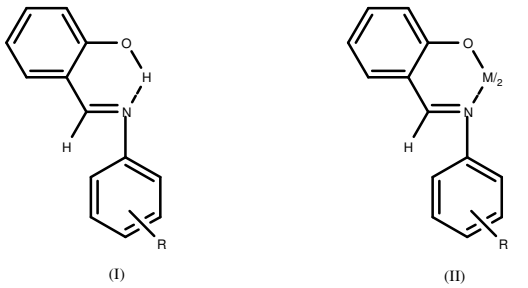

Fig. 1.2: N-arylsalicylaldimine Schiff bases (I) and metal chelates (II)

The assignments of the characteristic infrared bands were based on ^{15}N-labelling of *p*-tolysalicylaldimine. The NMR spectra established that the Schiff base ligands existed in phenol-imine form in deuterated chloroform at room temperature and that the electron withdrawing N-aryl substituents reduced the shielding on the hydroxyl proton. The two ^{15}N-sensitive bands ($\Delta\nu$ -5 and -8 cm^{-1}) near 1600 cm^{-1} in the IR spectrum of *p*-tolysalicylaldimine were assigned to coupled $\nu_{C=N}$ bands. The assignment of both bands to $\nu_{C=N}$ was supported by their sensitivity to metal ion complexation. Phenolic C-O stretching frequency was assigned to the band near 1287 cm^{-1} and the neighbouring band near 1310 cm^{-1}. The strong intramolecular hydrogen bonding present in the ligands led to very weak and broad hydroxyl absorption near 2700 cm^{-1}. However, in the NMR spectra of the Schiff base ligands, the azomethine proton absorbed at 8.70-8.35 ppm, while the phenolic hydroxyl proton absorbed far downfield at 13.46-11.83 ppm. Metal(II) [M= Ni, Co, Cu and Zn] chelates of the salicylaldimines were also discussed. The assignments were based on ^{15}N-labelling of the Cu(II) complex of *p*-tolysalicylaldimine. Support for the $\nu_{C=N}$ assignment in the IR spectra of the Cu(II) chelates is provided by observing the frequency shifts induced by metal ion substitution and by varying the N-aryl substituent.

The same authors [102] have equally extended their studies to N-alkyl salicylaldimines and their chelates.

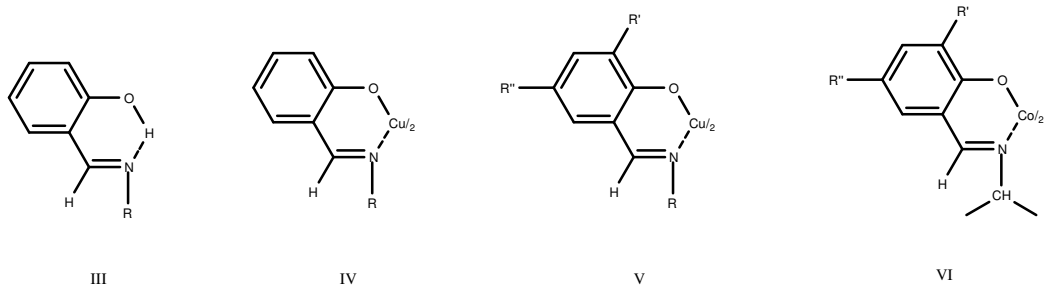

Fig. 1.3: N-arylsalicylaldimine Schiff bases (I) and metal chelates (II-VI)

The NMR spectra showed that the Schiff base ligands existed in phenol-imine form in deuterated chloroform. The strong intramolecular hydrogen bonding in the ligands led to a large downfield shift of the hydroxyl resonance which is related to the inductive effects of the substituents measured by their substituent parameters [103]. An increase in the shielding of the OH proton is produced by electron withdrawing substituents which have the effect of decreasing the electron density in the N-H bond [104].

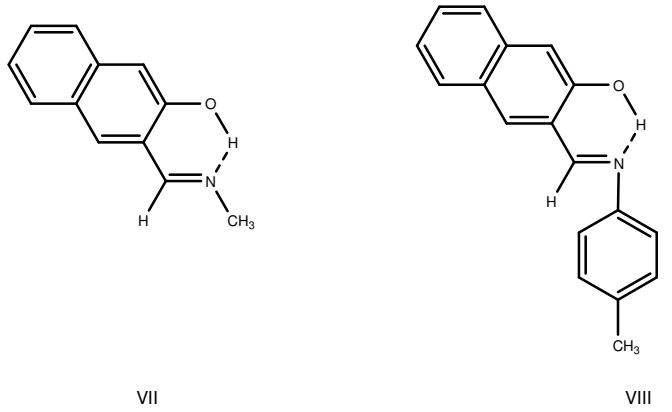

Fig. 1.4: N-arylsalicylaldimine Schiff bases (VII and VIII)

The IR spectra of the N-alkyl salicylaldimines are characterized by the presence of substantially fewer bands than are observed in the spectra of the N-aryl bases. This feature suggests less coupling in the N-alkyl compounds. Thus, there was only one ^{15}N-sensitive $\nu_{C=N}$ band in the 1600 cm^{-1} region of the spectrum of the N-alkyl base (VII). Also, the ^{15}N-induced shift of the single band in the spectrum of (VII) was relatively large ($\Delta\nu$ -18 cm^{-1}) compared with shifts of -5 and -8 cm^{-1} for the two bands in the spectrum of (VIII) and a theoretical shift of -40 cm^{-1} for vibrational pure $\nu_{C=N}$ band.

Marvel et al. [105] prepared a number of polymeric salicylaldimine complexes and found that the C=N absorption varied from 1637 to 1616 cm^{-1} in the free base and from 1656 to 1606 cm^{-1} in the metal chelates. These authors also assigned the phenolic C-O vibration in the chelates to the region 1390 cm^{-1} and 1310 cm^{-1}. The thermal stability of the Schiff base ligands and their metal chelates [M= Zn(II), Ni(II), Cu(II), and Fe(II)] were also studied in the presence and absence of air.

Adducts as well as deprotonated complexes of the forms : $MCl_2.2H_2PIS$, $M(HPIS)_2$ and $M(PIS).nH_2O$ [M= Mn(II), Co(II), Ni(II), Cu(II) and Zn(II)] were prepared from N-(picolinamido)salicylaldimine, H_2PIS, Schiff base ligand [81]. A partially deprotonated Cu(II) complex {$Cu(HPIS)Cl.H_2O$} was also prepared. The magnetic and UV/Visible studies suggested an octahedral geometry for all the complexes except those of Cu(II), which have distorted octahedral geometry.

The formation constants of some transition metal ions, Cr(III), Mn(II), Fe(III), Ni(II) and Cu(II), binary complexes containing Schiff bases from condensation of salicylaldehyde with aniline, 2-aminopyridine, 4-aminopyridine and 2-aminopyrimidine were determined pH-metrically in ethanolic medium (80%, v/v) [83]. The infrared (IR) spectral bands corresponding to the azomethine group of the free Schiff base ligands was observed at 1643–1650 cm^{-1}. The phenolic C–O of the free ligands was observed at 1275 cm^{-1}. Upon chelation, the C=N and the C-O bands underwent a red and blue shifts respectively. This indicated that it may be considered as a center of chelation. The thermal dehydration and decomposition of these complexes were studied kinetically using the integral method applying the Coats–Redfern equation [83].

Zinc(II) complex of Schiff base ligand derived from salicylaldehyde and 4-methyl-1,3-phen has been evaluated for their antimicrobial activity [106]. The complexes of formula $[Zn(HL)Cl(H_2O)_2] \cdot C_2H_5OH$ and $[Zn(H_2L)_2Cl(NO_3)(H_2O)] \cdot CH_3OH$ were characterized as powder solids and in solution by spectroscopic methods (IR, ^1H and ^{13}C NMR, FAB-MS, ESI-MS, UV–Vis), thermo-gravimetric and elemental analysis, as well as potentiometry. The

compounds were tested for antimicrobial activity against *Staphylococcus aureus* in a minimum inhibitory concentration (MIC) experiment.

The Schiff-base ligands derived from the reaction of 3-hydroxybenzaldehyde with three alkyl diamines [107] have been synthesized and characterized. The reactions of the three Schiff-base ligands with various MX_2 salts (M = Cu, Ni or Zn; X = chloride, perchlorate or acetate) resulted in the cleavage of the imine bond and formation of metal–amine complexes, as well as the entrapment of a two coordinate $CuCl_2$ molecule within the lattice in one particular case.

A binuclear Ni(II) complex of Schiff base ligand obtained from the condensation of *o*-vanillin and *p*-toluidine [108] was synthesized. The structure of the complex was characterized by FTIR and UV/Vis spectroscopy as well as thermogravimetric analyses (TG-DTG). It was further confirmed by single crystal X-ray diffraction. The crystal structure revealed the presence of a Ni.Ni core, with the Schiff base ligand coordinating to the nickel ions via the phenolic oxygen, the imne nitrogen and the methoxyl oxygen atoms.

Dubey et al. [109] reported the physicochemical characterization of some chromium complexes of Schiff base ligands derived from the condensation reaction of salicylaldehyde or vanillin with 2-aminopyridine, 2-aminophenol, *o*-toluidine, *p*-toluidine, 3-nitraniline and substituted benzimidazole / benzoxazole or mercaptobenzimidazole. The complexes were characterized by elemental analysis, infrared, UV-visible, FAB-mass and magnetic susceptibility techniques. Octahedral geometry was proposed for the complexes.

Valent et al. [110] reported the synthesis of some copper(II)salicylideneglycinate complexes as potential antimicrobial agents. The complexes were synthesized by reacting N-salicylideneglycinatoaqua copper(II) hemihydrate with urea, pyridine, 2,4-dimethylpyridine, 3,5-dimethylpyridine, quinoline, isoquinoline or 3-methyisoquinoline in an equimolar ratio. The complexes were of the type [Cu(salgly)L] with distorted square pyramidal coordination polyhedra. The products were characterized by elemental analysis, electronic and EPR spectra, and magnetic susceptibility measurements. The antimicrobial activity of the complexes was

evaluated by macro-dilution method using *G-Staphylococcus aureus, G-Escherichia coli* and *Candida parapsilosis.*

Mashaly et al. [111] reported the synthesis and the antimicrobial activity of Cu(II), Ni(II), Zn(II), and Fe(III) Schiff base complexes derived from 4-aminoantipyrine and salicylaldehyde as well as mixed ligand complexes obtained with 2-aminopyridine, 8-hydroxyquinoline and oxalic acid and their pyrolytical products. All the binary and mixed ligand complexes have octahedral configurations. The antibacterial activity of free ligand and its binary metal complexes were tested against *Staphylococcus aureus, Bacillus subtilis, Pseudomonas aeruginosa*, and *Escherichia coli*. The antifungal activity against *Aspergillus fumigatus, Penicillium italicum, Syncephalastrum racemosum, Alternaria alternata*, and *Candida albicans* were also evaluated.

Suresh et al. [112] reported that the Schiff base ligands obtained from vanillin and 4-aminoantipyrine formed stable chelates with transition metal ions such as Cr(III), Co(II), Ni(II), Cu(II), Zn(II) and Cd(II). The compounds were characterized by elemental analysis and thermo-gravimetric analysis, infrared, electronic, NMR as well as electron spin spectroscopy. The Schiff base ligands coordinated to the metal ions via the C=O and the azomethine CH=N group. Octahedral geometry was proposed for all the prepared metal complexes. The synthesized ligand and complexes were tested for their antibacterial activity against *Staphylococcus aureus* and *Escherichia coli.*

Sabaa et al. [113] reported the synthesis of vanillin–Schiff's bases as organic thermal stabilizers and co-stabilizers for rigid poly(vinyl chloride). The Schiff base ligands were derived from vanillin and aniline, *p*-anisidine or *p*-nitraniline and consequently reacted with Ni(II) and Co(II) ions to form the metal complexes. The compounds were characterized with elemental and thermo-gravimetric analysis, infrared as well as NMR spectroscopic techniques. All the compounds were investigated for their thermal efficiency.

Sivasankaran and Arish [114] have reported the synthesis of Schiff base ligand derived from vanillinidene-4-aminoantipyrine and o-phenylenediamine. The metal(II) complexes [M=Co(II),

Ni(II), Cu(II) and Zn(II)] of the ligand were equally prepared. The compounds were characterized by elemental analysis, ^{1}H-NMR ^{13}C-NMR, molar conductance, infrared, electronic, magnetic measurements, cyclic voltametry, powder XRD and SEM. The electronic spectral and magnetic measurement data indicate that the complexes exhibit octahedral geometry.

Rathore et al. [115] compared the synthesis of Schiff base metal complexes using the classical thermal and microwave-irradiation techniques. The Schiff base ligand derived from *o*-vanillin and *p*-chloroaniline was reacted with Cr(III), Ni(II), Co(II) and Cu(II). A tetragonal geometry was suggested for the Cu(II) complex of the Schiff base ligand due to broad absorption bands in the regions 637 nm (15699 cm^{-1}) and 411 nm (24320 cm^{-1}). All the compounds were screened against *Staphylococcus aureus, Escherichia coli, Aspergillus niger* and *Fusarium oxysporum.*

Bhunora et al. [116] reported the synthesis and characterization of a range of monomeric tetra-coordinate copper(II) and zinc(II) complexes of N,O-bidentate salicylaldimine Schiff base ligands. The X-ray crystal structures for the complexes revealed a distorted square planar and distorted tetrahedral geometry for the Cu(II) and Zinc(II) complexes respectively. The complexes were evaluated as initiators in ring-opening polymerization of lactides at 70 $^{\circ}$C and 110 $^{\circ}$C. It was discovered that the catalytic activity of the complexes depends on many factors which include the coordination geometry of the metal complexes, M-O bond length and substituents on the Schiff base ligands. Both the Zn and Cu complexes exhibit characteristics of living ring opening polymerization.

Al-Allaf and Sheet [117, 118] synthesized a series of Schiff bases from benzaldehyde, salicylaldehyde and 2- or 3-aminopyridine. Their Schiff base complexes with platinum, palladium and nickel compounds were reported. Noro et al. [119] reported the synthesis and crystal structure of copper(II) complex of N-salicylaldene-3-aminopyridine, while Al-Allaf et al. [120] prepared the diorganotin(IV) complexes of Schiff bases derived from 2- or 3-aminopyridine with 2-hydroxy, 3-hydroxy-or 2-hydroxy-3-methoxy-benzaldehyde. The complexes were screened against several strains of bacteria. In addition, Ayad et al. [121] has equally synthesized copper(II) complexes of Schiff base ligands derived from 2- amino or 3-

aminopyridine with salicylaldehyde. The compounds were characterized by elemental analysis, infrared and electronic spectra as well as DTA data. The electronic spectral data suggested a square planar geometry for the Cu(II) complexes due to the presence of an absorption band at around 700 nm with a shoulder at about 550 nm.

Coppola et al. [122] studied the mass spectrometric behaviour of polydentate Schiff bases derived from 2-(aminomethylpyridine) with 3-methoxylsalicylaldehyde and six other aldehydes while Datta [123] reported the synthesis and characterization of Cu(II) complex of the Schiff base ligand. The coordination geometry around the copper atom is slightly distorted square planar, formed by the N_2O donor set of the Schiff base and one Cl atom.

1.6.0 Benzimidazole

The benzimidazoles contain a phenyl ring fused to an imidazole nucleus as shown in figure 1.5 below. Benzimidazole which contain a hydrogen atom attached to nitrogen tautomerise easily.

Fig. 1.5: Structures of imidazole (I) and Benzimidazole (II)

Imidazole and benzimidazole are amphoteric in nature; they are moderately strong organic bases capable of accepting proton at N-3, as well as weak acids capable of losing a proton from N-1. Therefore, in neutral solutions, the unprotonated molecule usually functions as a unidentate ligand through the unshared pair of electrons on N-3. The probability of participation of the pair of electrons on N-1 in coordination is very small because these electrons are delocalized through the π- system. However, neutral imdazole undergoes deprotonation at N-1 in strongly basic solution, and the resulting aromatic imidazolate ion possesses two equivalent sites for coordination [124]. A large number of publications are available in the literature on studies conducted on benzimidazole and its derivatives with emphasis on pharmacological applications as well as metal complexes formation. Fabiola et al. [125] has written a review on coordination mode of benzimidazole and its derivatives.

1.6.1 Biological importance of Benzimidazole

The imidazole nucleus is found in a number of important natural products such as histidine, the purines and Vitamin B12. The structure of vitamin B12 contains 5, 6-dimethyl-(α-D-ribofuranosyl)benzimidazole. Consequently a massive research effort has been expended upon the chemistry of imidazoles and benzimidazoles with particular emphasis on the synthesis of new compounds for pharmacological screening. Benzimidazole derivatives were reported to possess antibacterial, antifungal, anti-inflammatory, antiviral, anti-tumour, anti-oxidant and anthelmintic activity [126-130].

Patil has written a comprehensive review on the anti-ulcer activity of some benzimidazole derivatives drugs [131]. Benzimidazole class of many substituted compounds such as 2-[[(2-pyridyl) methyl] thio]-1-H benzimidazole has shown selective activities against gastric pathogen *Helicobacter pylori,* the probable mechanism being as inhibitor of *H. pylori* [132].

Panneer Selvam et al. [133] reported the synthesis of a series of 2-benzimidazole derivatives as antimicrobial agents. The compounds were screened against *Staphylococcus aureus, Staphylococcus epidiermidis, Klebsiella pneumoniae, Escherichia coli, Candida albicans* and *Aspergillus niger*.The discovery of new antibacterial and anthelmintic agents has added momentum to investigations in these areas. Several benzimidazole derivatives have been marketed [133] in the past decades as anthelmintic and antimicrobial agents for both human and veterinary purposes (table 1.1).

Some metal complexes of benzimidazoles were screened for antibacterial activity against Gram-negative and Gram-positive bacteria. A majority of the compounds were found to be effective at moderate to high concentration levels [134]. Milanino et al. [135] prepared copper(II) chelates of some bis(2-benzimidazolyl)thioethers and orally administered to rats. They found that these chelates were most effective as anti-inflammatory agents. Benzimidazoles and imidazoles as axial bases facilitate oxygen binding by heme iron [136-138]. Such complexes can be considered as models for myoglobin. The oxygen binding constant is at least 3800 times greater for the

imidazole compound than that for the pyridine analogue. The π-donor ability of the imidazole ring is suggested as an explanation for its increased binding capacity [139].

Table 1.1: List of benzimidazole drugs in the market

Approved name	**Chemical name**	**Structure**	**Uses**
Thiabendazole	2-(3-triazolyl)-benzimidazole	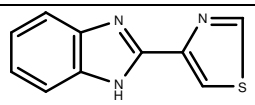	Anthelmintic
Mebendazole	Methyl-5-benzoyl-2-benzimidazole carbamate	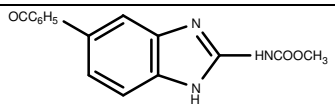	Anthelmintic
Bezitramide	1-(3-cyano-3,3-diphenylpropyl)-4-(2-oxo-3-priopionyl-1-benzimidazolinyl)piperidine	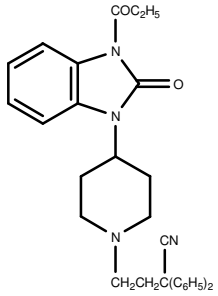	Analgesic
Clemizole	1-(*p*-chlorobenzyl)-2-(1-pyrrolidnylmethyl)-benzimidazole	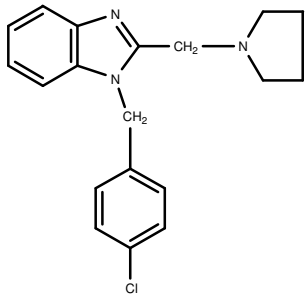	Antihistidine
Fuberidazole	2-(2-furanyl)benzimidazole	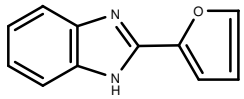	Fungicide
Cambendazole	5-isopropoxycarbonyl-amino-2-(4-thiazolyl)-benzimidazole	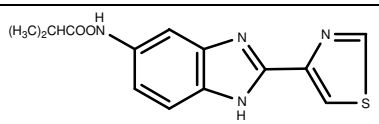	Anthelmintic

Cobaloximes are the most studied models [140] of vitamin B12. Interaction of cobaltous acetate and dimethylglyoxime in the presence of cyanide ion and benzimidazoles produces cobaloximes having cyanide ion and benzimidazole ligands at axial positions. Similar complexes having halide in place of cyanide have been prepared from cobaltous halides, dimethylglyoxime and benzimidazoles. The possible role of cobaloximes in the 40 mechanism of corrinoid based enzymatic reactions has been a subject of considerable discussion [141] .

1.6.2 Benzimidazole Schiff base complexes

Substituted benzimidazoles have received great attention, especially since it has been reported that the influence of the substitution at 1, 2, and 5 positions is very important for their pharmacological effects [142]. In the same vein, Schiff bases, derived mostly from variety of heterocyclic rings, were reported to possess a broad spectrum and a wide variety of biological activities including antiviral, anticancer, cytotoxic, antimicrobial and anticonvulsant among others [143].

Thus, the search for benzimidazole derivatives with higher pharmacological activity has led to increased interest in the synthesis of benzimidazole-based Schiff base compounds. Such compounds combine the biological potency of both the benzimidaziole nucleus and the azomethine functional group of the Schiff base ligands. Schiff base ligands have been used to prepare several metal complexes and have consequently been evaluated for their biological activity.

Marijana et al. [144] reported the synthesis of series of substituted benzimidazole Schiff bases from aromatic aldehydes with corresponding 2-aminobenzimidazoles. Majority of the Schiff bases exerted non-specific antiproliferative activity on the tested cell lines at the highest tested concentration.

Metal chelates [M = Fe(II), Co(II), Ni(II), Cu(II), Zn(II) and Cd(II)] of salicylidene-2-aminobenzimidazole Schiff base, (figure 1.4), have been prepared [145]. The base reacts with these metal ions to give 1:1 (M→L) complexes; in the case of Fe(III), Co(II), Cu(II), Zn(II) and

Cd(II) ions; and 1:2 (M→L) complex; in the case of Ni(II) ion. The IR spectra of the complexes indicated that the ligands coordinated to the metal ions in a terdentate manner with O, N, N donor sites of the phenolic -OH, azomethine -N and benzimidazole N-3. A square planar geometry was proposed for the Cu(II) complex based on the appearance of a single band at 566 nm (17667 cm^{-1}) in the solid reflectance spectrum of the complex. It was further confirmed by a magnetic moment of 2.92 B.M.

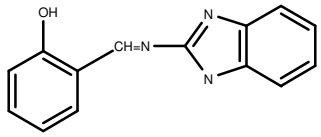

Fig. 1.6: 2-Aminobenzimidazole Schiff base ligand

Liu et al. [146] reported the single crystal structure of a dinuclear copper(II) complex, $[CuL(NO_3)]_2 \cdot 2MeOH$, obtained by the coordination reaction of $Cu(NO_3)_2 \cdot 3H_2O$ with ligand HL (HL = N-(methyl-2-benzimidazolmethylidene)- 2-hydroxylaniline), figure 1.7. The basic dinuclear copper(II) complex units $[CuL(NO3)]_2$ were formed by NO_3^- as co-bridging ligands and L as NNO tridentate chelate coordinating to the copper ions. The Cu(II) complex has a distorted octahedral geometry.

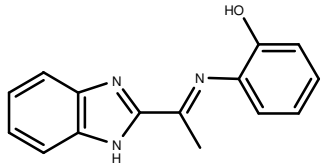

Fig. 1.7: N-(methyl-2-benzimidazolmethylidene)- 2-hydroxyaniline

Chhonker et al. [147] reported the synthesis of a series of Schiff base ligands using 2-aminophenylbenzimidazole, figure 1.8. The ligands were obtained by condensing 1, 2-phenylenediamine with anthranilic acid or *p*-benzoic acid in polyphophoric acid (PPA) at 190-195°C under reflux. The Schiff base ligands were screened for their *in vitro* antimicrobial activity against *Staphylococcus aureus, Bacillus subtilis, Escherichia coli* and *Pseudomonas aeruginosa*

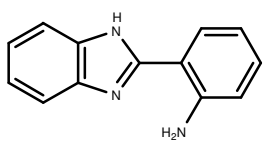

2-(2-aminophenyl) benzimidazole

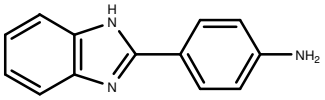

2-(4-aminophenyl) benzimidazole

Fig. 1.8: 2-Aminophenylbenzimidazoles

1.7.0 Geometrical structure and electronic spectra of Cu(II) complexes

The (+2) oxidation state of copper is by far the commonest state in which the copper ion has nine d-electrons, and most of the divalent compounds are four-coordinate [141]. There are a number of quite stable, five-coordinate complexes of Cu^{2+}, all involving ligands that are considered to be π-acceptors.

Copper(II) complexes are mostly blue or green [141, 148], however, the nature of the ligand does influence the colour of the isolated complexes in some cases. The origin of the colour is due to the presence of an absorption band in the 600-900 nm region of the spectrum. The envelopes of these bands are generally un-symmetrical seeming to encompass several transitions, but definitive resolution into the proper number of sub-bands with correct location is difficult. Only when the polarized spectra of single crystals have been measured has this resolution been achieved unambiguously. The cases of $[Cu(NH_3)_4]^{2+}$ ion in $[Cu(NH_3)_4][ClO_4]_3.NH_3$ and $Cu(DPM)_2$ are instructive [149].

There is a large number of copper(II) electronic spectra in the literature , where the structure is known but the assignment is not certain [149]. An example of this uncertainty can be found in the $^2T_{2g} \rightarrow {}^2E_g$ transition for octahedral copper(II) complexes in which the $t_{2g} \rightarrow e_g$ separations are from approximately 769 nm for CuO_2 to about 556 nm for CuN_6. Several absorption bands may be expected in this region for a tetragonally distorted octahedral copper(II) complex. These bands correspond to transitions from sub-levels (d_{xz}, d_{yz}, and d_{xy}) of $^2T_{2g}$ to $d_{x^2-y^2}$ and d_{z^2}. The ^2E_g and $^2T_{2g}$ ground terms of an octahedron splits, as shown in figure 1.9 [150], as a result of Jahn-Teller distortion and in turn results in overlapping of bands and a more complex spectrum, with the appearance of a low energy shoulder.

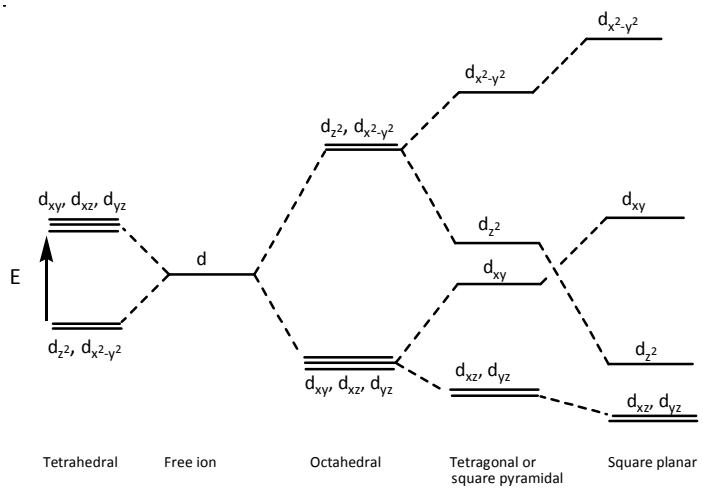

Fig. 1.9: Crystal field spliting of the d-orbitals of a central ion in complexes of various geometrical structures

Square planar geometry is more favoured for a tetra-coordinated copper(II) complex. The distortion of this system commonly leads to three transitions, namely $^2B_2 \rightarrow {}^2A_2$; $^2B_2 \rightarrow {}^2B_1$ and $^2B_2 \rightarrow {}^2A_1$ [149]. Absorptions above 500 nm have been observed [151] for distorted tetrahedral $[CuBr_4]^{2-}$ and $[CuCl_4]^{2-}$ while the tetra-amine coordinated copper(II) ion with stronger fields such as imines will appear blue shifted. Copper(II) ion complexes are susceptible to ligand-solvent exchange or the possibility of more than one species in equilibrium, depending on coordination number involved [152].

1.7.1 Jahn-Teller distortion

The Jahn-Teller theorem states that "in a non-linear molecule, if degenerate orbitals are asymmetrically occupied, the molecule will undergo distortion to remove the degeneracy by lowering the symmetry and thus by lowering the energy [153].

An electronically degenerate state represents the availability of more than one degenerate orbital for an electron. In this condition, the degenerate orbitals are asymmetrically occupied. For instance, in octahedral symmetry, the d^1 configuration is said to be electronically degenerate since three t_{2g} orbitals with the same energy are available for the electron to occupy. In this condition, the degenerate orbitals are said to be asymmetrically occupied by electrons. For

instance, in the case of octahedral d^9 configuration, the last electron may occupy either d_{z^2} or $d_{x^2-y^2}$ orbitals of e_g set.

The Jahn-Teller distortion is mostly observed in octahedral environments. Theoretically, the electronic degeneracy in octahedral symmetry is possible in all the configurations except d^3, d^8, d^{10}, high spin d^5 and low spin d^6 configurations. However, considerable distortions are usually observed in high spin d^4, low spin d^7 and d^9 configurations in the octahedral environment. This is because the Jahn-Teller distortion is usually significant for asymmetrically occupied e_g orbitals since they are directed towards the ligands and the energy gain is considerably more.

In the case of unevenly occupied t_{2g} orbitals, the Jahn-Teller distortion is very weak since the t_{2g} set does not point directly at the ligands and therefore the energy gain is much less. e.g. d^1; d^2; low spin d^4 & d^5 configurations. Likewise, for the same reason, the tetrahedral complexes do not exhibit Jahn-Teller distortion. Again, in this case also, the ligands are not pointing towards the orbitals directly and hence there is less stabilization to be gained upon distortion.

Z-out and Z-in Jahn-Teller distortions

The degeneracy of orbitals can be removed by lowering the symmetry of the molecule. This can be achieved by either elongation of bonds along the z-axis (Z-out distortion) or by shortening the bonds along the z-axis (Z-in distortion). Thus, an octahedrally symmetrical molecule is distorted to tetragonal geometry.

The Z-out distortion is the most preferred distortion and occurs in most of the cases, especially when the degeneracy occurs in e_g level. For example, the octahedral d^2, d^4 high spin, d^7 low spin and d^9 configurations usually show the z-out distortion. Theoretically, it is not however possible to predict the type of distortion that occurs when the degeneracy occurs in e_g level. On the other hand, the degeneracy in an octahedral d^1 configuration is removed by shortening the bonds along the z-axis (Z-in distortion). It should be noted that Jahn-Theorem does not predict how large a distortion should occur.

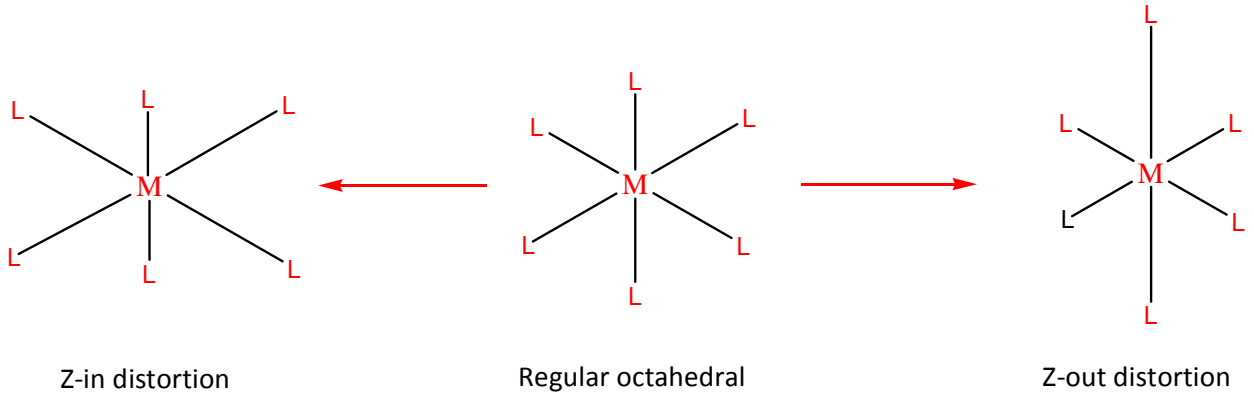

Fig. 1.10: Jahn-Teller distortion in octahedral environment

Jahn-Teller distortion provides extra stability to Cu(II) ions as observed in the Irving Williams series for relative stability of complexes formed by high spin divalent first row transition metal ions. The stability order is given shown below:

Mn(II) < Fe(II) < Co(II) < Ni(II) < Cu(II) > Zn(II)

It also results in the splitting of absorption bands in the UV/visible spectra of metal complexes. For example, the absorption band in the electronic spectrum of aqueous Ti(III), a d^1 octahedral system, is not symmetric but rather shows a distinct broad shoulder due to Jahn-Teller distortion. This absorption band is similar to that of Cu(II) complexes.

1.8.0 Biological importance of Cu(II) ion

The fundamental importance of copper is adduced to its involvement in several enzymes and proteins widely distributed in animals and plants; where it performs central functions in various fundamental biological processes [154]. In plants copper participates in the process of photosynthesis, assists in the assimilation of starch and nitrogen, enhances the stability of chlorophyll, and stimulates respiration. The vegetative parts of plants contain more copper than the reproductive. Copper is found in the tissue, liver, muscle and bone of animals. It is mainly absorbed in the acid medium of the stomach and upper intestine very probably in complexes with amino acids such as histidine and with peptides; copper can also be absorbed from the lower parts of the intestine [155].

In animals, copper is involved in the body's protective functions; pigmentation and keratinisation of hair and feathers; and the formation of copper-containing proteins with enzymatic functions [156]. Copper proteins play two main functions, namely; electron transport and di-oxygen transport and activation. For instance, cytochrome C oxidase is required by cells to produce the energy needed to drive biochemical reactions as in aerobic respiration; while hemocyanins acts as dioxygen transport proteins in several organisms. Dopamine B hydrolase is required in the conversion of dopamine to noradrenaline, a neural hormone that plays a vital part in the transmission of nerve impulses [157]. Likewise, lysyl oxidase is required for the proper cross-linking of elastin and collagen during the building, maintenance and repair of connective tissues [158]. Superoxidase dismutase is required to prevent the accumulation of the superoxide radicals which cause cellular damage; the enzyme responsible is a copper/zinc metallo-enzyme found in the cytosol of all cells [159].

In humans, copper has been associated with lipid metabolism since 1973 [160]. An imbalance of Zn over Cu has been associated with an increased incidence of hypercholesterolaemia in rats and to a greater risk of ischaemic heart disease in humans [161]. In the same vein, Wilson's disease has been linked to massive accumulation of Cu in the brain due to the inability of the patient to transport copper out of the affected tissues via the blood protein, caeruloplasmin or via biliary excretion [154]. Patients suffering from Wilson's disease are treated with such drugs as the copper chelating agent, penicillamine that removes or modulates copper distribution. Copper has been implicated in many other disorders; for example, as far back as 1938 [162], hypercupreama (associated with increased levels of caeruloplasmin) was observed in rheumatoid arthritis. It has been established that copper complexes can be effective in treating arthritis [163].

Acute copper poisoning is a rare event, largely restricted to young children who have accidentally drunk solutions of copper sulphate or copper nitrate. Inorganic copper salts are powerful emetics and inadvertent large dose are rejected by vomiting. Chronic copper poisoning is also very rare [164].

1.8.1 Therapeutic effects of metal complexes

Metal ions are involved in several mechanisms in the biological systems and thus the development of metal-based therapeutics has gained the much needed special attention. Metal centers, being positively charged, are favored to bind to negatively charged biomolecules; the constituents of proteins and nucleic acids offer excellent ligands for binding to metal ions. Bonding of metallo-elements with polydentate ligands to form ring structure, where the metal atom is part of the ring, is called chelation. In chelates, metal is firmly held by a number of ligand atoms usually nitrogen, oxygen or sulphur through coordinate covalent bonds. Some of the chelates are model analogues of certain metallo-enzymes [165, 166]. Furthermore, some of the chelates develop considerable antimicrobial activity. It has been demonstrated through several studies [134, 137, 167] [171] that the biological activity of chelating compounds is enhanced on chelation with metal atoms. Some of the inactive ligands developed such properties upon chelation. The antimicrobial activity of some Schiff bases has been attributed to their ability to chelate with trace transition metal [168, 169]. The pharmaceutical use of metal complexes therefore has excellent potential.

The earliest reports on the therapeutic use of metals or metal containing compounds in cancer and leukemia date back from the sixteenth century. They were forgotten until 1960s when the antitumor activity of the inorganic complex *cis*-diamminedichloroplatinum(II) (Cisplatin) was discovered. This led to the development of other types of non-organic cytostatic drugs. Cisplatin has developed into one of the most frequently used and most effective cytostatic drugs for the treatment of solid carcinomas and particular for testicular cancer [170].

Silver and mercury have a long history of use as antibactericidal agents [171-173], though the use of mercurochrome as a topical disinfection is now discouraged. Silver sulfadiazine finds use for the treatment of severe burns. Silver nitrate is still used in many countries to prevent ophthalmic disease in new born children [174]. The mechanism of action of silver and mercury is through slow release of the active metal ion; inhibition of thiol function in bacterial cell walls gives a rationale for the specificity of bactericidal action.

Bismuth compounds have been used for their antacid and astringent properties in a variety of gastrointestinal disorders [175, 176]. The effectiveness of bismuth is due to its bactericidal action against the gram-negative bacterium, *Helicobacter pylori*. The commonly used agents are colloidal bismuth subcitrate (CBS), and bismuth subsalicylate (BSS). The mechanism of action is complex and includes inhibition of protein and cell wall synthesis, membrane function, and ATP synthesis. The most notable salts are tripotassiumdicitratobismuth, bismuth salicylate, Pepto-Bismol (BSS), and De-Nol (CBS). The combination of ranitidine (a histamine H_2-receptor antagonist) and bismuth citrate is marketed as Ranitidine Bismutrex for the management of peptic ulcer and ulcers associated with *H. pylori* [177].

The clinical value of lithium has been recognized since 1949. Lithium carbonate is used in maniac depressive psychoses for the treatment of recurrent mood changes [178, 179].The drug is administered orally in doses up to 2 g day^{-1} (30 mmol day^{-1}) and the mood stability may only occur after months rather than weeks. It is of limited use in other psychiatric disorders such as pathological aggression, although additional benefit may also include a reduction in actual or attempted suicide.

Gold salts have had a long history of use in rheumatoid arthritis [180, 181]. The development of orally active auranofin (also known as Radaura); was a major improvement over the early "injectionable gold" preparations which were polymeric. However, use has declined with the popularity of non-steroidal anti-inflammatory drugs (NSAIDS) such as indomethacin. The mechanism of action is postulated to occur through thiolate exchange reactions [182].

The use of lanthanum carbonate is being promoted as an alternative aluminum-based therapy for the treatment of hyperphosphatemia [183, 184]. Patients with this end-stage renal disease are not able to filter excess phosphate that enters the body in the normal diet. Elevated phosphate produces the bone disorder renal osteodystrophy and skeletal deformity may occur possibly associated with cardiovascular disease. Forsenol (AnorMED), a lanthanide compound, allows systemic absorption of excess phosphate from the body and this demonstrates an intrigue use of lanthanide compound in therapy.

Historically, sodium vanadate was used to treat human diabetes mellitus (DM) as far back as 1899 [185] before the discovery of insulin in 1921. Recently, both vanadyl sulfate and sodium vanadate have been examined clinically to find out whether they improve human DM [186-188]. Orally active insulin-mimetic vanadyl complexes with the $VO(O_4)$ coordination mode have equally been developed [186, 189-191]. The most widely tested bis(maltolato) oxovanadium(IV) $[VO(ma)_2]$ and bis(ethylmaltolato)oxovanadium(IV) $[VO(ema)_2]$ complexes added in drinking water were reported to normalize the high blood glucose levels of STZ-rats, following useful studies of vanadyl complexes with the $VO(O_4)$ coordination mode in 1990 [192].

The anti-inflammatory activity of copper complexes of various ligands such as amino acids, anthranilic acids and of salicylic acid has been demonstrated [193]. These copper complexes are known to promote tissue repair. It has been found that the ligands, which may not be anti-inflammatory on their own, may well be effective forming copper complexes in vivo [194]. Intriguingly, copper devices such as bracelets, have been used for anti-inflammatory and anti-arthritic purposes and may serve as a source of copper taken into the body with cupriphores from sweat [195].

An intriguing aspect of the role of metal complexes in medicine is the role of nitric oxide (NO) [196, 197].The discovery of diverse biological roles for NO has stimulated and facilitated the development of NO targeted pharmaceuticals. Physiological processes mediated by NO include neurotransmission, blood pressure regulation and immunological responses. NO is an excellent ligand for metal ions, thus, metal nitrosyl complexes have therapeutic values. The nitroprusside ion, $[Fe(NO)(CN)_5]^{2-}$ is a vasodilator used in emergency situations to treat hypertensive patients in operating theatres [198, 199]. The complex is 30-100 more potent than simple nitrites. The mechanism is considered to be release of NO; an understanding prompted by the emergence of NO as a prominent cell signaling molecule [197].

Many of the well-known antibiotics viz: penicillin, streptomycin, bacitracin, tetracycline etc. are chelating agents and their action is improved by the presence of small amount of metal ion [200]. A couple of metal-based drugs have been developed in an attempt to address the spread of

resistance to the conventional anti-parasitic drugs such as chloroquine. One of the famous approaches is to complex metal ions to known anti-parasitic agents in attempts to gain selective uptake or selective action of the metal-drug conjugate. Gold and ruthenium complexes of chloroquine and chlortrimazole have been described [201-204]. In favourable cases, some of these complexes show good activity; the chloroquine complexes being useful even in chloroquine resistant cases.

1.9.0 Aim of the study

Ortho-hydroxyl Schiff bases have received overwhelming attention due to their fascinating chemistry. There is a great possibility of intramolecular hydrogen bonding, O-H----N-H, implying that they can exhibit circular dichroism. Likewise, they formed stable metal complexes readily with metal ions, especially, the transition metal series. In addition, reports have shown that ortho-hydroxyl Schiff bases do exhibit significant biological activity which often becomes enhanced upon chelation in some cases. Copper(II) ions on the other-hand is known to be involved in several copper proteins necessary for normal functioning of living systems, both in plants and animals. Also, the bactericidal action of copper(II) ions has been established since antiquity.

The aim of this study therefore was to synthesize copper(II) complexes of Schiff bases derived from *o*-hydroxybenzaldimine and its derivatives, and consequently evaluate the antimicrobial activity of the Schiff base ligands and the copper(II) complexes.

1.9.1 Scope of the study

Four different aldehydes were used for this study with a view to evaluate the effect of methoxyl group on the antimicrobial activity of the *o*-hydroxybenzaldimines. Thus, salicylaldehye, 3-methoxy-2-hydroxybenzaldehyde (*o*-vanillin), 4-methoxy-2-hydroxybenzaldehyde (*p*-vanillin) and 4-hydroxy-3-methoxybenzaldehyde (vanillin) were selected in order to consider the effect of having the methoxyl group at different positions on the aldehyde moiety of the Schiff base ligands. Likewise, the amines under study were of six different categories viz.: substituted anilines; 1-aminonaphthalene; aminopyridines; aminomethylpyridines; aminobenzimidazole and *o*-phenylenediamine amines.

In the substituted anilines group, the focus was to study the effect of different substituents of varying electronegativity at either the para or ortho position of the amino moiety of the Schiff base ligands. In the same vein, the influence of the fused ring system in aminonaphthalene was also considered with respect to the aniline-based Schiff base ligands. The aminopyridines and aminomethylpyridines are similar to pyridoxal phosphate (PLP), a co-factor of vitamin B6, which is involved in the metabolism of amino acids. The Schiff base ligands of these amines have equally be found to possess some biological activity, for instance, 2-aminopyridine Schiff base ligand of salicylaldehyde was found to possess anti-inflammatory activity. The interest in the benzimidazole derivative was borne on the fact that many antifungal drugs currently in the market have the imidazole or benzimidazole nucleus. Thus, the interest was to evaluate the synergistic effect of the azomethine group and the imidazole nucleus against the tested micro-organisms. Lastly, the condensation of *o*-phenylenediamine with ortho-hydroxybenzaldehyde yields symmetrical macrocyclic Schiff base ligand which imposes and stabilizes the geometrical configuration of metal ion in a chelate system.

1.9.2 Objectives

The objectives of the study are stated as follows:

- Synthesis of salicylaldehyde-based Schiff base ligands from salicylaldehyde and *p*-substituted anilines; *o*-substituted anilines; 1-aminonaphthalene; 2-aminopyridine; 3-aminopyridine; 2-aminomethylpyridine; 3-aminomethylpyridine or 2-aminobenzimidazole; as well as their copper(II) complexes.
- Synthesis of *o*-vanillin-based Schiff base ligands from 3-methoxy-2-hydroxybenzaldehyde (*o*-vanillin) and *p*-substituted anilines; *o*-substituted anilines; 1-aminonaphthalene; 2-aminopyridine; 3-aminopyridine; 2-aminomethylpyridine or 3-aminomethylpyridine; as well as their copper(II) complexes.
- Synthesis of *p*-vanillin-based Schiff base ligands from 4-methoxy-2-hydroxybenzaldehyde (*p*-vanillin) and *p*-substituted anilines; 1-aminonaphthalene; 2-aminopyridine; 3-aminopyridine; 2-aminomethylpyridine or 3-aminomethylpyridine or 1-aminonaphthalene; as well as their copper(II) complexes.

- Synthesis of vanillin-based Schiff base ligands from 3-methoxy-4-hydroxybenzaldehyde (vanillin) and *p*-substituted anilines; 1-aminonaphthalene; 2-aminopyridine; 3-aminopyridine; 2-aminomethylpyridine or 3-aminomethylpyridine or 1-aminonaphthalene as well as their copper(II) complexes.
- Synthesis of aminobenzimidazole-based Schiff base ligands derived from 2-aminobenzimidazole and salicylaldehyde, *o*-vanillin or *p*-vanillin; as well as their copper(II) complexes.
- Synthesis of *o*-phenylenediamine-based Schiff base ligand derived from *o*-phenylenediamine and *o*-vanillin or salicylaldehyde; as well as their copper(II) complexes.
- Evaluation of the Schiff base ligands and the copper(II) complexes for biological activity against two Gram positive and one Gram negative bacteria strains; as well as one fungal strain.

Though, the synthesis of some of the Schiff base ligands has been reported, the antimicrobial activity of their Cu(II) complexes is yet to be evaluated according to literature review. A summary of the previously reported Schiff bases, their complexes and antimicrobial activity with respect to this study is presented in scheme 1.4 below.

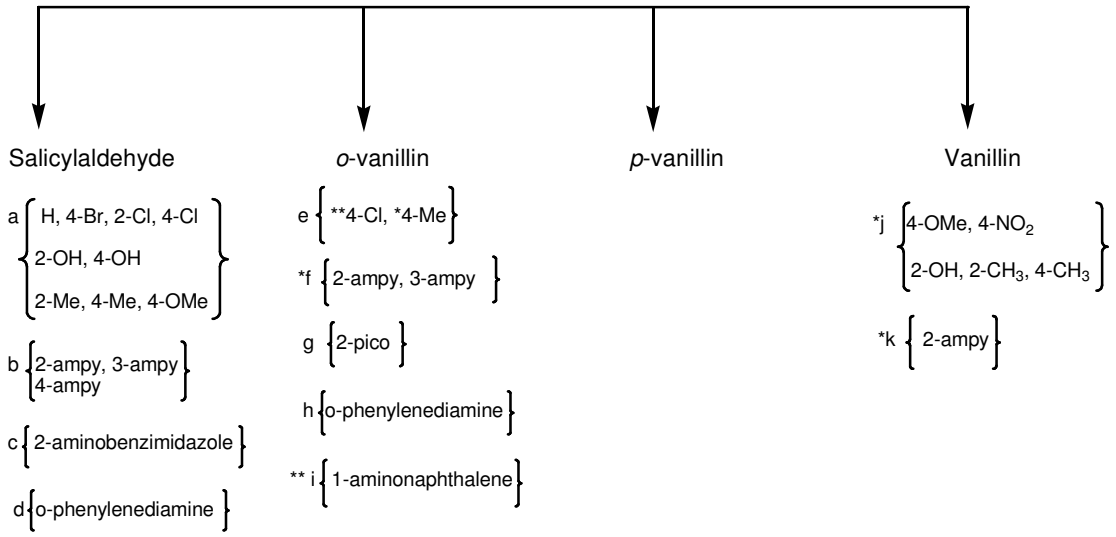

N.B: a: [12]; [101] b: [83, 117-119, 121]; c:[145]; d: [205] e: [108, 115]; f: [120]; g: [123]; h:[30]; i: [206]; j: [105, 109, 113]; k: [109]
*: Schiff bases only; **: antimicrobial study

Scheme 1.4: Summary of previous reports on Schiff bases, their Cu(II) complexes and antimicrobial activity relative to the current study

2.0.0 Physical Techniques

This chapter discusses the physical techniques that were used for elucidating the structures of the synthesized copper(II) complexes. The methods include:

UV/visible spectroscopy

Infrared spectroscopy

Conductivity measurement

X-ray crystallography

2.1.0 Ultraviolet and Visible spectroscopy

The visible and ultraviolet spectra of organic compounds are associated with transitions between electronic energy levels. The transitions are generally between a bonding or lone-pair orbital and an unfilled non-bonding or antibonding orbital [207]. The use of visible and ultraviolet spectroscopy to explain the structural aspects of chelates is a rather simple but powerful tool. The application of visible spectroscopy is limited to chelates of the transition metal ions, the lanthanides, and the actinides. Ultraviolet spectroscopy is more universal and can be useful in structural determinations of all chelates, since they all absorb in this region. In a typical transition metal chelate, the observed spectrum, in general, consists of a series of crystal field bands which are in the visible region and depend largely on the donor atom of the ligand and on the metal ion.

The crystal field transitions are of two types: the more intense spin-allowed transitions and the lower intensity spin-forbidden transition, which usually appear as shoulders on the spin allowed transitions.The ultrviolet spectrum is complicated and consists of electronic transitions between the ligand and the metal (charge transfer), and also transitions within the ligand itself which are usually $n \rightarrow \pi *$, $\pi \rightarrow \pi^{*}$or $\sigma \rightarrow \sigma^{*}$ transitions. The spectra of the non-transition metal ion chelates usually consist of the charge transfer and ligand transitions. The ligand transitions in all

cases are characteristic of the coordinated ligand and not of the free ligand; however, the spectrum of the free ligand aids in classifying the transitions of the coordinated ligand. The intensities of the crystal field transitions never exceeded a molar extinction coefficient of 500 ($\epsilon \leq 500$ mol^{-1} dm^3 cm^{-1}) whereas the charge transfer and ligand transitions in the ultraviolet usually exceed an extinction coefficient of 500 (≥ 500 mol^{-1} dm^3 cm^{-1}).

The visible spectra of transition metal ion chelates can be well understood and described quantitatively by crystal field theory or its extension, ligand field theory. These concepts are discussed extensively in common inorganic textbooks.

2.2.0 Infrared Spectroscopy

Vibrational spectra originate in the vibrations of the nuclei constituting a molecule, and are observed both as the infrared and the Raman spectra in the frequency region between approximately 10^4 cm^{-1} (1 μ) and 10 cm^{-1} (10^3 μ). The frequencies of the vibrational transitions are determined by the masses of constituent atoms, the molecular geometry (bond distances, bond angles, and angles of internal rotation), and the interatomic forces, whereas the intensities of infrared and Raman spectra are related to the changes in the dipole moment and polarizability, respectively, caused by molecular vibrations. Thus studies of vibrational spectra provide valuable information about molecular structure and chemical bonding.

Although, both infrared and Raman data are desirable, the lack of Raman data does not cause serious difficulty in vibrational analysis of metal chelate compounds, because, owing to the relatively low symmetry of these compounds, most vibrational transitions are allowed in the infrared spectrum [208].

For convenience, vibrational spectra of metal chelate compounds can be divided into the high frequency (4000-650 cm^{-1}) or mid-infrared region, and the low frequency (650-50 cm^{-1}) or far-infrared region. In general, vibrations which occur in the high frequency region originate in the ligand itself, whereas those in the low frequency region originate in the metal-ligand coordinate bonds. High frequency vibrations are ligand-sensitive and have already been the subject of a large number of studies. On the other hand, low frequency vibrations are metal-sensitive and

comparatively very little work has been done on them. This is because the spectra in the low frequency region are more difficult to interpret on an empirical basis than are those in the high frequency region.

Assignment of bands in the infrared spectra can be made either empirically or theoretically. The empirical method is simple and straight-forward, but its application is limited to a few well-known vibrations, and it often fail to give unambiguous band assignments even in the high frequency region. On the other hand, the theoretical method involves a tedious procedure of calculation, but leads to a quantitative description of each vibration in terms of the bond-stretching and angle bending coordinates chosen for the calculation.

The principle of the empirical method rests on the idea of "group vibrations" that is, the notion that the vibrations of a particular group in a molecule are relatively independent of those of the rest of the molecule. This idea is approximately correct if a group contains atoms which are relatively light, e.g. hydrogen, or relatively heavy, e.g. chlorine compared with the other atoms in the molecule. Such groups absorb in narrow frequency ranges regardless of the nature of the rest of the molecule.

2.2.1 Spectra and the strength of coordinate bonds

On coordination to a metal, the ligand bands are shifted to lower or higher frequencies with concomitant variation in intensity. In a series of metal complexes having the same structure, the magnitude of these band shifts becomes larger as the coordinate bond becomes stronger. It is therefore possible to determine the order of the strength of the coordinate bonds by comparing the magnitudes of the band shifts. A number of infrared studies have already been carried out to compare, on the basis of the band shifts observed, the strength of the coordinate bonds. However, there is a need for some caution in using this simple approach. Firstly, the direction of the band shift depends on the structure of the metal complex formed and secondly, the direction of the band shift also depends on the nature of the normal vibration and the effect of coordination on it.

It should be noted that the coordinate bond stretching bond vibrations, such as metal-nitrogen and metal-oxygen stretching modes which appear in the low frequency region, would be more

sensitive to the nature of the metal than the ligand vibrations in the high frequency region. These low frequency bands can only be fully assigned by carrying out a normal coordinate analysis of the whole chelate ring.

Several attempts have been made to establish a quantitative relationship between the band shift and the strength of the coordinate bond. For example, Bellamy and Branch [209] obtained a linear relationship from the plot of the C=O stretching against the stability constant ($\log k_1 k_2$) for a series of bis(salicylaldehydato) complexes of divalent metals. The C=O stretching band is shifted to lower frequency with increase in stability constant in the order of metals: Mg(II) < Zn(II) < Co(II) < Ni(II) < Cu(II) < Pd(II). This order is in perfect agreement with the well-known stability order of divalent metal complexes found by Mellor and Maley [210]; Mg(II) < Mn(II) < Cd(II) < Zn(II) < Co(II) < Ni(II) < Cu(II) < Pd(II). Sharma et al [211] also noted that a linear relationship holds between the stability constant and the N-H stretching frequency of bis(β-alanino) complexes of divalent metals; the N-H stretching frequency decreases linearly as the stability constant increases in the order Co(II) < Ni(II) < Cu(II) < Pd(II). This result was interpreted as an indication that the N-H bond is weakened as the metal -nitrogen bond is strengthened in this order of metals.

2.3.0 Conductivity measurements

Electrolytic conductivity is a measure of the ability of a solution to carry an electric current. Solutions of electrolyte conduct an electric current by the migration of ions under the influence of a potential gradient. The ions move at a rate dependent on their charge and size. Conductivity measurement gives an idea of the degree to which a substance is distorted in solution and consequently the number of species present in solution.

The electrical conductivity of a particular substance depends on a number of factors such as temperature and concentration. The unit of measurement commonly used is one millionth of a Siemen per centimeter (micro-Siemens per centimeter or μS/cm). However, when measuring more concentrated solutions, the units are expressed as milli-Siemens/cm (mS/cm) i.e. 10^{-3}.

2.3.1 Solvent considerations

For most purposes, the criteria most relevant to the selection of a solvent for conductivity determinations are its dielectric constant, viscousity, specific conductivity, ease of purification, and donor capacity towards metal ions. Some generally accepted values of the first three of these parameters for the commonly used organic solvents are presented in table 2.1 [212].

Table 2.1: Properties of non-aqueous solvents relative to their use for conductivity measurement

Solvent	**Dielectric constant**	**Viscousity ($g^{-1}. s^{-1}$)**	**Specific conductivity ($ohm^{-1}. cm^{-1}$)**
Acetone	20.7	0.295	5.8×10^{-8}
Nitromethane	35.9	0.595	6.56×10^{-7}
Nitrobenzene	34.8	1.634	9.1×10^{-7}
Methanol	32.6	0.545	1.5×10^{-9}
Ethanol	24.3	1.078	1.35×10^{-9}
Acetonitrile	36.2	0.325	5.9×10^{-8}
Dimethylformamide	36.7	0.796	$0.6 - 2.0 \times 10^{-7}$
Dimethylsulfoxide	46.6	1.96	3.0×10^{-8}
Pyridine	12.3	0.829	4.0×10^{-8}

In qualitative terms, a solvent with a high dielectric constant and low viscosity will be preferred for conductivity purposes, and on this basis; acetonitrile, nitromethane, and methanol may be selected as particularly useful. The use of both nitrobenzene and dimethylsulfoxide suffers from their high viscosity; there are, of course, other disadvantages, most notably the odour of nitrobenzene and the strong donor capacity of DMSO. Pyridine suffers from a low dielectric constant, unpleasant working effects, and strong donor properties; as a solvent for conductivity. Table 2.2 below lists the expected molar conductivity, $\Lambda_{M,}$ ranges for different electrolytes at 10^{-3} in the common organic solvents [212].

Table 2.2: Expected molar conductivity, $\Lambda_{M,}$ ranges for different electrolytes at 10^{-3} ($ohm^{-1}. cm^2. mol^{-1}$)

Solvent	**Electrolyte type**			
	1:1	**2:1**	**3:1**	**4:1**
Nitromethane	75-95	150-180	220-260	290-330
Nitrobenzene	20-30	50-60	70-82	90-100
Acetone	100-140	160-200	270?	380?
Acetonitrile	120-160	220-300	340-420	500?
Dimethylformamide	65-90	130-170	200-240	300?
Methanol	80-115	160-220	290-350	450?
Ethanol	35-45	70-90	120?	160?

2.4.0 X-ray crystallography

X-ray diffraction unlike the various spectroscopic techniques, gives detailed information about the whole molecular structure of a substance and in this case, metal chelates. Although, chemical methods of investigation leave no doubt about the existence of chelate rings and the general features of the structure of metal chelates, confirmation of the correctness of the structures by diffraction techniques has greatly strengthened our knowledge of chelation [213]. Such techniques have introduced a metrical element into the understanding of metal chelate rings by revealing the lengths of chemical bonds, the angles between them, and other structural details that could not be gained by purely chemical methods.

The determination of the precise location of all the atoms in the unit cell of a crystal by structural analysis provides the strongest and most detailed evidence for the existence of chelate rings. Moreover, the distance between the atoms of neighbouring molecules and ions can be measured with the same precision as those between the atoms in the molecule itself.

The quantitative knowledge of intermolecular distances gained in this way is of great importance, especially in structures involving special interactions, such as hydrogen bonds or

direct metal-metal interactions. If the wavelength of X-rays is properly chosen, it is possible to determine the absolute configuration of optically active complexes. The absolute configuration of one optically active complex determined by X-rays (in conjunction with rotatory dispersion studies) generally allows the configuration of many related coordination compounds to be settled with reasonable certainty.

The detailed theory and principles of X-ray diffraction is presented in many standard chemistry textbooks.

2.4.1 Limitations of the X-ray method

The scattering power of an atom depends on the number of its extranuclear electrons. It is difficult to locate accurately the positions of very light atoms in the presence of heavy atoms because their contribution to the diffracted beams is small. Thus in the presence of heavy central atoms it is not easy to ascertain the details of the chelate rings. Hydrogen atoms cannot be located accurately by X-rays except under favourable conditions. Their positions may, however, sometimes be inferred from considerations of symmetry from the distances between pairs of atoms between which the hydrogen atoms lie.

Also, it is difficult to distinguish between atoms of rather similar scattering power, for example, N and O, or to determine the state of ionization of atoms in a crystal. Finally, the shape and the size of molecules (or ions) in crystals are sometimes slightly different from those found in gases, liquids, or solution, because in crystals they are stabilized by specific intermolecular forces.

2.5.0 Linear Free Energy Relationships

The existence of a quantitative relationship between equilibrium constant and rate of a reaction was first observed by Bronsted and co-workers [214] in the study of reactions which show general acid-base catalysis. Linear free energy relationships are attempts to develop quantitative relationships between structure and activity. It allows a correlation of substituent with the rate of the reaction, biological activity, pKa, etc. In 1937, Hammett [215] described the influence of the meta- or para-substituents on the rate constants or equilibrium constants of the side chain reactions of substituted benzenes, based on the ionization of benzoic acid derivatives.

2.6.1 Hammett equation

Hammett equation relates reaction rates with acid dissociation constants

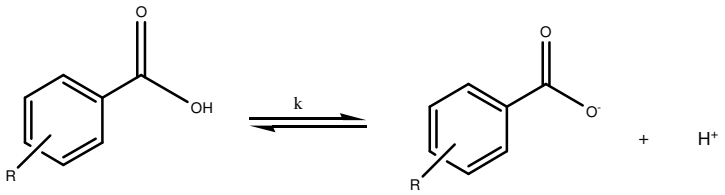

Fig. 2.1: Dissociation of benzoic acid

$$\log \frac{K}{K_\circ} = \rho\sigma \qquad 3.3$$

K is the reaction rate or equilibrium constant of ionization for a meta- or para-substituted benzoic acid; $K_\circ$ is the rate or equilibrium constant of ionization for unsubstituted benzoic acid in water at 25°C; σ is the substituent constant and ρ is the reaction constant. The substituent constant, σ, is a measure of the polar effect exerted by the substituent X, relative to no substituent, on the reaction centre, while the reaction constant, ρ, depends on the nature of the reaction, including conditions such as temperature. It measures the sensitivity of the reaction to the electronic effects of the substituents [216-218].

A positive σ value indicates that the substituent withdraws electrons relative to hydrogen; while substituents with negative σ values repel electrons relative to hydrogen. The effect of the substituent, X, in the meta-position on the aromatic ring is mostly inductive while the para substituents contribute both inductive and electronic effects. Hammett σ values, table 2.3, [215] indicate the combination of inductive (field) and mesomeric (resonance) effects produced by the electron withdrawing or donating substituent. The Hammett equation does not apply to ortho-substituted benzene derivatives, since the ortho substituents can give rise to steric interactions which may make the relationships unreliable.

Though, the Hammett methodology was a success in studying and describing the influence of structure on chemical behaviour, it failed to give values for some substituents that show strong interaction between the substituent and the reaction site, such as NO_2 and OH.

Table 2.3: Hammett substituent constants

Substituent-X	σ_p	σ_m
$-NH_2$	-0.66	-0.161
$-OCH_3$	-0.268	+0.115
$-OC_2H_5$	-0.25	+0.15
$-(CH3)_2NH_2$	-0.205	-0.211
$-CH_3$	-0.170	-0.069
H	0	0
-F	+0.062	+0.337
-Cl	+0.227	+0.373
-Br	+0.232	+0.393
-I	+0.276	+0.353
$-NO_2$	+0.778	+0.710
-CN	+1.000	+0.678

Jaffe re-calculated Hammett's substituent constants values using more recent values for ionization or equilibrium constants obtained for a wide series of reactions. McDaniel and Brown [219] re-defined σ_m and σ_p values for the ionization of substituted benzoic acids and suggested that these values be used for substituent constants rather than the mean values obtained from all available reactions. Taft and Lewis [220, 221] suggested that the resultant polar effects of substituents on chemical reactivities and physical properties should be quantitatively separated into inductive and resonance effects. Taff's equation is an extension of the Hammett equation, as shown in equation 2.

$$\log\frac{K}{K_\circ} = \rho_I\sigma_I + \rho_R\sigma_R \qquad 3.4$$

σ_I is the inductive effect and it is assumed to contribute a similar effect for the meta- and para-position. The resonance effect is denoted by σ_R and the contribution for meta- is different from

that of para-position. ρ_I and $\rho_R$are the contributions to the reaction constant due to the substituents.

Infrared and nuclear magnetic resonance spectroscopy have been used to establish a correlation between Hammett's substituent constant and electronic effects of substituents in substituted aromatic, heterocyclic and aliphatic compounds. Baker and Shulgin [13] obtained a qualitative linear relationship between the basicity of donor atoms and the energy of hydrogen bond from a plot of σ against ν_{OH} shift values. The downward deshielding effect of substituents in some N-arylsalicylaldimines has also been studied by plotting the chemical shift values of the hydroxyl proton, OH, against the Hammet substituent parameters [101]. Percy and Thornton equally obtained a correlation between substituent constants σ or σ^* and ν_{M-L} in metal(II) salicylaldimine complexes [101].

3.0.0 Experimental

All reagents and chemicals obtained from Sigma-Aldrich or Merck were of AnalaR grade and used without further purification. Chemicals and solvents used for the synthesis of Schiff base ligands and metal complexes are: salicylaldehyde, 3-methoxy-2-hydroxybenzaldehyde (*o*-vanillin), 4-methoxy-2-hydroxybenzaldehyde (*p*-vanillin), 4-hydroxy-3-methoxybenzaldehyde (vanillin), aniline, 4-chloroaniline, 4-bromoaniline, 4-methylaniline (*p*-toluidine), 4-methoxyaniline (*p*-anisidine), 4-nitroaniline (*p*-nitraniline), 4-hydroxyaniline, 2-chloroaniline, 2-bromoaniline, 2-methylaniline (*p*-toluidine), 2-methoxyaniline (*p*-anisidine), 2-hydroxyaniline, 1-aminonaphthalene, 2-aminopyridine, 3-aminopyridine, 2-aminomethylpyridine, 3-aminomethylpyridine, 2-aminobenzimidazole, *o*-phenylenediamine, absolute ethanol, petroleum ether (60-80 $^{\circ}$C), dimethylformamide, deuterated chloroform (d_1) and deuterated dimethylsufoxide (d_6).

3.1.0 Physical and analytical methods

The Schiff bases and the copper(II) complexes prepared in this study have been characterized by the combination of elemental analysis and spectral (infrared and electronic). In addition, the nuclear magnetic resonance, ^{1}H- and ^{13}C- NMR, study of the Schiff base ligands was conducted to confirm their structures. The Raman spectral study of the ligands was conducted to complement the infrared spectral data. Likewise, the conductivity measurement of the complexes was done to substantiate the proposed structures for the complexes. Lastly, the structures and geometry of some of the complexes were unequivocally established with X-ray single crystal diffraction.

3.1.1 Nuclear magnetic resonance spectroscopy (NMR)

The ^{1}H- and ^{13}C- NMR spectra were recorded on a Bruker Avance 400MHz NMR spectrometer in deuterated chloroform (d_1) or deuterated dimethylsulfoxide (d_6) with tetramethylsilane

($SiMe_4$) as internal standard. All spectra were recorded at ambient temperature and the chemical shifts were measured in parts per million (ppm) downfield to the reference signal.

3.1.2 Mid-infrared spectroscopy (MIR)

Mid-infrared spectra were recorded on a Perkin-Elmer Spectrum 100 FT-IR spectrometer in the region 4000-700 cm^{-1} with 4 scans at an average resolution of 8 cm^{-1}. The spectrometer was equipped with universal attenuated total reflectance (ATR) accessory, thus no sample preparation was required.

3.1.3 Far-infrared spectroscopy (FIR)

Far infrared spectra were recorded on a Perkin-Elmer Spectrum 400 FT-IR spectrometer in the region 700-30 cm^{-1} with 128 scans at an average resolution of 8 cm^{-1}. The samples were run as mulls in Nujol on polyethylene windows.

3.1.4 Raman spectroscopy

The Raman spectra for the Schiff base ligands were recorded on a Bruker Vertex 70 RAM 11 spectrophotometer using a 1064 nm Nd-YAG laser. The samples were run in solid state. Efforts to obtain the Raman spectra for the complexes were not successful due to fluorescence experienced with the 1064 nm laser (Nd-YAG) even when diluted with spectroscopic KBr.

3.1.5 UV/Visible spectroscopy

The UV/Visible spectra were obtained from Perkin Elmer Lambda 25 spectrophotometer. The Schiff base ligands were dissolved in methanol and dimethylformamide (DMF) to a concentration of approximately 2.0 x 10^{-5} M while the complexes spectra were recorded at 2.0 x10^{-3} M in methanol or DMF.

3.1.6 Microanalysis

Carbon, hydrogen and nitrogen combustion microanalysis was carried out on a Vario MICRO V1.6.2 elemental analysen systeme GmbH.

3.1.7 Metal analysis (AAS)

The percentage copper composition in the prepared complexes was evaluated using Perkin Elmer A Analyst 200 atomic absorption spectrometer. A known quantity of the Cu(II) complexes was digested using aqua regia (HNO_3/HCl) with a few drops of concentrated H_2SO_4.

3.1.8 Molar conductivity

Molar conductivity measurement for the complexes was done in methanol or dimethylformamide (DMF), depending on solubility of the complexes, using Az® 86555 pH/mV/Cond./TDS/Temp apparatus at a concentration of 1 x 10^{-3} M.

3.1.9 Melting point

The melting points of the compounds were determined using Galenkemp melting point apparatus. The values were uncorrected.

3.1.10 X-ray diffraction

Single crystals suitable for X-ray diffraction were obtained via slow evaporation of the saturated solution of the compounds in DMF or CH_2Cl_2/MeOH solvent system. [Cu(ovan-2-pico)Cl] crystals were grown as green needle-like crystals in CH_2Cl_2/MeOH (1:1) while the crystals of [Cu(ovan-$NH_3)_2$].H_2O, [Cu(bis-salphen)] and [Cu(bis-ovanphen)(H_2O)] were obtained as shining brown crystals in DMF.

The single crystal X-ray diffraction was done at Nelson Mandela Metropolitan University, Port Elizabeth, South Africa by Dr Van Brecht Bernadus. The data was collected using a Bruker KAPPA APEX II single crystal X-ray diffractometer, with a 4-circle Kappa goniometer and sensitive CCD detector. The instrument used a Molybdenum fine focus sealed X-ray tube as an X-ray source and an Oxford Cryostream 700 system for sample temperature control. Bruker's APEX2 software was used for instrument control.

3.2.0 Synthesis of the ligands

The Schiff base ligands were synthesized according to the general synthetic procedures in the literature [81-84, 128, 222]. Absolute ethanol was used as solvent for most of the synthesis. The ligands were prepared by condensing the aldehydes with the respective amines in a ratio 1:1.

3.2.1 Salicylaldehyde-based ligands

A hot 10 mmol (1.07 mL) of salicylaldehyde in 10 mL ethanol was mixed with 10 mmol (0.91 mL) of aniline in 10 mL ethanol. The resulting yellow solution was refluxed for 2 hr in a 100 mL round bottom flask equipped with an air-cooled condenser to obtain a yellow precipitate. The precipitate was filtered under suction, washed with ethanol and recrystallized from ethanol. It was dried over silica gel. The same procedure was repeated for all the *p*-substituted and *o*-substituted anilines; 1-aminonaphthalene; 2- and 3-aminopyridine as well as the 2- and 3-aminomethylpyridine analogues. It should be noted that the 1-aminonaphthalene derivative did not form readily and likewise, the 2-aminomethylpyridine and *o*-nitroaniline derivative could not be isolated. The proposed structures for all the members of this series are given in figures 3.1-3.3, while the names are presented in tables 3.1-3.3.

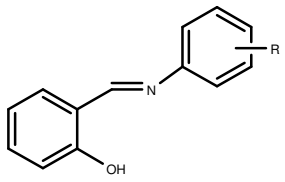

Fig. 3.1: Substituted aniline-based ligands(1)

Table 3.1: Salicylaldehyde-based substituted aniline ligands

No.	Ligand	IUPAC name	-R
1	salaani	(E)-2-((phenylimino)methyl)phenol	H
2	sal-4-cla	(E)-2-((4-chloro-phenylimino)methyl)phenol	4-Cl
3	sal-4-bra	(E)-2-((4-bromo-phenylimino)methyl)phenol	4-Br
4	sal-4-tol	(E)-2-((4-methyl-phenylimino)methyl)phenol	4-CH_3
5	sal-4-nis	(E)-2-((4-methoxy-phenylimino)methyl)phenol	4-OCH_3

6	sal-4-nit	(E)-2-((4-nitro-phenylimino)methyl)phenol	4-NO_2
7	sal-4-phen	(E)-2-((4-hydroxyl-phenylimino)methyl)phenol	4-OH
8	sal-2-cla	(E)-2-((2-chloro-phenylimino)methyl)phenol	2-Cl
9	sal-2-bra	(E)-2-((4-bromo-phenylimino)methyl)phenol	2-Br
10	sal-2-tol	(E)-2-((2-methyl-phenylimino)methyl)phenol	2-CH_3
11	sal-2-nis	(E)-2-((2-methoxy-phenylimino)methyl)phenol	2-CH_3
12	sal-2-phen	(E)-2-((2-hydroxyl-phenylimino)methyl)phenol	2-OH

Table 3.2: Salicylaldehyde-based 1-aminonaphthalene ligand

No.	Ligand	IUPAC name	Structure
13	sal-1-amnaph	(E)-2-((naphthalen-1-yl)methyl)phenol	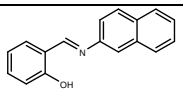

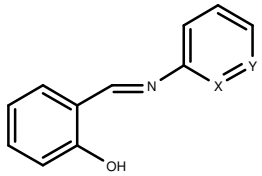

Fig. 3.2: Aminopyridine-based ligands(1)

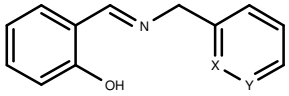

Fig. 3.3: Aminomethylpyridine-based ligands(1)

Table 3.3: Salicylaldehyde-based aminopyridine & aminomethylpyridine ligands

No.	Ligand	IUPAC name	X; Y
14	sal-3-ampy	(E)-2-((pyridin-3-ylimino)methyl)phenol	H; N
15	sal-3-pico	(E)-2-((pyridin-3-ylmethylimino)methyl)phenol	H; N

3.2.2 *o*-vanillin-based ligands

10 mmol (1.522 g) of 3-methoxyl-2-hydroxylbenzaldehyde (*o*-vanillin) was dissolved in 10 mL ethanol on heating. The hot solution was mixed with equimolar 10 mL ethanolic solution of aniline in a 100 mL round bottom flask equipped with an air-cooled condenser. The mixture was refluxed for 2 hr to obtain an orange solution. It was allowed to cool to room temperature and the volume was reduced using rotar vapour to obtain an orange precipitate. The precipitate was filtered under suction, washed with ethanol and recrystallized from ethanol. It was dried over silica gel. The same procedure was repeated for all the *p*-substituted and *o*-substituted anilines; 1-aminonaphthalene; 2- and 3-aminopyridine as well as the 2- and 3-aminomethylpyridine analogues. All attempts made at synthesizing *o*-nitroaniline and 3-aminomethylpyridine derivatives were not successful. The members of this series are typified in figures 3.4-3.6 and the names are listed in tables 3.4-3.6.

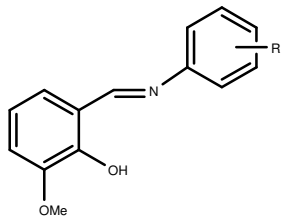

Fig. 3.4: Substituted aniline-based ligands (2)

Table 3.4: *o*-vanillin-based substituted aniline ligands

No.	Ligand	IUPAC name	-R
16	Ovaani	(E)-2-methoxy-6-((phenylimino)methyl)phenol	H
17	ovan-4-cla	(E)-2-methoxy-6-((4-chloro-phenylimino)methyl)phenol	4-Cl
18	ovan-4-bra	(E)-2-methoxy-6-((4-bromo-phenylimino)methyl)phenol	4-Br
19	ovan-4-tol	(E)-2-methoxy-6-((4-methyl-phenylimino)methyl)phenol	4-CH_3
20	ovan-4-nis	(E)-2-methoxy-6-((4-methoxy-phenylimino)methyl)phenol	4-OCH_3
21	ovan-4-nit	(E)-2-methoxy-6-((4-nitro-phenylimino)methyl)phenol	4-NO_2
22	ovan-4-phen	(E)-2-methoxy-6-((4-hydroxyl-phenylimino)methyl)phenol	4-OH

23	ovan-2-cla	(E)-2-methoxy-6-((2-chloro-phenylimino)methyl)phenol	2-Cla
24	ovan-2-bra	(E)-2-methoxy-6-((2-bromo-phenylimino)methyl)phenol	2-Bra
25	ovan-2-tol	(E)-2-methoxy-6-((2-methyl-phenylimino)methyl)phenol	2-CH_3
26	ovan-2-nis	(E)-2-methoxy-6-((2-methoxy-phenylimino)methyl)phenol	2-OCH_3
27	ovan-2-phen	(E)-2-methoxy-6-((2-hydroxyl-phenylimino)methyl)phenol	2-OH

Table 3.5: *o*-vanillin-based 1-aminonaphthalene ligand

No.	Ligand	IUPAC name	Structure
28	ovan-1-amnaph	(E)-2-methoxy-6-((naphthalen-1-yl)methyl)phenol	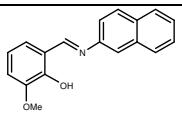

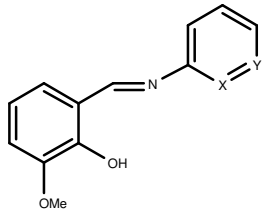

Fig. 3.5: Aminopyridine-based ligands (2)

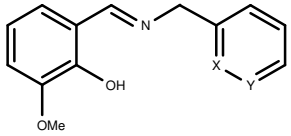

Fig. 3.6: Aminomethylpyridine-based ligands (2)

Table 3.6: *o*-vanillin-based aminopyridine & aminomethylpyridine ligands

No.	Ligand	IUPAC name	X; Y
29	ovan-2-ampy	(E)-2-methoxy-6-((pyridin-2-ylimino)methyl)phenol	N; H
30	ovan-3-ampy	(E)-2-methoxy-6-((pyridin-3-ylimino)methyl)phenol	H; N
31	ovan-2-pico	(E)-2-methoxy-6-((pyridin-2-ylmethylimino)methyl)phenol	N; H

3.2.3 *p*-vanillin-based ligands

10 mmol (1.522 g) of 4-methoxyl-2-hydroxylbenzaldehyde (*p*-vanillin) was dissolved in 10 mL ethanol on heating. The hot solution was mixed with equimolar 10 mL ethanolic solution of

aniline in a 100 mL round bottom flask equipped with an air-cooled condenser. The mixture was refluxed for 2 hr to obtain an orange solution. It was allowed to cool to room temperature and the volume was reduced using rotar vapour to obtain a yellow precipitate. The precipitate was filtered under suction, washed with ethanol and recrystallized from ethanol. It was dried over silica gel. The same procedure was repeated for all the *p*-substituted and *o*-substituted anilines; 1-aminonaphthalene; 2- and 3-aminomethylpyridine as well as the 2- and 3-aminomethylpyridine analogues. The *o*-anisidine, *o*-nitroaniline, 2-aminopyridine, as well as 2- and 3-aminomethylpyridine derivatives could not be isolated. The proposed structures for this series are typified in figures 3.7-3.9 while the names are listed in tables 3.7-3.9.

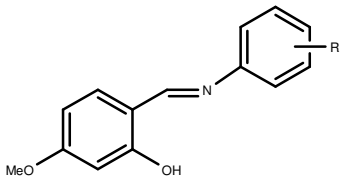

Fig. 3.7: Substituted aniline-based ligands(3)

Table 3.7: *p*-vanillin-based substituted aniline ligands

No.	**Ligand**	**IUPAC name**	**R**
32	pvaani	(E)-5-methoxy-2-((phenylimino)methyl)phenol	-H
33	pvan-4-cla	(E)-5-methoxy-2-((4-chloro-phenylimino)methyl)phenol	4-Cl
34	pvan-4-bra	(E)-5-methoxy-2-((4-bromo-phenylimino)methyl)phenol	4-Br
35	pvan-4-tol	(E)-5-methoxy-2-((4-methyl-phenylimino)methyl)phenol	4-CH_3
36	pvan-4-nis	(E)-5-methoxy-2-((4-methoxy-phenylimino)methyl)phenol	4-OCH_3
37	pvan-4-nit	(E)-5-methoxy-2-((4-nitro-phenylimino)methyl)phenol	4-NO_2
38	pvan-4-phen	(E)-5-methoxy-2-((4-hydroxyl-phenylimino)methyl)phenol	4-OH
39	pvan-2-cla	(E)-5-methoxy-2-((2-chloro-phenylimino)methyl)phenol	2-Cl
40	pvan-2-bra	(E)-5-methoxy-2-((2-bromo-phenylimino)methyl)phenol	2-Br
41	pvan-2-tol	(E)-5-methoxy-2-((2-methyl-phenylimino)methyl)phenol	2-CH_3
42	pvan-2-phen	(E)-5-methoxy-2-((2-hydroxyl-phenylimino)methyl)phenol	2-OH

Table 3.8: *p*-vanillin-based 1-aminonaphthalene ligand

No.	Ligand	IUPAC name	Structure
43	pvan-1-amnaph	(E)-5-methoxy-2-((naphthalen-1-ylimino)methyl)phenol	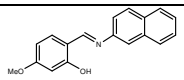

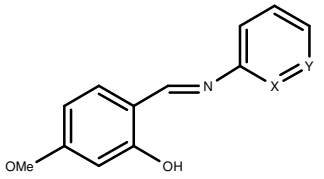

Fig. 3.8: Aminopyridine-based ligands (3)

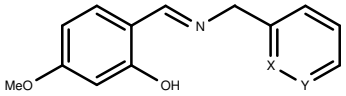

Fig. 3.9: Aminomethylpyridine-based ligands(3)

Table 3.9: *p*-vanillin-based aminopyridine & aminomethylpyridine ligand

No.	Ligand	IUPAC name	X; Y
44	pvan-3-ampy	(E)-2-methoxy-6-((pyridin-3-ylimino)methyl)phenol	H; N

3.2.4 Vanillin-based ligands

10 mmol (1.522 g) of 3-methoxyl-4-hydroxylbenzaldehyde (vanillin) was dissolved in 10 mL ethanol on heating. The hot solution was mixed with equimolar 10 mL ethanolic solution of aniline in a 100 mL round bottom flask equipped with an air-cooled condenser. The mixture was refluxed for 2 hr to obtain a brown solution. The volume was reduced using rotar vapour and consequently treated with petroleum ether to obtain a cream precipitate. The precipitate was filtered under suction, washed with ethanol and recrystallized from ethanol. It was dried over silica gel. The same procedure was repeated for all the *p*-substituted and *o*-substituted anilines; 1-aminonaphthalene; 2- and 3-aminomethylpyridine as well as the 2- and 3-aminomethylpyridine analogues. The 2-aminopyridine, 2-aminomethylpyridine and all the o-substituted analogues could not be isolated. The proposed structures for this series are typified in figures 3.10-3.12 while the names are listed in tables 3.10-3.12.

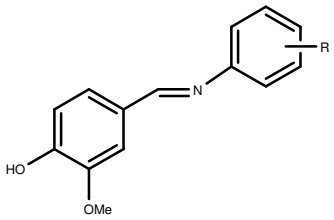

Fig. 3.10: Substituted aniline-based ligands (4)

Table 3.10: Vanillin-based substituted aniline ligands

No.	**Ligand**	**IUPAC name**	**-R**
45	vaani	(E)-2-methoxy-4-((phenylimino)methyl)phenol	-H
46	van-4-cla	(E)-2-methoxy-4-((4-chloro-phenylimino)methyl)phenol	4-Cl
47	van-4-bra	(E)-2-methoxy-4-((4-bromo-phenylimino)methyl)phenol	4-Br
48	van-4-tol	(E)-2-methoxy-4-((4-methyl-phenylimino)methyl)phenol	4-CH_3
49	van-4-nis	(E)-2-methoxy-4-((4-methoxy-phenylimino)methyl)phenol	4-OCH_3
50	van-4-phen	(E)-2-methoxy-4-((4-hydroxyl-phenylimino)methyl)phenol	4-OH

Table 3.11: Vanillin-based 1-aminonaphthalene ligand

No.	**Ligand**	**IUPAC name**	**Structure**
51	van-1-amanph	(E)-2-methoxy-4-((naphthalen-1-ylimino)methyl)phenol	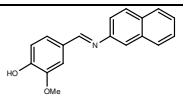

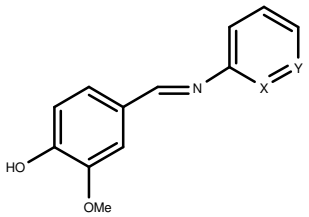

Fig. 3.11: Aminopyridine-based ligands (4)

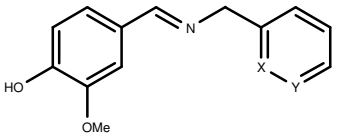

Fig. 3.12: Aminomethylpyridine-based ligands (4)

Table 3.12: Vanillin-based aminopyridine & aminomethylpyridine ligands

No.	Ligand	IUPAC name	X; Y
52	van-3-ampy	(E)-2-methoxy-2-((pyridin-3-ylimino)methyl)phenol	H; N
53	Van-3-pico	(E)-2-methoxy-2-((pyridin-2-ylmethylimino)methyl)phenol	H; N

3.2.5 2-aminobenzimidazole-based ligands

1.332 g (10 mmol) of 2-aminobenzimidazole was dissolved in 10 mL ethanol on heating. The hot solution was refluxed with equimolar 10 mL ethanolic solution of salicylaldehyde for 12 hr. The resulting solution was allowed to cool to room temperature and the volume was reduced using rotar vapour to obtain a yellow precipitate. The precipitate was filtered under suction, washed with ethanol and recrystallized from ethanol. It was dried over silica gel. The same procedure was repeated for the *o*-vanillin and *p*-vanillin analogues. All the members of this series are listed in table 3.13.

Table 3.13: 2-Aminobenzimidazole-based ligands

No.	Ligand	IUPAC name	Structure
54	sal-AmBZI	2-((2-benzimidazoylimino)methyl)phenol	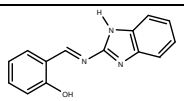
55	ovan-AmBZI	2-methoxy-6-((2-benzimidazoylimino)methyl)phenol	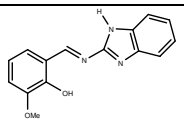
56	pvan-AmBZI	5-methoxy-2-((2-benzimidazoylimino)methyl)phenol)	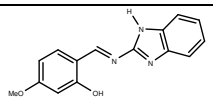

3.2.6 *o*-phenylenediamine-based ligands

10 mmol (1.522 g) of *o*-vanillin was dissolved in 10 mL ethanol and mixed with 10 mL ethanolic solution of *o*-phenylenediamine (5 mmol, 0.542 g) in a 100 mL round bottom flask. The resulting mixture was refluxed for 2hr to obtain some red precipitates. The precipitate was filtered under

suction, washed with ethanol and recrystallized from ethanol. It was dried over silical gel. The same procedure was employed for the salicylaldehyde analogue of the Schiff base ligand. Figure 3.13 below represents the synthesized ligands while the names are given in table 3.14.

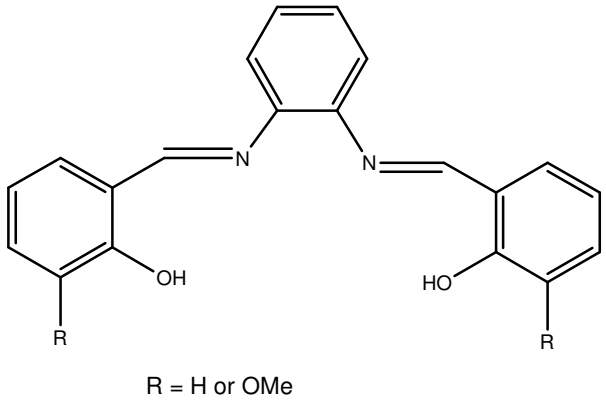

Fig. 3.13: o-phenylenediamine-based ligands

Table 3.14: *o*-phenylenediamine-based ligands

No.	**Ligand**	**IUPAC name**
L57	Bis-salphen	N, N'-bis(2-hydroxybenzalidene)-*o*-phenylenediamine
L58	Bis-ovanphen	N, N'-bis(3-methoxy-(2hydroxybenzalidene))-*o*-phenylenediamine

The Schiff base ligands are grouped into four major categories based on the type of aldehyde used for the synthesis. They include:

- salicylaldehyde-based ligands
- *o*-vanillin-based ligands
- *p*-vanillin-based ligands
- vanillin-based ligands

They are however, further sub-divided into six groups according to the nature of the amino moiety on the Schiff base ligands. Thus, we have the following groups:

- substituted aniline-based ligands
- 1-aminonaphthalene-based ligands
- aminopyridine-based ligands
- aminomethylpyridine-based ligands
- 2-aminobenzimidazole-based ligands
- *o*-phenylenediamine-based ligands

A total of 58 ligands were isolated all together and were consequently reacted with Cu(II) salt to prepare the corresponding metal complexes.

3.3.0 Synthesis of the complexes

The usual methods for preparation of metal-chelate complexes with an MN_2O_2 or MN, coordination sphere include (a) direct interaction of the Schiff base with the metal salts, (b) template condensation of aldehydes (ketones), primary amines and metal salts and (c) reaction of aldehydato complexes with amines [223]. The first method was employed for all the complexes isolated in this study except for [Cu(bis-salphen)] and [Cu(bis-ovanphen)] which were synthesized via the template route. Copper(II) chloride dihydrate ($CuCl_2.2H_2O$) and copper(II) acetate monohydrate, $Cu(CH_3COO)_2.H_2O$ were used for the synthesis. The general method employed for the synthesis of the complexes is highlighted below and the list of all the synthesized complexes is presented in table 3.14.

3.3.1 Method 1

Hot ethanolic solution of $CuCl_2.2H_2O$ was gradually added to a hot ethanolic solution of the ligand in a ratio 1:2 to obtain complexes of the forms ML_2. The resulting solution was stirred for 30 minutes with slight heating. Diethyl ether was used to induce precipitation in cases where the

precipitate did not form on stirring. The precipitate was filtered under suction, washed with ethanol and dried in a vacuum desiccator over silica gel. However, the elemental analysis results indicated that the isolated complexes were either $M(LH)_2Cl_2.xH_2O$ or $MLCl_x.xH_2O$. The complexes have been characterized by conductivity values as well as infrared and electronic spectral data. In addition, the structure of Cu(II) complex of ovan-2-pico Schiff base ligand was further confirmed by X-ray single crystal structure.

3.3.2 Method 2

0.114 g (0.573 mmol) of copper acetate monohydrate, $Cu(CH_3COO)_2.H_2O$, was dissolved in 10 mL ethanol and added drop-wisely to a vigorously stirring ethanolic solution of sal-2-cla, 0.30 g (1.15 mmole). The resulting solution was refluxed for 6 hr to obtain a brown precipitate. It was filtered under suction, washed thoroughly with ethanol and dried over silical gel in a desiccator. The procedure was repeated for all the other complexes. The elemental analysis results suggested complexes of the form ML_2 or ML and the complexes were further characterized by conductivity values as well as infrared and electronic spectral data.

3.3.3 Method 3

The procedure used here was the same as the second method with the exception that aqueous ammonia was used to precipitate the Cu(II) complexes from solution.

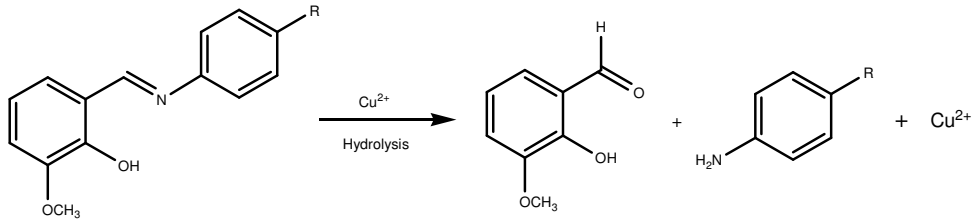

R = CH_3 or OCH_3

Scheme 3.1: Hydrolysis of the Schiff base ligands by Cu^{2+}

It is necessary to state that the introduction of the Cu(II) ions into the Schiff base system resulted in the hydrolysis of the imine bond in each case, scheme 3.1. It is assumed that the aldehyde moiety of the ligand reacted with aqueous ammonia to form a new imine bond. The Cu(II) complexes resulted from the Schiff base ligand is shown in scheme 3.2, and the structures have been confirmed with conductivity values, infrared and electronic spectral data, as well as X-ray single crystal structure.

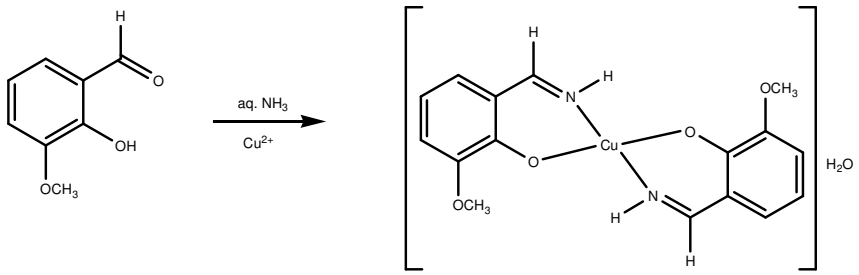

Scheme 3.2: Formation of Cu(II) complex from the hydrolysed Schiff base

3.3.4 Method 4

The synthesis of the copper(II) complexes of *o*-phenylenediamine-based ligand was achieved using template method as typified in scheme 3.3.

The resulting complex was of the form $[Cu(L)(H_2O)_x]$. 10 mL ethanolic solution of *o*-vanillin (5 mmol 0.761 g) was mixed with 10 mL ethanolic solution of *o*-phenylenediamine (2.5 mmol, 0.270 g) in a round bottom flask and refluxed for one hour to obtain an orange solution. Thereafter, 0.4262 g (2.50 mmol) of $CuCl_2.2H_2O$ was dissolved in 5 mL ethanol and added dropwisely to the ligand solution. The resulting solution was refluxed for another one hour to obtain some brown precipitates. The precipitates was filtered under suction, washed with ethanol and dried over silical gel. Single crystals suitable for X-ray diffraction were obtained from slow evaporation of the saturated solution of the complex in DMF.

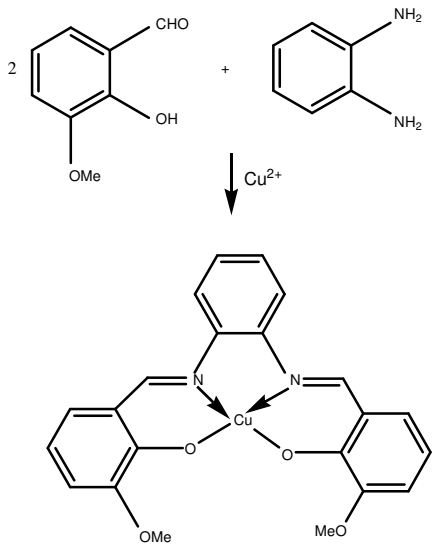

Scheme 3.3: Synthesis of [Cu(ovan-phen)(H_2O)]

Table 3.14: List of the isolated complexes

No.	**$Cu(LH)_2Cl_2.xH_2O$**	**[Cu(LH)Cl(H_2O)]Cl & [CuLCl]**	**$[CuL_2]$**	**$[Cu_2L_2]$**	**[CuL(H_2O)x]**
1	$Cu(salaani)_2Cl_2.2½H_2O$	$Cu(ovan\text{-}2\text{-}ampy)Cl_2.H_2O$	$Cu(sal\text{-}2\text{-}cla)_2$	Cu(sal-2-phen)	Cu(bis-salphen)
2	$Cu(sal\text{-}4\text{-}cla)_2Cl_2.2H_2O$	Cu(ovan-2-pico)Cl	$Cu(sal\text{-}2\text{-}bra)_2$	Cu(ovan-2-phen)	Cu(bis-ovanphen)(H_2O)
3	$Cu(sal\text{-}4\text{-}bra)_2Cl_2.H_2O$		$Cu(sal\text{-}2\text{-}tol)_2$	Cu(pvan-2-phen)	
4	$Cu(sal\text{-}4\text{-}tol)_2Cl_2.H_2O$		$Cu(sal\text{-}2\text{-}nit)_2$		
5	$Cu(ovaani)_2Cl_2.H_2O.½2EtOH$		$Cu(sal\text{-}2\text{-}nis)_2$		
6	$Cu(Ovan\text{-}4\text{-}bra)_2Cl_2.H_2O$		$Cu(sal\text{-}1\text{-}amnaph)_2$		
7	$Cu(ovan\text{-}4\text{-}tol)_2Cl_2.2½H_2O$		$Cu(ovan\text{-}2\text{-}cla)_2$		
8	$Cu(ovan\text{-}4\text{-}phen)Cl_2.H_2O$		$Cu(ovan\text{-}2\text{-}bra)_2$		
9	$Cu(sal\text{-}2\text{-}ampy)_2Cl_2$		*$Cu(ovan\text{-}NH)_2$		
10	$Cu(sal\text{-}3\text{-}ampy)_2Cl_2..½2H_2O$		$Cu(Ovan\text{-}4\text{-}nit)_2.2EtOH$		
11	$Cu(ovan\text{-}3\text{-}ampy)_2Cl_2$		$Cu(ovan\text{-}1\text{-}amanph)_2$		
12	$Cu(sal\text{-}3\text{-}pico)_2Cl_2.½2H_2O$				

*$Cu(ovan\text{-}NH)_2.H_2O$ was prepared from the hydrolysed Schiff base ligands using aqueous ammonia

It should be noted that, though, the synthesis of all the Schiff bases was attempted, only the complexes of the salicylaldehyde and *o*-vanillin based ligands are reported. This is because, the elemental analysis results of the *p*-vanillin and vanillin-based complexes remained unresolved. The difficulty in resolving the microanalysis results for the complexes can be attributed to the possibility of hydrolysis of the imine bond in the presence of copper(II) ions in which variety of mixed products are isolated.

Mahon et al. [107] has reported the hydrolysis and in some cases the decomposition of some Schiff base ligands in the presence of Cu(II), Ni(II) and Zn(II) ions. This was also evident from the crystal structure obtained from the synthesis of the Cu(II) complexes using, ovan-2-tol, ovan-4-tol and ovan-4-nis. The microanalysis results of Cu(II) complexes prepared from ovan-2-tol, ovan-2-nis and ovan-4-tol were initially ambiguous until the crystal structure was obtained, indicating the hydrolysis of the imine bond as shown in scheme 3.3.0 and 3.3.1 above.

4.0.0 Results

4.1.0 Physical and analytical data for the ligands

4.1.1 Aniline and substituted aniline ligands

Table 4.1: Physical and analytical data for the aniline-based ligands

No.	Ligand	Colour	%Yield	M.Pt (°C)	Molar mass	Molecular Formula	%Found (Calculated)		
							C	H	N
L1	salaani	Yellow	84	42-43	197.25	$C_{13}H_{11}NO$	79.34 (79.09)	5.73 (5.58)	7.13 (7.10)
L16	ovaani	Orange	85	78-80	227.28	$C_{14}H_{13}NO_2$	74.55 (73.98)	5.84 (5.77)	6.19 (6.16)
L32	pvaani	Yellow	45	60-62	227.28	$C_{14}H_{13}NO_2$	73.17 (73.98)	5.66 (5.77)	6.01 (6.16)
L45	vaani	Cream	63	149-150	227.28	$C_{14}H_{13}NO_2$	74.01 (73.98)	5.87 (5.73)	6.16 (6.16)

Table 4.2: Physical and analytical data for the chloroaniline-based ligands

No.	Ligand	Colour	%Yield	M.Pt (°C)	Molar mass	Molecular Formula	%Found (Calculated)		
							C	H	N
L2	sal-4-cla	Yellow	82	92-94	231.70	$C_{13}H_{10}NOCl$	67.50 (67.39)	4.29 (4.35)	6.02 (6.05)
L8	sal-2-cla	Yellow	53	72-74	231.70	$C_{13}H_{10}NOCl$	66.97 (67.39)	4.31 (4.35)	6.00 (6.05)
L5	ovan-4-cla	Orange	73	102-104	261.65	$C_{14}H_{12}NOCl$	64.09 (64.27)	4.87 (4.62)	5.34 (5.35)
L23	ovan-2-cla	Orange	45	110-112	261.65	$C_{14}H_{12}NO_2Cl$	63.82 (64.27)	4.62 (4.62)	5.10 (5.35)
L33	pvan-4-cla	Yellow	84	112-113	261.65	$C_{14}H_{12}NOCl$	63.12 (62.27)	4.58 (4.62)	5.24 (5.35)
L39	pvan-2-cla	Yellow	40	106-108	261.65	$C_{14}H_{12}NO_2Cl$	63.32 (64.27)	4.62 (4.62)	5.27(5.35)
L46	van-4-cla	Cream	61	120-122	261.65	$C_{14}H_{12}NOCl$	64.68 (64.27)	5.01 (4.62)	5.34 (5.35)

Table 4.3: Physical and analytical data for the bromoaniline-based ligands

No.	Ligand	Colour	%Yield	M.Pt (°C)	Molar mass	Molecular Formula	%Found (Calculated)		
							C	H	N
L3	sal-4-bra	Green	84	105-106	276.15	$C_{13}H_{10}NOBr$	56.72 (56.54)	3.69 (3.65)	5.06 (5.07)
L9	sal-2-bra	Yellow	78	76-78	276.15	$C_{13}H_{11}NOBr$	56.43 (56.54)	3.56 (3.65)	5.04 (5.07)
L18	ovan-4-bra	Orange	89	108-110	306.18	$C_{14}H_{12}NO_2Br$	55.10 (54.92)	3.78 (3.95)	4.64 (4.57)
L24	ovan-2-bra	Orange	29	102-104	306.18	$C_{14}H_{12}NO_2Br$	54.87 (54.92)	3.92 (3.95)	4.57 (4.57)
L34	pvan-4-bra	Yellow	86	144-145	306.18	$C_{14}H_{12}NO_2Br$	54.13 (54.92)	3.78 (3.95)	4.45 (4.57)
L40	pvan-2-bra	Yellow	82	82-84	306.18	$C_{14}H_{12}NO_2Br$	54.89 (54.92)	4.05 (3.95)	4.58 (4.57)
L47	van-4-bra	Green	86	108-110	306.18	$C_{14}H_{12}NO_2Br$	54.94 (54.92)	3.93 (3.95)	4.52 (4.57)

Table 4.4: Physical and analytical data for the methylaniline-based ligands

No.	Ligand	Colour	%Yield	M.Pt (°C)	Molar mass	Molecular Formula	%Found (Calculated)		
							C	H	N
L4	sal-4-tol	Yellow	95	85-87	211.28	$C_{14}H_{13}NO$	79.78 (79.59)	5.84 (5.77)	6.59 (6.63)
L10	sal-2-tol	Yellow	73	38-40	211.28	$C_{14}H_{13}NO$	78.84 (79.59)	6.19 (6.15)	6.60 (6.63)
L19	ovan-4-tol	Yellow	83	90-92	241.31	$C_{15}H_{15}NO_2$	74.17 (74.66)	6.47 (6.27)	5.58 (5.80)
L25	ovan-2-tol	Orange	48	50-52	241.31	$C_{15}H_{15}NO_2$	74.66 (74.66)	6.26 (6.27)	5.68 (5.80)
L35	pvan-4-tol	Yellow	70	80-82	241.31	$C_{15}H_{15}NO_2$	73.83 (74.66)	6.18 (6.27)	5.69 (5.80)
L41	pvan-2-tol	Yellow	57	92-94	241.31	$C_{15}H_{15}NO_2$	74.55 (74.66)	6.19 (6.27)	5.78 (5.80)
L48	van-4-tol	Cream	52	104-106	241.31	$C_{15}H_{15}NO_2$	74.64 (74.66)	6.24 (6.27)	5.56 (5.80)

Table 4.5: Physical and analytical data for the methoxyaniline-based ligands

No.	Ligand	Colour	%Yield	M.Pt (°C)	Molar mass	Molecular Formula	%Found (Calculated) C	H	N
L5	sal-4-nis	Green	78	74-75	227.27	$C_{14}H_{13}NO_2$	74.60 (73.99)	5.78 (5.77)	6.19 (6.16)
L11	sal-2-nis	Yellow	61	42-44	227.27	$C_{14}H_{13}NO_2$	73.18 (73.99)	5.89 (5.77)	6.13 (6.16)
L20	ovan-4-nis	Yellow	67	88-89	257.30	$C_{15}H_{15}NO_3$	70.20 (70.02)	6.41 (5.88)	5.44 (5.44)
L26	ovan-2-nis	Orange	89	74-76	257.30	$C_{15}H_{15}NO_3$	69.35 (70.02)	5.98 (5.88)	5.30 (5.44)
L36	pvan-4-nis	Yellow	82	118-120	257.30	$C_{15}H_{15}NO_3$	69.21 (70.02)	5.83 (5.88)	5.35 (5.44)
L49	van-4-nis	Brown	78	128-129	257.30	$C_{15}H_{15}NO_3$	70.76 (70.02)	6.41 (5.88)	5.47 (5.44)

Table 4.6: Physical and analytical data for the nitroaniline-based ligands

No.	Ligand	Colour	%Yield	M.Pt (°C)	Molar mass	Molecular Formula	%Found (Calculated) C	H	N
L6	sal-4-nit	Yellow	90	153-155	242.25	$C_{13}H_{10}N_2O_3$	64.38 (64.46)	4.18 (4.16)	11.54 (11.56)
L21	ovan-4-nit	Orange	76	164-166	272.28	$C_{14}H_{12}N_2O_4$	61.38 (61.76)	4.42 (4.44)	10.05 (10.29)
L37	pvan-4-nit	Yellow	50	140-142	272.28	$C_{14}H_{12}N_2O_4$	61.42 (61.76)	4.40 (4.44)	10.28 (10.29)

Table 4.7: Physical and analytical data for the hydroxyaniline-based ligands

No.	Ligand	Colour	%Yield	M.Pt (°C)	Molar mass	Molecular Formula	%Found (Calculated) C	H	N
L7	sal-4-phen	Brown	78	126-128	213.25	$C_{13}H_{11}NO_2$	72.88 (73.23)	5.54 (5.20)	6.57 (6.57)
L13	sal-2-phen	Orange	91	180-182	213.25	$C_{13}H_{11}NO$	73.01 (73.23)	5.29 (5.20)	6.44 (6.57)
L22	ovan-4-phen	Wine	70	134-136	261.28	$C_{14}H_{13}NO_3$	69.11 (69.12)	5.77 (5.39)	5.62 (5.76)
L27	ovan-2-phen	Red	97	186-188	261.28	$C_{14}H_{13}NO_2$	68.89 (69.12)	5.43 (5.39)	5.72 (5.76)

L38	pvan-4-phen	Yellow	77	178-180	261.28	$C_{14}H_{13}NO_3$	68.71 (69.12)	5.46 (5.39)	5.79 (5.76)
L42	pvan-2-phen	Yellow	91	210-212	261.28	$C_{14}H_{13}NO_2$	69.31 (69.12)	5.45 (5.39)	5.70 (5.76)
L50	van-4-phen	Chocolate	76	191-193	261.28	$C_{14}H_{13}NO_3$	68.38 (69.12)	5.72 (5.39)	5.57 (5.76)

4.1.2 1-Aminonaphthalene-based ligands

Table 4.8: Physical and analytical data for the 1-aminonaphthalene-based ligands

No.	**Ligand**	**Colour**	**%Yield**	**M.Pt ($°C$)**	**Molar mass**	**Molecular Formula**	**%Found (Calculated)**		
							C	**H**	**N**
L14	sal-1-amnaph	Yellow	85	35-36	247.29	$C_{17}H_{13}NO$	82.52 (82.57)	5.24 (5.30)	5.67 (5.66)
L28	ovan-1-amnaph	Red	68	86-88	277.34	$C_{18}H_{15}NO_2$	77.99 (77.95)	5.37 (5.45)	5.09 (5.05)
L43	pvan-1-amnaph	Yellow	34	64-66	277.34	$C_{18}H_{15}NO_2$	77.28 (77.95)	5.36 (5.45)	4.90 (5.05)
L51	van-1-amnaph	Cream	66	107-109	277.34	$C_{18}H_{15}NO_2$	77.95 (77.95)	5.54 (5.42)	5.04 (5.05)

4.1.3 Aminopyridine-based ligands

Table 4.9: Physical and analytical data for the aminopyridine-based ligands

No.	**Ligand**	**Colour**	**%Yield**	**M.Pt ($°C$)**	**Molar mass**	**Molecular Formula**	**%Found (Calculated)**		
							C	**H**	**N**
L15	sal-2-ampy	Yellow	98	53-54	198.24	$C_{12}H_{10}N_2O$	72.94 (72.71)	5.09 (5.09)	14.17 (14.13)
L16	sal-3-ampy	Yellow	88	57-58	198.24	$C_{12}H_{10}N_2O$	72.79 (72.71)	5.22 (5.09)	14.13 (14.13)
L29	ovan-2-ampy	Orange	90	86-88	228.27	$C_{13}H_{12}N_2O_2$	68.50 (68.40)	5.20 (5.29)	12.30 (12.27)
L30	ovan-3-ampy	Yellow	88	109-110	228.27	$C_{13}H_{12}N_2O_2$	68.43 (68.40)	5.35 (5.29)	12.11 (12.27)
L44	pvan-3-ampy	Yellow	60	106-108	228.27	$C_{13}H_{12}N_2O_2$	67.63 (68.40)	5.29 (5.29)	12.09 (12.27)
L52	van-3-ampy	Yellow	37	108-109	228.27	$C_{13}H_{12}N_2O_2$	68.35 (68.40)	5.48 (5.29)	12.03 (12.27)

4.1.4 Aminomethylpyridine-based ligands

Table 4.10: Physical and analytical data for the aminomethylpyridine-based ligands

No.	Ligand	Colour	%Yield	M.Pt (°C)	Molar mass	Molecular Formula	%Found (Calculated) C	H	N
L17	sal-3-pico	Yellow	72	41-43	212.26	$C_{13}H_{12}N_2O$	73.56 (74.00)	5.69 (5.88)	13.20 (13.28)
L31	ovan-2-pico	Yellow	88	99-101	242.29	$C_{14}H_{14}N_2O_2$	69.65 (69.34)	5.94 (5.82)	11.59 (11.56)
L53	van-3-pico	Cream	59	136-138	242.29	$C_{14}H_{14}N_2O_2$	69.54 (69.34)	5.90 (5.78)	11.57 (11.56)

4.1.5 2-Aminobenzimidazole-based ligands

Table 4.11: Physical and analytical data for the 2-aminobenzimidazole-based ligands

No.	Ligand	Colour	%Yield	M.Pt (°C)	Molar mass	Molecular Formula	%Found (Calculated) C	H	N
L54	sal-AmBZI	Yellow	56	216-218	237.20	$C_{14}H_{11}N_3O$	71.75 (70.89)	4.52 (4.67)	17.71 (17.72)
L55	ovan-AmBZI	Orange	65	214-216	267.30	$C_{15}H_{13}N_3O_2$	67.67 (67.40)	4.90 (4.92)	15.68 (15.72)
L56	pvan-BZI	Yellow	60	206-207	267.30	$C_{15}H_{13}N_3O_2$	67.39 (67.40)	4.92 (4.92)	15.64 (15.72)

4.1.6 *o*-phenylenediamine-based ligands

Table 4.11: Physical and analytical data for the *o*-phenylenediamine-based ligands

No.	Ligand	Colour	% Yield	M. Pt °C	Molar mass	Molecular formula	% Found (calculated) C	H	N
L57	bis-salphen	Yellow	87	152-154	316.39	$C_{20}H_{14}N_2O_2$	75.26 (75.93)	5.20 (5.10)	8.65 (8.85)
L58	bis-ovanphen	Orange	90	159-161	376.45	$C_{24}H_{18}N_2O_4$	70.22 (70.19)	5.60 (5.36)	7.41 (7.44)

4.2.0: Physical and analytical data for the complexes

Table 4.12: Physical and analytical data for the aniline-based complexes

No.	Complex	Colour	%Yield	M.Pt (°C)	Molar mass	Molecular Formula	%Found (Calculated) C	H	N	Cu	Λ_M ($\Omega^{-1}.cm^2.mol^{-1}$)
1	$Cu(salaani)_2Cl_2.2½\,2H_2O$	Brown	69	128-130	572.05	$CuC_{26}H_{22}N_2O_2Cl_2.2½\,2H_2O$	54.59 (54.69)	4.41 (4.26)	4.90 (5.91)	11.11 (11.62)	183.00 (1:1) Methanol
2	$Cu(ovaani)_2Cl_2.H_2O.½\,2EtOH$	Brown	88	124-126	629.42	$CuC_{28}H_{26}N_2O_4Cl_2.H_2O\,.½\,2EtOH$	55.34 (55.52)	4.97 (4.69)	4.45 (4.44)	10.10 (9.80)	134.2 (1:1) Methanol

Table 4.13: Physical and analytical data for the chloroaniline-based complexes

No.	Complex	Colour	%Yield	M.Pt (°C)	Molar mass	Molecular Formula	%Found (Calculated) C	H	N	Cu	Λ_M ($\Omega^{-1}.cm^2.mol^{-1}$)
3	$Cu(sal\text{-}4\text{-}cla)_2Cl_2.2H_2O$	Brown	55	160-162	633.95	$CuC_{26}H_{20}N_2O_2Cl_4.2H_2O$	49.26 (49.61)	3.82 (3.33)	4.42 (4.72)	11.02 (10.15)	138 (1:1) Methanol
4	$Cu(ovan\text{-}4\text{-}cla)_2$	Green	84	194-196	584.85	$CuC_{28}H_{22}N_2O_4Cl_2$	57.30 (57.50)	4.05 (3.79)	4.76 (4.79)	11.01 (10.87)	1.57[a] DMF
5	$Cu(sal\text{-}2\text{-}cla)_2$	Brown	81	250-252	524.93	$CuC_{26}H_{18}N_2O_2Cl_2$	59.24 (59.49)	3.36 (3.46)	5.29 (5.34)	(12.30 (12.10)	1.65[a] DMF
6	$Cu(ovan\text{-}2\text{-}cla)_2$	Brown	60	174-176	584.85	$CuC_{28}H_{22}N_2O_4Cl_2$	57.37 (57.50)	3.80 (3.79)	4.71 (4.79)	10.50 (10.87)	2.90[a] DMF

(a) Neutral complex

Table 4.14: Physical and analytical data for the bromoaniline-based complexes

No.	Complex	Colour	%Yield	M.Pt (°C)	Molar mass	Molecular Formula	%Found (Calculated) C	H	N	Cu	Λ_M ($\Omega^{-1}.cm^2.mol^{-1}$)
7	$Cu(sal\text{-}4\text{-}bra)_2Cl_2.H_2O$	Brown	75	171-172	704.77	$CuC_{26}H_{20}N_2O_2Br_2Cl_2.H_2O$	44.31 (44.56)	3.15 (2.82)	3.97 (4.07)	9.02 (8.72)	126.50 (1:1) Methanol
8	$Cu(ovan\text{-}4\text{-}bra)_2Cl_2.H_2O$	Brown	56	179-180	764.93	$CuC_{28}H_{24}N_2O_2Br_2Cl_2.H_2O$	43.97 (43.47)	3.43 (3.16)	3.66 (3.61)	8.31 (7.72)	99.80 (1:1) Methanol
9	$Cu(sal\text{-}2\text{-}bra)_2$	Brown	76	248-249	613.83	$CuC_{26}H_{18}N_2O_2Br_2$	51.92 (51.87)	2.93 (2.96)	4.51 (4.56)	10.60 (10.35)	1.59[a] DMF
10	$Cu(ovan\text{-}2\text{-}bra)_2$	Brown	68	172-174	673.91	$CuC_{28}H_{22}N_2O_4Br_2$	49.97 (49.90)	3.36 (3.29)	4.12 (4.16)	9.57 (9.43)	6.59[a] DMF

(a) Neutral complex

Table 4.15: Physical and analytical data for the methylaniline-based complexes

No.	Complex	Colour	%Yield	M.Pt (°C)	Molar mass	Molecular Formula	%Found (Calculated) C	H	N	Cu	Λ_M ($\Omega^{-1}.cm^2.mol^{-1}$)
11	$Cu(sal\text{-}4\text{-}tol)_2Cl_2.H_2O$	Brown	57	156-158	575.01	$CuC_{28}H_{26}N_2O_2Cl_2.H_2O$	58.49 (58.68)	4.91 (4.71)	4.85 (5.00)	11.79 (11.05)	83.00 (1:1) Methanol
12	$Cu(ovan\text{-}4\text{-}tol)_2Cl_2.2½H_2O$	Brown	60	168-170	671.19	$CuC_{30}H_{30}N_2O_4Cl_2.2½H_2O$	53.69 (54.41)	5.41 (5.33)	4.17 (4.23)	9.47 (9.60)	82.70 (1:1) Methanol

13	*Cu(ovan-NH_3)$_2$.H_2O	Green	75	166-168	399.90	$CuC_{16}H_{20}N_2O_6$	47.70 48.06	5.07 (5.04)	6.97 (7.01)	15.80 (15.89)	1.80[a] DMF
14	Cu(sal-2-tol)$_2$	Brown	91	230-232	484.09	$CuC_{28}H_{24}N_2O_2$	70.52 (69.47)	5.11 (5.00)	5.73 (5.79)	12.87 (13.13)	2.71[a] DMF
15	Cu(pvan-2-tol)$_2$.½ $2H_2O$	Green	78	196-198	553.15	$CuC_{30}H_{28}N_2O_4$.½ $2H_2O$	65.55 (65.14)	5.40 (5.28)	4.96 (5.06)	11.60 (11.48)	2.60[a] DMF

(a) Neutral complex; *Cu(ovan-NH_3)$_2$.H_2O was prepared from *o*-vanillin and ammonia, starting with ovan-2-tol

Table 4.16: Physical and analytical data for the methoxyaniline-based complexes

No.	**Complex**	**Colour**	**%Yield**	**M.Pt** ($°C$)	**Molar mass**	**Molecular Formula**	**%Found (Calculated)**				Λ_M ($\Omega^{-1}.cm^2.mol^{-1}$)
							C	**H**	**N**	**Cu**	
16	Cu(sal-4-nis)$_2$	Red	77	170-172	516.074	$CuC_{28}H_{24}N_2O_4$	65.08 (65.16)	4.92 (4.69)	5.34 (5.43)	11.98 (12.31)	1.60[a] DMF
17	Cu(sal-2-nis)$_2$	Brown	76	208-210	516.074	$CuC_{28}H_{24}N_2O_4$	64.66 (65.16)	4.74 (4.69)	5.38 (5.43)	12.02 (12.31)	4.65[a] DMF
18	*Cu(ovan-NH_3)$_2$	Green	67	166-168	399.900	$CuC_{16}H_{20}N_2O_6$	47.82 (48.06)	5.13 (5.04)	7.03 (7.01)	16.00 (15.89)	1.80[a] DMF
19	*Cu(ovan-NH_3)$_2$	Green	70	166-168	399.900	$CuC_{16}H_{20}N_2O_6$	47.93 (48.06)	5.04 (5.04)	7.00 (7.01)	15.75 (15.89)	1.80[a] DMF

(a) Neutral complex; *Cu(ovan-NH_3)$_2$ were prepared from ammonia and *o*-vanillin starting with ovan-4-nis or ovan-2-nis.

Table 4.17: Physical and analytical data for the nitroaniline-based complexes

No.	Complex	Colour	%Yield	M.Pt (°C)	Molar mass	Molecular Formula	%Found (Calculated) C	H	N	Cu	Λ_M ($\Omega^{-1}.cm^2.mol^{-1}$)
20	$Cu(sal\text{-}4\text{-}nit)_2.½H_2O$	Orange	90	> 250	555.034	$CuC_{26}H_{18}N_4O_6.½H_2O$	56.60 (56.26)	3.48 (3.48)	10.13 (10.09)	11.12 (11.45)	6.39[a] DMF
21	$Cu(ovan\text{-}4\text{-}nit)_2.2EtOH$	Brown	78	>250	698.09	$CuC_{28}H_{22}N_4O_8.2EtOH$	55.17 (55.06)	4.91 (4.38)	8.03 (8.00)	9.10 (8.79)	6.61[a] DMF

(a) Neutral complex

Table 4.18: Physical and analytical data for the hydroxyaniline-based complexes

No.	Complex	Colour	%Yield	M.Pt (°C)	Molar mass	Molecular Formula	%Found (Calculated) C	H	N	Cu	Λ_M ($\Omega^{-1}.cm^2.mol^{-1}$)
22	$Cu(sal\text{-}4\text{-}phen)_2Cl_2.H_2O$	Brown	60	150-152	640.584	$CuC_{26}H_{20}N_2O_4Cl_2$	48.29 (48.76)	3.48 (3.46)	(4.37)	(9.92)	95.00 (1:1) Methanol
23	$Cu(ovan\text{-}4\text{-}phen)_2Cl_2.H_2O$	Brown	67	178-180	637.09	$CuC_{28}H_{26}N_2O_6Cl_2.H_2O$	52.79 (52.44)	4.11 (4.31)	4.40 (5.03)	9.98 (9.77)	131.00 (1:1) Methanol
24	$Cu_2(sal\text{-}2\text{-}phen)_2$	Green	93	> 250	274.784	$Cu_2C_{26}H_{18}N_2$	56.01 (56.82)	3.11 (3.3)	4.93 (5.10)	23.5 (23.13)	*ns
25	$Cu_2(ovan\text{-}2\text{-}phen)_2$	Green	60	> 250	304.814	$Cu_2C_{28}H_{22}N_2$	54.98 55.17	3.39 (3.64)	4.55 (4.60)	20.95 (20.85)	*ns

26	Cu_2(pvan-2-phen)$_2$	Green	85	> 250	304.814	$Cu_2C_{28}H_{22}N_2$	54.98 (55.17)	3.37 (3.64)	4.60 (4.60)	20.70 (20.85)	*ns

(*ns) Not soluble

Table 4.19: Physical and analytical data for the 1-aminonaphthalene-based complexes

No.	**Complex**	**Colour**	**%Yield**	**M.Pt ($°C$)**	**Molar mass**	**Molecular Formula**	**%Found (Calculated)**				**Λ_M ($\Omega^{-1}.cm^2.mol^{-1}$)**
							C	**H**	**N**	**Cu**	
27	Cu(sal-1-amnaph)$_2$.1½H_2O	Brown	20	> 250	583.122	$CuC_{34}H_{24}N_2O_4$ .1½H_2O	69.87 (70.03)	4.30 (4.67)	(4.80)	(10.90)	94.95 (1:1) DMF
28	Cu(ovan-1-amnaph)$_2$	Brown	34	222-224	616.214	$CuC_{36}H_{28}N_2O_4$	69.51 (70.17)	4.83 (4.91)	4.52 (4.55)	10.10 (10.31)	5.21[a] DMF

(a) Neutral complex

Table 4.20: Physical and analytical data for the aminopyridine-based complexes

No.	**Complex**	**Colour**	**%Yield**	**M.Pt ($°C$)**	**Molar mass**	**Molecular Formula**	**%Found (Calculated)**				**Λ_M ($\Omega^{-1}.cm^2.mol^{-1}$)**
							C	**H**	**N**	**Cu**	
29	Cu(sal-2-ampy)$_2$.Cl_2	Brown	46	196-198	594.58	$CuC_{24}H_{20}N_4O_2Cl_2$	48.48 (48.48)	3.25 (3.39)	9.99 (9.42)	9.80 (9.22)	57.95[a] DMF

30	$Cu(sal\text{-}3\text{-}ampy)_2Cl_2.{}^{1}/_{2}H_2O$	Green	73	198-200	540.03	$CuC_{24}H_{20}N_4O_2Cl_2 .{}^{1}/_{2}H_2O$	53.63 (53.36)	3.94 (3.92)	10.64 (10.37)	11.77 (10.70)	48.55[a] DMF
31	$Cu(ovan\text{-}2\text{-}ampy)Cl_2.H_2O$	Brown	55	180-182	379.81	$CuC_{13}H_{12}N_2O_2Cl_2.H_2O$	40.79 (41.00)	3.33 (3.71)	7.51 (7.36)	16.50 (16.73)	79.75 (1:1) DMF
32	$Cu(ovan\text{-}3\text{-}ampy)_2Cl_2.H_2O$	Green	81	193-195	609.09	$CuC_{26}H_{24}N_4O_4Cl_2 .H_2O$	51.92 (51.27)	4.14 (4.30)	9.42 (9.20)	10.87 (10.43)	50.70[a] DMF

(a) Neutral complex

Table 4.21: Physical and analytical data for the aminomethylpyridine-based complexes

No.	**Complex**	**Colour**	**%Yield**	**M.Pt** ($°C$)	**Molar mass**	**Molecular Formula**	**%Found (Calculated)** **C**	**H**	**N**	**Cu**	Λ_M ($\Omega^{-1}.cm^2.mol^{-1}$)
33	$Cu(ovan\text{-}2\text{-}pico)Cl$	Green	87	172-174	340.332	$CuC_{14}H_{13}N_2O_2Cl$	49.86 (49.41)	4.02 (3.85)	8.41 (8.23)	18.50 (18.67)	47.50[a] DMF
34	$Cu(sal\text{-}3\text{-}pico)_2Cl_2.{}^{1}/_{2}H_2O$	Green	56	161-162	631.62	$CuC_{26}H_{24}N_4O_2Cl_2.{}^{1}/_{2}H_2O$	49.16 (49.44)	3.95 (3.99)	9.84 (8.87)	10.06 (9.22)	52.90[a] DMF

(a) Neutral complex

Table 4.22: Physical and analytical data for the 2-aminobenzimidazole-based complexes

No.	Complex	Colour	%Yield	M.Pt (°C)	Molar mass	Molecular Formula	%Found (Calculated) C	H	N	Cu	Λ_M ($\Omega^{-1}.cm^2.mol^{-1}$)
35	Cu(sal-AmBZI)$_2$.½ 2H$_2$O	Brown	73	238*	545.074	$CuC_{28}H_{20}N_6O_2$.½ 2H$_2$O	61.75 (61.70)	3.57 (3.88)	15.34 (15.42)	11.32 (11.66)	13.13[a] DMF
36	Cu(ovan-AmBZI)$_2$.H$_2$O	Brown	80	241*	614.134	$CuC_{30}H_{24}N_6O_4$.½ 2H$_2$O	58.93 (59.55)	4.00 (4.17)	13.65 (13.8)	10.10 (10.35)	7.73[a] DMF
37	Cu(pvan-AmBZI)$_2$	Brown	72	230*	596.134	$CuC_{30}H_{24}N_6O_4$	60.17 (60.44)	4.11 (4.06)	14.00 (14.10)	10.43 (10.66)	7.46[a] DMF

*decomposition temperature

Table 4.23: Physical and analytical data for the *o*-phenylenediamine-based complexes

No.	Ligand	Colour	% Yield	M. Pt °C	Molar mass	Molecular formula	% Found (calculated) C	H	N	Λ_M ($\Omega^{-1}.cm^2.mol^{-1}$)
38	Cu(bis-salphen)Cl$_2$.2H$_2$0	Green	78	159-161	459.94	$CuC_{20}H_{16}N_2O_5Cl_2$.2H$_2$0	52.02 (51.45)	3.54 (3.45)	6.09 (6.00)	41.80[a] Methanol
39	Cu(bis-ovanphen)Cl$_2$.½H$_2$O	Greenish-yellow	82	> 250	520.00	$CuC_{22}H_{19}N_2O_5Cl_2$.½H$_2$O	51.08 (51.01)	3.93 (3.70)	5.94 (5.41)	42.60[a] DMF

(a) Neutral complex

4.3.0 Mid-infrared data for the ligands

4.3.1 Aniline-based ligands

Table 4.24: Mid-infrared frequencies (cm^{-1}) for the aniline-based ligands

No.	Compound	Structure	ν_{OH}	$\nu_{C=N_{(imine)}}$	ν_{C-O}	$\Delta\nu_{C=N_{(imine)}}$
Ref.	Benzylideneaniline	-		1630	-	-
L1	salaani	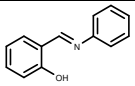	3114-2106	1613	1273	-17
L16	ovaani	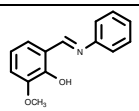	3205-2370	1613	1267	-17
L32	pvaani	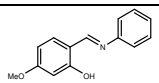	3139-2365	1613	1287	-17
L45	vaani	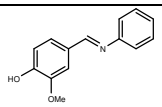	3453-2365	1622	1282	-8

4.3.2 Substituted aniline-based ligands

Table 4.25: Mid-infrared frequencies (cm^{-1}) for the chloroaniline-based ligands

No.	Compound	ν_{OH}	$\nu_{C=N_{(imine)}}$	ν_{C-O}	$\Delta\nu_{C=N_{(imine)}}$
Ref.	Benzylideneaniline	-	1630	-	-
L2	sal-4-cla	3114-1965	1608	1272	-22
L8	sal-2-cla	3220-2359	1612	1273	-14
L17	ovan-4-cla	3114-2375	1611	1272	-19
L23	ovan-2-cla	3149-2365	1613	1277	-17
L33	pvan-4-cla	3119-2349	1607	1286	-23

L39	pvan-2-cla	3206-2349	1607	1291	-24
L46	van-4-cla	3443-2314	1623	1276	-7

Table 4.26: Mid-infrared frequencies (cm^{-1}) for the bromoaniline-based ligands

No.	**Compound**	ν_{OH}	$\nu_{C=N_{(imine)}}$	ν_{C-O}	$\Delta\nu_{C=N_{(imine)}}$
Ref.	Benzylideneaniline	-	1630	-	-
L3	sal-4-bra	3215-2162	1608	1281	-22
L9	sal-2-bra	3220-2339	1612	1277	-14
L18	ovan-4-bra	3114-2370	1611	1273	-19
L24	ovan-2-bra	3099-2375	1613	1277	-17
L34	pvan-4-bra	3094-2375	1607	1288	-23
L40	pvan-2-bra	3271-2370	1606	1290	-24
L47	van-4-bra	3408-2354	1622	1279	-8

Table 4.27: Mid-infrared frequencies (cm^{-1}) for the methylaniline-based ligands

No.	**Compound**	ν_{OH}	$\nu_{C=N_{(imine)}}$	ν_{C-O}	$\Delta\nu_{C=N_{(imine)}}$
Ref.	Benzylideneaniline	-	1630	-	-
L4	sal-4-tol	3063-2334	1616	1281	-14
L10	sal-2-tol	3104-2334	1615	1279	-14
L19	ovan-4-tol	3094-2370	1616	1270	-14
L25	ovan-2-tol	3104-2349	1612	1277	-17
L35	pvan-4-tol	3094-2344	1613	1288	-17
L41	pvan-2-tol	3109-2339	1610	1292	-20
L48	van-4-tol	3382-2349	1623	1277	-7

Table 4.28: Mid-infrared frequencies (cm^{-1}) for the methoxyaniline-based ligands

No.	Compound	ν_{OH}	$\nu_{C=N_{(imine)}}$	ν_{C-O}	$\Delta\nu_{C=N_{(imine)}}$
Ref.	Benzylideneaniline	-	1630	-	-
L5	sal-4-nis	3073-2071	1616	1280	-14
L11	sal-2-nis	3084-2284	1615	1280	-14
L20	ovan-4-nis	3094-2375	1613	1269	-17
L26	ovan-2-nis	3104-2344	1614	1280	-17
L36	pvan-4-nis	3271-2157	1614	1286	-16
L49	van-4-nis	3392-2365	1623	1275	-7

Table 4.29: Mid-infrared frequencies (cm^{-1}) for the nitroaniline-based ligands

No.	Compound	ν_{OH}	$\nu_{C=N_{(imine)}}$	ν_{C-O}	$\Delta\nu_{C=N_{(imine)}}$
Ref.	Benzylideneaniline	-	1630	-	-
L6	sal-4-nit	3139-2147	1598	1287	-14
L21	ovan-4-nit	3144-2375	1611	1273	-17
L37	pvan-4-nit	3120-2158	1614	1286	-16

Table 4.30: Mid-infrared frequencies (cm^{-1}) for the hydroxyaniline-based ligands

No.	Compound	ν_{OH}	$\nu_{C=N_{(imine)}}$	ν_{C-O}	$\Delta\nu_{C=N_{(imine)}}$
`	Benzylideneaniline	-	1630	-	-
L7	sal-4-phen	3301; 3289-2162	1615	1280, 1289	-15
L12	sal-2-phen	3134-1949	1626	1272, 1304	-19

L22	ovan-4-phen	3413	1611	1278, 1295	-17
L27	ovan-2-phen	3129-1952	1626	1277, 1306	-14
L38	pvan-4-phen	3190-2064	1614	1286	-16
L42	pvan-2-phen	3313; 3158-2043	1624	1276, 1286	-20
L50	van-4-phen	3469-2477	1623	1275	-7

4.3.3 1-Aminonaphthalene-based ligands

Table 4.31: Mid-infrared frequencies (cm^{-1}) for the 1-aminonaphthalene-based ligands

No.	**Compound**	**Structure**	ν_{OH}	$\nu_{C=N_{(imine)}}$	ν_{C-O}
L13	sal-1-amnaph	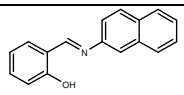	3215-2167	1609	1278
L28	ovan-1-amnaph	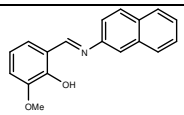	3099-2157	1606	1279
L43	pvan-1-amnaph	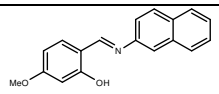	3170-2344	1607	1287
L51	van-1-amnaph	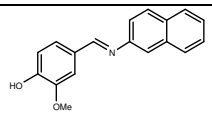	3362-2349	1622	1283

4.3.4 Aminopyridine-based ligands

Table 4.32: Mid-infrared frequencies (cm^{-1}) for the aminopyridine-based ligands

No.	Compound	Structure	ν_{OH}	$\nu_{C=N(imine)}$	$\nu_{C=N(py)}$	ν_{C-O}
L14	sal-2-ampy	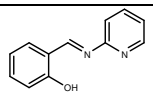	3210-2071	1588	1575	1278
L15	sal-3-ampy	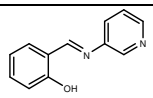	3109-2127	1611	1563	1284
L29	ovan-2-ampy	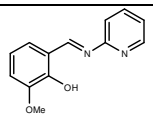	3114-2375	1587	1560	1275
L30	ovan-3-ampy	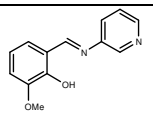	3109-2390	1613	1562	1272
L44	pvan-3-ampy	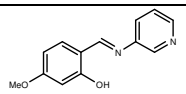	3165-2365	1608	1564	1285
L52	van-3-ampy	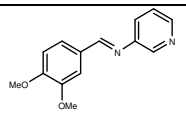	3367-2137	1620	1577	1271

4.3.5 Aminomethylpyridine-based ligands

Table 4.33: Mid-infrared frequencies (cm^{-1}) for the aminomethylpyridine-based ligands

No.	Compound	Structure	ν_{OH}	$\nu_{C=N(imine)}$	$\nu_{C=N(py)}$	ν_{C-O}
L16	sal-3-pico	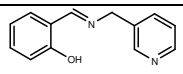	3089-2284	1627	1606	1274
L31	ovan-2-pico	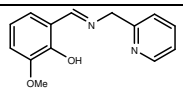	3104-2152	1631	1605	1282

L53	van-3-pico	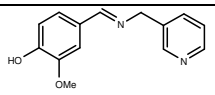	3337-2081	1634	1603	1285

4.3.6 2-Aminobenzimidazole-based ligands

Table 4.34: Mid-infrared frequencies (cm^{-1}) for the 2-aminobenzimidazole-based ligands

No.	**Compound**	**Structure**	ν_{OH}	$\nu_{C=N_{(imine)}}$	$\nu_{C=N_{(Im)}}$	ν_{C-O}
L54	sal-2-AmBZI	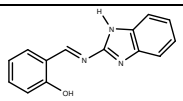	3175-2344	1606	1619	1276
L55	ovan-2-AmBZI	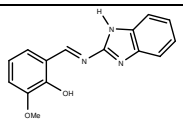	3087-2339	1600	1623	1249
L56	pvan-2-AmBZI	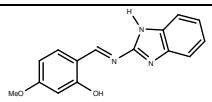	3109-2287	1598	1624	1278

4.3.7 *o*-Phenylenediamine-based ligands

Table 4.35: Mid-infrared frequencies (cm^{-1}) for the 2-aminobenzimidazole-based ligands

No.	**Compound**	ν_{OH}	$\nu_{C=N_{(imine)}}$	ν_{C-O}
L57	bis-salphen	3099-2370	1610	1275
L58	bis-ovanphen	3087-2370	1610	1269

4.4.0 Mid and far infrared data for the complexes

4.4.1 Aniline-based complexes

Table 4.36: Mid and far infrared data for the aniline-based complexes

No.	Compound	Structure	$\nu_{OH/NH}$	ν_{C-H}	$\nu_{C=N_{(imine)}}$	ν_{C-O}	ν_{Cu-O}	ν_{Cu-N}	ν_{Cu-Cl}
	Salaani	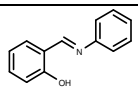	3114-2106	3053	1613	1273	----	----	----
1	$Cu(salaani)_2Cl_2.2½2H_2O$		3261, 3215	3127,3053	1606,1634	1315	-----	515	386, 316
	Ovaani	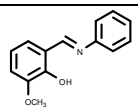	3205-2370	3080, 3052	1613	1267	-----	----	-----
2	$Cu(ovaani)_2Cl_2.H_2O.½2EtOH$		3494, 3438; 3109-2668	3038, 2932	1608, 1633	1309	-----	425	248

4.4.2 Substituted aniline-based complexes

Table 4.37: Mid and far infrared data for the chloroaniline-based complexes

No.	Compound	Structure	$\nu_{OH/NH}$	ν_{C-H}	$\nu_{C=N_{(imine)}}$	ν_{C-O}	ν_{Cu-O}	ν_{Cu-N}	ν_{Cu-Cl}
	sal-4-cla	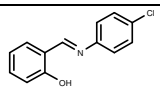	3114-1965	3089, 3058	1608	1272	-----	-----	-----
3	$Cu(sal-4-cla)_2Cl_2.2H_2O$		3322, 3241 3205	3124, 3058	1606, 1628	1309	-----	513, 428	334, 274
	sal-2-cla	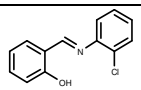	3220-2359	3068, 2987	1612	1273	-----	-----	-----
4	$Cu(sal-2-cla)_2$		-----	3076, 3057	1603	1325	595, 556	468, 430	-----

	ovan-4-cla	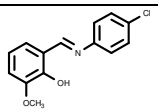	3114-2375	3091, 3053	1611	1272	-----	-----	-----
5	$Cu(ovan\text{-}4\text{-}cla)_2$		------	3084, 3065	1598	1318	584, 561	497, 440	-----
	ovan-2-cla	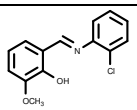	3149-2365	3077, 3063	1613	1277	-----	-----	-----
6	$Cu(ovan\text{-}2\text{-}cla)_2$		-----	3079, 3054	1603	1336	575, 559	518, 437	-----

Table 4.38: Mid and far infrared data for the bromoaniline-based complexes

No.	**Compound**	**Structure**	$\nu_{OH/NH}$	ν_{C-H}	$\nu_{C=N_{(imine)}}$	ν_{C-O}	ν_{Cu-O}	ν_{Cu-N}	ν_{Cu-Cl}
	sal-4-bra	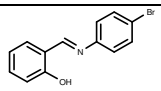	3215-2162	3082, 3066	1608	1281	-----	-----	-----
7	$Cu(sal\text{-}4\text{-}bra)_2Cl_2.2H_2O$		3119-2780	3058, 3037	1603, 1633	1309	-----	511	368
	sal-2-bra	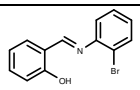	3220-2359	3067	1612	1277	-----	-----	-----
8	$Cu(sal\text{-}2\text{-}bra)_2$		-----	3044	1602	1325	556	539, 466	-----
	ovan-4-bra	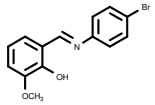	3114-2370	3099, 3048	1611	1273	-----	-----	-----
9	$Cu(ovan\text{-}4\text{-}bra)_2Cl_2.H_2O$		3114-2648	3089, 3028	1613, 1637	1308	-----	530, 435	372
	ovan-2-bra	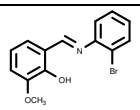	3114-2370	3075, 3059	1613	1277	-----	-----	-----
10	$Cu(ovan\text{-}2\text{-}bra)_2$		-----	3052	1604	1331	562	515, 432	-----

Table 4.39: Mid and far infrared data for the methylaniline-based complexes

No.	Compound	Structure	$\nu_{OH/NH}$	ν_{C-H}	$\nu_{C=N_{(imine)}}$	ν_{C-O}	ν_{Cu-O}	ν_{Cu-N}	ν_{Cu-Cl}
	sal-4-tol	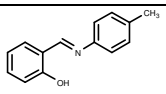	3063-2334	3055, 3023	1616	1281	-----	-----	-----
11	$Cu(sal\text{-}4\text{-}tol)_2Cl_2.H_2O$		3251, 3210	3127, 3043	1606,1638	1316	-----	503	364
	sal-2-tol	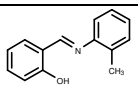	3104-2334	3064, 3048	1615	1279	-----	-----	-----
12	Cu(sal-2-tol)2		-----	3075, 3043	1606	1325	545, 531	489, 429	-----
	ovan-4-tol	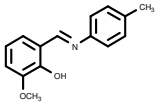	3094-2370	3061, 3050	1616	1270	-----	-----	-----
13	$Cu(ovan\text{-}4\text{-}tol)_2Cl_2.\ 2^1/_2H_2O$		3207, 3160	3055, 3033	1611, 1641	1305	-----	495, 441	347
	Ovan-2-tol	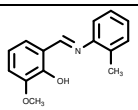	3104-2349		1612	1277	-----	-----	-----
14	$Cu(ovan\text{-}NH)_2.H_2O$		3413; 3294	3051	1623	1331	513	484, 421	-----
	pvan-2-tol	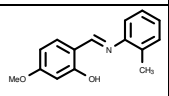	3109-2339	3063, 3002	1610	1292	-----	-----	-----
15	Cu(pvan-2-tol)		-----	3063	1605	1310	522	490, 465	-----

Table 4.40: Mid and far infrared data for the methoxyaniline-based complexes

No.	Compound	Structure	$\nu_{OH/NH}$	ν_{C-H}	$\nu_{C=N_{(imine)}}$	ν_{C-O}	ν_{Cu-O}	ν_{Cu-N}	ν_{Cu-Cl}
	sal-4-nis	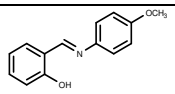	3073-2071	3063, 3053	1616	1280	-----	-----	-----
16	$Cu(sal\text{-}4\text{-}nis)_2$		------	3086, 3076	1600	1325	591	497, 424	-----
	sal-2-nis	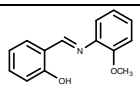	3084-2284	3064, 3014	1615	1280	-----	-----	-----
17	$Cu(sal\text{-}2\text{-}nis)_2$		-----	3058, 3020	1606	1329	580	489,	-----
	ovan-4-nis	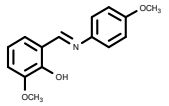	3094-2375	3078	1613	1269	-----	-----	-----
18	$Cu(ovan\text{-}NH)_2.H_2O$		3413; 3294	3051	1623	1331	513	484, 421	-----
	Ovan-2-nis	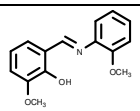	3104-2344	3063	1614	1280	-----	-----	-----
19	$Cu(ovan\text{-}NH)_2.H_2O$		3413; 3294	3051	1623	1331	513	484, 421	-----

Table 4.41: Mid and far infrared data for the nitroaniline-based complexes

No.	Compound	Structure	$\nu_{OH/NH}$	ν_{C-H}	$\nu_{C=N_{(imine)}}$	ν_{C-O}	ν_{Cu-O}	ν_{Cu-N}	ν_{Cu-Cl}
	sal-4-nit	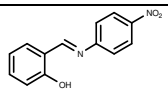	3139-2147	3055, 3023	1598	1270	-----	-----	-----
20	$Cu(sal\text{-}4\text{-}nit)_2$		-----	3109, 3079	1610, 1578	1320	587	491, 424	-----
	ovan-4-nit	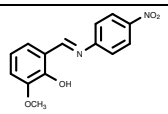	3144-2375	3124, 3058	1611	1273	-----	-----	-----
21	$Cu(ovan\text{-}4\text{-}nit)_2.2EtOH$		3210	3103, 3063	1603	1330	573	466, 412	-----

Table 4.42: Mid and far infrared data for the hydroxyaniline-based complexes

No.	Compound	Structure	$\nu_{OH/NH}$	ν_{C-H}	$\nu_{C=N_{(imine)}}$	ν_{C-O}	ν_{Cu-O}	ν_{Cu-N}	ν_{Cu-Cl}
	sal-4-phen	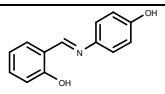	3286-2147	3051	1615	1280,1289	-----	-----	-----
22	$Cu_2(sal\text{-}4\text{-}phen)_2Cl_2.H_2O$		3678-2344	3058	1598	1317S	-----	-----	-----
	sal-2-phen	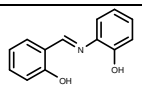	3134-1949	3043	1626	1272, 1304	-----	-----	-----
23	$Cu_2(sal\text{-}2\text{-}phen)_2$		-----	3058, 3011	1613	1341, 1379	604,	489, 449	-----
	ovan-4-phen	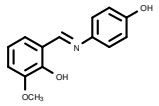	3413	3040, 3013	1611	1278, 1295	-----	-----	-----
24	$Cu(ovan4\text{-}phen)_2Cl_2.\ H_2O$		3448, 3180	3033	1608, 1641	1311	538	492, 448	386
	ovan-2-phen	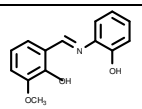	3129-1952	3056	1626	1277, 1306	-----	-----	-----
25	$Cu_2(ovan\text{-}2\text{-}phen)_2$		-----	3052, 3012	1610	1355, 1317	583, 535	473, 371	-----
	pvan-2-phen	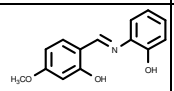	3158-2043	2971	1624	1276, 1286	-----	-----	-----
26	$Cu_2(pvan\text{-}2\text{-}phen)_2$		-----	3058	1599	1357, 1304	578, 511	484, 464	-----

4.4.3 1-Aminonaphthalene-based complexes

Table 4.43: Mid and far infrared data for the 1-aminonaphthalene-based complexes

No.	Compound	Structure	$\nu_{OH/NH}$	ν_{C-H}	$\nu_{C=N_{(imine)}}$	ν_{C-O}	ν_{Cu-O}	ν_{Cu-N}	ν_{Cu-Cl}
	sal-1-amnaph	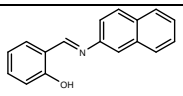	3104-1970	3060	1609	1278	-----	-----	-----
27	Cu(sal-1-amnaph)$_2$. 1½H_2O		3210	3048	1607	1314	584, 561	501, 458	-----
	ovan-1-amnaph	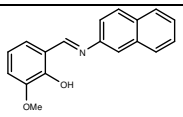	3099-2157	3074	1606	1279	-----	-----	-----
28	Cu(ovan-1-amnaph)$_2$		-----	3046	1600	1332	594, 567	502, 435	-----

4.4.4 Aminopyridine-based complexes

Table 4.44: Mid and far infrared data for the aminopyridine-based complexes

No.	Compound		$\nu_{OH/NH}$	ν_{C-H}	$\nu_{C=N_{(imin}}$	$\nu_{C=N_{(py)}}$	ν_{C-O}	ν_{Cu-O}	ν_{Cu-N}	ν_{Cu-Cl}
	sal-2-ampy	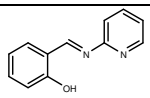	3210-2071	3048	1588	1575	1278	-----	-----	-----
29	Cu(sal-2-ampy)$_2Cl_2$		3327	3104	1584	1563	1292	441	388	358
	sal-3-ampy	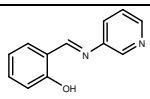	3109-2127	3053	1611	1565	1284	-----	-----	-----
30	Cu(sal-3-ampy)$_2Cl_2$. ½H_2O		3119-2395	3094	1613	1568	1327	419	380	358
	ovan-2-ampy	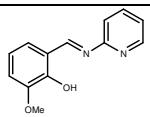	3114-2375	3058	1607	1587	1275	-----	-----	-----
31	Cu(ovan-2-ampy)Cl_2. H_2O		3413; 3195-2856	3094	1598	1567	1299	502	424	276

	ovan-3-ampy	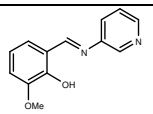	3109-2390	3084	1613	1565	1272	-----	-----	-----
32	Cu(ovan-3-ampy)Cl_2. H_2O		3205-2385	3068	1606	1572	1284	482	427	293

4.4.5 Aminomethylpyridine-based complexes

Table 4.45: Mid and far infrared data for the aminomethylpyridine-based complexes

No.	**Compound**	**Structure**	$\nu_{OH/NH}$	ν_{C-H}	$\nu_{C=N_{(imin}}$	$\nu_{C=N_{(py)}}$	ν_{C-O}	ν_{Cu-O}	ν_{Cu-N}	ν_{Cu-Cl}
	ovan-2-pico	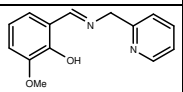	3104-2152	3058	1631	1602	1258	-----	-----	------
33	Cu(ovan-2-pico)Cl		-----	3098	1624	1605	1281	501	421	------
	sal-3-pico	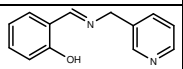	-----	3058	1627	1609	1274	-----	-----	-----
34	Cu(sal-3-pico)Cl_2. $^1/_2H_2O$		3464; 3124-2527	3056	1620	1606	1328	442	372	269

4.4.6 Aminobenzimidazole-based complexes

Table 4.46: Mid and far infrared data for the 2-aminobenzimidazole-based complexes

No.	Compound	Structure	$\nu_{OH/NH}$	ν_{C-H}	$\nu_{C=N_{(imine)}}$	$\nu_{C=N_{(BZI)}}$ / $\nu_{C=C}$	ν_{C-O}	ν_{Cu-O}	ν_{Cu-N}	$\nu_{Cu-N_{(BZI)}}$
	sal-2-AmBZI	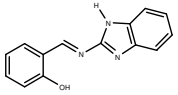	3175-2344	3052	1606	1619, 1570	1276	-----	-----	-----
35	$Cu(sal\text{-}AmBZI)_2.½2H_2O$		3357-2744	3048	1581	1622, 1543	1321	445, 436	393	339, 317
	ovan-2-AmBZI	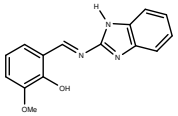	3296; 3087-2339	3069	1600	1622, 1574	1249	-----	-----	-----
36	$Cu(ovan\text{-}AmBZI)_2.H_2O$		3291-2724	3054	1585	1606, 1547	1276	466, 435	399	364
	pvan-2-AmBZI	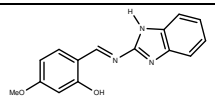	3261; 3109-2287	3053	1597	1628, 1568	1278	-----	-----	-----
37	$Cu(pvan\text{-}AmBZI)_2$		3301	3053	1583	1614, 1542, 1504	1313	513, 468	389	339

4.4.7 *o*-phenylenediamine-based complexes

Table 4.47: Mid and far infrared data for the *o*-phenylenediamine-based complexes

No.	Compound	ν_{OH}	ν_{C-H}	$\nu_{C=N_{(imine)}}$	ν_{C-O}	ν_{Cu-O}	ν_{Cu-N}	ν_{Cu-Cl}
	bis-salphen	3099-2370	3053	1610	1275	-----	-----	-----
38	Cu(bis-salphen)	3468	3018	1607	1310	404	368	-----
	bis-ovanphen	3087-2370	3058	1611	1269	-----	-----	-----
39	Cu(bis-ovan-phen).H_2O	3463	3018	1604	1313	445, 404	366	-----

4.5.0 Raman frequencies (cm^{-1}) for the ligands

4.5.1 Aniline-based ligands

Table 4.48: Raman frequencies (cm^{-1}) for the aniline-based ligands

No.	Compound	Structure	ν_{C-H}	$\nu_{C=N_{(imine)}}$	$\nu_{C=C}$	δ_{C-H}
L1	salaani	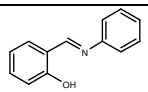	3060	1617	1590, 1572	1188, 1170, 1150
L16	ovaani	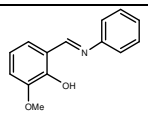	3009, 3002	1614	1591, 1576	1198, 1172
L32	pvaani	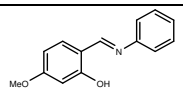	3058	1613	1592, 1575	1195, 1175
L45	vaani	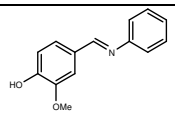	3066, 2938	1623	1586, 1515	1162

4.5.2 Substituted aniline-based ligands

Table 4.49: Raman frequencies (cm^{-1}) for the chloroaniline-based ligands

No.	Compound	ν_{C-H}	$\nu_{C=N(imine)}$	$\nu_{C=C}$	δ_{C-H}
L2	sal-4-cla	3064	1612	1570	1179, 1154
L8	sal-2-cla	3071, 3046	1613	1588, 1574	1191, 1151
L17	ovan-4-cla	3069, 3002	1614	1574	1196, 1173
L23	ovan-2-cla	3064, 3005	1614	1570	1203, 1166
L33	pvan-4-cla	3064, 3017	1615	1591, 1572	1193, 1170
L39	pvan-2-cla	3067, 3015	1607	1581, 1563	1195, 1159
L46	van-4-cla	3062	1624	1600, 1584	1187, 1174, 1158

Table 4.50: Raman frequencies (cm^{-1}) for the bromoaniline-based ligands

No.	Compound	ν_{C-H}	$\nu_{C=N(imine)}$	$\nu_{C=C}$	δ_{C-H}
L3	sal-4-bra	3064	1616	1570	1187, 1173, 1152
L9	sal-2-bra	3069, 3045	1613	1572	1189, 1151
L18	ovan-4-bra	3059	1612	1572	1194, 1174
L24	ovan-2-bra	3077, 3062,	1614	1567	1201, 1167
L34	pvan-4-bra	3062, 3014	1614	1584, 1570	1193, 1172
L40	pvan-2-bra	3062, 3013	1607	1562	1194, 1160
L47	van-4-bra	3061, 2043	1622	1599, 1579	1176, 1159

Table 4.51: Raman frequencies (cm^{-1}) for the methylaniline-based ligands

No.	Compound	ν_{C-H}	$\nu_{C=N(imine)}$	$\nu_{C=C}$	δ_{C-H}
L4	sal-4-tol	3056	1621	1599, 1572	1177, 1155
L10	sal-2-tol	3063, 3020	1619	1598, 1571	1179, 1153
L19	ovan-4-tol	3061, 3024	1616	1599, 1578	1201, 1178
L25	ovan-2-tol	3069, 3053	1615	1594, 1572	1211, 1162, 1115
L35	pvan-4-tol	3059	1628	1605, 1573	1195, 1177
L41	pvan-2-tol	3062, 3032	1611	1592, 1564	1211, 1160,1111
L48	van-4-tol	3054, 2941	1624	1592	1179, 1158

Table 4.52: Raman frequencies (cm^{-1}) for the methoxyaniline-based ligands

No.	Compound	ν_{C-H}	$\nu_{C=N(imine)}$	$\nu_{C=C}$	δ_{C-H}
L5	sal-4-nis	3063, 3014	1626	1603 1572	1190, 1169
L11	sal-2-nis	3071, 3016	1614	1588, 1572	1190, 1171, 1151
L20	ovan-4-nis	3075, 3056	-----	1597, 1578	1199, 1169
L26	ovan-2-nis	3084, 3031	1616	1576	1201, 1168
L36	pvan-4-nis	3072, 3011	-----	1595, 1571	1188, 1171
L49	van-4-nis	3061, 3012	1623	1594	1188, 1153

Table 4.53: Raman frequencies (cm^{-1}) for the nitroaniline-based ligands

No.	Compound	ν_{C-H}	$\nu_{C=N(imine)}$	$\nu_{C=C}$	δ_{C-H}
L6	sal-4-nit	3072	1618	1588, 1566	1178, 1153
L21	ovan-4-nit	3075, 3012	1616	1573	1200, 1177
L37	pvan-4-nit	3070	-----	1585, 1558	1188, 1169

N.B: (-) not observed

Table 4.54: Raman frequencies (cm^{-1}) for the hydroxyaniline-based ligands

No.	Compound	ν_{C-H}	$\nu_{C=N(imine)}$	$\nu_{C=C}$	δ_{C-H}
L7	sal-4-phen	3066	-----	1598, 1572	1188, 1171
L10	sal-2-phen	3077, 3047	1625	1596	1166, 1143
L22	ovan-4-phen	3069	1615	1598, 1576	1197, 1166
L27	ovan-2-phen	3066	1626	1598	1166
L38	pvan-4-phen	3072, 3049	1632	1609	1209, 1171
L42	pvan-2-phen	3076	1627	1593	1180, 1160
L50	van-4-phen	3059	1624	1588	1185, 1159

4.5.3. 1-Aminonaphthalene-based ligands

Table 4.55: Raman frequencies (cm^{-1}) for the 1-aminonaphthalene-based ligands

No.	Compound	Structure	ν_{C-H}	$\nu_{C=N(imine)}$	$\nu_{C=C}$	δ_{C-H}
L13	sal-1-amnaph	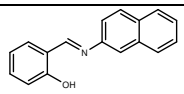	3063	1610	1570	1151
L28	ovan-1-amnaph	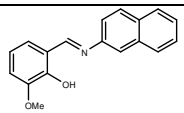	3083, 3059	1609	1565	1223, 1081,1041
L43	pvan-1-amnaph	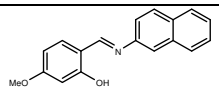	3059	1613	1567	1218, 1118, 1043
L51	van-1-amnaph	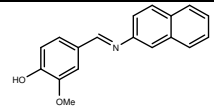	3057, 3013	1621	1596, 1572	1228, 1194, 1151

4.5.4 Aminopyridine-based ligands

Table 4.56: Raman frequencies (cm^{-1}) for the aminopyridine-based ligands

No.	Compound	Structure	ν_{C-H}	$\nu_{C=N(imine)}$	$\nu_{C=C}$	δ_{C-H}
L14	sal-2-ampy	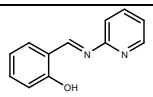	3083, 3062	1614	1568	1209
L15	sal-3-ampy	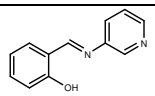	3062, 3008	1616	1567	1197, 1184, 1151
L29	ovan-2-ampy	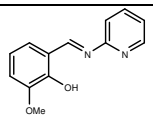	3086, 3061	1609	1588, 1559	1202, 1196
L30	ovan-3-ampy	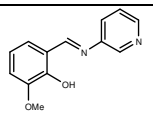	3082, 3062	1615	1567	1209
L44	pvan-3-ampy	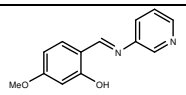	3057, 3018	1611	1565	1186, 1145
L52	van-3-ampy	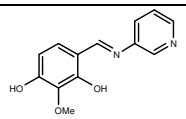	3058	1622	1598, 1579	1179, 1155

4.5.5 Aminomethylpyridine-based ligands

Table 4.57: Raman frequencies (cm^{-1}) for the aminomethylpyridine-based ligands

No.	Compound	Structure	ν_{C-H}	$\nu_{C=N(imine)}$	$\nu_{C=C}$	δ_{C-H}
L31	ovan-2-pico	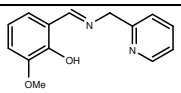	3067	1627	1582	------
L16	sal-3-pico	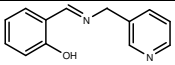	3057	1628	1591, 1575	1236, 1148,1041
L53	van-3-pico	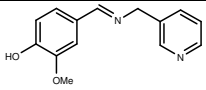	3067	1635	1601, 1582	1217, 1187

4.5.6 2-Aminobenzimidazole-based ligands

Table 4.58: Raman frequencies (cm^{-1}) for the 2-aminobenzimidazole-based ligands

No.	Compound	Structure	ν_{C-H}	$\nu_{C=N(imine)}$	$\nu_{C=C}$	δ_{C-H}
L54	sal-2-AmBZI	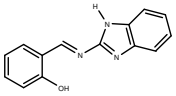	3062	1607	1589, 1568	1150
L55	ovan-2-AmBZI	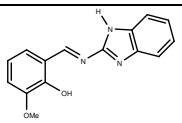	3069	1601	1574	1144
L56	pvan-2-AmBZI	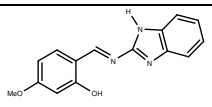	3064	1607	1572	1160

4.6.0 ^{1}H- and ^{13}C-NMR spectral data for the ligands

4.6.1 Aniline-based ligands

Table 4.59: ^{1}H- and ^{13}C-NMR data for the aniline-based ligands

No.	Compound		Ar-O**H**	**H**C=N	**Ar**-N=C	**Ar**-OCH$_3$	Ar-O**C**H$_3$
L1	salaani	^{1}H	13.26 (1H, s)	8.66 (1H, s)	-------	--------	---------
		^{13}C	163.08	161.60	149.00		
L16	ovaani	^{1}H	13.68 (1H, s)	8.67 (1H, s)	---------	---------	3.98 (3H, s)
		^{13}C	(148.66)	163.02	151.99	148.97	56.63
L32	pvaani	^{1}H	13.84 91H,	8.57 (1H, s)	--------	---------	3.88 93H,
		^{13}C	s) 164.44	161.90	148.79	164.47	s) 55.90
L45	vaani	^{1}H	6.15 (1H, s)	8.38 (1H, s)	---------	---------	4.01 (3H, s)
		^{13}C	147.56	160.43	152.70	149.48	56.51

Table 4.60: ^{1}H- and ^{13}C-NMR data for the chloroaniline-based ligands

No.	Compound		Ar-O**H**	**H**C=N	**Ar**-N=C	**Ar**-OCH$_3$	Ar-Cl	Ar-O**C**H$_3$
L2	sal-4-cla	^{1}H	13.01 (1H, s)	8.63 (1H, s)	--------	--------	---------	---------
		^{13}C	163.39	161.56	147.53		133.83	
L8	sal-2-cla	^{1}H	13.21 (1H, s)	8.66 (1H, s)	-------	--------	--------	--------
		^{13}C	163.74	161.81	145.86		130.65	
L17	ovan-4-cla	^{1}H	13.36 (1H, s)	8.64 (1H, s)	---------	---------	---------	3.97 (3H, s)
		^{13}C	148.66	163.44	148.96	151.85	-132.93	56.68
L23	ovan-2-cla	^{1}H	13.65 (1H, s)	8.68 (1H, s)	--------	--------	3.98	3.98 (3H,s)
		^{13}C	149.06	163.51	145.49	152.09	(3H, s)	56.62
L33	pvan-4-cla	^{1}H	13.54 (1H, s)	8.53 (1H, s)	---------	----------	---------	3.88 (3H, s)
		^{13}C	164.16	162.30	147.52	164.60	134.08	55.93
L39	pvan-2-cla	^{1}H	13.77 (1H, s)	8.57 (1H, s)	---------	---------	--------	3.89 (3H, s)
		^{13}C	164.47	162.46	145.76	164.79	134.21	55.95
L46	van-4-cla	^{1}H	6.10 (1H, s)	8.35 (1H, s)	--------	---------	--------	4.02 (3H, s)
		^{13}C	147.56	160.68	149.68	151.17	131.48	56.52

Table 4.61: ^{1}H- and ^{13}C-NMR data for the bromoaniline-based ligands

No.	Compound		Ar-O**H**	**H**C=N	**Ar**-N=C	**Ar**-OCH_3	Ar-Br	Ar-O**C**H_3
L3	sal-4-bra	^{1}H	12.97 (1H, s)	8.63 (1H, s)	---------	---------	133.88	----------
		^{13}C	163.45	161.57	148.03			
L9	sal-2-bra	^{1}H	13.13 (1H, s)	8.64	---------	---------	--------	----------
		^{13}C	163.64	161.73	147.26		134.13	
L18	ovan-4-bra	^{1}H	13.39 (1H, s)	8.63 (1H, s)	---------	----------	---------	3.97 (3H, s)
		^{13}C	147.23	163.38	148.95	151.84	133.01	56.68
L24	ovan-2-bra	^{1}H	13.73 (1H, s)	8.68 (1H, s)	---------	----------	----------	3.98 (3H, s)
		^{13}C	145.41	163.47	149.02	152.02	115.44	56.51
L34	pvan-4-bra	^{1}H	13.52 (1H, s)	8.53 (1H, s)	---------	----------	----------	3.88 (3H, s)
		^{13}C	164.18	162.33	148.01	164.64	134.10	55.93
L40	pvan-2-bra	^{1}H	13.61 (1H, s)	8.55 (1H, s)	---------	---------	---------	3.89 (3H, s)
		^{13}C	147.26	164.85	162.46	164.33	101.60	55.94
L47	van-4-bra	^{1}H	6.10 (1H, s)	8.30 (1H, s)	--------	---------	--------	4.00 (1H, s)
		^{13}C	147.57	160.71	149.70	151.68	132.57	56.54

Table 4.62: ^{1}H- and ^{13}C-NMR data for the methylaniline-based ligands

No.	Compound		Ar-O**H**	**H**C=N	**Ar**-N=C	**Ar**-OCH_3	**Ar**-CH_3	Ar-**C**H_3	Ar-O**C**H_3
L4	sal-4-tol	^{1}H	13.37 (1H, s)	8.66 (1H, s)	---------	---------	----------	2.48 (3H, s)	----------
		^{13}C	162.11	161.56	146.37		137.29	21.42	
L10	sal-2-tol	^{1}H	13.48 (1H, s)	8.62 (1H, s)	----------	----------	---------	2.44 (3H, s)	----------
		^{13}C	162.69	161.65	147.93		133.56	18.68	
L19	ovan-4-tol	^{1}H	13.82 (1H, s)	8.66 (1H, s)	---------	----------	----------	2.42 (3H, s)	3.97 (3H, s)
		^{13}C	148.96	162.03	146.01	151.99	137.40	21.42	56.68
L25	ovan-2-tol	^{1}H	13.85 (1H, s)	8.64 (1H, s)	---------	----------	----------	2.44 (3H, s)	3.99 (3H, s)
		^{13}C	147.37	162.36	148.96	152.12	133.01	18.66	56.57
L35	pvan-tol	^{1}H	13.96 (1H, s)	8.56 (1H, s)	---------	---------	----------	2.41 (3H, s)	3.88 (3H, s)
		^{13}C	164.27	161.01	146.13	164.51	136.73	21.45	55.87

L41	pvan-2-tol	^{1}H ^{13}C	14.04 (1H, s) 147.63	8.52 (1H, s) 164.74	--------- 161.43	--------- 164.49	--------- 133.88	2.44 (3H, s) 18.64	3.89 (3H, s) 55.90
L48	van-4-tol	^{1}H ^{13}C	6.10 (1H, s) 147.53	8.40 (1H, s) 159.87	--------- 149.30	--------- 150.01	---------- 135.86	2.4 (3H, s) 21.45	4.00 (3H, s) 56.52

Table 4.63: ^{1}H- and ^{13}C-NMR data for the methoxyaniline-based ligands

No.	**Compound**		**Ar-O<u>H</u>**	**<u>H</u>C=N**	**<u>Ar</u>-N=C**	**<u>Ar</u>-OCH$_3$**	**Ar-O<u>C</u>H$_3$**	**Ar-O<u>C</u>H$_3$**
L5	sal-4-nis	^{1}H ^{13}C	13.41 (1H, s) 161.44	8.64 160.88	-------- 141.81	--------- 159.30	3.88 (3H, s) 55.95	----------
L11	sal-2-nis	^{1}H ^{13}C	13.41 (1H, s) 161.44	8.64 160.88	-------- 141.81	--------- 159.30	3.88 (3H, s) 55.95	----------
L20	ovan-4-nis	^{1}H ^{13}C	13.85 (1H, s) 148.92	8.64 (1H, s) 160.78	--------- 141.54	---------- 159.36, 151.80,	3.97 (3H, s) 56.66	3.87 (3H, s) 55.95
L26	ovan-2-nis	^{1}H ^{13}C	14.42 149.19	8.74 161.77	--------- 136.79	---------- 153.49, 153.08,	3.97 (3H, s) 56.57	3.93 (3H, s) 56.28
L36	pvan-4-nis	^{1}H ^{13}C	13.97 (1H, s) 164.06	8.54 (1H, s) 160.03	--------- 141.81	---------- 164.18, 158.84	3.87 (3H, s) 55.86	3.87 (3H, s) 55.86
L49	van-4-nis	^{1}H ^{13}C	6.10 (1H, s) 147.52	8.40 (1H, s) 158.64	--------- 149.18	---------- 158.41, 145.62	4.01 (3H, s) 56.49	3.86 (3H, s) 55.90

Table 4.64: ^{1}H- and ^{13}C-NMR data for the nitroaniline-based ligands

No.	**Compound**		**Ar-O<u>H</u>**	**<u>H</u>C=N**	**<u>Ar</u>-N=C**	**<u>Ar</u>-OCH$_3$**	**<u>Ar</u>-NO$_2$**	**Ar-O<u>C</u>H$_3$**
L6	sal-4-nit	^{1}H ^{13}C	12.54 165.84	8.63 161.74	--------- 154.64	----------	--------- 146.50	---------
21	ovan-4-nit	^{1}H ^{13}C	12.86 (1H, s) 149.04	8.68 (1H, s) 165.80	--------- 154.43	---------- 152.04	--------- 146.64	3.98 (3H, s) 56.74
L37	pvan-4-nit	^{1}H ^{13}C	13.10 (1H, s) 165.46	8.58 (1H, s) 164.42	--------- 154.74	--------- 164.47	---------- 146.08	3.90 (3H, s) 56.05

Table 4.65: ^{1}H- and ^{13}C-NMR data for the hydroxyaniline-based ligands

No.	Compound		Ar-O**H**	**H**C=N	**Ar**-N=C	Ar-OCH_3	**Ar**-OH	-OCH_3
L7	sal-4-phen	^{1}H	13.40 (1H, s)	8.80 (1H, s)	---------	---------	9.64 (1H, s)	---------
		^{13}C	157.83	161.03	140.12		157.83	
L13	sal-2-phen	^{1}H	13.78 (1H, s)	8.97 (1H, s)	----------	---------	9.77 (1H, s)	----------
		^{13}C	162.55	161.60	135.80		152.00	
L22	ovan-4-phen	^{1}H	13.58 (1H, s)	8.88 (1H, s)	---------	---------	9.62 (1H, s)	3.82 (3H, s)
		^{13}C	148.74	161.15	139.90	151.32	157.83	56.78
L27	ovan-2-phen	^{1}H	14.44 (1H, s)	8.86 (1H, s)	---------	----------	9.79 (1H, s)	3.80 (3H, s)
		^{13}C	160.73	166.54	151.32	164.68	164.68	56.24
L38	pvan-4-phen	^{1}H	13.97 (1H, s)	8.80 (1H, s)	--------	----------	9.63 (1H, s)	3.80 (3H, s)
		^{13}C	163.76	160.48	139.97	163.94	157.33	56.27
L42	pvan-2-phen	^{1}H	14.40 (1H, s)	8.85 (1H, s)	--------	----------	9.77 (1H, s)	3.80 (3H, s)
		^{13}C	164.70	160.73	137.37	166.52	151.29	56.55
L50	van-4-phen	^{1}H	9.53 (1H, s)	8.43 (1H, s)	---------	---------	9.53 (1H, s)	3.84 (3H, s)
		^{13}C	148.80	157.99	144.02	150.52	156.54	56.36

Table 4.66: ^{1}H- and ^{13}C-NMR data for the 1-aminonaphthalene based ligands

No.	Compound		Ar-O**H**	**H**C=N	**Ar**-N=C	**Ar**-OCH_3	Ar-O**C**H_3
L14	sal-1-amnaph	^{1}H	13.40 (1H, s)	8.75 (1H, s)	----------	----------	----------
		^{13}C	164.05	161.67	146.68		
L28	ovan-1-amnaph	^{1}H	13.91 (1H, s)	8.77 (1H, s)	---------	----------	4.02 (1H, s)
		^{13}C	149.04	163.82	146.20	152.05	56.67
L43	pvan-1-amnaph	^{1}H	13.90 (1H, s)	8.66 (1H, s)	----------	---------	3.87 (3H, s)
		^{13}C	164.28	162.99	146.67	164.59	55.86
L51	van-1-amnaph	^{1}H	6.06 (1H, s)	8.47 (1H, s)	---------	----------	4.07 (3H, s)
		^{13}C	147.57	160.43	149.54	150.02	56.58

Table 4.67: ^{1}H- and ^{13}C-NMR data for the aminopyridine-based ligands

No.	Compound		Ar-OH	N=C**H**,py	**H**C=N	**Ar**-N=C	Ar-OCH_3	-OCH_3
L15	sal-2-ampy	^{1}H	13.50 (1H, s)	9.50(1H, s)	8.60 (1H, s)	---------	---------	---------
		^{13}C	165.20	149.40	162.31	158.04		
L16	sal-3-ampy	^{1}H	12.80 (1H, s)	8.60(1H, d); 8.57(1H, d)	8.67 (1H, s)	---------	---------	----------
		^{13}C	164.97	148.41,	161.56	143.49		
L29	ovan-2-ampy	^{1}H	14.00 (1H, s)	9.40 (1H, s)	8.40 (1H, s)	---------	----------	3.97 (1H, s)
		^{13}C	152.92	149.40	165.03	157.62	148.90	56.60
L30	ovan-3-ampy	^{1}H	13.10 (1H, s)	8.68 (1H, s); 8.60(1H, s)	8.59 (1H, s)	---------	---------	3.82 (3H, s)
		^{13}C	148.94	148.48, 144.92	165.00	143.46	151.73	56.78
L44	pvan-3-ampy	^{1}H	13.27 (1H, s)	8.56(1H, s); 8.52(1H, d)	8.56 (1H, s)	--------	----------	3.87 (3H, s)
		^{13}C	163.99)	147.84, 144.93	163.81	143.53	164.83	55.95
L52	van-3-ampy	^{1}H	7.02 (1H, s)	8.51(1H,d); 8.49(1H, dd)	8.38 (1H, s)	----------	----------	4.00 (3H, s)
		^{13}C	147.83	148.59, 146.94	162.16	142.98	150.30	56.51

Table 4.68: ^{1}H- and ^{13}C- NMR data for the 2-aminomethylpyridine-based ligands

No.	Compound		Ar-OH	N=C**H**,py	**H**C=N	-CH_2	Ar-OCH_3	-OCH_3
L31	ovan-2-pico	^{1}H	13.74	8.60 (1H, d)	8.56 (1H, s)	4.99 (2H, s)	-------	3.94 (3H, s)
		^{13}C	152.09	148.93	167.25	65.16	149.79	56.60
L17	sal-3-pico	^{1}H	13.00 (1H, s)	8.60 (1H, d)8.558 (1H, d)	8.50 (1H, s)	4.85 (2H, s)	---------	---------
		^{13}C	166.88	149.60, 149.32	161.33	61.19		
L53	van-3-pico	^{1}H	6.36 (1H, s)	8.65 (1H, s); 8.55 (1H, d)	8.34 (1H, s)	4.82 (2H, s)	----------	3.96 (3H, s)
		^{13}C	149.53	148.49, 147.91	163.18	62.54	149.62	56.35

Table 4.69: ^{1}H- and ^{13}C-NMR for the 2-aminobenzimidazole ligands

No.	Compound		Ar-OH	N-H	HC=N	C=N$_{(Im)}$	Ar-OCH$_3$	Ar-OCH$_3$
L54	sal-2-AmBZI	^{1}H ^{13}C	12.76 (1H, s) 166.40	12.15 (1H, s)	9.67 (1H, s) 161.43	---------- 154.82	--------	---------
L55	pvan-2-AmBZI	^{1}H ^{13}C	12.70 (1H, s) 165.71	12.63 (1H, s)	9.54 (1H, s) 164.04	---------- 154.09	---------- 166.03	3.85 (3H, s) 56.55
L56	ovan-2-AmBZI	^{1}H ^{13}C	12.76 (1H, s) 148.89	12.05 (1H, s)	9.66 (1H, s) 166.58	---------- 154.74	---------- 151.42	3.86 (3H, s) 56.77

Table 4.70: ^{1}H- and ^{13}C-NMR for the *o*-phenylenediamine-based ligands

No.	Compound		Ar-OH	HC=N	Ar-N=C	Ar-OCH$_3$	Ar-OCH$_3$
L57	bis-salphen	^{1}H ^{13}C	13.09 (2H, s) 164.17	8.67 (2H, s) 161.79	-------- 143.01	--------	---------
L58	bis-ovanphen	^{1}H ^{13}C	13.23 (2H, s) 148.96	8.64 (2H, s) 164.69	-------- 142.96	---------- 152.00	3.85 (6H, s) 56.57

4.7.0 UV/Visible spectral data for the ligands

Table 4.71: UV/Visible data for the aniline-based ligands

No.	Compound	Structure	Solvent	200-240 nm	250-300 nm	305-350 nm	> 350 nm
L1	salaani	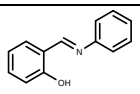	Methanol DMF	----- -----	268, 298 271, 300	314, 334 316, 340	----- -----
L16	ovaani	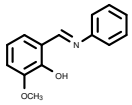	Methanol DMF	210, 225 -----	279 279	312 311	460 -----
L32	pvaani	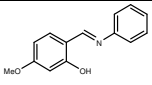	Methanol DMF	224, 236 -----	285 288 (bra)	334 337	412 -----

L45	vaani	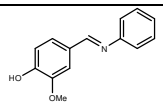	Methanol DMF	227 -----	284 284	326 327	441 -----

Table 4.72: UV/Visible data for the chloroaniline-based ligands

No.	**Compound**	**Solvent**	**200-240 nm**	**250-300 nm**	**305-350 nm**	**> 350 nm**
L2	sal-4-cla	Methanol DMF	208, 230 (sh) -----	271, 317 274	341 304, 320, 342	----- -----
L8	sal-2-cla	Methanol DMF	209, 227 -----	272 277	324, 342 327, 344	----- ------
L17	ovan-4-cla	Methanol DMF	227 -----	280 283	315 318	459 -----
L23	ovan-2-cla	Methanol DMF	215, 227 -----	284 284	320 321	471 373
L33	pvan-4-cla	Methanol DMF	228, 237 -----	291 292	339 341	415 -----
L39	pvan-2-cla	Methanol DMF	----- -----	287 284	336 337	413 -----
L46	van-4-cla	Methanol DMF	231 -----	285 284	330 333	442 -----

Table 4.73: UV/Visible data for the bromoaniline-based ligands

No.	Compound	Solvent	200-240 nm	250-300 nm	305-350 nm	> 350 (nm)
L3	sal-4-bra	Methanol	-----	268	301, 318, 340	-----
		DMF	-----	274	304, 320, 343	-----
L9	sal-2-bra	Methanol	214, 227	285	319	470
		DMF	-----	280	327, 345	-----
L18	ovan-4-bra	Methanol	-----	278	315	458
		DMF	------	282	318	------
L24	ovan-2-bra	Methanol	211, 228	273	325, 344	------
		DMF	-----	287	322	371
L34	pvan-4-bra	Methanol	227, 237	292	340	415
		DMF	-----	291	343	-----
L40	pvan-2-bra	Methanol	-----	289	337	414
		DMF	-----	291	337	-----
L47	van-4-bra	Methanol	230	285	331	444
		DMF	------	288	333	-----

Table 4.74: UV/Visible data for the methylaniline-based ligands

No.	Compound	Solvent	200-240 nm	250-300 nm	305-350 nm	> 350 nm
L4	sal-4-tol	Methanol	-----	268	302(sh),318,340	441
		DMF	-----	268	302,318,340	-----
L10	sal-2-tol	Methanol	208, 224	266	337	442
		DMF	-----	-----	326, 342	-----
L19	ovan-4-tol	Methanol	240	272	317	447
		DMF	-----	280	319	-----

L25	ovan-2-tol	Methanol DMF	212, 225 -----	276 279	320 322	455 -----
L35	pvan-4-tol	Methanol DMF	224, 238 -----	283 282	336 343 (br)	414 -----
L41	pvan-2-tol	Methanol DMF	----- -----	281 285	328 340	404 420
L48	van-4-tol	Methanol DMF	227 -----	283 285	329 331	430 -----

Table 4.75: UV/Visible data for the methoxyaniline-based ligands

No.	**Compound**	**Solvent**	**200-240 nm**	**250-300 nm**	**305-350 nm**	**> 350 nm**
L5	sal-4-nis	Methanol DMF	208 -----	268 273, 293 (sh), 304(sh)	348 325 9sh)	434 -----
L11	sal-2-nis	Methanol DMF	205, 228 -----	268 272	346 352 (br)	450 -----
L20	ovan-4-nis	Methanol DMF	226 -----	276 280, 292(sh), 304 (sh)	335 333	463 374 (br)
L26	ovan-2-nis	Methanol DMF	216, 229 -----	280 280	346 327, 338	462 -----
L36	pvan-4-nis	Methanol DMF	213, 236 -----	286, 293 282 (br)	343 349 (br)	420 -----
L49	van-4-nis	Methanol DMF	227 -----	284 286	336 337	441 -----

Table 4.76: UV/Visible data for the nitroaniline-based ligands

No.	Compound	Solvent	200-240 nm	250-300 nm	305-350 nm	> 350 nm
L6	sal-4-nit	Methanol	212 (sh)	322 (br)	356	------
		DMF	-----	-----	330(br)	358(br)
L21	ovan-4-nit	Methanol	220	-----	336	-----
		DMF	-----	-----	336 (br)	-----
L37	pvan-4-nit	Methanol	-----	-----	-----	359 (br)
		DMF	-----	-----	-----	372 (br)

Table 4.77: UV/Visible data for the hydroxyaniline-based ligands

No.	Compound	Solvent	200-240 nm	250-300 nm	305-350 nm	> 350 nm
L7	sal-4-phen	Methanol	-----	275, 301	301, 342	-----
		DMF	-----	271, 294	306, 325	352
L12	sal-2-phen	Methanol	-----	275	334	444
		DMF	-----	271	348	431
L22	ovan-4-phen	Methanol	240	275, 293	336	459
		DMF	-----	279	333	374
L27	ovan-2-phen	Methanol	-----	257, 280	350	450
		DMF	-----	279	347 (br)	466
L38	pvan-4-phen	Methanol	-----	244,283,295	342	419
		DMF	-----	293	3440	370
L42	pvan-2-phen	Methanol	-----	-----	337	421
		DMF	-----	285	351	430
L50	van-4-phen	Methanol	-----	243, 282	337	-----
		DMF	-----	287	338	-----

Table 4.78: UV/Visible data for the 1-aminonaphthalene-based ligands

No.	Compound	Structure	Solvent	200-240 nm	250-300 nm	305-350 nm	> 350 nm
L13	sal-1-amnaph	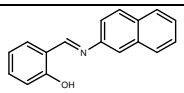	Methanol	-----	266	294	352
L28	ovan-1-amnaph	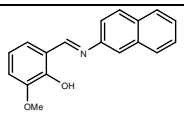	Methanol DMF	----- -----	263 275, 294	347 346	----- -----
L43	pvan-1-amnaph	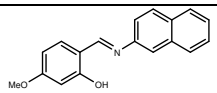	Methanol DMF	228 -----	----- 284	342 347	381 -----
L51	van-1-amnaph	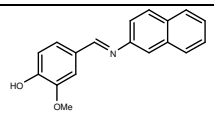	Methanol DMF	210, 231 -----	----- 284	320, 337 323, 346	----- -----

Table 4.79: UV/Visible data for the aminopyridine-based ligands

No.	Compound	Structure	Solvent	200-240 nm	250-300 nm	301-350 nm	> 350 nm
L14	sal-2-ampy	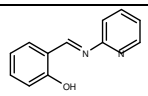	Methanol DMF	207 -----	268 275 (sh)	304, 345 307, 349	----- ------
L15	sal-3-ampy	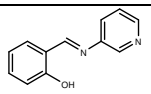	Methanol DMF	203, 217 (sh) -----	275 278	340 341	------ -----
L29	ovan-2-ampy	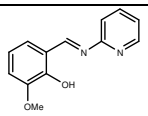	Methanol DMF	------ -----	----- 278	312 318	475 371
L30	ovan-3-ampy	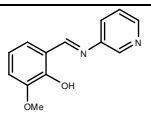	Methanol DMF	225 -----	286 -----	`----- -----	----- 363
L44	pvan-3-ampy	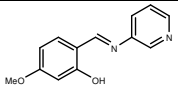	Methanol DMF	235 -----	288 293	331 338	415 -----

L52	van-3-ampy	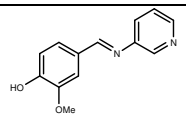	Methanol DMF	239 -----	289 284	328 327	----- -----

Table 4.80: UV/Visible data for the aminomethylpyridine-based ligands

No.	**Compound**	**Structure**	**Solvent**	**200-240 nm**	**250-300 nm**	**305-350 nm**	**> 350 nm**
L16	sal-3-pico	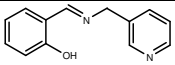	Methanol DMF	215 -	256 -	316 317	- -
L31	ovan-2-pico	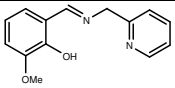	Methanol DMF	234 -----	277 ------	----- 334	388, check again -----
L53	van-3-pico	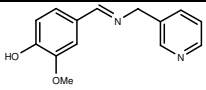	Methanol DMF	206, 228 -----	270 272	305 303	401 -----

Table 4.81: UV/Visible data for the 2-aminobenzimidazole-based ligands

No.	**Compound**	**Structure**	**Solvent**	**200-240 nm**	**250-300 nm**	**305-350 nm**	**> 350**
L54	sal-2-AmBZI	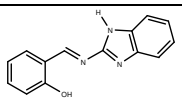	DMF	-----	-----	-----	367
L55	ovan-2-AmBZI	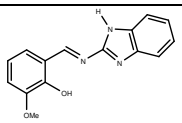	DMF	-----	282	-----	357
L56	pvan-2-AmBZI	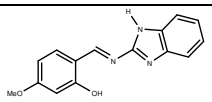	DMF	-----	284	-----	370

Table 4.82: UV/Visible data for the *o*-phenylenediamine-based ligands

No.	Compound	Solvent	200-240 nm	250-300 nm	305-350 nm	> 350
L57	bis-salphen	DMF	-----	260,	332,	446
L58	bis-ovanphen	DMF	-----	282	336	------

4.8.0 UV/Visible spectral data for the complexes

Table 4.83: UV/Visible data for the aniline-based complexes

No.	Compound	Solvent	200-240 nm	250-300 nm	305-350 nm	> 350 nm
	salaani	Methanol	-----	268, 298	314, 334	-----
1	$Cu(salaani)_2Cl_2.2½\,2H_2O$	Methanol	230	280	-----	383, 713
	ovaani	Methanol	210, 225	279	312	460
2	$Cu(ovaani)_2Cl_2.H_2O.½\,2EtOH$	Methanol	231	287	-----	391, 748

Table 4.84: UV/Visible data for the chloroaniline-based complexes

No.	Compound	Solvent	200-240 nm	250-300 nm	305-350 nm	> 350 nm
	sal-4-cla	Methanol	208, 230 (sh)	271, 317	341	-----
3	$Cu(sal\text{-}4\text{-}cla)_2Cl_2.2H_2O$	Methanol	240	282	386	810
	sal-2-cla	Methanol	209, 227	272	324, 342	-----
4	$Cu(sal\text{-}2\text{-}cla)_2$	Methanol	213, 238	398	-----	667
	ovan-4-cla	Methanol	227	280	315	459
5	$Cu(ovan\text{-}4\text{-}cla)_2$	Methanol	234	293	396	405, 517
	ovan-2-cla	Methanol	215, 227	284	320	471
6	$Cu(ovan\text{-}2\text{-}cla)_2$	Methanol	236	292	------	403, 661

Table 4.85: UV/Visible data for the bromoaniline-based complexes

No.	Compound	Solvent	200-240 nm	250-300 nm	305-350 nm	> 350 (nm)
	sal-4-bra	Methanol	-----	268	301, 318, 340	-----
7	$Cu(sal\text{-}4\text{-}bra)_2Cl_2.H_2O$	Methanol	223, 240	282	-----	385, 804
	sal-2-bra	Methanol	214, 227	285	319	470
8	$Cu(sal\text{-}2\text{-}bra)_2$	Methanol	226	281	-----	393, 663
	ovan-4-bra	Methanol	-----	278	315	458
9	$Cu(ovan\text{-}4\text{-}bra)_2Cl_2.H_2O$	Methanol	-----	284	-----	394, 756, 819
	ovan-2-bra	Methanol	211, 228	273	325, 344	-----
10	$Cu(ovan\text{-}2\text{-}bra)_2$	Methanol	235	292	-----	404, 665

Table 4.86: UV/Visible data for the methylaniline-based complexes

No.	Compound	Solvent	200-240 nm	250-300 nm	305-350 nm	> 350 nm
	sal-4-tol	Methanol	-----	268	302(sh),318,340	441
11	$Cu(sal\text{-}4\text{-}tol)_2Cl_2.H_2O$	Methanol	------	282	-----	383, 750
	sal-2-tol	Methanol	208, 224	266	337	442
12	$Cu(sal\text{-}2\text{-}tol)_2$	Methanol	229	-----	-----	373, 394, 657
	ovan-4-tol	Methanol	240	272	317	447
13	$Cu(ovan\text{-}4\text{-}tol)_2Cl_2.2½H_2O$	Methanol	231	288	-----	288, 388, 794
	Ovan-2-tol	Methanol	212, 225	276	320	455
14	$Cu(ovan\text{-}NH)_2.H_2O$	Methanol	237	274	------	378, 654
	pvan-2-tol	Methanol	-----	281	328	404
15	Cu(pvan-2-tol)	DMF	------	2286	351	472

Table 4.87: UV/Visible data for the methoxyaniline-based complexes

No.	Compound	Solvent	200-240 nm	250-300 nm	305-350 nm	> 360 nm
	sal-4-nis	Methanol	208	268	348	434
16	$Cu(sal\text{-}4\text{-}nis)_2$	Methanol	230	273, 299	-----	384, 501, 674
	sal-2-nis	Methanol	205, 228	268	346	450
17	Cu(sal-2-nis)2	Methanol	216	283	-----	390, 683
	ovan-4-nis	Methanol	226	276, 280, 292(sh), 304(sh)	333, 335	463
18	$Cu(ovan\text{-}NH)_2.H_2O$	Methanol	237	274	------	378, 654
	ovan-2-nis	Methanol	216, 229	280	346	462
19	$Cu(ovan\text{-}NH)_2.H_2O$	Methanol	237	274	------	378, 654

Table 4.88: UV/Visible data for the nitroaniline-based complexes

No.	Compound	Solvent	200-240 nm	250-300 nm	305-350 nm	> 360 nm
	sal-4-nit	DMF	-----	322 (br)	356	-----
20	$Cu(sal\text{-}4\text{-}nit)_2$	DMF	-----	-----	-----	374, 423 (br)
	ovan-4-nit	DMF	-----	-----	336	-----
21	$Cu(ovan\text{-}4\text{-}nit)_2Cl_2.2EtOH$	DMF	-----	-----	307	412, 770

Table 4.89: UV/Visible data for the hydroxyaniline-based complexes

No.	Compound	Solvent	200-240 nm	250-300 nm	305-350 nm	> 360 nm
	sal-4-phen	DMF	------	271, 294	306, 325	352
22	$Cu(Sal\text{-}4\text{-}phen)_2$	DMF	------	-----	341	470
	sal-2-phen	Methanol	-----	275	334	444
23	$Cu_2(sal\text{-}2\text{-}phen)_2$	Solid reflectance	-----	-----	-----	409, 676

	ovan-4-phen	Methanol	240	275, 293	336	459
24	Cu(ovan-4-phen)$_2$.Cl$_2$H$_2$O	Methanol	-----	280	313	389, 502
	ovan-2-phen	Methanol	-----	280	350	450
25	Cu$_2$(ovan-2-phen)$_2$	Solid reflectance	-----	-----	-----	435, 628
	pvan-2-phen	Methanol	-----	-----	337	421
26	Cu$_2$(pvan-2-phen)$_2$	Solid reflectance	-----	-----	-----	421, 641

Table 4.90: UV/Visible data for the 1-aminonaphthalene-based complexes

No.	**Compound**	**Solvent**	**200-240 nm**	**250-300 nm**	**305-350 nm**	**> 360 nm**
	sal-1-amnaph	DMF	-----	265	294	352
27	Cu(sal-1-amnaph)$_2$	DMF	-----	291	335	515
	ovan-1-amnaph	Methanol	209, 226	274	346	458
28	Cu(ovamnaph)$_2$	Methanol	218	284	-----	403, 532

Table 4.91: UV/Visible data for the aminopyridine-based complexes

No.	**Compound**	**Solvent**	**200-240 nm**	**250-300 nm**	**301-350 nm**	**> 360 nm**
	sal-2-ampy	Methanol	207	268	304, 345	-----
29	Cu(sal-2-ampy)$_2$Cl$_2$	Methanol	210, 236	-----	-----	403, 647
	sal-3-ampy	DMF	-----	278	340	-----
30	Cu(sal-3-ampy)$_2$Cl$_2$.$^1/_2$H$_2$O	DMF	-----	279	340	804
	ovan-2-ampy	Methanol	-----	-----	312	475
31	Cu(ovan-2-ampy)Cl$_2$.H$_2$O	Methanol	233	300	-----	416, 715
	ovan-3-ampy	DMF	-----	-----	301	363
32	Cu(ovan-3-ampy)$_2$Cl$_2$.H$_2$O	DMF	-----	293	-----	486, 634

Table 4.92: UV/Visible data for the aminomethylpyridine-based complexes

No.	Compound	Solvent	200-240 nm	250-300 nm	305-350 nm	> 360 nm
	sal-3-pico	DMF	-----	-----	317	-----
33	$Cu(sal\text{-}3\text{-}pico)_2Cl_2.{}^1/_2H_2O$	DMF	-----	268	306	370, 513, 685
	ovan-2-pico	Methanol	221	262, 299	335	425
34	Cu(ovan-2-pico)Cl	Methanol	234	277	-----	388, 629

Table 4.93: UV/Visible data for the 2-aminobenzimidazole-based complexes

No.	Compound	Solvent	200-240 nm	250-300 nm	305-350 nm	> 360 nm
	sal-AmBZI	DMF	----	-----	-----	367
35	$Cu(sal\text{-}AmbZI)_2.½H_2O$	DMF	-----	-----	322	359, 415, 692
	ovan-AmBZI	DMF	-----	282	-----	357
36	$Cu(ovan\text{-}AmbZI)_2.H_2O$	DMF	-----	-----	-----	352, 412, 755
	pvan-AmBZI	DMF	-----	284	-----	370
37	$Cu(pvan\text{-}AmBZI)_2$	DMF	----	-----	319	375, 702

Table 4.94: UV/Visible data for the *o*-phenylenediamine-based complexes

No.	Compound	Solvent	200-240 nm	250-300 nm	305-350 nm	> 360 nm
	bis-salphen	DMF	----	260	332	446
38	Cu(bis-salphen)	DMF	-----	-----	307	422, 540
	bis-ovanphen	DMF	-----	282	336	-----
39	$Cu(bis\text{-}ovanphen).H_2O$	DMF	-----	-----	322, 341	360, 438, 554

4.9.0 Selected bond lengths and bond angles for the crystals

Table 4.95: Selected bond lengths and bond angles for $[Cu(ovan\text{-}NH)_2].H_2O$

Bond lengths	(Å)	**Bond angles**	(°)
Cu1-O1	1.9447	O1-Cu1-N1	92.19
Cu1-N1	1.915	O1-Cu1-O1	180.00
Cu1-O1	1.9447	O1-Cu1-N1	87.81
Cu1-N1	1.915	N1-Cu1-O1	87.81
N1-H1	0.78	N1-Cu1-N1	180.00
N1-C7	1.279	O1-Cu1-N1	92.19
O3-H3A	0.79		
O3-H3B	0.73		

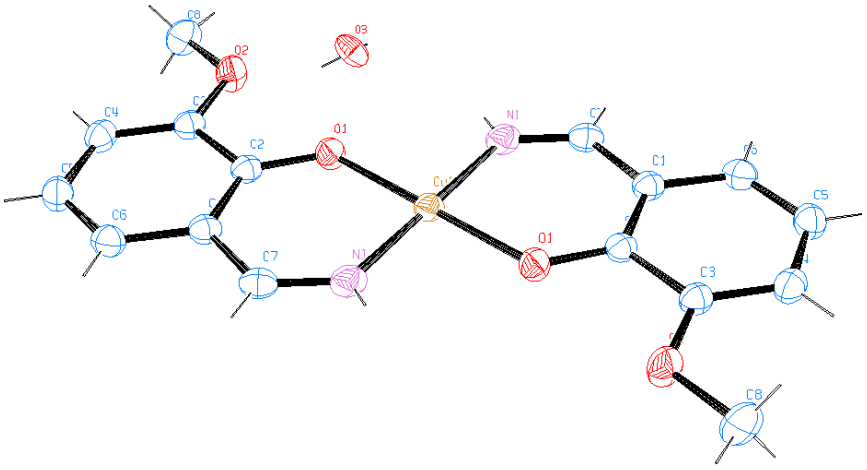

Fig. 4.1: Labelled diagram of the ORTEP view of the monomeric unit of $[Cu(ovan\text{-}NH)_2].H_2O$

Table 4.96: Selected bond angles and bond lengths for [Cu(ovan-2-pico)Cl]

Bond lengths	(Å)	**Bond angles**	(°)
Cu1-Cl1	2.2510	Cl1-Cu1-O1	89.76
Cu1-O1	1.912	Cl1-Cu1-N1	174.24
Cu1-N1	1.941	Cl-Cu1-N2	95.94
Cu1-N2	2.012	O1-Cu1-N1	92.43
N1-C8	1.292	O1-Cu1-N2	174.17
N1-C9	1.464	N1-Cu1-N2	82.01
N2-C10	1.343	Cu1-O1-C2	127.9
N2-C14	1.349	Cu1-N1-C8	126.4

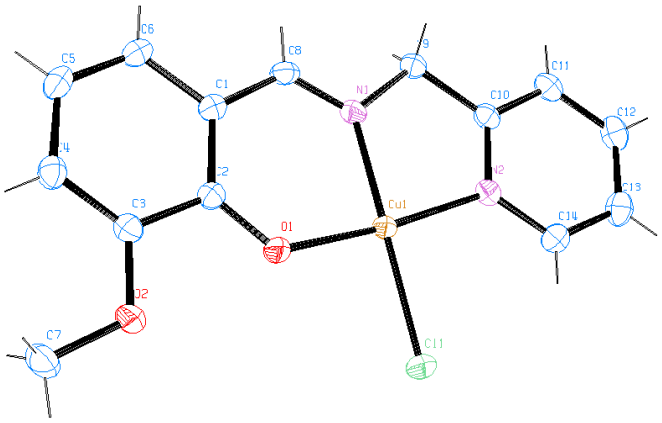

Fig.4.2: Labelled diagram of the ORTEP view of the monomeric unit of [Cu(ovan-2-pico)Cl]

Table 4.97: Selected bond angles and bond lengths for the monomeric unit of [Cu(bis-salphen)]

Bond lengths	(Å)	**Bond angles**	(°)
Cu1-O1	1.841	O1-Cu1-O2	84.56
Cu1-O2	1.846	O1-Cu1-N1	94.4
Cu1-N1	1.864	O1-Cu1-N2	178.9
Cu1-N2	1.864	O2-Cu1-N1	178.4
O1-C1	1.294	O2-Cu1-N2	94.54
O2-C20	1.284	N1-Cu1-N2	86.5
N1-C7	1.285	Cu1-O1-C1	128.5
N1-C8	1.424	Cu1-O2-C20	128.1
N2-C13	1.434	Cu1-O2-C7	125.9
N2-C14	1.295	Cu1-N1-C7	112.4

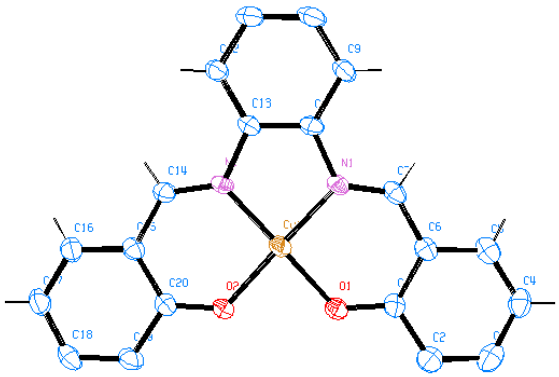

Fig. 4.3: Labelled diagram of the ORTEP view of the monomeric unit of [Cu(bis-salphen)]

Table 4.98: Selected bond lengths and bond angles for the monomeric unit of [Cu(bis-ovanphen)(H_2O)]

Bond lengths	(Å)	**Bond angles**	(°)
Cu1-O1	1.927	O1-Cu1-O2	88.58
Cu-O2	1.912	O1-Cu1-O3	96.23
Cu1-O3	2.327	O1-Cu1-N1	93.08
Cu1-N1	1.966	O1-Cu1-N2	171.51
Cu-N2	1.966	O2-Cu1-O3	95.82
O3-H3B	0.83	O2-Cu1-N1	170.25
O3-H3C	0.83	O2-Cu1-N2	93.53
N1-C7	1.298	O3-Cu1-N1	93.56
N1-C8	1.415	O3-Cu1-N2	91.75
N2-C13	1.410		
N2-C14	1.299		
C2-O4	1.356		
C19-O5	1.358		
O4-C21	1.423		
O5-C22	1.435		

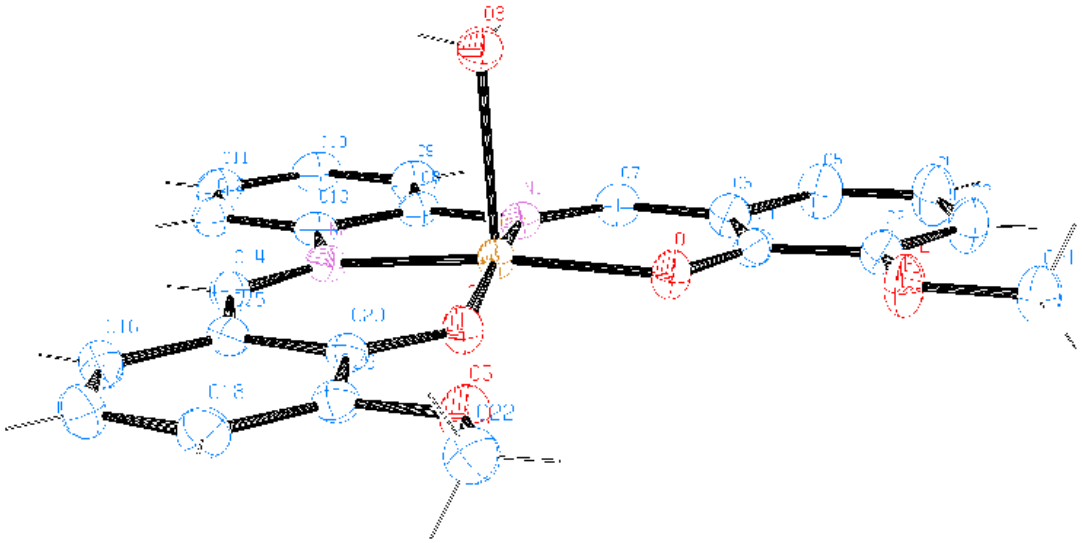

Fig. 4.4: Labelled diagram of the ORTEP view of the monomeric unit of [Cu(bis-ovanphen)(H_2O)]

5.0.0 Discussion

The Schiff base ligands were grouped into four categories based on the type of the aldehyde used for the synthesis. Salicylaldehyde, *o*-vanillin, *p*-vanillin and vanillin were condensed respectively with aniline and substituted anilines, 1-aminonaphthalene, aminopyridine, aminomethylpyridine, 2-aminobenzimidazole and *o*-phenylenediamine. Thus, the ligands were further categorized into six sub-divisions depending on the nature of the amino moiety. Though, synthesis of all the proposed Schiff bases were attempted, the isolation of all the vanillin analogues of the *o*-substituted anilines could not be achieved, probably due to electronic effect. Also, not all the aminopyridine and aminomethylpyridine were isolated and this might be due to a decrease in the basicity of the lone pairs on the amino group, occasioned by the position of the azine nitrogen and the acidity of the carbonyl on the aldehyde. For instance, the pKa value of 2-picolylamine is 8.8 while 3-picolylamine has a pKa value of 8.34 and likewise, 2-ampy with a pKa value of 6.9, is less basic than 4-aminopyridine, pKa value of 9.2. Those that were not synthesized include sal-2-pico, sal-4-ampy, pvan-2-ampy, pvan-4-ampy, pvan-2-pico, pvan-3-pico, van-2-ampy and van-4-ampy.

All the Schiff base ligands were obtained in high purity with good yield. The analytical and physicochemical data for the ligands are presented in tables 4.1-4.12. The rate and ease of formation of the ligands were influenced by the nature of the aldehydes and the amines that were used in the synthesis. Salicylaldehyde, *o*-vanillin and *p*-vanillin Schiff bases formed more readily compared with their vanillin analogues. This was probably due to the presence of the hydroxyl group at the ortho position of the carbonyl functional group which results in stabilization of the condensed product through tautomerization. Likewise, the Schiff base ligands were intensely coloured, varying between creamy to orange and suffices to mention that the presence and position of the hydroxy and methoxy groups on the aldehyde moeity highly influenced the intensity of the observed colour. The *o*-vanillin analogues of the synthesized ligands have the most intense colour. For instance, ligands L1 (salaani) and L32 (pvaani) have yellow colour

while ligand L16 (ovaani) was orange; ligand L45 (vaani) was however creamy. Likewise, the nature of the Schiff base ligands equally impact on the colour of the isolated complexes; for instance all the ortho-hydroxyl-based complexes were green while most of the *p*-substituted analogues were brownish in colour. All the complexes melted at a higher temperature than the corresponding Schiff base ligands.

Kovacic [12] reported only the synthesis of some of the salicylaldehyde analogues of the substituted anilines based Schiff bases while Shaibu [224] have equally prepared the Co(II) complexes derivatives of aniline, 1-aminonaphthalene, 2-,3- and 4-aminopyridine as well as 2- and 3-aminomethylpyridine, using salicylaldehyde, *o*-vanillin, *p*-vanillin and vanillin.

However, the biological study of the Cu(II) complexes of the Schiff base ligands has not been previously conducted.

5.1.0: ^{1}H- and ^{13}C-NMR study of the ligands

The question of the exact structure of Schiff bases has long been controversial [7]. This is because the keto-amine / enol-imine tautomer is sensitive to the physical state, the nature of solvent, as well as the effects of substituents. In particular, some cases have been reported [7] where a ketimine form seems to have greater stability than the enol-imine tautomer . The azomethine proton and the enol proton chemical shifts can be used to evaluate the position of the keto-amine / enol tautomer equilibrium of Schiff bases. Any significant presence of the keto-amine tautomer is expected to split the methine proton, with the concomitant loss of the hydroxyl proton. The positions of the chemical shifts are also sensitive to the electronic effects of substituents, and this may be correlated with the Hammett substituent parameters [101, 225, 226]. Any significant presence of the keto-amine tautomer is also expected to be reflected in the aromatic protons, with the quinoidal form undergoing downfield shifts [227]. A better differentiation between the quinoidal and the benzoid forms can be obtained from the ^{13}C-NMR spectra.

The NMR spectra of all the compounds were run in deuterated chloroform, the only exception being the 2-and 4-aminophenol Schiff base ligands which were done in dimethylsufoxide.

5.1.1: The NMR spectral data of the aniline-based ligands

In this group, the focus is principally on the methine and the hydroxyl protons. The prevalence of the enol form for Schiff bases derivatives of 2-hydroxynaphthone and salicylaldehyde has been reported [7]. It has been shown that salicylaldimine Schiff base ligand (figure 1.2, page 11), with R=H, exists solely in the enol form [228], since no splitting of the methine proton was noted.

Likewise, the NMR spectra of some substituted N-arylsalicylaldimines have been studied and the hydroxyl protons were found at δ 13.46-11.83 pap while the methine proton, N=CH, appeared as a singlet at δ 8.70-8.35 ppm. It was discovered that a correlation existed between the hydroxyl proton shielding and the electronic effects of the substituents. The methine proton chemical shift was not substituent-dependent. The electronic effect of the substituents on hydrogen bonding was understood to occur directly by modifying the capacity of the nitrogen atom for participation in hydrogen bonding rather than through the conjugation of the heterocyclic ring which would have favoured a keto-imine tautoumer. It has been shown [225, 226] that the electronic structure of the azomethine group is more sensitive to substitution in the benzaldehyde ring rather than in the aniline ring, with an electron donating substituent causing a small shift to higher field of the azomethine proton by increasing the electron density on the carbon atom.

The characteristic NMR spectral data for the aniline based Schiff base ligands under study are presented in tables 4.59-4.65. The OH proton absorbed downfield at δ 13.97-12.54 ppm due to hydrogen bonding with the imine nitrogen while the methine proton (HC=N) appeared as a singlet at δ 8.97-8.30 ppm. It should be mentioned that the electronic effect of the methoxyl group equally affected the extent of the hydrogen bonding as reflected in the chemical shift values for the salicylaldimine, *o*-vanillin and *p*-vanillin analogues. It has been reported [101] that the strong intramolecular bonding in the ligands leads to a large downfield shift of the hydroxyl proton resonance which is related to the electronic effects of the substituents measured by their Taft [103] substituent's parameters, σ^*. A plot of OH chemical shift values of the *p*-substituted anils under study against Hammett substituent parameters is presented in figure 5.1. An r^2 value of 0.98205 indicates a good correlation between the electronic effect of the substituents and the resonance frequency of the hydroxyl proton in aprotic solvent. According to Percy and Thornton

[101], an increase in the shielding of the OH proton is produced by electron withdrawing effects which have the effect of decreasing the electron density in the N-H bond.

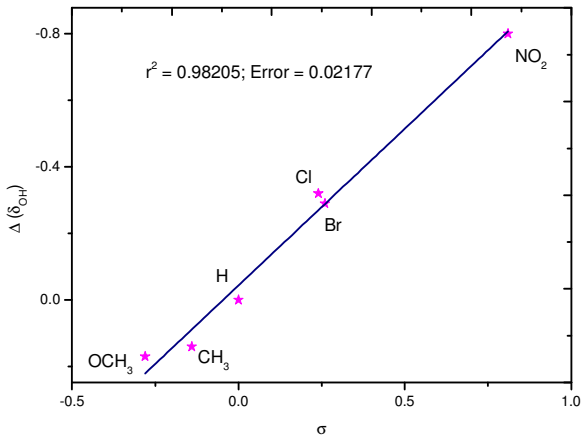

Fig. 5.1: Plot o f δ_{OH} of o-vanillin analogues of p-substituted anilines against Hammet substituent parameters (σ)

Introduction of the methoxyl group to the salicylaldimines resulted in a slight increased acidity and a downfield shift of the OH signal. However, the effect of hydrogen bonding was not seen in the vanillin analogue of the Schiff bases, since the hydroxyl proton is on the 4-position. The OH proton for the vanillin series absorbed at δ 6.15-6.10 ppm, except in the case of 4-hydroxy substituent, where it absorbed at δ 9.35 ppm. A representative ^{1}H-NMR spectrum for the aniline based ligand is presented in figure 5.2 below, while the electronic copies of all the spectra are included in the appendix.

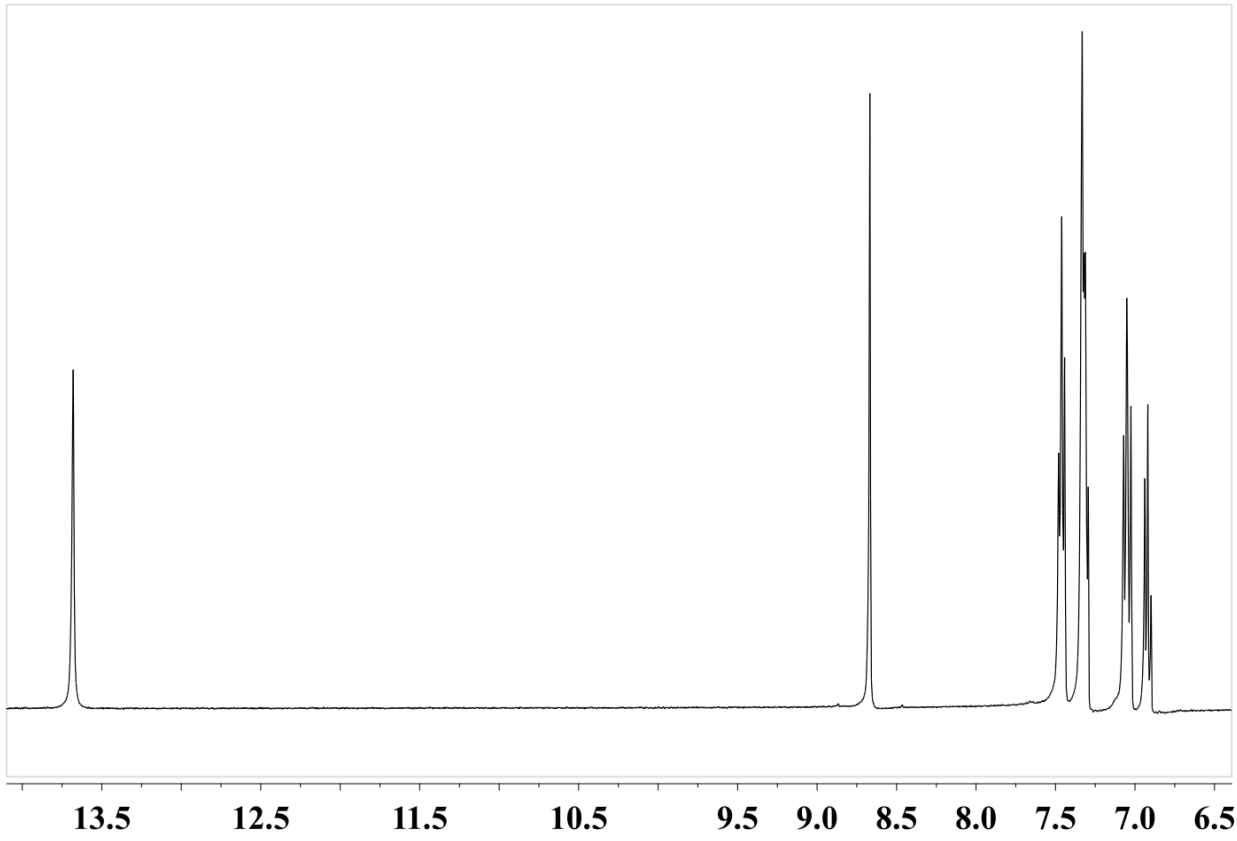

Fig. 5.2: NMR spectrum of ligand L16 (Ovaani) showing the non-splitting of the methine proton at 8.67 ppm

5.1.2: The NMR spectral data of the 1-aminonaphthalene-based ligands

The NMR spectral data for the 1-aminonaphthalene based Schiff bases are presented in table 4.66. In comparism with the substituted anils, the methine proton equally appeared as a singlet at δ 8.47-8.75 ppm while the OH proton appeared at δ 13.91-13.40 ppm for ortho-hydroxyl Schiff bases of this series and 6.10 ppm for the vanillin analogues. The azomethine carbon absorbed at 160.43 - 163.82 ppm. Thus, the keto-enol form is again predominant in chloroform.

5.1.3: The NMR spectral data of the aminopyridine-based ligands

Aminopyridines are weak bases and they can exist in neutral and protonated form at physiological pH [229]. With $pKa_{(py)}$ for the 2- and 3- aminopyridnes of 6.82 and 5.94 respectively [229] the 2-aminopyridine is the most likely to be protonated at the pyridine

nitrogen site. In the same vein, a $pKa_{(NH2)}$ of 7.6 for 2-aminopyridine indicates that the 2-aminopyridine-based salicylaldimine is expected to favour the keto-amine of the pyridine systems. The pyridine nitrogen, $pKa_{(py)}$ = 7.09 [230], is more basic than the free pyridine, $pKa_{(py)}$ 5.34 [80] and is protonated before the pyridine nitrogen. In addition, the 2-aminopyridine-based salicylaldimine in the solid state is planar with benzene ring and is stabilized by hydrogen bonding with the proton in the E configuration. This would permit the delocalization of the pi system over the whole molecule, thus favouring the keto enamine tautomer of the Schiff base. However, Cameraman et al. [66, 231] maintained that for the 2-aminopyridine based salicylaldimine the keto-amine tautomer does not exist even in polar solutions.

On the other hand, 3-aminopyridine has a $pKa_{(NH2)}$ of 1.5 and thus the 3-aminopyridine based salicylaldimine is expected to have an equilibrium less shifted to the keto-amine than the 2-aminopyridine analogues. With $pKa_{(py)}$ of 5.94 for 3-aminopyridine, the pyridine nitrogen site in the Schiff bases would likely be the receptor site in any proton transfer. This means that the imine nitrogen would be the receptor site in any proton transfer, allowing the splitting of the methine proton to be used to indicate any presence of keto-amine tautomer

The NMR spectral data for the 2-and 3-aminopyridine based Schiff bases are presented in table 4.67. The observation seen in the study was in agreement with previously reported values [224]. The azomethine proton appeared as a singlet at 8.38-8.68 ppm. Using UV spectroscopy, Galic et al. [80] noted the prevalence of enol-imine form for salicylaldehyde Schiff bases of 2-aminopyridine and 3-aminomethylpyridine, amongst other. However, rapid tautomeric interconversion of enol-imines to keto-imines as well as slow hydrolysis were noted in polar solvents [80].

5.1.4: The NMR spectral data of the aminomethylpyridine-based ligands

The NMR spectral data for the 2- and 3-aminomethylpyridine based Schiff bases are presented in table 4.68 and the methine proton equally appeared as a singlet in all the cases. In the solid state, the pyridine ring in the 3-aminommethylpyridine salicylaldimine is non-planar with the benzene ring, and thus the delocalized benzene π electrons involve only the imine and the methane groups [66]. Though, on the other hand, the pyridine ring is planar (within 4°) with the benzene

ring [66] in the case of 2-aminomethylpyridine, the lack of the quinoid ring skeletal stretches in the infrared spectra indicated the dominance of the enol-imine tautomer, even in polar solvents. Thus, the non-splitting of the methine proton of the Schiff base ligands of this series is indicative.

5.1.5: The NMR spectral data of the 2-aminobenzimidazole-based ligands

The NMR spectral data for this series is presented in table 4.69. The OH proton appeared less de-shielded compared to all the other groups of Schiff bases studied in this work. Its signal appeared as a broad singlet at 12.76-12. 70 ppm, while the imidazole N-H proton signal was equally broad at 1215-1205 ppm. The methine proton, however, absorbed far downfield as a singlet at 9.54-9.67 ppm probably due to the electronic effect of the two imidazole N-atoms. Marijana et al. [144] reported a range of 9.62-9.15 ppm for the methine proton in a series of Schiff base ligands derived from 2-aminobenzimidazole and aromatic aldehydes.

5.1.6: The NMR spectral data of the *o*-phenylenediamine-based ligands

The NMR spectra data of the *o*-phenylenediamine bis-Schiff base ligands are similar to the aniline and substituted aniline-based ligands excepting that both the azomethine and the hydroxy protons absorbed as 2H singlet in the Schiff base ligands. The hydroxyl protons absorbed at 13.23-13.09 ppm while the azomethine signal was observed at 8.67-8.64 ppm respectively. The spectra data are presented in table 4.70.

5.2.0: Mid-infrared study of the ligands

The significant infrared data for all the Schiff base ligands and the metal complexes are presented in tables 4.24-4.35. Generally, the diagnostic infrared bands for salicylaldimine Schiff base ligands are due to the absorption associated with the hydroxyl symmetric stretching (ν_{OH}); imine symmetric stretching $\nu_{C=N}$ as well as the phenoxy symmetric stretching (ν_{C-O}). The hydroxyl absorption bands for all the ortho-hydroxyl based ligands were not observed at the expected frequency range, 3400-3300 cm^{-1}, in the mid-infrared spectra of the free Schiff base ligands. Instead, a broad, weak band having some fine structure is found in the region 3100-2000 cm^{-1} of the IR spectra. Most of the fine structure is due to CH modes; and the bands near 2730

cm^{-1} have been previously assigned to the internally hydrogen bonded O-H stretching vibration [12, 101]. The mid-infrared data will be discussed according to the nature of amine moiety of the ligands.

5.2.1: Mid-infrared data for the aniline-based ligands

The mid-infrared data for the aniline and substituted aniline-based Schiff bases are presented in tables 4.24-4.30. The azomethine symmetric stretching frequency, $\nu_{C=N,}$ for the salicylaldehyde-based Schiff bases derived from aniline and substituted anils falls in the range 1616-1598 cm^{-1}. A value of 1630 cm^{-1} has been reported for benzylideneaniline while a frequency range of 1650-1638 cm^{-1} [9] was found for Schiff bases of the type Ar-CH=N-R where Ar is an un-substituted phenyl group. Suydam [10] has, however, reported a smaller range of 1650-1645 cm^{-1}. Frequency region of 1631-1613 cm^{-1} were found for the compounds of the type Ar-CH=N-Ar [11]. In the present study, the observed infrared frequency of the salicylaldehyde-based ligands reflected the effect of hydrogen bonding on the imine bond, occasioned by the presence of the hydroxyl group at the ortho position of the aldehyde moiety of the Schiff bases.

Intramolecular hydrogen bonds in Schiff bases may form six- or five -membered cycles as shown in figure, page 11. The hydrogen bonding participating in six-membered rings are essentially stronger than those of five-membered rings due to acquisition of a quasi-aromatic type in the former case [223].

The presence of an OH group at the 2-position of the phenyl ring effects a red shift with a frequency shift of about -8 cm^{-1} using N-benzylidene-aniline as a reference [11]. It was also observed that the electron withdrawing substituents caused a further reduction (Δ= -5 cm^{-1}) in the azomethine absorption frequency while slightly higher values (Δ= +3 cm^{-1}) were obtained in the presence of the electron donating groups. The length of the imine bond decreases with electron donating group and consequently it absorbs at a higher frequency, while on the other hand, electron withdrawing group reduces the π-electron density in the bond and thus lead to a lower frequency. In contrast to the *p*-substituents, the imine absorption frequencies of the ortho-

substituted anils were not substituent dependent as there was only a narrow difference (Δ =+/-2 cm^{-1}) in the observed values.

The phenolic C-O frequencies for the ligands were observed at 1289-1273 cm^{-1}. A range of 1288-1265 cm^{-1} has been reported [12, 101] for Schiff ligands of this series. The ν_{C-O} values for both *o*-vanillin and *p*-vanillin analogues were similar to their salicylaldimine counterparts and agreed well with reported values for similar structures [115]. It should be noted that two strong C-O bands were obtained for the *o*-and *p*-hydroxyaniline substituted ligands as expected.

In the same vein, the $\nu_{C=N}$ value for the *o*-vanillin Schiff base ligands fall between 1616 cm^{-1} and 1611 cm^{-1}. There was not much deviation from the un-substiuted aniline (Δ = +2 cm^{-1}) except for the methyl substituent with Δ = +3 cm^{-1}). The observed $\nu_{C=N}$ values for the *p*-vanillin analogues were, however, similar to the values obtained for the salicylaldehyde based ligands. The imine frequency was lowered by -5 cm^{-1} for both the chloro- and bromo substituents while the values for other members of the series were typically non-substituents dependent. This is a reflection of the influence of mass of substituent on the extent of vibrational coupling in benzene ring systems; Br and Cl are classified as heavy substituents by Varsányi and Zöke [232] whereas other substituents are classified as light.

The vanillin-based analogues showed a great deviation from the ortho-hydroxyl series; the OH is on the 4-position and thus not involved in intramolecular hydrogen bonding with the imine bond. Thus, a range of 1623-1622 cm^{-1} for $\nu_{C=N}$ was obtained for the members of this series. The $\nu_{C=N}$ values were however, similar.

5.2.2: Mid-infrared data for the 1-aminonaphthalene-based ligands

The infrared data for the 1-aminonaphthalene-based Schiff bases are presented in table 4.31. The strength of the imine bond for the 1-aminonaphthalene Schiff bases was influenced by three factors, namely; the bulkiness of the naphthalene ring, hydrogen bonding effect as observed in the aniline-based ligands, and the presence of the methoxyl group at the ortho or para position of ligands L28 (ovan-1-amnaph) and L43 (pvan-1-amnaph). The later extends the conjugation of the imine double bond and consequently resulted in a much lower frequency compared to ligand

L14 (sal-1-amnaph). Thus, the $\nu_{C=N}$ values for ligands L14, L28 and L43 were 1609 cm^{-1}, 1606 cm^{-1} and 1607 cm^{-1} respectively. However, the vanillin analogue of the series did not seem to be affected by these factors as the observed $\nu_{C=N}$ value for ligand L51 (van-1-amnaph) was 1622 cm^{-1} and this was similar to ligand L45 (vaani).

The ν_{C-O} values for all the members of the series were similar to the substituted aniline-based ligands. It varied from 1297 cm^{-1} to 1278 cm^{-1}.

5.2.3: Mid-infrared data for the aminopyridine-based ligands

The infrared data for the 2-aminopyridine-based Schiff bases are presented in table 4.32. In this group, consideration was also given to the heterocyclic C=N vibrational frequency, $\nu_{C=N_{(py)}}$, in addition to $\nu_{C=N}$ and ν_{C-O}. There was a greater decrease in the $\nu_{C=N}$ values for this series as compared to the first two groups. This is probably due to the fact that the pyridine ring is involved in conjugation with the imine bond and consequently decreased the double bond character of the imine bond. The observed $\nu_{C=N}$ values for ligands L14 (sal-2-ampy) and L29 (ovan-2-ampy) were 1588 and 1587 cm^{-1} respectively. This shows that the effect of the methoxyl group was not pronounced in this case, suggesting the conjugation from the pyridine ring is more dominant than the electronic effect of the methoxy moeity. The $C=N_{(py)}$ bands appeared in the 1575-1560 cm^{-1} region while the observed ν_{C-O} values agreed well with the substituted anils series.

The effect of having the N atom at different position on the pyridine ring was reflected on the observed $\nu_{C=N}$ values for the 2- and 3-aminopyridine Schiff bases. As explained above, lower frequency values were obtained for the former due to conjugation of the pyridine N with the imine bond. In contrast, the observed $\nu_{C=N}$ values for the 3-aminopyridine analogues were similar to the substituted anils series and thus suggesting that the presence of the 3-N in the pyridine ring does not permit extended conjugation through the ligand. The $\nu_{C=N}$ values for ligands L15 (sal-3-py) and L30 (ovan-3-py) were 1611 cm^{-1} and 1613 cm^{-1} respectively. The presence of the methoxyl group at the para position of ligand L433 (pvan-3-py) extends the conjugation in the ligand system and consequently lowered the frequency of absorbtion to 1608 cm^{-1}. The absence of intramolecular hydrogen bonding in the vanillin analogues of the Schiff

bases was once again noticed in the $\nu_{C=N}$ value, 1620 cm^{-1}, for ligand L52 (van-3-ampy). The $C=N_{(py)}$ and the C-O bands appeared in the same region as the 2-aminopyridine analogues.

5.2.4: Mid-infrared data for the aminomethylpyridine-based ligands

The infrared data is presented in table 4.33. The difference between this group and the aminopyridine analogues was the inclusion of a methylene group between the imine bond and the pyridine ring. The increase in the mass effect is expected to lower the observed frequency, but higher values were observed for this series. This reflects the simple harmonic diatomic oscillator approximation in action. The increase in the $\nu_{C=N}$ values can be understood to be due to the presence of the methylene group which separates the pyridine ring from the π conjugation of the rest of the molecule preventing conjugation with the imine bond. The $\nu_{C=N}$ values for ligands L31 (ovan-2-pico), L16 (sal-3-pico) and L53 (van-3-pico) were 1627, 1631 and 1634 cm^{-1}. Ligand L53 has the highest value, due to the absence of hydrogen bonded hydroxyl group. The same explanation also holds for the observed values of the $\nu_{C=N_{(py)}}$; 1606 - 1606 cm^{-1}. The ν_{C-O} values were equally similar to the substituted anils analogues.

5.2.5: Mid-infrared data for the 2-aminobenzimidazole-based ligands

The mid-infrared spectral data for the 2-aminobenzimidazole Schiff base ligands are presented in table 4.34. The infrared spectra of benzimidazoles are very complex. Benzimidazoles are known to be strongly associated through intermolecular hydrogen bonding and this is evident from the appearance of a strong broad band from 3300-2800 cm^{-1} [233]. The strong band observed in the region 3357-2744 cm^{-1} was thus assigned as the $\nu_{N-H_{(stretch)}}$ of the imidazole ring. The imine bands of this series appeared at a much lower frequency than the aniline based analogues, in the region 1606-1597 cm^{-1}, indicating the presence of extended conjugation through the ligand system. The strong band at 1628-1606 cm^{-1} was however assigned to the heterocyclic, C=N band of the benzimidazole while the phenolic C-O stretching bond appeared at 1278-1249 cm^{-1}.

5.2.6: Mid-infrared data for the *o*-phenylenediamine-based ligands

The mid-infrared spectral data for the *o*-phenylenediamine Schiff base ligands are presented in table 4.35 with the $\nu_{C=N}$ band absorbing at around 1610 cm^{-1} similar to the aniline-based analogues, due to strong intramolecular hydrogen bonding. The phenolic C-O stretch of the ligands equally absorbed at 1275-1269 cm^{-1}.

5.3.0: Mid-infrared study of the complexes

The infrared data for the isolated complexes of the Schiff base ligands are presented in tables 4.36-4.47. The assignment of the characteristic absorption bands was done based on previous assignment of similar system in the literature. This was carried out to determine the mode of coordination of the Schiff base ligands to Cu(II) ion. Thus, the far infrared data of the complexes was also studied in order to substantiate the proposed coordination mode.

5.3.1: Mid-infrared data for the aniline-based complexes

In order to determine the mode of coordination of the Schiff base ligands to the metal ion, the observed $\nu_{C=N}$ and ν_{C-O} values for free ligands were compared with those of the complexes based on previous assignment. The mid-infrared spectral data for aniline-based complexes are presented in tables 3.34-3.40. It is well known that the ligand bands are shifted to lower or higher frequencies with simultaneous variation in intensity when a chelate is formed [223, 234].

A shift to higher frequency has been reported for ortho-hydroxysalicylaldimine chelates prepared from metal halides [235]. In such cases, the Schiff base ligand acted as a neutral base coordinating only through the imine nitrogen [235]. In this study, a shift of 30-20 cm^{-1} was observed in the complexes of the form $Cu(LH)_2Cl_2.xH_2O$, thus indicating that the ligand coordinated only through the imine nitrogen; $[Cu(LH)_2Cl(H_2O)]Cl$. The broad hydroxyl band of the Schiff base ligand was persistent in the infrared spectra of the complexes, indicating that the hydroxyl proton was not deprotonated and probably non-coordinating. A conductivity value of 1:1 electrolyte for these complexes indicated the presence of one chlorine atom and at least one water molecule in the inner coordination sphere. The presence of coordinated water was supported by the presence of the broad band at around 3400-3100 cm^{-1} while the ν_{Cu-Cl} band is

discussed under the far-infrared section. Alternatively, and more probably, the Schiff base ligands could be considered to coordinate as bidentates via the imine nitrogen and the non-deprotonated oxygen atoms as shown in figure 5.3.

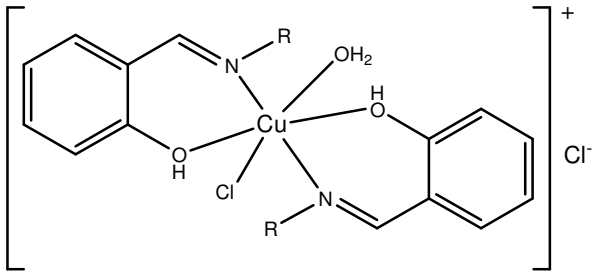

Fig. 5.3: Proposed structure for the $M(LH)_2Cl_2.xH_2O$ complexes (1:1)

On the other hand, the imine bond absorbed at a slightly lower value, 1616-1610 cm^{-1} to 1606-1598 cm^{-1}, in the complexes of the form ML_2. These complexes were prepared from copper(II) acetate monohydrate. The differences in the complexes is a reflection of the Bronsted base strength of acetate ion (pKa 4.75) against that of the phenolic moiety (pKa 7.95), whereas the chloride ion as a spectator ion cannot deprotonate phenolic moiety, but as a strong Lewis base may coordinate to the metal ion. The phenolic C-O stretching vibrational bond absorbed at higher values, 1292-1272 cm^{-1} to 1331-1310 cm^{-1}, than the free ligands in these complexes and this indicates that the ligands acted as bidentate ligands coordinating through the imine nitrogen and the deprotonated phenolic oxygen atoms. The broad OH bands observed at 3200-2300 cm^{-1} in the spectra of the free Schiff base ligands were not observed in the spectra of the complexes. Further confirmation of the mode of coordination of the Schiff base ligands is discussed under the far infrared section.

All the ortho-hydroxyaniline Schiff base ligands formed complexes of the form CuL, which must thus dimerise in order to form the required tetra- or hexa- coordinated Cu(II) complexes. The ν_{OH} value observed at 3158-1949 cm^{-1} in the free ligands was not observed in the spectra of the complexes indicating the dibasic tridentate nature of the Schiff base ligands. The insolubility of the Cu(II) complexes in common coordinating solvent and high melting or decomposition temperature (greater than 250 $°C$) has been used to support the dimeric or polymeric nature of the complexes [236]. The $\nu_{C=N}$ band shifted to a lower frequency, 1626-1624 cm^{-1} to 1613-1599

cm^{-1}; while the ν_{C-O} band shifted to a higher value, 1276-1272 cm^{-1} to 1341-1304 cm^{-1}, thus confirming the coordination of the Schiff base ligand via the imine nitrogen and phenolic oxygen atoms. A ν_{C-O} band shift at 1540 cm^{-1} to higher frequency by 10-20 cm^{-1} has been used unambiguously to indicate the formation of phenolic oxygen bridge in magnetically condensed Cu(II) complexes [237, 238]. The band was observed at 1530-1494 cm^{-1} in the free ligands and at 1527-1479 cm^{-1} in the spectra of the complexes. The proposed structure for the complexes is presented in figure 5.4.

Fig. 5.4: 2-Aminophenol Schiff base ligands and their Cu(II) complexes

Lastly, the ammonia-based Schiff base ligands equally coordinated to the Cu(II) ions in a bidentate manner via the protonated imine nitrogen and the phenolic oxygen as shown in figure 5.5 below.

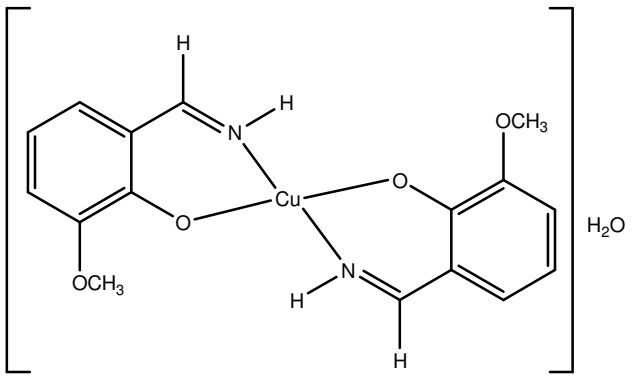

Fig. 5.5: Structure of Cu(II) complex of the ammonia-based base ligand, [Cu(ovan-NH)$_2$].H_2O

The imine band in these complexes consistently absorbed at 1623 cm^{-1} while the phenolic C-O band appeared at a higher frequency, 1331 cm^{-1}, compared to the free Schiff base ligands (1280-1269 cm^{-1}). The two conspicuous strong bands at 3413 cm^{-1} and 3294 cm^{-1} in the spectra of the complexes are attributable to ν_{OH} and ν_{N-H} of the water molecule and the N-H group respectively. The labelled ORTEP diagram of the monomeric unit of the crystals is presented in figure 4.1, while the selected bond lengths and bond angles are presented in table 4.94.

5.3.2: Mid-infrared data for the 1-aminonaphthalene-based complexes

The mid-infrared data for the 1-aminonaphthalene-based complexes are presented in table 3.41. The observed trend in this series is similar to the substituted anils complexes. The two complexes prepared from the 1-aminonaphthalene based Schiff base ligands were of the form $[CuL_2]$, figure 5.6 and thus a negative shift of -3 cm^{-1} and -7 cm^{-1} were observed for the imine azomethine vibrational frequency in the metal chelate. This was accompanied by a shift to higher frequency, 1279-1278 cm^{-1} to 1332-1314 cm^{-1}, of the phenolic ν_{C-O} frequencies indicating the coordination of the ligand via the imine nitrogen and the phenolic oxygen. The non-coordination of the chloride ion in the complex of sal-1-amnaph, which was prepared from $CuCl_2.2H_2O$, could be attributed to steric factor occasioned by the bulkiness of the aminonaphthalene rings.

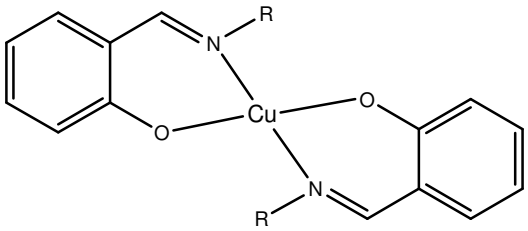

Fig. 5.6: Proposed structure for the [CuL_2] complexes

5.3.3: Mid-infrared data for the aminopyridine-based complexes

The mid-infrared data for the amininopyridine based complexes are presented in tables 3.42. Ayad et al. [121] reported the synthesis of Cu(II) complexes of the salicylaldehyde analogues of the 2-and 3-aminopyridine Schiff base ligands. The Schiff base ligand behaved as bidentate via

the imine nitrogen and phenolic oxygen forming complexes of the form $Cu(L)_2$ or $CuLCl.H_2O$ depending on the nature of the Cu(II) salt used for the synthesis.

In this study, the elemental analysis results suggested that the complexes of this series were of the form $Cu(LH)_2Cl_2.xH_2O$, similar to the aniline based analogues, but the conductivity measurement values indicated non-electrolyte complexes, figure 5.7. This implies that the ligands coordinate via the imine nitrogen and the non-deprotonated phenolic oxygen atoms; $[Cu(LH)_2Cl_2].xH_2O$. The imine vibrational frequency was observed at lower frequencies (1631-1588 cm^{-1} to 1624-1584 cm^{-1}) in the Cu(II) chelates compared to the free ligands. However, the infrared spectrum of Cu(sal-3-ampy) showed a higher value for the imine vibrational frequency, suggesting the possibility of M→L antibonding, increasing the bond order and consequently leading to higher frequency of absorption. The ν_{C-O} values for the complexes were observed at higher frequencies (1284-1258 cm^{-1} to 1328-1284cm^{-1}) in all the complexes. Likewise, the broad hydroxyl proton band of the Schiff base ligand was still evident in the spectra of the complexes, undergoing blue or red shift due to the involvement of the hydroxyl proton in chelation to the Cu(II) ions.

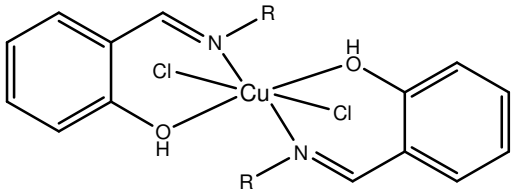

Fig. 5.7: Proposed structure for the neutral $[Cu(LH)_2Cl_2].xH_2O$ complex

The *o*-vanillin analogue of the 2-aminopyridine complex was 1:1 electrolyte in DMF, with the elemental analysis result suggesting complex of the form $[M(LH)Cl(H_2O)]Cl$. A cationic complex, figure 5.8, with one chlorine atom as counter ion was thus suggested for the complex. The presence of the coordinated water molecule was confirmed by the appearance of a strong band attributed to ν_{OH} at 3413 cm^{-1} and a shift in the broad hydroxyl band at 3114 -2375 cm^{-1} to 3195-2856 cm^{-1} equally indicated the coordination of the Schiff base legend via the non-deprotonated phenolic oxygen atom. Al-Allaf et al. [120] have equally reported the synthesis of the cationic diorganotin (IV) complexes of 2- and 3- aminopyridine using salicylaldehyde. The

Schiff base ligands coordinated as bidentate ligand through the imine nitrogen and the phenolic oxygen atoms.

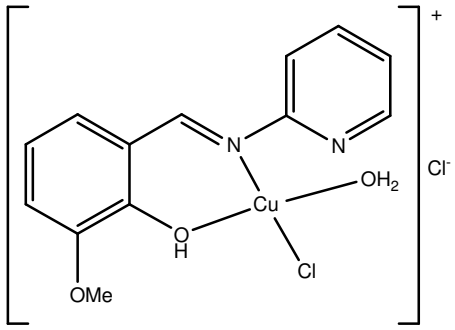

Fig. 5.8: Proposed structure for the Cu(II) complex of ovan-2-ampy-based ligand, [Cu(LH)Cl(H_2O)]Cl

5.3.4: Mid-infrared data for the aminomethylpyridine-based complexes

The isolated complexes for this series were prepared from sal-3-pico and ovan-2-pico. The copper(II) complexes of the Schiff base ligands conformed to the forms, $[Cu(LH)_2Cl_2].xH_2O$ and [CuLCl] respectively. The complexes were non-electrolyte in DMF. The Cu(II) ion in sal-3-pico is involved in coordination via the imine nitrogen, the two chlorine ions and the non-deprotonated phenolic oxygen. The $\nu_{C=N}$ band of the free ligand shifted by -7 cm^{-1} in the spectra of the complex, while the ν_{C-O} band appeared at a higher frequency, 1274 cm^{-1} to 1328 cm^{-1} confirming the coordination of the Schiff base ligand via the imine nitrogen and the non-deprotonated phenolic oxygen atoms. The broad band at 3089-2284 due to the ν_{OH} of the free ligand did not disappear in the spectra of the complex, but rather underwent a positive shift to 3124-2527 cm^{-1}. The involvement of the chloride ions in coordination to the Cu(II) ions is discussed under the far-infrared section.

The elemental analysis result and the infrared spectra data for the Cu(II) complex of the 2-picolylamine based ligand suggested coordination via the phenolic oxygen, the imine nitrogen and the azine nitrogen atoms; with one chlorine atom completing the square planar environment as shown in figure 5.9. The structure of the complex has been confirmed by X-ray single crystal diffraction and the labelled ORTEP diagram of the monomeric unit of the crystals is presented in figure 4.2. The $\nu_{C=N}$ band absorbed at lower frequency in the complex, 1631 cm^{-1} to 1624 cm^{-1},

while the ν_{C-O} and the $\nu_{C=N_{(pyridine)}}$ underwent positive shift, suggesting the coordination of the Schiff base ligand as monobasic tridentate ligand via the imine nitrogen, the deprotonated oxygen and the azine nitrogen atoms. The broad ν_{OH} band of the ligand which appeared at 3104-2152 cm^{-1} was not observed in the spectrum of the complex. The mode of coordination of the Schiff base ligand is further discussed under the far-infrared section. Datta [123] has equally reported the crystal structure of this complex, with the ligand acting as tridentate through the imine nitrogen, the phenolic oxygen and the pyridine nitrogen.

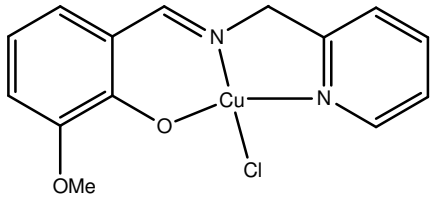

Fig. 5.9: Proposed structure for [Cu(ovan-2-pico)Cl]

5.3.5: Mid-infrared data for the 2-aminobenzimidazole-based complexes

The mid-infrared spectral data for this series are presented in table 3.44. All the complexes prepared from the 2-aminobenzimidazole Schiff base ligands were of the form $[CuL_2].xH_2O$. However, complexes of the form $ML.xH_2O$ have been reported for the salicylaldehyde analogues of this series [145].

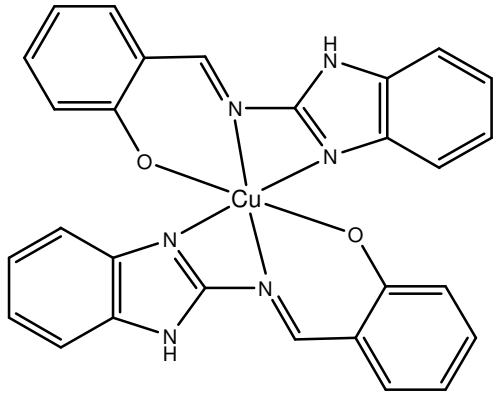

Fig. 5.10: Proposed structure for the 2-aminobenzimidazole-based complexes

It has been reported [145] that Schiff base ligands derived from 2-aminobenzimidazole and salicylaldehyde coordinated to metal ions via the imine N, phenolic oxygen and the imidazole N_3 atoms as in figure 5.10. In this study, the imine functional group underwent a red-shift from 1606-1597 cm^{-1} to 1585-1581 cm^{-1}, upon chelation in all the complexes, while the phenolic C-O stretching vibration was observed at higher frequencies, 1278-1249 cm^{-1} to 1321-1276 cm^{-1}, when compared with the free Schiff base ligands. In the same vein, the imidazole C=N vibrational bands were observed at higher frequencies in all the complexes viz: 1628-1606 cm^{-1} to 1622 cm^{-1} to 1606 cm^{-1}.

5.3.6: Mid-infrared data for the *o*-phenylenediamine-based complexes

Neutral N_2O_2 Schiff base ligands form stable macrocyclic chelates with metal ions, coordinating via the imine nitrogen and the phenolic oxygen atoms, in a tetradentate manner [205, 239]. The $\nu_{C=N}$ bands of ligands L57 (bis-salphen) and L58 (bis-ovanphen) underwent a red shift to 1607 cm^{-1} and 1602 cm^{-1} respectively in the spectra of the complexes. This indicates that the ligands coordinate to the Cu(II) ions through the azomethine functional group. Likewise, the ν_{C-O} of the free ligands that were observed at 1275 cm^{-1} and 1269 cm^{-1} underwent red shifts in the complexes, suggesting coordination via the phenolic oxygen atoms.

In addition, the presence of coordinated water in [Cu(bis-ovanphen)(H_2O)] is supported by the appearance of a strong ν_{OH} band at 3463 cm^{-1} in the infrared spectra of the complexes. However, the broad ν_{OH} band of the free ligands was not observed in the spectra of the complexes; this equally support coordination via the deprotonated phenolic oxygen atoms and further complement the non-elecrtolytic nature of the complexes as suggested by the conductivity values of between 42.60-41.80 ($\Omega^{-1}.cm^2.mol^{-1}$).

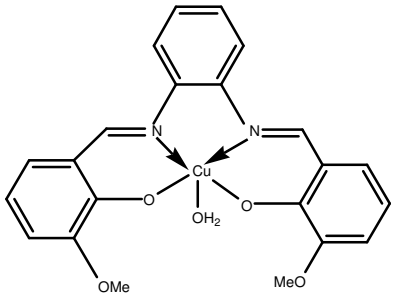

Fig. 5.11: Proposed structure for [Cu(bis-ovanphen)(H_2O)] complex

Further evidence for the mode of coordination is discussed under the far-infrared and molecular structure sections. The proposed structure for [Cu(bis-ovanphen)(H_2O)] is presented in figure 5.11. Though, elemental analysis result indicates chloro complexes for complexes of both ligands L57 and L58, the X-ray single crystal structures of the complexes proved otherwise.

5.4.0: Far-infrared study of the complexes

The emphasis on the far-infrared spectra of the complexes was on the metal to ligand vibrational frequency. The metal-ligand frequencies are expected to occur below 600 cm^{-1}. In N-arylsalicylaldimine complexes, both M-O and M-N bands are associated with the imine and hydroxyl groups. In this case, the frequencies of interest were $\nu_{M-N,}$ ν_{M-O} and possibly ν_{M-Cl}. Percy and Thornton [101, 240] noted extensive vibrational coupling between ν_{M-O} and ν_{M-N}; encountering as many as five M-L bands below 600 cm^{-1}. In their study on infrared spectra of some N-aryl salicylaldimine complexes, Percy and Thornton employed three different approaches to assign the M-L bands of some iso-structural complexes. They studied the effect of ^{15}N-labelling; the effect of metal ion substitution; and the influence of varying the substituents on the significant bands in the spectrum of the complexes [101, 240]. There were three bands below 600 cm^{-1} which show significant ^{15}N-induced shifts, but only the bands at 505 cm^{-1} and 427 cm^{-1} were assigned to ν_{Cu-N} because these bands were influenced by both metal ion and substituent substitution. However, the possibility of coupling to each band was not ruled out from the ν_{Cu-O} bands. The assignment of the ν_{Cu-N} bands was further substantiated by studying the correlation between Hammett substituent parameter and ν_{Cu-N} of a series of Cu(II) N-arylsalicylaldimine complexes variously substituted in the 4-position of the N-aryl ring. It was found that electron

withdrawing substituents increase ν_{Cu-N} and that was consistent with the expectation that such substituents will facilitate Cu→N π bonding.

In a supplementary study, Percy and Thornton showed that substitution of the phenyl ring introduces additional variations to the extent of the coupling between ν_{Cu-O} and ν_{Cu-N} [241]. Based on ^{15}N-isotope labelling of N-*p*-tolysalicylaldimine, two to four bands between 550-490 cm^{-1} were identified as being strongly coupled ν_{Cu-O} / ν_{Cu-N}, the extent of coupling being dependent on the phenyl ring substitution [241]. They however, noted an additional band, constantly existing below 450 cm^{-1}, which was the purest ν_{Cu-N}.

The complexes studied in this work have additional potential donors as a result of using chloride salt for the synthesis. It should be noted that an increase in coordination number shifts the frequency of M-L to a lower value [242]. The size of the shift is a reflection of the strength of the additional donor atom.

5.4.1: Far-infrared spectral data for the aniline-based complexes

The characteristic spectral data for the isolated aniline-based ligands and their copper(II) complexes are presented in tables 4.36-4.42. The microanalysis results suggested that the complexes in this series were of two categories, $[M(LH)_2Cl(H_2O)]Cl$ and $[ML_2]$. The bands appearing at 539-468 cm^{-1} and 430-424 cm^{-1} were assigned to the asymmetric and symmetric Cu-N vibrational frequencies, ν_{Cu-N}, of the Cu(II) chelate while the bands at 595-531 cm^{-1} were tentatively proposed to be due to Cu-O vibrations. This corroborates the coordination of the Schiff base ligands to the Cu(II) ions via the imine nitrogen and the phenolic oxygen atoms. For complexes of the form $[M(L)_2Cl_2]$, the ν_{Cu-Cl} values fall within 386-246 cm^{-1}, and this indicated a terminal M-Cl bond in the complexes [242]. Thornton and Percy [240] have proposed a square planar structures for Cu(II) complexes of N-aryl Schiff base ligands of the type, $[CuL_2]$ studied in this work.

5.4.2: Far-infrared spectral data for the 1-aminonaphthalene-based complexes

The characteristic group frequencies for the spectral data for the 1-aminonaphthalene ligands and their complexes are presented in table 4.43. The bands at 594-584 cm^{-1} and 567-561 cm^{-1} were

assigned to the asymmetrical and symmetrical Cu-O vibrational frequencies of the complexes, while the $\nu_{C=N}$ values fall at 502-501 cm^{-1} and 458-435 cm^{-1}. This, corroborate the coordination of the Schiff base ligands as bidentate via the imine nitrogen and the phenolic oxygen atoms.

5.4.3: Far-infrared spectral data for the aminopyridine-based complexes

The characteristic group frequencies for the isolated aminopyridine ligands and their copper(II) complexes are presented in table 4.44. The azine nitrogen in the pyridine ring of this group present another site for coordination, but formation of a chelate through the nitrogen atom is not expected because of high ring strain in a four-membered chelate.

All the complexes of this series conformed to the general formular, $[Cu(LH)_2Cl_2].xH_2O$, excepting complex Cu(ovan-2-ampy), which was $[Cu(LH)Cl(H_2O)]Cl$. A value of 511-483 cm^{-1} and 427-388 cm^{-1} were obtained for the asymmetric and symmetric Cu-N vibrational frequencies of the complexes while the ν_{Cu-O} values fall at 562-531 cm^{-1}. The ν_{Cu-Cl} values for these complexes fall within 358-351 cm^{-1} region indicating a terminal Cu−Cl bond.

5.4.4: Far-infrared spectral data for the aminomethylpyridine-based complexes

The characteristic group frequencies for the isolated aminomethylpyridine ligands and their copper(II) complexes are presented in table 4.45. Again, this group possesses another donor site for coordination and possibility of chelate formation via the azine nitrogen is very high. However, the position of the nitrogen atom in the 3-aminomethylpyridine does not favour chelation unlike with the 2-aminomethylpyridine analogues.

The 2-aminomethylpyridine based ligands favoured both six-membered chelate ring (C-O; $C-N_{(imine)}$) and a five-membered ring ($C-N_{(imine)}$; $C-N_{(py)}$). The ν_{Cu-O} and ν_{Cu-N} values for the complexes fall at 562-554 cm^{-1} and 514-427 cm^{-1} respectively, while the terminal Cu-Cl vibrational band was observed at 362-357 cm^{-1}. An octahedral geometry was proposed for the copper(II) complex of sal-3-pico based Schiff base ligand, $[Cu(LH)_2Cl_2]$, while ovan-2-pico complex is a four-coordinate complex, [CuLCl], as was confirmed by X-ray crystal structure to be square planar as shown in figure 4.2.

5.4.5: Far-infrared spectra for the 2-aminobenzimidazole-based complexes

The characteristic far-infrared frequencies for the 2-aminobenzimidazole based complexes are presented in table 4.46. It has been reported that Schiff base ligands derived from salicylaldehyde and 2-aminobenzimidazole coordinate to metal ions [145] as tridentate via the imine nitrogen, phenolic oxygen and the benzimidazole, N3 atoms.

Thus, the bands at 564-513 cm^{-1}, 470-389 cm^{-1} and 366-303 cm^{-1} were assigned to the metal-ligand vibrations of the complexes respectively, corresponding to $\nu_{C-O}; \nu_{Cu-N}$ and $\nu_{Cu-N_{(Im)}}$.

5.4.6: Far-infrared spectra for the *o*-phenylenediamine-based complexes

The characteristic far-infrared frequencies for the *o*-phenylenediamine-based complexes are presented in table 4.47. The $M-L$ bands substantiating the coordination of the Schiff base ligands to the Cu(II) ions were observed in the region 445-323 cm^{-1}. The bands at 445-404 cm^{-1} were assigned to ν_{Cu-O} while bands attributable to ν_{Cu-N} appeared at 368-366 cm^{-1}.

5.5.0 Raman spectral data for the ligands

The Raman spectra for the Schiff base ligands were obtained in solid state to complement the infrared spectral data. It should be noted that not all vibrations that were observed in the infrared spectra of the Schiff bases were seen in the Raman spectra. This is because infrared spectroscopy measures absorption due to change in dipole moment of the bonds while the Raman peaks results from difference in bonds polarizability. Thus, a bond that is infrared active might be Raman inactive and vice versa. For, instance, the phenolic C-O stretching vibration that was observed as a strong band at 1285-1265 cm^{-1} in the infrared spectra of the complexes was not seen in the Raman spectra. However, the azomethine group (C=N) absorbed with a very strong Raman intensity at 1626-1612 cm^{-1}; very close to the ring stretch (C=C) which appeared as intense doublets in the Raman spectra of most of the ligands. The doublets band is typical of a di-substituted benzene ring stretch vibrations [243]. The aromatic C-H stretch absorbed in the range 3159-3002 cm^{-1} while the C-H deformations bands were observed at 1201-1107cm^{-1} [243].

The Raman spectral data for the Schiff base ligands are presented in tables 4.48-4.58. A plot of change in $\nu_{C=N}$ values for the *p*-substituted salicylaldimines against Hammett's substituent parameters is presented in figures 5.12 and 5.13. The nitro substituent is an outlier as indicated by the r^2 values of the plots, with and without NO_2. It is also evident from the poor r^2 values (0.81528), that the solid state correlation is less sensitive compared to the solution studies discussed earlier. Efforts to obtain the Raman spectra for the complexes were not successful due to fluorescence experienced with the 1064nm laser (Nd-YAG), even in the presence of spectroscopic KBr.

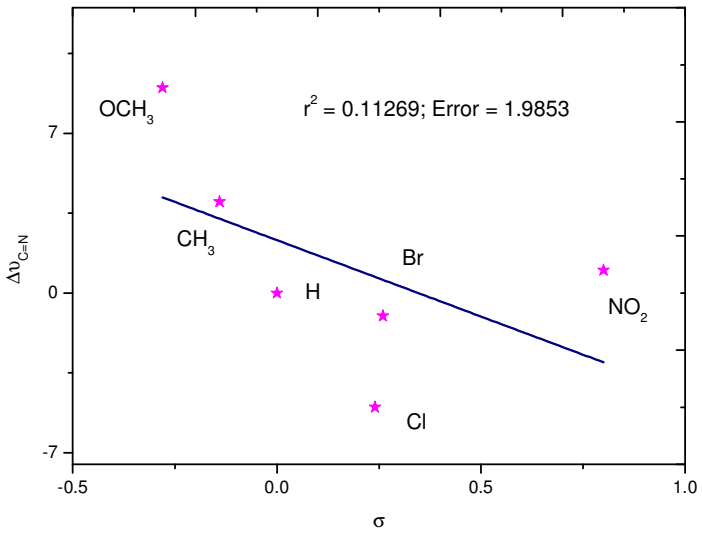

Fig. 5.12: Plot of $\Delta\nu_{C=N}$ against Hammet substituent parameter, σ , of the p-substituted salicyaldimines showing NO_2 as an outlier

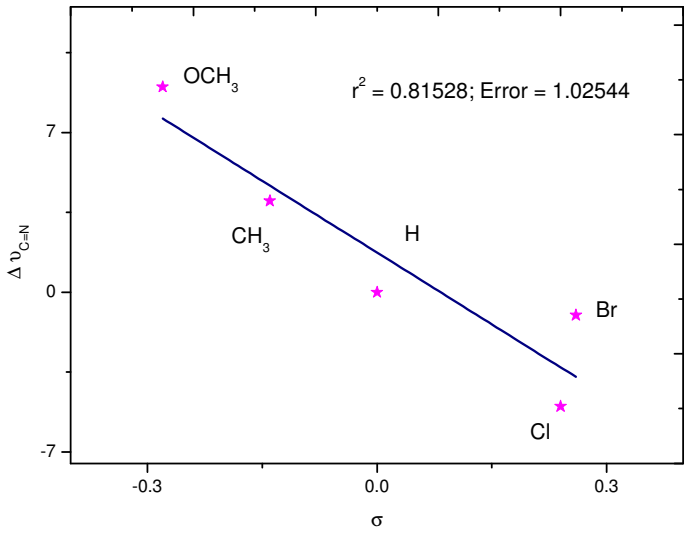

Fig. 5.13: Plot of $\Delta\nu_{C=N}$ against Hammet substituent parameter, σ, of the p-substituted salicylaldimines

5.6.0: Electronic transitions of the compounds

The UV spectra of the Schiff base ligands were obtained using methanol and DMF respectively at 700-200 nm. In this study, the effect of solvents as well as the electronic effects of the substituent on the keto-enol tautomerism of the Schiff base ligands was examined. Solvents may induce shifts of the ligand bands (solvochromatism), particularly with polar solvents, and may also cause other changes as a result of solvent coordination, or even dissociation of the complex. Protic solvents can stabilise both cations and anions by lone pair of electrons and hydrogen bonding respectively. In summary, for keto-enone tautomers (and by extension, to the keto-imine tautomers in the present series of ligands), removal of lone pairs from possible conjugation will induce a blue shift, while enhancement of the phenolate ion will induce a red shift.

In addition, the effect of having the methoxyl group on the aldehyde moiety was equally considered with respect to band position. The UV spectral data for the Schiff base ligands are presented in tables 4.71-4.82.

Likewise, the visible region of the electromagnetic spectrum provides information about the possible electronic transitions in a metal center and consequently, the nature of such transitions indicates the probable geometry of metal complexes. The UV/Visible spectral data for copper(II) complexes of the isolated ligands were obtained in methanol or DMF at 900-200 nm. The spectral data are presented in tables 4.83-4.94.

5.6.1 Electronic spectral data for the ligands

As stated above, this section deals with the study on three different aspects which determined the observed transitions in the ligand spectra. Thus, we shall consider solvent effect, substituent effect and lastly, the nature of the amine on the absorption bands of the Schiff base ligands, mainly for the aniline-based ligands, while efforts will be made at assigning possible transitions to the observed bands in the other series.

5.6.1.1 Electronic spectral data for the aniline-based ligands

The spectral data for the aniline-based ligands are presented in tables 4.71-4.77. The first striking feature of this group is the appearance of a band at greater than 400 nm in the visible region of the spectra of *o*-vanillin, *p*-vanillin and vanillin analogues in methanol (figure 5.14), all having a methoxy group on the aldehyde moiety of the Schiff base ligands. The absorption band at greater than 400 nm indicates a keto-imine form of the Schiff bases; the enol form has no appreciable absorbance in this region [21, 22, 28].

The band position also suggests the extent of the tautomerism, hence, it can be deduced that the presence of the methoxyl group at the 3-position favoured the keto-imine tautomer than at the 4-position (figure 5.14).

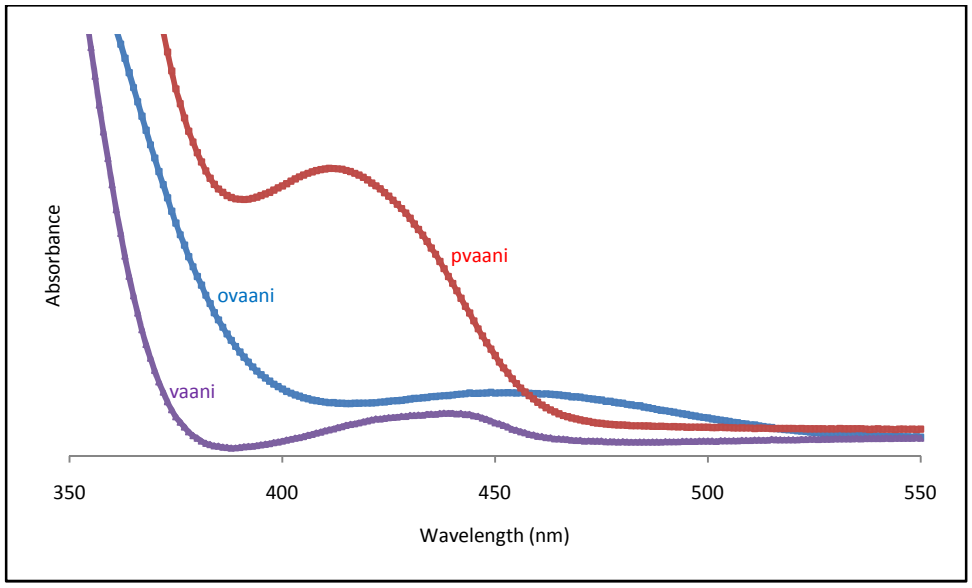

Fig. 5.14: UV spectra of ovaani, pvaani and vaani; showing the quinoid band at > 400 nm

The extent of tautomerism as measured by the molar absorptivity of the band at greater than 400 nm was then plotted against Hammett substituent parameter, σ, (with and without Br) and the pKa of the corresponding amine.

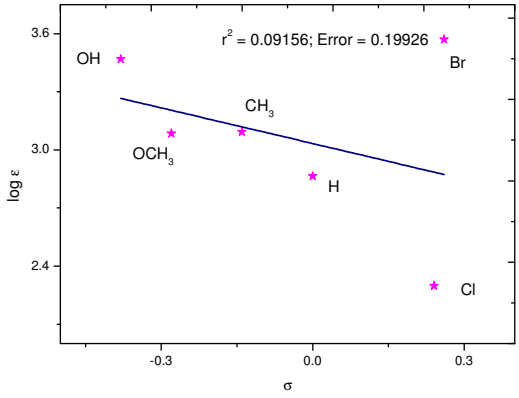

Fig. 5.15: Correlation of the intensity of the Quinoid band of the o-vanillin analogues with the Hammett's substituent parameters, showing the electronic effect of the p-substituent on band intensity (Br is an outlier)

It was observed that the band intensity increases with the electron donating ability of the substituents and equally with the basicity of the imine nitrogen. Bromine was an outlier as indicated by the poor correlation value, 0.09156.

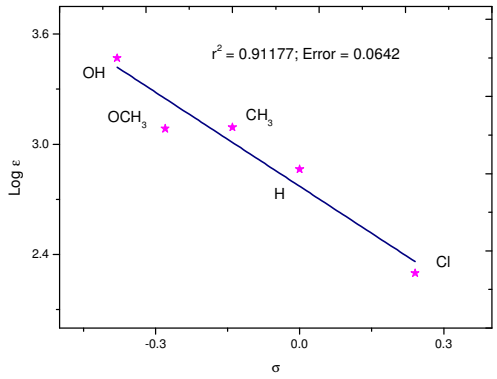

Fig. 5.16: Corellation of the 'Quinoid band' of the o-vanillin analogues with the Hammett's substituent parameters, showing the electronic effect of the p-substituents on band intensity

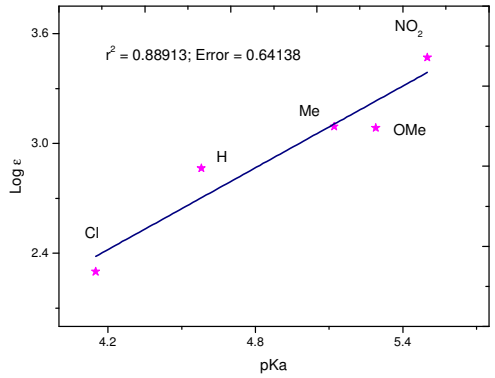

Fig. 5.17: Correlation of the intensity of the 'quinoid band' of the o-vanillin analogues against ionization constant of the p-substituted anilines

The DMF spectra of the ligands did not show any band in the visible region. It should be noted that bands similar to the methanol spectra were observed with slight shift and broadness in some cases, figure 5.18. However, the bands below 270 nm were obscured in the DMF spectra of the Schiff bases by solvent absorption.

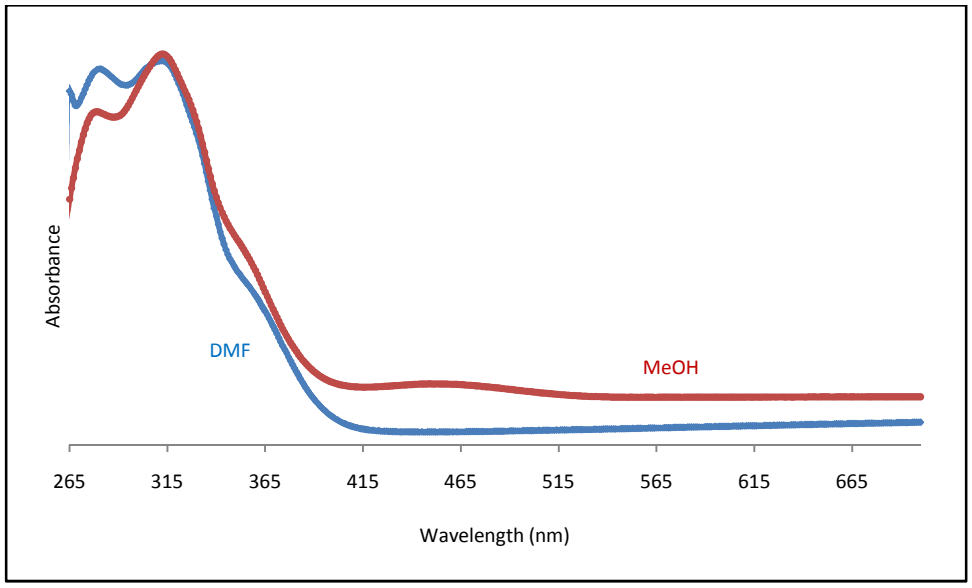

Fig 5.18: MeOH and DMF spectra of the aniline-based (ovaani) ligand

5.6.1.2 Electronic spectral data for the 1-aminonaphthalene-based ligands

The electronic spectral data for the 1-aminonaphthalene based ligands are presented in tables 4.78 and efforts were made to examine the effect of substituting the aniline moiety with the naphthalene ring. In the same vein, solvent effect and presence of the methoxyl group were noted.

Firstly, the band at greater than 400 nm was absent in all the spectra of the Schiff base ligands as compared with the aniline analogues, figure 5.19.This is probably because the extended conjugation in the naphthalene ring decreases the basicity of the amine nitrogen and consequently shifted the equilibrium to the enol form.

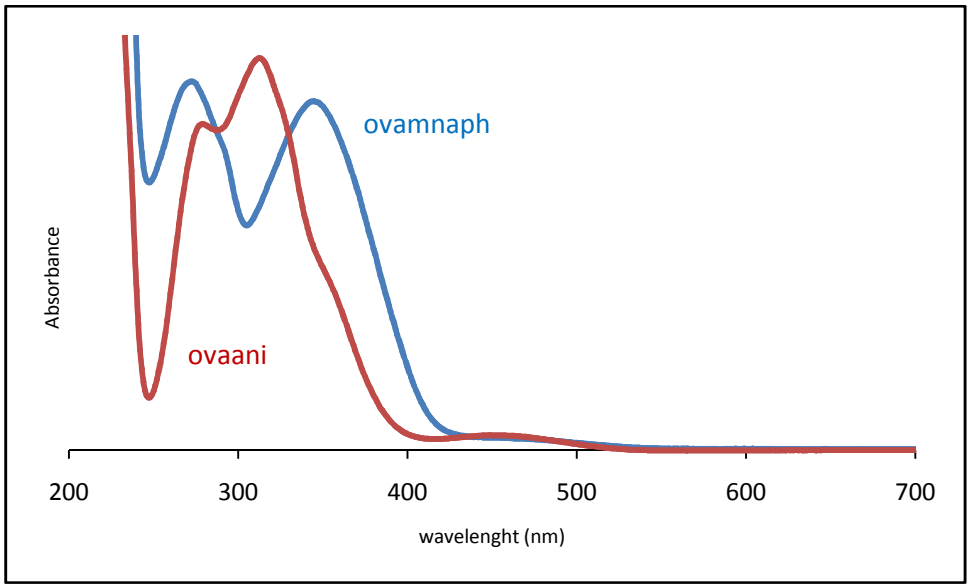

Fig. 519: UV spectra of ovamnaph and ovaani in MeOH

5.6.1.3 Electronic spectral data for the aminopyridine-based ligands

The spectral data for the 2-and 3-aminopyridine based Schiff bases are presented in table 4.79. Basically, three types of transitions are expected in this type of compound viz: $\pi \rightarrow \pi^*, n \rightarrow \pi^*$, and possibly intra-ligand charge transfer. The bands at 270, 333 and 295-249 nm have been previously assigned to $\pi \rightarrow \pi^*$ of the benzene ring while the azomethine $n \rightarrow \pi^*$ transition has been assigned to the bands at 372 nm and 330-346 nm [30, 31]. In the 2-aminopyridine analogues of the Schiff base ligands in this study, the bands at 207 nm was due to intra-ligand charge transfer, while the bands at 268-318 nm was of $\pi \rightarrow \pi^*$ origin. The bands associated with the imino $n \rightarrow \pi^*$ transition appeared at 345-318 nm. A band however appeared in the visible region of ligand ovan-2-ampy, suggesting the predominance of the keto-imine form for the Schiff base ligand. The band at greater than 400 nm was not observed in the DMF spectra of the ligands, thus indicating the effect of solvent on the observed tautomerism. The UV spectrum of ovan2-ampy is presented in figure 5.20.

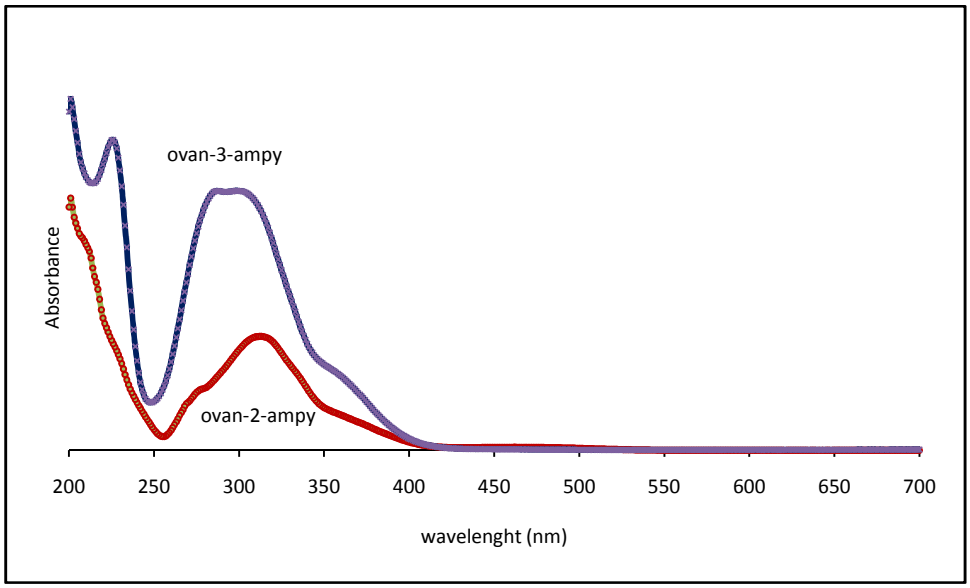

Fig. 5.20: UV spectra of ovan-2-ampy and ovan-3-ampy in MeOH

In the same vein, the $\pi \rightarrow \pi^*$ bands appeared at 275-301 nm in the UV spectra of 3-aminopyridine based Schiff bases; the imine $n \rightarrow \pi^*$ at 328-363 nm, while the bands at higher energy of 303-239 nm was assumed to be of charge transfer origin. There was no band in the visible region of both the methanol and DMF spectra of the ligands, suggesting the existence of the Schiff bases in purely enol form. The UV spectrum of ovan-3-ampy is presented in figure 5.20.

5.6.1.4 Electronic spectral data for the aminomethylpyridine-based ligands

The spectral data for the 2-and 3-aminomethylpyridine Schiff bases are presented in table 4.80. As with the aminopyridine analogues, the assignment of the possible transitions is intended in this section. In ligand ovan-2-pico, the band at 234 nm was due to charge transfer while the $\pi \rightarrow \pi^*$ bands appeared at 277 nm. The imino $n \rightarrow \pi^*$ transition was responsible for bands at 334 and 388 nm. The band at greater than 400 nm did not appear in both the methanol and DMF spectra of the ligands.

The transitions observed in the spectra of the 3-aminomethylpyridine analogues differ from the 2-aminomethylpyridine Schiff bases, appearing at a slightly higher energy. For instance, the charge transfer bands appeared at 215-228 nm; $\pi \rightarrow \pi^*$ at 256-272 nm while the imino $n \rightarrow \pi^*$

band was observed at 303-316 nm. There was however, a band at 401 nm of the vanillin analogue (figure 5.21), indicating the existence of a keto-imine tautomer of the Schiff base ligand.

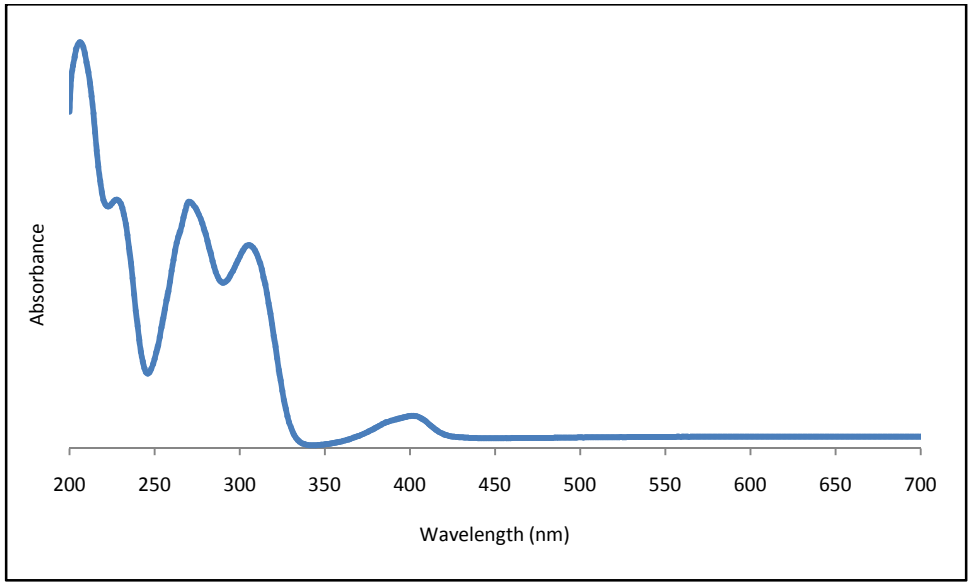

Fig. 5.21: UV spectrum of van-3-pico in MeOH

5.6.1.5 Electronic spectra data of the 2-aminobenzimidazole-based ligands

The UV spectra of the 2-aminobenzimidazole based Schiff base ligands are presented in table 4.81. Type equation here.Only two absorption bands were observed in this series, figure 5.22. The absorption due to the conjugated aromatic system, comprising the imidazole and the benzimidazole rings, was observed at 284 - 282 nm as the $\pi \rightarrow \pi^*$ transition band while the azomethine $n \rightarrow \pi^*$ band absorbed at a lower energy in the region 370 - 357 nm.

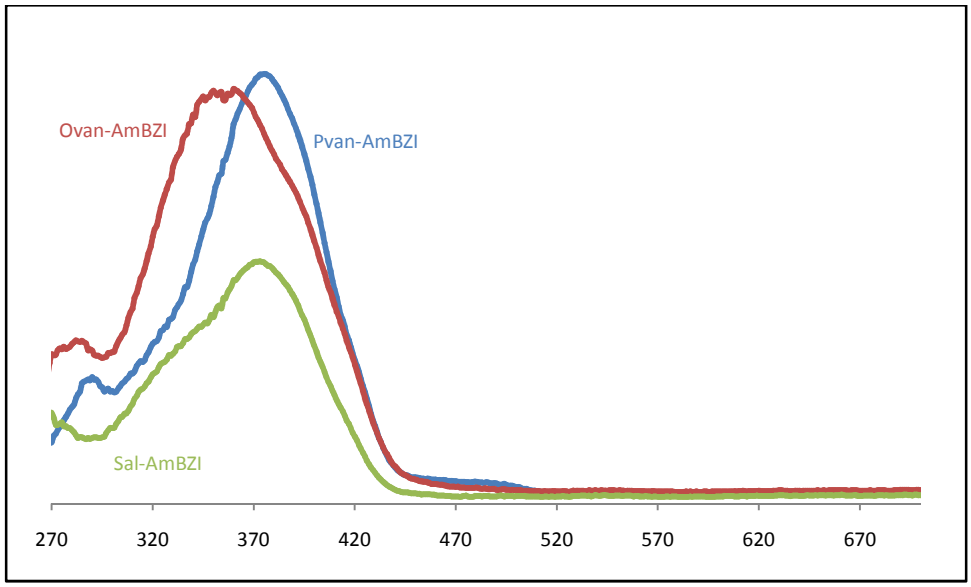

Fig. 5.22: UV spectra of 2-aminobenzimidazole Schiff base ligands

5.6.1.6 Electronic spectral data for the *o*-phenylenediamine-based ligands

The UV/visible spectral data for the *o*-phenylenediamine-based ligands are presented in table 4.82.

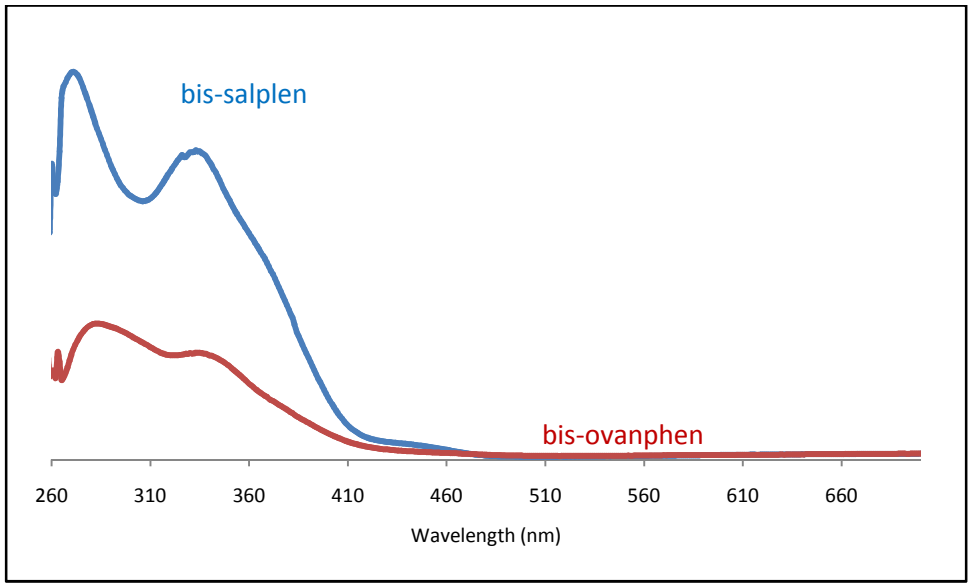

Fig. 5.23: UV/visible spectra of o-phenylenediamine ligands

Two similar absorption bands were observed in the UV/visible spectra of the two ligands, figure 5.23. The bands at 282-262 nm are due to $\pi \rightarrow \pi *$ of the aromatic system, while the bands at 336-332 nm have been previously assigned to the $n \rightarrow \pi *$ transition of the azomethine bond of Schiff base ligands.

5.7.0 Electronic transitions of the complexes

The electronic spectra of the synthesized Cu(II) complexes were extended to include both the UV and the visible region. In the UV region of the spectra, attention is given to the possible shift of the ligands bands described above as an indication of coordination of the ligands donor atoms to the Cu(II) ion. On the other hand, the visible region of the spectrum gives bands due to the metal ion and thus allowing the prediction of probable geometry for the corresponding Cu(II) complex. For, a regular six coordinate Cu(II) complexes, a single transition is expected, $T_2 \rightarrow E_g$, however, this is not always the case, as Jahn-Teller distortion causes non-degeneracy of a previously degenerate d-orbital, and consequently resulting in several transitions which appear as a single broad band. This phenomenon makes the electronic spectra of Cu(II) complexes to be ambiguous and difficult to interpret. The synthesized Cu(II) complexes are categorized into seven groups based on the elemental analysis results and conductivity values viz: (a) $[Cu(LH)_2Cl(H_2O)]Cl$ (b) $[Cu(LH)_2Cl_2].xH_2O$ (c) $[Cu(LH)Cl(H_2O)]Cl$ (d) [CuLCl] (e) $[CuL_2]$ (f) $[Cu_2L_2]$ (g) $[Cu(L)(H_2O)x]$. Thus, the electronic spectra of the complexes will be discussed accordingly. The electronic spectra for the isolated Cu(II) complexes are presented in tables 4.83-4.94.

5.7.1 Group 1: Electronic spectral data for the $[Cu(LH)_2Cl(H_2O)]Cl$ complexes

Most of the *p*-substituted aniline Schiff base complexes belong to this group and they were prepared using $CuCl_2.2H_2O$. A general trend was observed in UV/visible spectra of all the complexes. The azomethine $n \rightarrow \pi^*$ bands observed in the ligands spectra underwent a significant red shift in all the complexes, indicating the involvement of the imine nitrogen in chelation with the Cu(II) ion. Also, a broad band due to d-d transition of the Cu(II) ion was observed at 850-600 nm in the visible region of the complexes.

5.7.2 Group 2: Electronic spectral data for the $[Cu(LH)_2Cl_2].xH_2O$ complexes

All the Cu(II) complexes of the aminopyridine and aminomethylpyridine, excepting ovan-2-ampy and ovan-2-pico, Schiff bases belong to this group. The elemental analysis results, the infrared spectral data and the conductivity values suggested a six-coordinate Cu(II) complexes. The electronic spectra of the complexes are characterized by a broad d-d absorption band in the region 804-634 nm. Aggarwal et al. [81] has assigned a distorted octahedral geometry to similar band observed at 700-674 nm in the spectra of some Cu(II) Schiff base complexes.

5.7.3 Group 3: Electronic spectral data for the $[Cu(LH)Cl(H_2O)]Cl$ and [CuLCl] complexes

The Cu(II) complex of ovan-2-ampy and ovan-2-pico were of the forms $[Cu(LH)Cl(H_2O)]Cl$ and [MLCl] respectively.

The elemental analysis result and the infrared spectral data of ovan-2-ampy suggested coordination to the Cu(II) ions in 1:1 stoichiometric ratio via the imine nitrogen and the phenolic oxygen atoms. The azomethine $n \rightarrow \pi^*$ at 312 nm in the ligand spectrum was shifted by -12 nm in the complex and this supported the shift on complexation in the infrared band of the imine band, C=N, from 1607-1598 cm^{-1}. The d-d absorption band was equally broad and it appeared at 715 nm in the visible spectrum of the complex. The conductivity measurement data indicated a 1:1 electrolyte for this complex and thus one chlorine atom must be in the outer coordination sphere as counter ion.

The Cu(II) complex obtained from the ovan-2-pico Schiff base ligand conform to the form [CuLCl] and the X-ray single crystal structure indicated a four-coordinate Cu(II) ions in a planar environment. The imine $n \rightarrow \pi^*$ band underwent a red shift in the complex, 335-388 nm, indicating the involvement of the imine nitrogen in chelation to the Cu(II) ions. A broad band at 629 nm, typical of a four-coordinate Cu(II) complex [78] was unequivocally attributed to the $d \rightarrow d$ transition of the Cu(II) ions.

5.7.4 Group 3: Electronic spectral data for the $[ML_2]$ complexes

All the complexes prepared from $Cu(OAc)_2.H_2O$ belong to this group, except the 2-hydroxyaniline analogues. The elemental analysis results suggested four coordinate complexes for this series with the conductivity values suggesting neutral non-electrolyte complexes. The imine $n \rightarrow \pi^*$ absorption band underwent a large red shift in energy in all the spectra of the complexes, implying the coordination of the Schiff base ligands through the imine nitrogen. Unlike in the case of the first two groups, the d-d transition bands appeared at higher energy, 591-667 nm, in the visible spectra of the complexes. A square planar geometry has been assigned for 4-coordinate Cu(II) complexes of N-arylsalicylaldimines [240, 244] having single absorption band at 667-588 nm. The Cu(II) complex of the hydrolyzed Schiff base ligand, $[Cu(ovan\text{-}NH)_2].H_2O$ equally belongs to this group and the X-ray single crystal structure confirmed the predicted square planar geometry.

5.7.5 Group 4: Electronic spectral data for the $[M_2L_2]$ complexes

The Schiff base ligands derived from 2-hydroxyaniline behaved as tridentate dibasic coordinating to the copper(II) ion with 1:1 stoichiometry. The d-d transition of the complexes was observed in the visible region of the solid diffuse reflectance spectra as a single broad band at 676-628 nm. All the complexes exhibit a strong band at 421-409 nm, the origin of which is due to the symmetry forbidden $L \rightarrow M$ charge transfer transition rather than to the binuclear species [236] [245].

5.7.6 Group 5: Electronic spectral data for the $[Cu(L)(H_2O)]$ complexes

The isolated complexes of the *o*-phenylenediamine-based ligands conform to the formular, $[Cu(L)(H_2O)]$ as revealed by the X-ray single crystal structure of $[Cu(bis\text{-}ovanphen)(H_2O)]$. It suffices to mention that, though the elemental analysis result suggested chloro complexes for both complexes, the X-ray crystal structure prove otherwise, thus the complexes are treated as five-coordinate Cu(II) complexes, since they both have similar electronic data typical of a five coordinate Cu(II) complexes.

The electronic spectra of the complexes have five absorption bands. The higher energy band at 322 nm has been assigned [29] to the $n \rightarrow \pi*$ transition of the azomethine functional group of Schiff base ligand while the bands at 341 nm and 357 nm were attributed to the $\pi \rightarrow \pi*$ transition of the imine and the aromatic system of the ligand. The broad band at 558 nm is due to the $d \rightarrow d$ transition of the Cu(II) ions while the sharp band at 448 nm can be attributed to ligand-metal or metal-ligand charge transfer. Five-coordinate Cu(II) complexes showing absorption in the 588–769 nm region approximate a square-pyramidal geometry, while complexes with a trigonal-bipyramidal geometry show absorption bands in the 685–952 nm region, with highest absorption intensities in the range 666-877 nm [246]. The electronic transition of [Cu(bis-ovanphen)(H_2O)] is thus in agreement with square pyramidal and has been confirmed by X-ray single crystal structure.

5.9.0 Molecular structures of the complexes

Single crystal structures were obtained for three of the complexes synthesized in this study. The selected bond lengths and bond angles for the crystal structures are presented in tables 4.95-4.97, while electronic copy of the crystal data and structure refinements are presented as appendix.

5.9.1 [Cu(ovan-NH)$_2$].H_2O

The labelled ORTEP diagram of [Cu(ovan-$NH)_2$].H_2O is presented in figure 4.1 while the bond lengths and angles are presented in table 4.95. The Cu(II) ion crystallizes in monoclinic system with a space group of P21/c having a = 10.9309, b = 4.85600, c= 17.7030, $\alpha = \gamma = 90$ ° and $\beta =$ 119.658 °. The bidentate Schiff base ligand formed a four coordinate chelate with the Cu(II) ion in a trans configuration through the imine nitrogen and the phenolic oxygen atoms. The geometry is slightly distorted from planarity with O1-Cu1-N1 bond angles of 92.19 ° and 87.81 °.

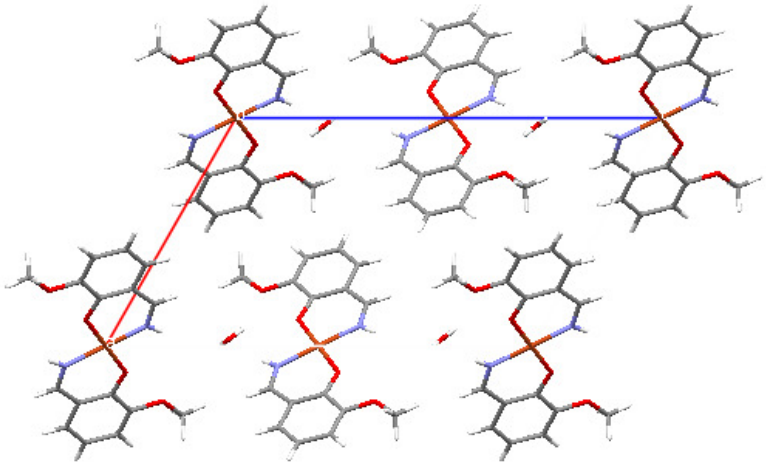

Fig. 5.24: Crystal packing of [Cu(ovan-NH)$_2$].H$_2$O viewed along the b axis

5.9.2 [Cu(ovan-2-pico)Cl]

The labelled ORTEP diagram of [Cu(ovan-2-pico)Cl] is presented in figure 4.2 while the bond lengths and angles are presented in table 4.96. In the same vein, the Cu(II) ion is in a square planar environment in which the Schiff base ligand coordinates as tridentate via the imine nitrogen, the azine nitrogen and the phenolic oxygen. The apical position is occupied by the chlorine atom having Cu1-Cl bond length of 2.2510 Å; Cl1-Cu1-O1, Cl1-Cu1-N1 and Cl1-Cu1-N2 bond angles of 89.76, 174.24 and 95.94 Å respectively, indicating a slight distortion from planarity. The crystals are monoclinic in a space group of P21/c having a = 7.01350, b = 18.1484, c= 10.3959, $\alpha = \gamma = 90$ ° and $\beta = 104.2050$ °.

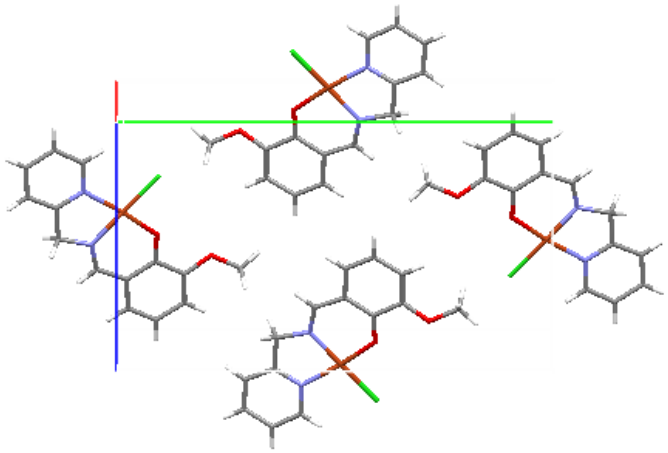

Fig. 5.25: Crystal packing of [Cu(ovan-2-pico)Cl] viewed along the b-axis

5.9.3 [Cu(bis-salphen)]

The labelled ORTEP diagram of the monomeric crystal structure of [Cu(bis-salphen)] is presented in figure 4.3 while the bond lengths and angles are presented in table 4.97. The Cu(II) complex crystallizes in orthorhombic system with space group P 212121 having a = 5.3938, b = 16.6580, and c = 17.2671. The neutral tetradendate Schiff base molecule is bonded to the Cu(II) ion in a planar form via the imine nitrogen and the phenolic oxygen atoms. The CIF file of the crystals is presented in the appendix. A slight distortion from square palanar geometry is evident in the structure with the bond lengths: O1-Cu1-N2 (178.90 Å); O2-Cu1-N1 (178.40 Å) and bond angles: N2-Cu1-O2 (94.54 °.); O1-Cu1-N1 (94.40 °.) O1-Cu1-O2 (84.56 °.); and N1-Cu1-N2 (86.50 °).

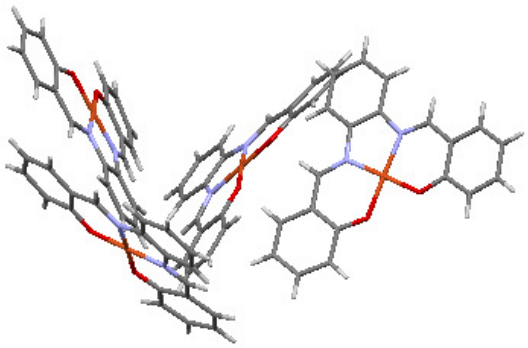

Fig. 5.26: Crystal packing of [Cu(bis-salphen)] viewed along the b-axis

5.9.3 [Cu(bis-ovanphen)(H_2O)]

The labelled ORTEP diagram of the monomeric crystal structure of [Cu(bis-ovanphen)(H_2O)] is presented in figure 4.4 while the bond lengths and angles are presented in table 4.98. The Cu(II) complex equally crystallizes in monoclinic system with space group P 21/n. The neutral tetradendate Schiff base molecule is bonded to the Cu(II) ion in a planar form via the imine nitrogen and the phenolic oxygen atoms with the water molecule occupying the apical site to form a square-pyramidal Cu(II) complex. The bond length of the axial coordination of the water molecule, Cu1-O3 was 2.327 Å while the bond angles O1-Cu1-O2 (88.58 °), O1-Cu1-O3 (96.23 °) and O1-Cu1-N2 (171.51 °) indicatating a distorted square pyramidal geometry for the complex.

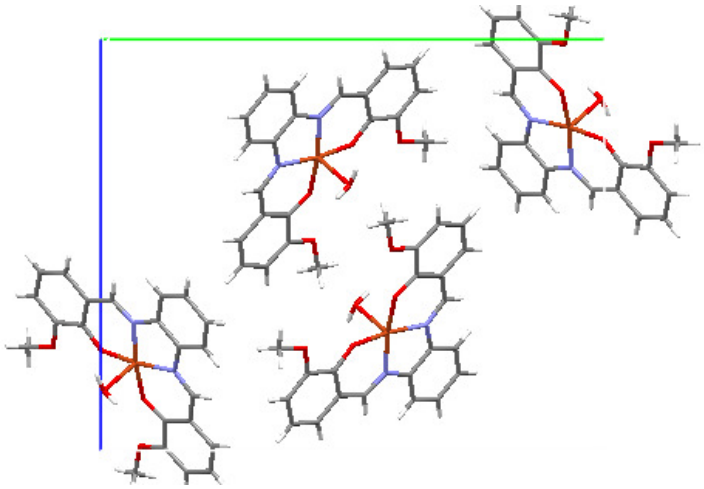

Fig. 5.26: Crystal packing of [Cu(bis-ovanphen)(H_2O)] viewed along the a axis

Chapter six

6.0.0 Antimicrobial study

6.1.0 Chemotherapy at a glance

Chemotherapy is the treatment of disease in which a chemical is specifically targeted for a microbial agent or a specific tissue. Chemotherapy as a science began with Paul Ehrlich in the late 1890s. He defined it as the use of drugs to injure the invading organism without injury to the host [247]. Before 1890, only three agents could be considered chemotherapeutic agents: cinchona, for the treatment of malaria; mercury for the treatment of syphilis; and ipecacuanha, for the treatment of amebic dysentery.

Ehrlich realized that like human and animal cells, certain bacteria cells coloured with certain dyes while others did not. He postulated that it might be possible to make certain dyes, or chemicals, that would kill bacteria while not harming the host organisms. He predicted that the function of the drug would be to upset the parasite's metabolism, after which the host's natural defenses would take over. The only chemotherapeutic agent of significance importance discovered by Ehrlich was Salvarsan-606, an arsenical used in the treatment of syphilis. The number 606 refers to the trials employed by Ehrlich research team to find the correct dosage for treatment of humans.

Another milestone in the history of chemotherapy was reached in 1935 by Domagk's discovery of prontosil, a dye used to treat streptococcal infections [247]. Prontosil in the mammalian body is converted to sulfanilamide, which inhibits microbial activity by binding to bacterial enzymes. Penicillin was described years before sulfonamides but it was not concentrated for practical use until 1940. The isolation of penicillin, the antimicrobial substance produced by the fungus penicillium, was a significant achievement in microbiology. Penicillin not only saved lives in World War II but its discovery encouraged others to search for chemotherapeutic agents produced by other microorganisms. Penicillin was discovered serendipitously by Alexander Fleming in 1928 [248]

6.3.0 Micro-organisms

Microorganisms are microscopic organisms too small to be seen by the naked eyes. They are often described as unicellular organisms and they include virus, bacteria, archaea, fungi, and protista. Bacteria and archaea have prokaryotic cell structure while fungi are eurakaryotes. The prokaryote cells lack a distinct nuclear membrane and do not have complex internal organelles, such as mitochondria or chloroplasts which are associated with energy generation in eurakaryotes. Prokaryotes have neither endoplasmic reticulum, nor Golgi apparatus. On the other hand, eukaryotes have a nucleus and complex internal organelles.

6.3.1 Bacteria

Bacteria are a large domain of prokaryotic organisms. Bacteria have relatively simple cell structure lacking a cell nucleus, cytoskeleton, and organelles such as mitochondria and chloroplasts. Most bacteria species are either spherical called cocci or rod-shaped called bacilli. Bacteria are categorized as gram positive or gram negative, based on the composition of their cell wall and their reaction to staining reagent. Gram positive bacteria possess thick peptidoglycan layer and are stained blue or violet by staining reagent. On the other hand, Gram negative bacteria do not retain the crystal violet colour in the staining protocol. They have thin peptidoglycan layer and an additional outer layer made of lipopolysaccharide (figure 6.1). The lipopolysaccharide layer provides additional fortification to the cell membrane and thus gram negative bacteria are more resistant to antibiotics treatment compared to the gram positive bacteria.

In the laboratory, bacteria are usually grown using solid or liquid media. Solid growth media such as agar plates are used to isolate pure cultures of a bacterial strain. However, liquid growth media are used when measurement of growth or large volumes of cells are required. Two Gram positive bacterial strains; *Staphylococcus aureus subsp. aureus ATCC® 6538™** and *Bacillus subtilis* subsp. *spizizeni ATCC® 6633™**; and one Gram negative bacterial strain, *Escherichia coli ATCC® 8739™*,* were used for this study.

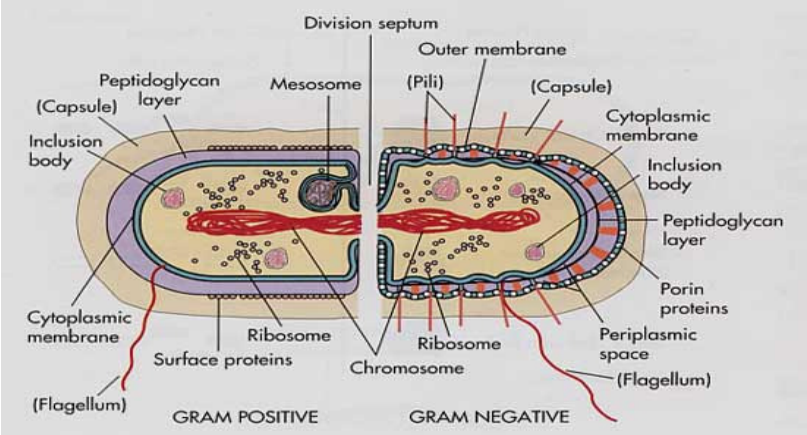

Fig. 6.1: Gram positive and Gram negative bacteria showing different in cell membranes

Bacillus substilis

Bacillus substilis also known as the hay bacillus or grass bacillus is a gram-positive, catalase-positive bacterium commonly found in soil. *B. substilis* is only known to cause disease in severely immuno-compromised patients, and can conversely be used as a probiotic in healthy individuals. It may contaminate food, but rarely causes food poisoning [249]. *B. substilis* spores can survive the extreme heat during cooking.

Staphylococcus aureus

Staphylococcus aureus is a Gram positive, coccus-shaped facultative anaerobic bacterium. It is frequently part of the skin flora found in the nose and on skin [250]. It can however, causes a wide range of illness from minor skin infections, such as pimples, impetigo, and scalded skin syndrome to life-threatening such as pneumonia, meningitis, osteomyelitis, endocarditis and toxic shock syndrome. Infections of the blood can carry the bacteria to various deep tissues, including bones, joints, organs and the respiratory system. Methicillin-resistant *S. aureus*, abbreviated MRSA, is one of a number of greatly-feared strains of *S. aureus* which have become resistant to most antibiotics.

Escherichia coli

Escherichia coli are Gram-negative, rod-shaped bacterium that is commonly found in the lower intestine of warm-blooded organisms (endotherms). Most *E. coli* strains are harmless but some serotypes are pathogenic and can cause serious food poisoning in humans, and are occasionally responsible for products recalls [251].

The harmless strains are part of the normal flora of the gut, and can benefit their hosts by producing vitamin K2 and by preventing the establishment of pathogenic bacteria within the intestine [251].

There are many strains, over 700 serotypes, of *E. coli*. Most of the *E. coli* are normal inhabitants of the small intestine and colon and do not cause disease in the intestines (non-pathogenic). Nevertheless, these non-pathogenic *E. coli* can cause disease if they spread outside the intestines, for example into the urinary tract, where they cause bladder or kidney infections, or into the blood stream causing sepsis. Other *E. coli* strains (enterovirulent *E. coli* strains or EEC) cause poisoning or diarrhea even though they usually remain within the intestine by producing toxins or intestinal inflammation.

The regular presence of *E.coli* in the human intestine and faeces has led to tracking the bacterium in nature as an indicator of fecal pollution and water contamination. As such, it is taken to mean that, wherever *E.coli* is found, there may be fecal contamination by intestinal parasites of humans.

6.3.2 Fungi

A fungus is a member of a large group of eukaryotic organisms that includes microorganisms, yeast and molds, as well as the more familiar mushrooms [252]. Fungal cells have cell walls that contain chitin, unlike the cell wall of plants, which contain cellulose. Like other eukaryotes, fungal cells contain membrane-bound nuclei with chromosomes that contain DNA with noncoding and coding regions. In addition, fungi possess membrane-bound cytoplasmic organelles such as mitochondria, sterol-containing membranes and ribosomes of the 80S type [252]. They resemble animals in that they lack chloroplasts and are heterotrophic organisms,

requiring preformed organic compounds as energy sources. They however, possess a cell wall and vacuoles. Fungi reproduce by both sexual and asexual means and like basal groups, such as ferns and mosses, produce spores.

Fungi can be true pathogens, such as Histoplasmosis and Coccodioidomycosis, that cause infections in healthy persons; or they can be opportunistic pathogens, such as Aspergillosis, Candidiasis, and Cryptococcosis, that cause infections in immuno-compromised persons including cancer patients, transplant recipients, and persons with AIDS. An example of a common fungus is the yeast organism which causes thrush and diaper rash (diaper dermatitis). Fungi are also used for the development of antibiotics, antitoxins and other drugs used to control human diseases. The fungus of choice for this study was *Candida albicans ATCC® 2091™**.

Candida albicans

Candida albicans is a diploid fungus that grows both as yeast and filamentous cells and a causal agent of opportunistic oral and genital infections in humans [253]. *Candida albicans* is commensal and a constituent of the normal gut flora comprising microorganisms that live in the human mouth and gastrointestinal tract. The fungus can also travel through the blood stream and affect the throat, intestines, and heart valves [254].

A common cause of candida infections may be the use of antibiotics that destroy beneficial, as well as harmful microorganisms in the body, permitting candida to multiply in their place. The resulting condition is known as candidiasis moniliasis or a "yeast infection".

Candida moniliasis is called thrush when it grows in the mouth, especially in infants; shows up on skin as a red, inflammed, and sometimes scaly rashy, such as diaper rash; causes vaginalitis moniliasis, commonly known as yeast infection in the vagina; causes candidal onchomycosis in the nails or paronychia next to the nails; and can also affect the oesophagus and the digestive tract. In rare instances, when body resistance is low as in leukemia or AIDS, *Candida albicans* can enter the bloodstream and cause serious infection of vital organs.

6.4.0 Microbial growth control

An antimicrobial agent is a chemotherapeutic agent used to treat the underlying cause of infectious disease, i.e., by inhibiting microbial growth and microbial survival. The single most important characteristic (of an antimicrobial agent) is selective toxicity, meaning that the antibiotic is far more toxic to the microorganism than to the host. It should be noted that no antimicrobial possesses no toxicity at all possible doses. Antimicrobial agents could be described as being antibiotics, synthetic drugs or semi-synthetic drugs depending on the mechanism of production. Antibiotics referred to chemical substances produced by bacteria or molds, which has the capacity to inhibit the growth of bacteria and even destroy bacteria and other organisms. Synthetic drugs on the other hand, are synthesized in the laboratory rather than by microorganisms while the semi-synthetic antimicrobials are obtained by chemically modifying a natural product, e.g., the chemical modification of an antibiotic or its precursor. However, antibiotics are now loosely used to include synthetic and semi-synthetic drugs; they are generally referred to as antibacterial.

6.5.0 Types of antimicrobial agents

Traditionally, antimicrobial agents have been classified based on their mechanism of action, chemical structure, or spectrum of activity. The primary mode of action is the inhibition of vital steps in the growth of the microorganism [255]. These steps include: bacterial or fungal cell wall synthesis; protein synthesis; nucleic acid synthesis; cell membrane function; and action as antimetabolites. The table 6.1 [256] below gives the classification of some antibiotics based on their mode of action.

Table 6.1: Classification of antibiotics

Site of action	**Antibiotic**
Cell wall (peptidoglycan) synthesis	Glycopeptides; β-lactams
Replication or transcription of general material	Quinolones; Nitroimidazoles; Rifampicin
Protein synthesis	Aminoglycosides; Chloramphenicol; Macrolides
Cell membrane functions (fungi)	Polymyxins

An antimicrobial drug that is effective against a large variety of microorganisms is said to have a broad spectrum of activity. Such a drug for instance would be effective against both Gram-

negative and Gram-positive bacteria. Advantages of using a broad-spectrum antibiotic are a high likelihood of efficacy against an unidentified pathogen. However, there is a high risk of the drug also destroying the non-pathogenic microorganisms normally found associated with a host. Normal flora can compete with pathogenic bacteria (microbial antagonism), thus preventing disease; removing these flora can thus make an individual more susceptible to subsequent disease. An example of broad spectrum antibiotic is tetracycline.

On the other hand, a narrow-spectrum antibiotic is effective against only a relatively small subset of bacteria and as such, its use allows an avoidance of some of the destruction of normal flora associated with antibiotic use. Penicillin is an example of an antibiotic possessing a relatively narrow spectrum of activity, acting particularly against Gram-positive bacteria. The main problem of narrow-spectrum antibiotics, however, is the need for identification of pathogen and, in some cases, pathogen antibiotic susceptibility before treatment can commence.

An antibiotic can be bactericidal or bacteriostatic. A bactericidal effect occurs when the antibiotic interaction results in an irreversible disruption or binding whereas a bacteriostatic effect involves lower affinity binding and as such is reversible when the antibiotic is removed from the environment. A bacteriostatic effect causes inhibition of the bacterial growth while bactericidal effect results in the death of the microorganisms.

6.6.0 Antimicrobial activity

The earliest methods for assessing the effects of antibiotics on bacterial involved the use of ditches cut into agar plates. Antibiotic solution poured into the ditch was allowed to diffuse out to inhibit the growth of the bacteria streaked perpendicular to the ditch. In 1943, Foster and woodruff used paper strips impregnated with antibiotics as an alternative source of diffusion [257]. The agar diffusion principles used in the bioassay of penicillin G were further used to develop the disk diffusion test [258]. Antibiotic reservoirs that initially consisted of antibiotic solutions in agar wells or cylinders were soon replaced by paper disks impregnated with antibiotics.

6.6.1 Disk diffusion techniques

Disk diffusion is a relatively "inexpensive", easy to use, flexible agar-based method that provides qualitative results for rapidly growing aerobic bacteria. However, disc diffusion is based on the use of a relatively unstable antibiotic concentration gradient generated from a point source diffusion centre, that is, the disk. The disk diffusion procedure is summarized as follows: A Petri dish containing an agar medium evenly inoculated with the test organism is prepared. Known amounts of the antimicrobial agent (synthetic or natural) are added to sterile antibiotic assay disks, which are then placed firmly on the surface of the agar. The inoculated agar plate and antimicrobial agent containing assay disks are incubated at a specific temperature for 10-24 hours or more. During the incubation, the agent diffuses from the assay disk into the agar; a zone of inhibition is created. The diameter of the zone is used to determine the effectiveness of the agent. This method is routinely used to test for antibiotic sensitivity in pathogens [259].

Many *in vitro* variables such as pre-diffusion, inoculum density, and growth phase, and variations in the agar plate, for example, depth, can directly influence zone sizes and therefore give unreliable results. Larger zones will be obtained with slow growing, fastidious organisms compared with rapidly growing aerobic bacteria directly as a consequence of a longer critical time and not necessarily a lower level of susceptibility. High molecular weight compounds such as vancomycin and polymyxin will not diffuse well in agar and are therefore difficult or inappropriate to test by disk diffusion.

Disk testing is an indirect qualitative method that has to be calibrated against reference MIC methods to generate clinically meaningful zone size-MIC-based interpretive criteria.

6.6.2 Minimal inhibitory concentration (MIC)

The lowest concentration of an antibiotic that will inhibit the growth of the organism being tested is known as the minimal inhibitory concentration (MIC). The MIC may assist in deciding the concentration of the antibiotic needed to inhibit the pathogen. The MIC test can be performed on agar or on liquid medium. The traditional method of determining the MIC is with the broth dilution technique [256], where serial dilutions of antibiotics are incorporated into the broth media in either the wells or microtitre plates or in culture tubes. The concentration of antibiotic

used may vary with the antimicrobial, organism identification, and site of infection. Each tube or well contains a different concentration of the antimicrobial agent and is inoculated with a fixed amount of the organism being tested. After appropriate incubation, the lowest concentration showing no invisible growth is considered as the MIC. MIC is a quantitative test and the result is expressed in micrograms per milli liter ($\mu g/ml$).

6.6.3 Enumeration of microorganisms

In order to ascertain the quantity of bacteria in a given sample, it is often necessary to determine the number of bacteria as well as to compare the amount of growth under various conditions [224]. Plate count, direct microscopic method and turbidity using spectrophotometer are some of the techniques used in determining the number as well as the growth of bacteria in a given sample.

6.7.0 Experimental

6.7.1 Materials and methods

All the ligands and the Cu(II) complexes were screened for antimicrobial activity against three bacterial strains (viz: *Escherichia coli ATCC® 8739™*, Staphylococcus aureus subsp. aureus ATCC® 6538™** and *Bacillus subtilis* subsp. *spizizeni ATCC® 6633™*)* and one fungal strain (*Candida albicans ATCC® 2091™**) using agar diffusion technique [256]. The minimum inhibitory concentration (MIC) values were determined using two-fold serial dilution method [260].

The microorganisms were purchased from Microbiologics, Cape Town, South Africa. Mueller Hinton agar (MH), Potato dextrose assay (PDA), agar bacteriological, nutrient broth and sterile Petri dishes (90 mm) were supplied by Merck (Pty) Ltd. Sterile antibiotic assay disks, 6.5 mm, were purchased from Davies diagnostics (Pty) limited, Randburg, South Africa. Other standard materials used were small stainless steel forceps, plastic loop, glass spreaders, sterile Petri dishes, disposable gloves, wooden swab, Eppendorf micropipettes, test-tubes, sterile 96-well microtitre plates, autoclave, incubator, incubator shaker and 0.50 McFarland standard.

6.7.2 Preparation of Mueller Hinton agar

A solution of the Mueller Hinton agar powder was prepared in accordance with the manufacturer's instructions. 22 g of Mueller Hinton agar powder and 17 g of agar bacteriological powder were dissolved in 1000 mL milli Q water and autoclaved for 15 minutes at 121 $^{\circ}$C. The solution was allowed to cool to about 50 $^{\circ}$C and 15-20 ml was aseptically poured into each of the required number of sterile Petri dishes. The dishes were covered with lids, allowed to set, then inverted and incubated for 24 hours at 37 $^{\circ}$C. The incubated plates were checked after the incubation period to ensure that bacteria free plates were used for the antimicrobial testing.

In the same vein, the potato disk assay (PDA) plates for the antifungal testing were prepared in similar manner.

6.7.3 Preparation of Turbidity standard (0.5 McFarland standard)

McFarland standard provides laboratory guidance for the standardization of numbers of bacteria for susceptibility testing or other procedures requiring a standardization of the inoculum. A 0.5 Mc Farland is comparable to bacteria suspension of 10^8 CFU/mL.

The 0.5 McFarland standard was prepared by adding 0.5 mL of a 1.175% (wt/vol) barium chloride dihydrate ($BaCl_2.2H_2O$) solution to 99.5 mL of 1% (vol/vol) sulfuric acid and shaken vigorously for five minutes. The accuracy of the density of the prepared McFarland standard was checked using PerkinElmer 25 spectrophotometer at a wavelength of 625 nm. The absorbance was between 0.08 and 0.1 and this corresponds to $1x10^6$ - 10^8 CFU/mL. The turbidity standard was then aliquoted into test tubes identical to those used to prepare the inoculum suspension.

6.7.4 Antibacterial susceptibility screening

The antimicrobial activity was evaluated using the disc diffusion technique [256]. Each test organism was inoculated onto a Mueller Hinton plate and incubated at 37 $^{\circ}$C for 24 hrs to obtain the primary culture. Several discrete colonies were picked from the culture to make a bacterial suspension (10 mL) in a test tube using saline water. The turbidity of the suspension was compared with 0.5 McFarland standard to obtain 10^6-10^8 CFU/mL. The bacterial suspension

(100 µL) was inoculated onto Mueller Hinton plate and the sterile discs that had been impregnated with the test compounds were firmly placed on it. The assay was inoculated at 37 ˚C for 16 hrs and the zone of inhibition was measured as millimeters diameter. Ampicillin was used as standard antibacterial drug, because it is the common antibacterial normally used for most antimicrobial screening. The test was repeated in triplicate for those compounds that showed activity of more than 6.5 mm and their activity was recorded as average zone of inhibition in tables 7.1-7.29.

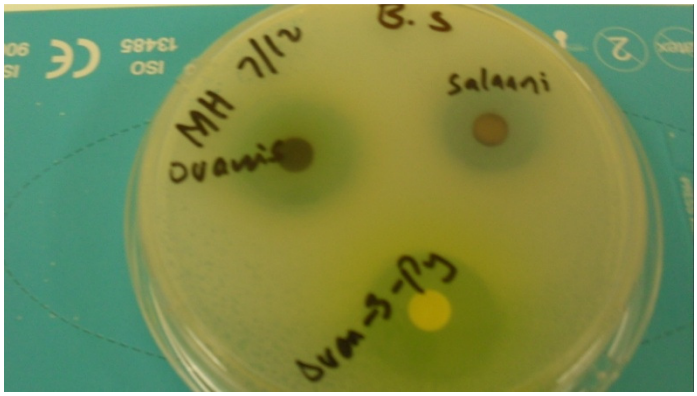

Fig. 6.2: Antimicrobial activity of the Schiff base ligands showing zone of inhibition against B. substilis

6.7.5 Minimum inhibitory concentration (MIC) assay

The quantitative antimicrobial activity of the test compounds was evaluated using macro dilution broth method according to Clinical and Laboratory Standard Institute (formally NCCLS) [260, 261]. Two-fold serial dilutions of the compounds were prepared in 96 wells microtitre plates using sterile nutrient broth as diluent. The plates were inoculated with 5 µL bacterial suspensions containing 10^6-10^8 CFUs and incubated at 37 ˚C for 16-18 hrs. The MIC value was defined as the lowest concentration of the compounds giving complete inhibition of visible growth. The MIC values for the compounds varied from 6.10 x 10^{-3} to 3.125 mg/mL and the results are presented in tables 7.30-7.46.

6.7.6 Antifungal susceptibility testing

The test compounds were screened for their antifungal activity against *Candida albicans ATCC® 2091™** using disc diffusion technique [256]. The fungus was grown on potato disc assay

(PDA) and the incubation was done at 28 °C for 48 hrs. Ketoconazole was used as standard antifungal drug and the zone of inhibition was measured as millimeters diameter. The test was repeated in triplicate for those compounds that showed activity of more than 6.5 mm and their activity was recorded as average zone of inhibition in table 7.10-7.29.

7.0.0 Antimicrobial assay results

The diameters of zone of inhibition and the minimum inhibitory concentration (MIC) values for the Schiff base ligands and the isolated Cu(II) complexes are presented in this chapter.

7.1.0 Disc diffusion results for the ligands

Table 7.1: Diameter of zone (mm) of inhibition for the aniline-based ligands

No.	**Compounds**	**Gram-positive**		**Gram-negative**	**Fungus**
		S. aureus	**B. substilis**	**E.coli**	**C. albicans**
L1	salaani	08	10	-	18
L16	ovaani	08	14	11	30
L32	pvaani	08	09	08	24
L45	vaani	-	08	-	-
	DMF (control)	-	-	-	-
	ampicillin (antibacterial)	52	38	28	
	ketoconazole (antifungal)				20

N.B: (-) non-active; blank--not tested

Table 7.2: Diameter of zone (mm) of inhibition for the chloroaniline-based ligands

No.	**Compounds**	**Gram-positive**		**Gram-negative**	**Fungus**
		S. aureus	**B. substilis**	**E.coli**	**C. albicans**
L2	sal-4-cla	-	08	-	-
L8	sal-2-cla	-	08	-	08
L17	ovan-4-cla	7.5	10	-	17
L23	ovan-2-cla	12	-	8.5	20

L33	pvan-4-cla	-	08	-	-
L39	pvan-2-cla	-	07	-	-
L46	van-4-cla	-	-	-	-
	DMF (control)	-	-	-	-
	ampicillin (antibacterial)	52	38	28	
	ketoconazole (antifungal)				20

Table 7.3: Diameter of zone (mm) of inhibition for the bromoaniline-based ligands

No.	**Compounds**	**Gram-positive**		**Gram-negative**	**Fungus**
		S. aureus	**B. substilis**	**E.coli**	**C. albicans**
L3	sal-4-bra	-	-	-	-
L9	sal-2-bra	-	08	-	-
L18	ovan-4-bra	-	9.5	-	15
L24	ovan-2-bra	12	-	09	21
L34	pvan-4-bra	-	08	-	-
L40	pvan-2-bra	-	-	-	07
L47	van-4-bra	-	-	-	-
	DMF (control)	-	-	-	-
	ampicillin (antibacterial)	52	38	28	
	ketoconazole (antifungal)				20

Table 7.4: Diameter of zone (mm) of inhibition for the methylaniline-based ligands

No.	Compounds	Gram-positive		Gram-negative	Fungus
		S. aureus	B.substilis	E.coli	C. albicans
L4	sal-4-tol	-	07	-	-
L10	sal-2-tol	-	08	08	07
L19	ovan-4-tol	-	10	10	21
L25	ovan-2-tol	16	10	11.5	26
L35	pvan-4-tol	-	08	-	-
L41	pvan-2-tol	-	-	-	08
L48	van-4-tol	-	-	-	-
	DMF (control)	-	-	-	-
	ampicillin (antibacterial)	52	38	28	
	ketoconazole (antifungal)				20

Table 7.5: Diameter of zone (mm) of inhibition for the methoxyaniline-based ligands

No.	Compounds	Gram-positive		Gram-negative	Fungus
		S. aureus	B.substilis	E.coli	C. albicans
L5	sal-4-nis	07	-	-	-
L11	sal-2-nis	-	09	-	07
L20	ovan-4-nis	-	10	-	20
L26	ovan-2-nis	16	16	14	44
L36	pvan-4-nis	-	08	-	-
L39	van-4-nis	-	08	-	-
	DMF (control)	-	-	-	-
	ampicillin (antibacterial)	52	38	28	
	ketoconazole (antifungal)				20

Table 7.6: Diameter of zone (mm) of inhibition for the nitroaniline-based ligands

No.	**Compounds**	**Gram-positive**		**Gram-negative**	**Fungus**
		S. aureus	**B. substilis**	**E.coli**	**C. albicans**
L6	sal-4-nit	-	-	-	12
L21	ovan-4-nit	8.5	10	08	29
L37	pvan-4-nit	-	-	-	-
	DMF (control)	-	-	-	-
	ampicillin (antibacterial)	52	38	28	
	ketoconazole (antifungal)				20

Table 7.7: Diameter of zone (mm) of inhibition for the hydroxyaniline-based ligands

No.	**Compounds**	**Gram-positive**		**Gram-negative**	**Fungus**
		S. aureus	**B. substilis**	**E.coli**	**C. albicans**
L7	sal-4-phen	14	17	09	-
L12	sal-2-phen	28	28	12	08
L22	ovan-4-phen	12	15	11.5	25
L27	ovan-2-phen	25	21	14	25
L38	Pvan-4-phen	13	14	10	21
L42	pvan-2-phen	-	11	-	07
L50	van-4-phen	20	20	09	-
	DMF (control)	-	-	-	-
	ampicillin (antibacterial)	52	38	28	
	ketoconazole (antifungal)				20

Table 7.8: Diameter of zone (mm) of inhibition for the 1-aminonaphthalene-based ligands

No.	**Compounds**	**Gram-positive**		**Gram-negative**	**Fungus**
		S. aureus	**B. substilis**	**E.coli**	**C. albicans**
L13	sal-1-amnaph	-	-	-	-
L28	ovan-1-amnaph	-	10	-	18
L43	pvan-1-amnaph	-	09	-	-
L51	van-1-amnaph	-	-	-	11
	DMF (control)	-	-	-	-
	ampicillin (antibacterial)	52	38	28	
	ketoconazole (antifungal)				20

Table 7.9: Diameter of zone (mm) of inhibition for the aminopyridine-based ligands

No.	**Compounds**	**Gram-positive**		**Gram-negative**	**Fungus**
		S. aureus	**B. substilis**	**E.coli**	**C. albicans**
L14	sal-2-ampy	-	-	-	-
L15	sal-3-ampy	-	-	-	-
L29	ovan-2-ampy	16	14	13	36
L30	ovan-3-ampy	17	12	16	36
L44	pvan-3-ampy	09	11	12	30
L52	van-3-ampy	-	-	-	-
	DMF (control)	-	-	-	-
	ampicillin (antibacterial)	52	38	28	
	ketoconazole (antifungal)				20

Table 7.10: Diameter of zone (mm) of inhibition for the aminomethylpyridine-based ligands

No.	Compounds	Gram-positive		Gram-negative	Fungus
		S. aureus	B. substilis	E.coli	C. albicans
L16	sal-3-pico	09	09	11	-
L31	ovan-2-pico	14	11	11	27
L51	van-3-pico	-	08	-	-
	DMF (control)	-	-	-	-
	ampicillin (antibacterial)	52	38	28	
	ketoconazole (antifungal)				20

Table 7.11: Diameter of zone (mm) of inhibition for the 2-aminobenzimidazole-based ligands

No.	Compounds	Gram-positive		Gram-negative	Fungus
		S. aureus	B. substilis	E.coli	C. albicans
L54	sal-2-AmBZI	07	08	09	08
L55	ovan-2-AmBZI	12	07	16	36
L56	ovan2-AmBZI	10	15	08	-
	DMF (control)	-	-	-	-
	ampicillin (antibacterial)	52	38	28	
	ketoconazole (antifungal)				20

Table 7.12: Diameter of zone (mm) of inhibition for the *o*-phenylenediamine-based ligands

No.	**Compounds**	**Gram-positive**		**Gram-negative**	**Fungus**
		S. aureus	**B. substilis**	**E.coli**	**C. albicans**
L57	bis-salphen				08
L58	bis-ovanphen	08	13	07	28
	DMF (control)	-	-	-	-
	ampicillin (antibacterial)	52	38	28	
	ketoconazole (antifungal)				20

7.2.0 Disc diffusion results for the complexes

Table 7.13: Diameter of zone (mm) of inhibition for ligands L1 and L6 with their complexes

No.	**Compounds**	**Gram-positive**		**Gram-negative**	**Fungus**
		S. aureus	**B. substilis**	**E.coli**	**C. albicans**
L1	salaani	08	10	-	18
	$Cu(salaani)_2Cl_2.2½\,2H_2O$	10	12	07	-
L6	ovaani	13	14	12	30
	$Cu(ovaani)_2Cl_2.H_2O.½\,2EtOH$	11	12	11	34.5
	DMF (control)	-	-	-	-
	ampicillin (antibacterial)	52	38	28	
	ketoconazole (antifungal)				20

Table 7.14: Diameter of zone (mm) of inhibition for ligands L2 and L8 with their complexes

No.	Compounds	Gram-positive		Gram-negative	Fungus
		S. aureus	B. substilis	E.coli	C. albicans
L2	sal-4-cla	-	08	-	-
	$Cu(sal\text{-}4\text{-}cla)Cl_2.2H_2O$	-	08	-	-
L8	sal-2-cla	-	08	-	08
	$Cu(sal\text{-}2\text{-}cla)_2$	*ns	*ns	*ns	*ns
	DMF (control)	-	-	-	-
	ampicillin (antibacterial)	52	38	28	
	ketoconazole (antifungal)				20

*ns: not soluble

Table 7.15: Diameter of zone (mm) of inhibition for ligands L17 and L23 with their complexes

No.	Compounds	Gram-positive		Gram-negative	Fungus
		S. aureus	B. substilis	E.coli	C. albicans
L17	ovan-4-cla	7.5	10	-	17
	$Cu(ovan\text{-}4\text{-}cla)_2$	*ns	*ns	*ns	*ns
L23	ovan-2-cla	12	-	8.5	20
	$Cu(ovan\text{-}2\text{-}cla)_2$	-	-	-	16
	DMF (control)	-	-	-	-
	ampicillin (antibacterial)	52	38	28	
	ketoconazole (antifungal)				20

*ns: not soluble

Table 7.16: Diameter of zone (mm) of inhibition for ligands L3 and L9 with their complexes

No.	**Compounds**	**Gram-positive**		**Gram-negative**	**Fungus**
		S. aureus	**B. substilis**	**E.coli**	**C. albicans**
L3	sal-4-bra	-	-	-	-
	$Cu(sal\text{-}4\text{-}bra)Cl_2.H_2O$	-	-	-	13
L9	sal-2-bra	-	08	-	-
	$Cu(sal\text{-}2\text{-}bra)_2$	*ns	*ns	*ns	*ns
	DMF (control)	-	-	-	-
	ampicillin (antibacterial)	52	38	28	
	ketoconazole (antifungal)				20

*ns: not soluble

Table 7.17: Diameter of zone (mm) of inhibition for ligands L18 and L24 with their complexes

No.	**Compounds**	**Gram-positive**		**Gram-negative**	**Fungus**
		S. aureus	**B. substilis**	**E.coli**	**C. albicans**
L18	ovan-4-bra	-	9.5	-	15
	$Cu(ovan\text{-}4\text{-}bra)Cl_2.H_2O$	-	10	-	23
L24	ovan-2-bra	12	-	09	21
	$Cu(ovan\text{-}2\text{-}bra)_2$	-	08	07	16
	DMF (control)	-	-	-	-
	ampicillin (antibacterial)	52	38	28	
	ketoconazole (antifungal)				20

Table 7.18: Diameter of zone (mm) of inhibition for ligands L4 and L10 with their complexes

No.	Compounds	Gram-positive		Gram-negative	Fungus
		S. aureus	B. substilis	E.coli	C. albicans
L4	sal-4-tol	-	07	-	-
	Cu(sal-4-tol)$Cl_2.H_2O$	09	12	-	13
L10	sal-2-tol	-	08	08	07
	Cu(sal-2-tol)$_2$	-	-	-	-
	DMF (control)	-	-	-	-
	ampicillin (antibacterial)	52	38	28	
	ketoconazole (antifungal)				20

Table 7.19: Diameter of zone of inhibition for ligands L19 and L25 complexes

No.	Compounds	Gram-positive		Gram-negative	Fungus
		S. aureus	B. substilis	E.coli	C. albicans
L19	ovan-4-tol	-	10	-	21
	Cu(ovan-4-tol)$Cl_2.2½2H_2O$	10	12	10	27
L25	ovan-2-tol	11.5	10	16	26
	Cu(ovan-2-tol)$_2$	*ns	*ns	*ns	*ns
	DMF (control)	-	-	-	-
	ampicillin (antibacterial)	52	38	28	
	ketoconazole (antifungal)				20

*ns: not soluble

Table 7.20: Diameter of zone (mm) of inhibition for ligands L5 and L11 with their complexes

No.	**Compounds**	**Gram-positive**		**Gram-negative**	**Fungus**
		S. aureus	**B. substilis**	**E.coli**	**C. albicans**
L5	sal-4-nis	07	**-**	-	12
	$Cu(sal\text{-}4\text{-}nis)_2$	09	09	-	07
L11	sal-2-nis	-	09	-	07
	$Cu(sal\text{-}2\text{-}nis)_2$	07	-	08	16
	DMF (control)	-	-	-	-
	ampicillin (antibacterial)	52	38	28	
	ketoconazole (antifungal)				20

Table 7.21: Diameter of zone (mm) of inhibition for ligands L20 and L26 with their complexes

No.	**Compounds**	**Gram-positive**		**Gram-negative**	**Fungus**
		S. aureus	**B. substilis**	**E.coli**	**C. albicans**
L20	ovan-4-nis	-	10	-	21
L26	ovan-2-nis	16	16	14	44
	$Cu(ovan\text{-}2\text{-}nis)_2$	-	-	-	21
	DMF (control)	-	-	-	-
	ampicillin (antibacterial)	52	38	28	
	ketoconazole (antifungal)				20

Table 7.22: Diameter of zone (mm) of inhibition for ligands L6 and L21 with their complexes

No.	**Compounds**	**Gram-positive**		**Gram-negative**	**Fungus**
		S. aureus	**B. substilis**	**E.coli**	**C. albicans**
L6	sal-4-nit	-	-	-	12
	$Cu(sal\text{-}4\text{-}nit)_2$	*ns	*ns	*ns	*ns
L21	ovan-4-nit	-	10	-	29
	Cu(ovan-4-nit).2EtOH	-	-	-	15
	DMF (control)	-	-	-	-
	ampicillin (antibacterial)	52	38	28	
	ketoconazole (antifungal)				20

*ns: not soluble

Table 7.23: Diameter of zone (mm) of inhibition for ligands L7 and L12 with their complexes

No.	**Compounds**	**Gram-positive**		**Gram-negative**	**Fungus**
		S. aureus	**B. substilis**	**E.coli**	**C. albicans**
L7	sal-4-phen	-	10	-	29
	$Cu(sal\text{-}4\text{-}phen)_2Cl_2.H_2O$	07	10	-	-
L12	sal-2-phen	28	28	12	08
	$Cu_2(sal\text{-}2\text{-}phen)_2$	*ns	*ns	*ns	*ns
	DMF (control)	-	-	-	-
	ampicillin (antibacterial)	52	38	28	
	ketoconazole (antifungal)				20

*ns: not soluble

Table 7.24: Diameter of zone of inhibition for ligands L22 and L27 with their complexes

No.	Compounds	Gram-positive		Gram-negative	Fungus
		S. aureus	B. substilis	E.coli	C. albicans
L22	ovan-4-phen	12	15	11.5	25
	$Cu(ovan\text{-}phen)Cl_2.H_2O$	08	11	08	30
L27	ovan-2-phen	25	21	14	25
	$Cu_2(ovan\text{-}2\text{-}phen)_2$	*ns	*ns	*ns	*ns
	DMF (control)	-	-	-	-
	ampicillin (antibacterial)	52	38	28	
	ketoconazole (antifungal)				20

*ns: not soluble

Table 7.25: Diameter of zone (mm) of inhibition for ligands L13 and L28 with their complexes

No.	Compounds	Gram-positive		Gram-negative	Fungus
		S. aureus	B. substilis	E.coli	C. albicans
L13	sal-1-amnaph	-	-	-	-
	$Cu(sal\text{-}1\text{-}amnaph)_2$	-	18	08	13
L28	ovan-1-amnaph	-	10	-	18
	$Cu(ovan\text{-}1\text{-}amnaph)_2$	09	09	08	-
	DMF (control)	-	-	-	-
	ampicillin (antibacterial)	52	38	28	
	ketoconazole (antifungal)				20

Table 7.26: Diameter of zone (mm) of inhibition for ligand L14 and L15 with their complexes

No.	Compounds	Gram-positive		Gram-negative	Fungus
		S. aureus	B. substilis	E.coli	C. albicans
L14	sal-2-ampy	-	-	-	-
	$Cu(sal\text{-}2\text{-}ampy)_2Cl_2$	-	12	-	-
L15	sal-3-ampy	-	-	-	-
	$Cu(sal\text{-}3\text{-}ampy)_2Cl_2 / 2H_2O$	-	11	-	-
	DMF (control)	-	-	-	-
	ampicillin (antibacterial)	52	38	28	
	ketoconazole (antifungal)				20

Table 7.27: Diameter of zone of inhibition for ligands L29 and L30 with their complexes

No.	Compounds	Gram-positive		Gram-negative	Fungus
		S. aureus	B. substilis	E.coli	C. albicans
L29	ovan-2-ampy	16	14	13	36
	$Cu(ovan\text{-}2ampy)Cl_2.H_2O$	14	15	08	09
L30	ovan-3-ampy	17	12	16	36
	$Cu(ovan\text{-}3\text{-}ampy)_2Cl_2.H_2O$	15	16	13	31
	DMF (control)	-	-	-	-
	ampicillin (antibacterial)	52	38	28	
	ketoconazole (antifungal)				20

Table 7.28: Diameter of zone (mm) of inhibition for ligands L16 and L31 with their complexes

No.	Compounds	Gram-positive		Gram-negative	Fungus
		S. aureus	B. substilis	E.coli	C. albicans
L16	sal-3-pico	09	09	11	-
	$Cu(sal\text{-}3\text{-}pico)_2Cl_2/2H_2O$	-	14	-	12
L31	ovan-2-pico	14	11	11	27
	Cu(ovan-2-pico)Cl	16	15	08	22
	DMF (control)	-	-	-	-
	ampicillin (antibacterial)	52	38	28	
	ketoconazole (antifungal)				20

Table 7.29: Diameter of zone of inhibition for ligands L54, L55, L56 and their complexes

No.	Compounds	Gram-positive		Gram-negative	Fungus
		S. aureus	B. substilis	E.coli	C. albicans
L54	sal-2-AmBZI	07	08	09	08
	$Cu(sal\text{-}2\text{-}AmBZI)_2$	09	10	08	-
L55	ovan-2-AmBZI	12	07	16	36
	$Cu(ovan\text{-}2\text{-}AmBZI)_2$	10	10	10	22
L56	pvan-2-AmBZI	10	15	08	-
	$Cu(pvan\text{-}2\text{-}AmBZI)_2$	-	-	-	-
	DMF (control)	-	-	-	-
	ampicillin (antibacterial)	52	38	28	
	ketoconazole (antifungal)				20

Table 7.30: Diameter of zone of inhibition for ligands L57 and L58 their complexes

No.	Compounds	Gram-positive		Gram-negative	Fungus
		S. aureus	B. substilis	E.coli	C. albicans
L54	bis-salphen	10	10	08	08
	Cu(bis-salphen)	10.5	08	-	07
L55	bis-ovanphen	08	13	07	28
	Cu(bis-ovanphen).H_2O	-	09	10	-
	DMF (control)	-	-	-	-
	ampicillin (antibacterial)	52	38	28	
	ketoconazole (antifungal)				20

7.3.0 MIC results for the ligands and the complexes

Table 7.31: MIC values for ligands L1 and L6 with their complexes (1 x 10^{-1} mg/mL)

No.	Compounds	Gram-positive		Gram-negative
		S. aureus	B. substilis	E.coli
	salaani	08	7.8125 (10)	-
	Cu(salaani)$_2Cl_2.2½\,2H_2O$	3.9062 (10)	3.9062 (12)	7.8125 (07)
	ovaani	3.9062 (13)	3.9062 (14)	7.8125 (12)
	Cu(ovaani)$_2Cl_2.H_2O.½\,2EtOH$	0.2441 (11)	1.9531 (12)	0.3125 (11)

N.B: The diameter of zone of inhibition (mm) is given in paranthesis

Table 7.32: MIC values for ligands L2 and L8 with their complexes (1 x 10^{-1} mg/mL)

No.	Compounds	Gram-positive		Gram-negative
		S. aureus	B. substilis	E. coli
L2	sal-4-cla	-	3.9062 (08)	-
	Cu(sal-4-cla)Cl_2.2H_2O	-	3.9062 (08)	-
L8	Sal-2-cla	-	31.25 (08)	-
	Cu(Sal-2-cla)$_2$	*ns	*ns	*ns

*ns: not soluble

Table 7.33: MIC values for ligands L17 and L23 with their complexes (1x 10^{-1} mg/mL)

No.	Compounds	Gram-positive		Gram-negative
		S. aureus	B. substilis	E.coli
L17	ovan-4-cla	7.8125 (7.5)	7.8125 (10)	-
	Cu(ovan-4-cla)$_2$	*ns	*ns	*ns
L23	ovan-2-cla	1.9531 (12)	-	1.9531 (8.5)
	Cu(ovan-2-cla)$_2$	-	-	-

*ns: not soluble

Table 7.34: MIC values for ligands L3 and L9 with their complexes (1 x 10^{-1} mg/mL)

No.	Compounds	Gram-positive		Gram-negative
		S. aureus	B. substilis	E.coli
L3	sal-4-bra	-	-	-
	Cu(sal-4-bra)Cl_2.H_2O	-	-	-
L9	sal-2-bra	-	31.250 (08)	-
	Cu(sal-2-bra)$_2$	*ns	*ns	*ns

*ns: not soluble

Table 7.35: MIC values for ligands L18 and L24 with their complexes (1 x 10^{-1} mg/mL)

No.	Compounds	Gram-positive		Gram-negative
		S. aureus	**B. substilis**	**E.coli**
L18	ovan-4-bra	-	31.25 (9.5)	-
	Cu(ovan-4-bra)$Cl_2.H_2O$	-	31.25 (10)	-
L24	ovan-2-bra	7.8125 (12)	-	7.8125 (09)
	Cu(ovan-2-bra)$_2$	-	7.8125 (08)	62.50 (07)

Table 7.36: MIC for ligands L4 and L10 with their complexes (1 x 10^{-1} mg/mL)

No.	Compounds	Gram-positive		Gram-negative
		S. aureus	**B. substilis**	**E.coli**
L4	sal-4-tol	-	7.8125 (07)	-
	Cu(sal-4-tol)$Cl_2.H_2O$	0.9766 (09)	7.8125 (12)	-
L10	sal-2-tol	-	15.625 (08)	7.8125 (08)
	Cu(sal-2-tol)$_2$	-	-	-

Table 7.37: MIC values for ligands L19 and L25 complexes (1 x 10^{-1} mg/mL)

No.	Compounds	Gram-positive		Gram-negative
		S. aureus	**B. substilis**	**E.coli**
L19	ovan-4-tol	-	3.9062 (10)	-
	Cu(ovan-4-tol)$Cl_2.2½H_2O$	0.1220 (10)	7.812 (12)	31.250 (10)
L25	ovan-2-tol	3.9063 (11.5)	7.8125 (10)	1.9531 (16)
	Cu(ovan-2-tol)$_2$	*ns	*ns	*ns

*ns: not soluble

Table 7.38: MIC values for ligands L5 and L11 with their complexes (1 x 10^{-1} mg/mL)

No.	Compounds	Gram-positive		Gram-negative
		S. aureus	B. substilis	E.coli
L5	sal-4-nis	-	-	-
	$Cu(sal\text{-}4\text{-}nis)_2$	31.250 (09)	7.8125 (09)	-
L11	sal-2-nis	-	15.625 (09)	-
	$Cu(sal\text{-}2\text{-}nis)_2$	31.250 (07)	-	31.250 (08)

Table 7.39: MIC values for ligands L20 and L26 with their complexes (1 x 10^{-1} mg/mL)

No.	Compounds	Gram-positive		Gram-negative
		S. aureus	B. substilis	E.coli
L20	ovan-4-nis	-	3.9063 (10)	-
	$Cu(ovan\text{-}4\text{-}nis)_2$	-	-	-
L26	Ovan-2-nis	3.9063 (16)	3.9063 (16)	3.9063 (14)
	$Cu(ovan\text{-}2\text{-}nis)_2$	-	-	-

Table 7.40: MIC values for ligands L6 and L21 with their complexes (1 x 10^{-1} mg/mL)

No.	Compounds	Gram-positive		Gram-negative
		S. aureus	B. substilis	E.coli
L6	sal-4-nit	-	-	-
	$Cu(sal\text{-}4\text{-}nit)_2$	*ns	*ns	*ns
L21	ovan-4-nit	15.6250 (8.5)	3.9062 (10)	3.9062 (08)
	Cu(ovan-4-nit).2EtOH	-	-	-

*ns: not soluble

Table 7.41: MIC values for ligands L7 and L12 with their complexes (1 x 10^{-1} mg/mL)

No.	Compounds	Gram-positive		Gram-negative
		S. aureus	B. substilis	E.coli
L7	sal-4-phen	-	1.9531 (10)	-
	$Cu(sal\text{-}4\text{-}phen)_2Cl_2.H_2O$	1.9531 (07)	7.8125 (10)	-
L12	sal-2-phen	3.9063 (28)	0.1221 (28)	3.9063 (12)
	$Cu_2(Sal\text{-}2\text{-}phen)_2$	*ns	*ns	*ns

*ns: not soluble

Table 7.42: MIC values for ligands L22 and L27 with their complexes (1 x 10^{-1} mg/mL)

No.	Compounds	Gram-positive		Gram-negative
		S. aureus	B. substilis	E.coli
L22	ovan-4-phen	0.4883 (12)	0.9766 (15)	3.9062 (11.5)
	$Cu(ovan\text{-}phen)Cl_2.H_2O$	7.8125 (08)	0.9766 (11)	1.9531 (08)
L27	ovan-2-phen	0.4883 (25)	0.1221 (21)	0.9766 (14)
	$Cu_2(ovan\text{-}2\text{-}phen)_2$	*ns	*ns	*ns

*ns: not soluble

Table 7.43: MIC values for ligands L13 and L28 with their complexes (1 x 10^{-1} mg/mL)

No.	Compounds	Gram-positive		Gram-negative
		S. aureus	B. substilis	E.coli
L13	sal-1-amnaph	-	-	-
	$Cu(sal\text{-}1\text{-}amnaph)_2$	-	0.4883 (18)	15.625 (08)
L28	ovan-1-amnaph	-	3.9063 (10)	-
	$Cu(ovan\text{-}1\text{-}amnaph)_2$	09 (15.625)	7.8125 (09)	15.625 (08)

Table 7.44: MIC values for ligand L14 and L15 with their complexes (1 x 10^{-1} mg/mL)

No.	Compounds	Gram-positive		Gram-negative
		S. aureus	B. substilis	E.coli
L14	sal-2-ampy	-	-	-
	$Cu(sal\text{-}2\text{-}ampy)_2Cl_2$	-	1.9531 (12)	-
L15	sal-3-ampy	-	-	-
	$Cu(sal\text{-}3\text{-}ampy)_2Cl_2{}^1/2H_2O$	-	0.9766 11)	-
	DMF (control)	-	-	-

Table 7.45: MIC for ligands L29 and L30 with their complexes (1 x 10^{-1} mg/mL)

No.	Compounds	Gram-positive		Gram-negative
		S. aureus	B. substilis	E.coli
L29	ovan-2-ampy	3.9064 (16)	1.9531 (14)	15.625 (13)
	$Cu(ovan\text{-}2ampy)Cl_2.H_2O$	3.9062 (14)	0.2441 (15)	1.9531 (08)
L30	ovan-3-ampy	3.9062 (17)	0.9765 (12)	31.250 (16)
	$Cu(ovan\text{-}3\text{-}ampy)_2Cl_2.H_2O$	3.9062 (15)	0.1220 (16)	7.8125 (13)

Table 7.46: MIC values for ligands L16 and L31 with their complexes (1 x 10^{-1} mg/mL)

No.	Compounds	Gram-positive		Gram-negative
		S. aureus	B. substilis	E.coli
L16	sal-3-pico	7.8125 (09)	3.9063 (09)	1.9531 (11)
	$Cu(sal\text{-}3\text{-}pico)_2Cl_2{}^1/2H_2O$	-	14 (3.1250)	-
L31	ovan-2-pico	7.8125 (14)	11 (1.9531)	31.2500 (11)
	Cu(ovan-2-pico)Cl	0.1220 (16)	0.4883 (15)	31.2500 (08)

Table 7.47: MIC values for ligands L54, L55 and L56 with their complexes

No.	Compounds	Gram-positive		Gram-negative
		S. aureus	B. substilis	E.coli
L54	sal-2-AmBZI	7.8125 (07)	7.8125 (08)	7.8125 (09)
	$Cu(sal\text{-}2\text{-}AmBZI)_2$	1.9531 (09)	0.9766 (10)	7.8125 (8)
L55	ovan-2-AmBZI	7.8125 (12)	1.9531 (07)	1.9531 (16)
	$Cu(ovan\text{-}2\text{-}AmBZI)_2$	3.9063 (10)	1.9531 (10)	62.50 (10)
L56	pvan-2-AmBZI	125.00 (10)	3.9063 (15)	250.00 (08)
	$Cu(pvan\text{-}2\text{-}AmBZI)_2$	-	-	-

Table 7.48: Diameter of zone of inhibition for ligands L57 and L58 their complexes

No.	Compounds	Gram-positive		Gram-negative
		S. aureus	B. substilis	E.coli
L54	bis-salphen	3.9063 (10)	1.9531 (10)	7.8125 (8)
	Cu(bis-salphen)	1.9531 (10.5)	3.9063 (08)	-
L55	bis-ovanphen	7.8125 (08)	0.9766 (13)	125.00 (07)
	$Cu(bis\text{-}ovanphen).H_2O$	-	7.8125 (09)	62.50 (10)

8.0.0 Discussion of the antimicrobial activity of the compounds

The Schiff base ligands and the isolated complexes were screened for their antimicrobial activity against *Escherichia coli ATCC® 8739™*, Staphylococcus aureus subsp. aureus ATCC® 6538™*, Bacillus subtilis* subsp. *spizizeni ATCC® 6633™** and *Candida albicans ATCC® 2091™** using agar disc diffusion and broth dilution techniques. The qualitative susceptibility of the test organisms was evaluated using agar disc diffusion technique while the minimum inhibitory concentration (MIC) values were obtained using broth dilution technique. The MIC values gave the quantitative evaluation of the activity of the synthesized compounds against the microorganisms.

Summarily, the presence of the methoxyl and hydroxyl groups at the para position of the aniline groups gave the most promising potency of all the compounds tested. Also, it was observed that the *o*-vanillin analogues of the studied compounds exhibited the highest activity compared to the salicylaldehyde, *p*-vanillin and vanillin analogues with the vanillin analogues being virtually non-active. All the *o*- and *p*-hydroxyaniline Schiff base ligands excepting ligand L42 (pva-2-phen) exhibited potency against all the tested organisms. The study also revealed that the fungus, *Candida albicans ATCC® 2091™**, was the most susceptible of all the microorganisms tested with the gram negative bacteria, *Escherichia coli ATCC® 8739™**, being the least susceptible. All the test compounds were active slightly against *Bacillus subtilis* subsp. *spizizeni ATCC® 6633™**. None of the compounds was as active as penicillin, the standard antibacterial drug, but compete favourably well in several cases with ketoconazole, the standard antifungal drug.

The Cu(II) complexes are expected to be more potent than the corresponding free Schiff base ligands. This is because, according to Tweedy's chelation theory [262], chelation reduces the polarity of the metal ion by sharing its positive charge with the donor atoms and also through the delocalization of π electrons in the whole chelate ring. This in turn, increases the lipophilicity of the compound across the lipolayer of the microbial cell wall. However, a general trend was not

observed in this study. The copper(II) complexes enhanced the activity in some cases, while the introduction of the metal ion caused a decrease in activity of the free ligands in the other.

8.1 Antimicrobial activity of the aniline-based compounds

The diameter of zone of inhibition for the aniline-based ligands is presented in table 7. As explained above, ligand L16 (ovaani) showed the highest activity in this series and it was active against all the tested organisms with highest potency being against the fungal strain. Salaani and pvaani (L1 and L32) showed similar activity against the gram positive bacteria while vaani, ligand L45, was virtually non-active against all the tested organisms except with the *Bacillus substilis* species where it showed slight activity. Ovaani and pvaani exhibited higher potency than the standard antifungal drug, ketoconazole.

The antibacterial activity of salaani was slightly enhanced upon chelation while a complete loss of antifungal activity of the free Schiff base ligand occured in the complex. On the other hand, chelation of ovaani with copper(II) ions resulted in a slight reduction in its antibacterial activity associated with an enhancement of its antifungal activity. The diameters of zone of inhibition for the aniline-based complexes are presented in table 7.12.

The MIC values for the Schiff base ligands and the complexes are presented in table 7.12. The values agreed quite well with the disc diffusion results, for instance, the minimum concentration of ovaani required to inhibit the growth of E. coli was higher (7.8125×10^{-1} mg/mL) than the amount required for *S. aureus* and *B. substilis* (3.9062×10^{-1} mg/mL).

8.2 Antimicrobial activity of the chloroaniline-based compounds

The diameters of zone of inhibition for the chloroaniline-based Schiff base ligands are presented in table 7.2. All the members of this series, except ovan-2-cla (L23) and ovan-4-cla (L17), are not active against the tested pathogenic microorganisms; *S. aureus, E. coli and C. albicans.* The antifungal activity of the two ligands was very close to that observed for the standard antifungal drug, ketoconazole.

However, on chelation, ovan-2-cla (L23) Schiff base lost its antibacterial activity accompanied with a slight reduction in its antifungal activity. The Cu(II) complex of ovan-4-cla (L17) was however, not soluble in both DMF and DMSO. In the same vein, chelation had no impact on the activity of the other members of the series. The diameters of zone of inhibition of the chloroaniline based complexes are presented in tables 7.13 and 7.14.

8.3 Antimicrobial activity of the bromoaniline-based compounds

The diameters of zone of inhibition for the bromoaniline-based Schiff base ligands are presented in table 7.3. As with the chloroaniline analogues, the members of this series exhibited no antimicrobial activity excepting ovan-2-bra (L24) Schiff base ligand. It has similar activity with the standard antifungal drug, ketoconazole.

On chelation, ovan-2-bra (L24) lost its antibacterial activity with a corresponding decrease in its antifungal activity. Copper(II) complexes of sal-4 bra (L3) and ovan-4-bra (L18) complexes, however, exhibited higher antifungal activity. The diameters of zone of inhibition for the bromoaniline-based complexes are presented in tables 7.15 and 7.16.

8.4 Antimicrobial activity of the methylaniline-based compounds

The diameters of zone of inhibition for the methylaniline-based Schiff base ligands are presented in table 7.4. Once again, the presence of the methyl substituent lead to a complete lost of antimicrobial activity of the aniline-based Schiff base ligands except for the ovan-2-tol (L25) ligand. The antifungal activity of ovan-2-tol (L25) Schiff base ligand is slightly higher than ketoconazole.

Chelation resulted in good improvement of the antimicrobial activity of sal-4-tol (L4) and ovan-4-tol (L19) Schiff base ligands, enhancing the antifungal activity significantly. The Cu(II) complex of ovan-2-tol (L25) was not soluble in DMF and DMSO. The diameters of zone of inhibition for the methylaniline-based complexes are presented in tables 7.17 and 7.18.

8.5 The antimicrobial activity of the methoxyaniline-based compounds

The diameters of zone of inhibition for the methoxyaniline-based Schiff bases are presented in table 7.5. In compliance with all the other substituted aniline-based Schiff bases, only the Schiff base ligand of ovan-2-nis (L26) exhibited antimicrobial activity against the tested micro-organisms and it possessed twice the antifungal activity of ketoconazole. This could be adduced to the synergistic effect of the methoxyl group on both the aniline and the aldehyde moiety at position 4 and 2 respectively. Ovan-4-nis (L20) Schiff base ligand equally has a comparative antifungal activity; 20 mm.

On chelation with copper(II) ions, the antibacterial activity of ovan-2-nis (L16) Schiff base ligand was lost completely with the antifungal activity drastically reduced by 50%. On the other hand, the antimicrobial activity of sal-4-nis (L5) Schiff base ligand became enhanced upon complexation with copper(II) ions. The diameters of zone of inhibition for the methoxyaniline-based complexes are presented in tables 7.19 and 7.20.

8.6 The antimicrobial activity of the nitroaniline-based compounds

The diameters of zone of inhibition for the nitroaniline-based Schiff bases are presented in table 7.6. In this series, only the ovan-4-nit (L21) Schiff base ligand was active against the tested microorganism, having a higher antifungal activity than ketoconazole.

On complexation however, the antimicrobial activity of the free ligand was lost completely, with the concomitant reduction of the antifungal activity by 50%. The diameters of zone of inhibition for the nitroaniline-based complexes are presented in table 7.21.

8.7 The antimicrobial activity of hydroxyaniline-based compounds

The diameters of zone of inhibition for the hydroxyaniline-based Schiff bases are presented in tables 7.7. In contrast to all the other analogues of the substituted aniline-based Schiff base ligands, all the members of this series exhibited significant potency, excepting pvan-2-phen (L42) Schiff base, against the tested micro-organisms. This could be adduced to the electron donating ability of the hydroxyl substituent, probably increasing the lipophilicity of the compound and thus resulting in the observed activity. The low activity of the pvan-2-phen

analogue might be due to the presence of the hydroxyl group at the 2-position on both the aldehyde and the amine moieties of the Schiff base respectively. It should be noted that the salicylaldehyde analogues of this series exhibited very low antifungal activity, perhaps due to the absence of the methoxyl group on the aldehyde moiety.

On chelation, the antimicrobial activity of sal-4-phen (L7) was lost completely, while there was a slight reduction in the activity of the ovan-4-phen Schiff base ligand with a corresponding enhancement of its antifungal activity. The complexes of sal-2-phen (L12), ovan-2-phen (L27) and pvan-2-phen (L42) were however not soluble in organic solvents. The diameters of zone of inhibition for the hydroxyaniline-based complexes are presented in tables 7.21 and 7.23.

8.8 The antimicrobial activity of 1-aminonaphthalene-based compounds

The diameters of zone of inhibition for the 1-aminonaphthalene-based Schiff bases are presented in tables 7.8. The presence of the fused ring system in the amino moiety of the Schiff base ligands did not result in an increase in the antimicrobial activity of the aniline-based ligands; rather there was almost complete loss of activity against the tested pathogenic organisms. The *o*-vanillin analogue of the Schiff base ligands however showed a significant antifungal activity against *Candida albicans*.

In the same vein, the Cu(II) complexes of the Schiff base ligands were completely non-potent against the tested organisms.

8.9.0 Antimicrobial activity of the aminopyridine-based compounds

The diameters of zone of inhibition for the aminopyridine-based Schiff bases are presented in table 7.9. The salicylaldehyde and the vanillin analogues of this series showed no activity against all the tested organisms. However, the *o*-vanillin analogues exhibited significant antimicrobial activity with corresponding higher antifungal activity than the standard antifungal drug, ketoconazole.

Chelation has no impact on the activity of the salicylaldehyde analogues as the complexes were equally non active. On the other hand, there was a slight reduction in the activity of ovan-2-py (L29) and ovan-3-py (L30) Schiff base ligands with the antifungal activity of ovan-2-py (L29) reduced to 25%. The diameters of zone of inhibition for the aminopyridine-based complexes are presented in tables 7.25 and 7.26.

8.10 The antimicrobial activity of the aminomethylpyridine-based compounds

The diameters of zone of inhibition for the aminomethylpyridine-based Schiff bases are presented in table 7.10. Sal-3-pico (L16) Schiff base ligand has slight antimicrobial activity, suggesting the influence of methylene inclusion between the imine functional group and the pyridine ring on the antimicrobial activity of sal-3-py (L15) which was completely non-active. On the other hand, the methylene inclusion resulted in a slight reduction in the activity of ovan-2-py (L29).

On chelation, the antifungal activity of sal-3-pico (L16) was enhanced on chelation with a concomitant loss of activity against the gram negative bacteria, *Escherichia coli*. In the same vein, a slight enhancement of activity was observed in the activity of ovan-2-pico (L31) against the gram positive bacteria with an associated reduction in its activity against *E.coli and Candida albicans*. The diameters of zone of inhibition for the aminopyridine-based complexes are presented in table 7.27.

8.11 The antimicrobial activity of the 2-aminobenzimidazole-based compounds

The diameters of zone of inhibition for the 2-aminobenzimidazole based Schiff base ligands are presented in table 7.28. All the members of this series are were active against the tested pathogenic bacteria with the *o*-vanillin analogue exhibiting the most significant activity, 12 mm and 16 mm for *S. aureus and E.coli* respectively. In addition, the *o*-vanillin analogue was also more potent than the standard antifungal agent, ketoconazole. It thus portends a promising antifungal activity.

On chelation, ligand L56 (pvan-AmBZI) suffered a complete loss of activity against all the tested organisms. In the same vein, the antifungal activity of ligands L54 (sal-AmBZI) and L55 was negatively affected. Cu(sal-AmBZI), however, exhibited a slightly higher activity against the two gram positive bacteria, *S. aurues* and *B. Substilis*.

8.12 The antimicrobial activity of the o-phenylenediamine-based compounds

The diameters of zone of inhibition for the *o*-phenylenediamine-based Schiff base ligands are presented in table 7.29. Both the two ligands, L57 (bis-salphen) and L58 (bis-ovanphen) were slightly active against the tested organisms, with the *o*-vanillin analogue (L58) once again exhibiting higher activity, 13 mm, against *Bacillus substilis* and compared fairly well with the standard antifungal drug of choice, ketoconazole.

Chelation, however, did not enhance the activity of the ligands, rather a lot in activity of L57 (bis-salphen) against *E. coli* was observed. [Cu(bis-ovanphen)(H_2O)] was equally not active against *S. aureus* and *C. albicans*.

9.0.0 General conclusion

The syntheses of the hydroxylbenzaldimine Schiff bases were achieved through the condensation of four different aldehydes viz: salicylaldehyde, 3-methoxy-2-hydroxylbenzaldehye, 4-methoxy-3-hydroxylbenzaldehyde or 4-hydroxy-3-methoxybenzaldehyde, with aniline, p-substituted aniline, o-substituted aniline, 1-aminonaphthalene, 2-aminopyridine, 3-aminopyridine, 2-aminomethylpyridine, 3-aminomethylpyridine, 2-aminobenzimidazole or *o*-phenylenediamine. Thus, the Schiff base ligands were grouped into four categories based on the nature of the aldehyde used for the synthesis and six groups depending on the amino moiety of the Schiff base compounds.

The structures of the Schiff base ligands have been confirmed by a combination of elemental analysis and spectral (viz: ^{1}H-and ^{13}C-NMR, UV/Visible, infrared and Raman) data. The microanalysis result agreed quite well with the calculated values and that indicated that the prepared ligands were pure and free of the starting materials. This was corroborated by the NMR, infrared and Raman spectral data. The azomethine proton, HC=N, signal absorbed at 8.70-8.35 ppm in the ^{1}H-NMR spectra of the ligands while the azomethine carbon, C=N, absorbed at 167.25-157.99 ppm. On the other hand, the hydroxyl proton resonates at a very high frequency and absorbed far downfield at 13.46-11.83 ppm in all the ortho-hydroxyl analogues of the prepared Schiff base ligands, due to the existence of hydrogen bonding between the hydroxyl proton and the imine nitrogen. A linear correlation was obtained between the strength of the hydrogen bonding and the electronic effect of the *p*-substituted aniline analogues of the Schiff base ligands. This was done by plotting the chemical shift values, δ_{OH}, of the Schiff base ligands against the Hammett substituent parameters, σ.

All the Schiff base ligands exist in pure enol form as neither the methine split nor was there any shifting of the aromatic protons in the ^{1}H-NMR spectral of the Schiff base ligands. Likewise, there was no signal or band attributable to the carbonyl functional group in the ^{13}C-NMR and infrared spectra respectively. However, UV/Visible study of the ligands in protic solvent,

methanol indicated the presence of keto-enol form in solution. A band at greater than 400 nm indicating the presence of the keto form was observed in the UV/Visible spectral of most of the Schiff base ligands. The intensity of the keto-tautomer band increased with the electronegativity of the *p*-substituents. On the other hand, there is poor correlation of $\nu_{C=N}$ in the solid state (Raman) suggesting that solid state effects such as crystal packing, dominate the electronic effects.

Different types of Cu(II) complexes were prepared from the Schiff base ligands by reacting the ligands with either $CuCl_2.2H_2O$ or $Cu(OAc)_2.H_2O$ in a stoichiometric ratio of 2:1. The complexes have been characterized by elemental analysis, infrared and UV/Visible spectral data, conductivity values and x-ray single crystal structures.

The first group of the complexes was of the form $Cu(LH)_2Cl_2.xH_2O$ and was 1:1 electrolyte in methanol / DMF. These complexes were prepared from $CuCl_2.2H_2O$ and the infrared spectral data indicated that the Schiff base ligands coordinated only through the imine nitrogen as neutral base and thus suggesting the presence of at least one molecule of coordinated water in the inner coordination sphere, since the conductivity measurement indicated a 1:1 electrolyte. The UV/visible spectra showed a broad single absorption band at 819-713 nm.

Complexes of the form $[ML_2]$ were obtained for the Cu(II) complexes prepared from $Cu(OAc)_2.H_2O$. The infrared spectral data showed that the Schiff base ligands coordinated to the Cu(II) ions via the imine nitrogen and the deprotonated phenolic oxygen atoms. All the complexes were non-electrolyte in DMF. The d-d absorption band for this series was observed at 683-517 nm and square planar geometry has been previously assigned to Cu(II) complexes of similar structures. X-ray single crystal structure of $[Cu(ovan\text{-}NH)_2].H_2O$ indicated a square planar geometry for the complex with the Schiff base ligand coordinating via the imine nitrogen and the phenolic oxygen in a trans manner. $[Cu(ovan\text{-}NH)_2].H_2O$ was precipitated out of solution using aqueous ammonia.

The third group however, was equally prepared from $CuCl_2.H_2O$ with the elemental analysis result suggesting similar structure as the first group. On the other hand, the conductivity values in DMF indicated non-electrolyte complexes. Thus, it was suggested from the infrared spectral

data that the Schiff base ligands coordinated to the Cu(II) ions via the imine nitrogen and the non-protonated phenolic oxygen atoms with the two chlorine atoms at the axial position to balance the +2 charges on the Cu(II) ions; $[Cu(LH)_2Cl_2].H_2O$. The d-d absorption band for this group appeared at 804-634 nm.

The copper(II) complexes of ovan-2-ampy and ovan-2-pico were of the forms $[Cu(LH)Cl(H_2O)]Cl$ and [CuLCl]. [Cu(ovan-2-pico)Cl] was non-electrolyte in DMF while ovan-2-py complex was 1:1 electrolyte, suggesting a cationic complex with a chloride counter ion. The X-ray single crystal structure of [Cu(ovan-2-pico)Cl] confirmed the proposed square planar geometry for the complex. The d-d absorption band for complex was observed at 629 nm.

The next group comprises of the Cu(II) complexes prepared from the ortho-hydroxyaniline Schiff base ligands and they conformed to the general formula, $[M_2L_2]$. All the complexes were not soluble in common organic solvents including DMF and DMSO. However a dinuclear complex structure has been proposed for these complexes. The solid diffuse reflectance spectra of the complexes have a single broad absorption band in the region 676-641 nm.

Lastly, the N_2O_2 macrocyclic ligand coordinated to the Cu(II) ions in a tetradentate fashion with one water molecule occupying the apical site to form a square pyramidal Cu(II) complex; $[Cu(L)(H_2O)]$. The complex was non-electrolyte in DMF and the d-d transition band was observed as a broad band at 558 nm.

All the prepared complexes were screened against three bacterial strains (viz: *Bacillus substilis, Staphylococcus aureus and Esherichia coli*) and one fungal strain, *Candida albicans,* using disc diffusion technique. The minimum inhibitory concentration (MIC) values of the compounds were equally evaluated using broth dilution technique.

This study revealed that the observed activity of the Schiff base ligands is related to the following factors: (1) nature of the aldehyde (2) nature of the substituent on the amino moiety of the Schiff base ligands (3) presence of fused ring system (4) presence of heterocyclic ring system.

Firstly, it was observed that the presence of the methoxyl group at the ortho position of the aldehyde moiety of the Schiff base ligands did enhanced the activity of the compounds and thus the *o*-vanillin Schiff base ligands were more potent than the salicylaldehyde, *p*-vanillin and the vanillin analogues. Likewise, the hydroxyaniline analogues of the Schiff base ligands equally exhibited the most significant activity against the tested organisms. Ligands L25 (ovan-2-tol) and L26 (ovan-2-nis) equally possessed significant activity against all the microorganisms, thus relating the activity of the Schiff bases to the electronic effects of the substituents since the chloro-, bromo- and the nitro- analogues showed little or no activity. Ansari et al. [263] reported significant antimicrobial activity for the *o*-chloro, *o*-methyl, *o*-methoxyl and *p*-amino analogues in a series of substituted benzimidazole Schiff base ligands

The *o*-vanillin analogues of the aminopyridine and aminomethylpyridne Schiff base ligands were also found to be potent against the tested micro-organisms. All the members of the 2-aminobenzimidalole series were potentially active, with activity ranging from moderate to significant. The 1-aminonaphthalene Schiff base ligands were virtually non-active indicating the ineffectiveness of the fused ring system against the tested organisms. Thus, the presence of heterocyclic rings in the Schiff base ligands induces activity, while the fused ring did not.

On chelation, the antimicrobial activity did not seem to improve as most of the Schiff base ligands lost their activity in the Cu(II) complexes, with only a few showing slight increase in activity. Though, it is believed that chelation increases the lipophilicity of the metal ion and consequently increases the antimicrobial activity of metal complexes relative to the free ligands. It has however been observed that the free ligand do possess higher activity in some cases, an indication that activity does not depend solely on the presence of metal ions but rather a synergistic effect of many factors. Thus, understanding the mechanisms of action of potential antimicrobial agent is thus considered a study for the future.

In general, all the prepared compounds exhibited significant activity against the non-pathogenic *Bacillus substilis*; moderate activity towards *Staphlococcus aureus* and least activity against *Escherichia coli.* The highest activity was however, against the fungus of choice, *Candida albicans*, with the anifungal activity in some cases almost double that for the standard antifungal

agent, ketoconazole. The variation in the susceptibility or resistance of the test organisms to the compunds could be adduced to the composition of the cell membrane of each of the organisms. *S. aureus* and *B. substilis*, being Gram positive, have thick peptidoglycan cell wall, while *E. coli* has an additional outer protective layer, lipopolysaccharide, figure 6.1. The lipopolysaccharide layer provides additional fortification to the cell membrane and thus gram negative bacteria are more resistant to antibiotics treatment compared to the gram positive bacteria as evident in this study. The fungi cell wall is however comprise of chitin. None of the compounds was as active as penicillin, the standard antibacterial drug used for the study.

References

1. Schiff, H., Justus Liebigs Ann. Chem., 1864. **131**: p. 2.

2. Hine, J. and C.Y. Yeh, *Equilibrium in formation and conformational isomerization of imines derived from isobutyraldehyde and saturated aliphatic primary amines.* J. Am. Chem. Soc., 1967. **89**(11): p. 2669-76.

3. Campbell, K.N., A.H. Sommers, and B.K. Campbell, *Preparation of unsymmetrical secondary aliphatic amines.* J. Am. Chem. Soc., 1944. **66**: p. 82-4.

4. Brewster, C.M., *Schiff's bases from 3,5-dibromosalicylaldehyde.* J. Am. Chem. Soc., 1924. **46**: p. 2463-8.

5. Fessenden, R.J. and J.S. Fessenden, *Organic Chemistry, Pt. 2. 5th Ed.* 1995: Tokyo Kagaku Dozin Co., Ltd. 680 pp.

6. Pratt, E.F. and M.J. Kamlet, *Reaction rates by distillation. IX. The condensation of anilines with benzaldehydes.* J. Org. Chem., 1961. **26**: p. 4029-31.

7. Charette, J., *A nuclear magnetic resonance proof of phenol-imine form in isopropylsalicylaldimine.* Spectrochim. Acta, 1963. **19**: p. 1275-6.

8. Patai, S. and Editor, *The Chemistry of the Carbon-Nitrogen Double Bond (Chemistry of Functional Groups).* 1970: Wiley-Interscience. 794 pp.

9. Fabian, J. and M. Legrand, *Intensity of infrared absorption of the imine [C=N] group.* Bull. Soc. Chim. Fr., 1956: p. 1461-3.

10. Suydam, F.H., *C:N stretching frequency in azomethines.* Anal. Chem., 1963. **35**: p. 193-5.

11. Clougherty, L.E., J.A. Sousa, and G.M. Wyman, *C:N stretching frequency in infrared spectra of aromatic azomethines.* J. Org. Chem., 1957. **22**: p. 462.

12. Kovacic, J.E., *The carbon:nitrogen stretching frequency in the infrared spectra of Schiff's base complexes. I. Copper complexes of salicylidene anilines.* Spectrochim. Acta, 1967. **23A**(1): p. 183-7.

13. Baker, A.W. and A.T. Shulgin, *Intramolecular hydrogen bonding. II. The determination of Hammett sigma constants by intramolecular hydrogen bonding in Schiff's bases.* J. Am. Chem. Soc., 1959. **81**: p. 1523-9.

14. Dudek, G.O. and R.H. Holm, *A nuclear magnetic resonance study of keto-enol equilibria in Schiff bases. II.* J. Am. Chem. Soc., 1961. **83**: p. 3914.

15. Dudek, G.O. and R.H. Holm, *Nuclear magnetic resonance (N.M.R.) studies of ketoenol equilibria. III. α,β-Unsaturated β-ketoamines.* J. Am. Chem. Soc., 1962. **84**: p. 2691-6.

16. Dudek, G.O. and R.H. Holm, *A proton resonance study of bis(acetylacetone)monoethylenediamine [Schiff base] and related Schiff bases.* J. Am. Chem. Soc., 1961. **83**: p. 2099-2104.

17. Hadjoudis, E., *Photochromism and thermochromism of N-salicylideneanilines and N-salicylideneaminopyridines.* J. Photochem., 1981. **17**(3-4): p. 355-63.

18. Yeap, G., S. Ha, N. Ishizawa, K. Suda, P. Boey, and M.W. Kamil, *Synthesis, crystal structure and spectroscopic study of para substituted 2-hydroxy-3-methoxybenzylideneanilines.* J. Mol. Struct., 2003. **658**(1-2): p. 87-99.

19. Yildiz, M., Z. Kilic, and T. Hokelek, *Intramolecular hydrogen bonding and tautomerism in Schiff bases. Part I. Structure of 1,8-bis[2-(salicylidenamino)phenoxy]-3,6-dioxaoctane.* J. Mol. Struct., 1998. **441**(1): p. 1-10.

20. Nazir, H., M. Yildiz, H. Yilmaz, M.N. Tahir, and D. Ulku, *Intramolecular hydrogen bonding and tautomerism in Schiff bases. Structure of N-(2-pyridyl)-2-oxo-1-naphthylidenemethylamine.* J. Mol. Struct., 2000. **524**: p. 241-250.

21. Salman, S.R., S.H. Shawkat, and G.M. Al-Obaidi, *Tautomerism in o-hydroxy Schiff bases: Effect of alkyl group.* Can. J. Spectrosc., 1990. **35**(2): p. 25-7.

22. Ledbetter, J.W., Jr., *Substituent effects on the tautomerism of Schiff bases.* J. Phys. Chem., 1968. **72**(12): p. 4111-15.

23. Antonov, L., W.M.F. Fabian, D. Nedeltcheva, and F.S. Kamounah, *Tautomerism of 2-hydroxynaphthaldehyde Schiff bases.* Journal of the Chemical Society. Perkin Transactions 2, 2000(6): p. 1173-1179.

24. FernÃ¡ndez-G, J.M., F. Del Rio-Portilla, B. Quiroz-GarcÃa, R.A. Toscano, and R. Salcedo, *The structures of some ortho-hydroxy Schiff base ligands.* Journal of Molecular Structure, 2001. **561**(1-3): p. 197-207.

25. Kamounah, F.S., S.R. Salman, and A.A.K. Mahmoud, *Substitution and solvent effect of some substituted hydroxy schiff bases.* Spectroscopy Letters, 1998. **31**(7): p. 1557-1567.

26. Rospenk, M., I. Krol-Starzomska, A. Filarowski, and A. Koll, *Proton transfer and self-association of sterically modified Schiff bases.* Chem. Phys., 2003. **287**(1-2): p. 113-124.

27. Asiri, A.M. and K.O. Badahdah, *Synthesis of some new anils: Part 1. Reaction of 2-hydroxybenzaldehyde and 2-hydroxynaphthaldehyde with 2-aminopyridine and 2-aminopyrazine.* Molecules, 2007. **12**(8): p. 1796-1804.

28. Saeed, A.A.H., A.A.K. Mahmoud, and H.A. Saed, *Electronic spectrophotometric study on the molecular structure of some hydroxy Schiff bases.* Can. J. Spectrosc., 1988. **33**(4): p. 89-93.

29. Abd-Elzaher, M.M., *Spectroscopic characterization of some tetradentate Schiff bases and their complexes with nickel, copper and zinc.* J. Chin. Chem. Soc. , 2001. **48**(2): p. 153-158.

30. Zhou, Y., X. Ye, F. Xin and X. Xin, *Solid state self-assembly synthesis of cobalt(II), nickel(II), copper(II) and zinc(II) complexes with a bis-Schiff base.* Transition Met. Chem., 1999. **24**(1): p. 118-120.

31. Ramesh, R. and S. Maheswaran, *Synthesis, spectra, dioxygen affinity and antifungal activity of Ru(III) Schiff base complexes.* J. Inorg. Biochem., 2003. **96**(4): p. 457-462.

32. Sharma, V.B., S.L. Jain, and B. Sain, *Copper(II) Schiff base catalyzed aerobic oxidative coupling of 2-naphthols: an efficient and simple synthesis of binaphthols.* J. Mol. Catal. A: Chem., 2004. **219**(1): p. 61-64.

33. Wang, R.M., C.J. Hao, Y.P. Wang, S.B. Li, *Amino acid Schiff base complex catalyst for effective oxidation of olefins with molecular oxygen.* J. Mol. Catal. A: Chem., 1999. **147**(1-2): p. 173-178.

34. May, J.P., R. Ting, L. Lermer, J.M. Thomas, Y. Roupioz, and D.M. Perrin *Covalent Schiff Base Catalysis and Turnover by a DNAzyme: A M2+-Independent AP-Endonuclease Mimic.* J. Am. Chem. Soc., 2004. **126**(13): p. 4145-4156.

35. Ershad, S., L. Sagathforoush, G. Karim-nezhad, and S. Kangari, *Electrochemical behavior of N2SO Schiff-base Co(II) complexes in non-aqueous media at the surface of solid electrodes.* Int. J. Electrochem. Sci., 2009. **4**(6): p. 846-854.

36. Elizondo, M.P., M.B. Najera, and d.B.C. Rodriguez, *A Schiff base nickel complex. A new material as modifier for selective electrodes.* Adv. Technol. Mater. Mater. Process. J., 2006. **8**(1): p. 41-48.

37. Tanaka, H., H. Dhimane, H. Fujita, Y. Ikemoto, and S. Torii, *Reductive dimerization of imines in a lead-aluminum bimetal redox system.* Tetrahedron Lett., 1988. **29**(31): p. 3811-14.

38. Brown, M.J., *Literature review of the ester enolate imine condensation.* Heterocycles, 1989. **29**(11): p. 2225-44.

39. Mathews, I.I. and H. Manohar, *Isolation and characterization of a novel multibridged tetradentate dianionic form of pyridoxic acid. Crystal structure of tetranuclear [Cu4(PAA)2(Bipyram)4(H2O)2Cl2](NO3)2.CH3OH.10H2O.* Polyhedron, 1991. **10**(23-24): p. 2851-3.

40. Pasini, A. and L. Casella, *Reactivity of amino acids coordinated to metal ions.* J. Inorg. Nucl. Chem., 1974. **36**(9): p. 2133-44.

41. Sacconi, L., P.L. Orioli, P. Paoletti, and M. Ciampolini, *Existence of tetrahedral nickel(II) chelates.* Proc. Chem. Soc., London, 1962: p. 255-6.

42. Gupta, K.C., A.K. Sutar, *Catalytic activities of Schiff base transition metal complexes.* Coord. Chem. Rev., 2008. **252**(12-14): p. 1420-1450.

43. Guan, Z., P.M. Cotts, E.F. McCord, and S.J. McLain, *Chain walking: a new strategy to control polymer topology.* Science, 1999. **283**(5410): p. 2059-2062.

44. Meneghetti, S.P., J. Kress, and P.J. Lutz, *Structural investigation of poly(olefin)s and copolymers of ethylene with polar monomers prepared under various reaction conditions in the presence of palladium catalysts.* Macromol. Chem. Phys., 2000. **201**(14): p. 1823-1832.

45. Small, B.L. and M. Brookhart, *New iron and cobalt catalysts for the polymerization of olefins.* Polym. Prepr. , 1998. **39**(1): p. 213.

46. Small, B.L., M. Brookhart, and A.M.A. Bennett, *Highly Active Iron and Cobalt Catalysts for the Polymerization of Ethylene.* J. Am. Chem. Soc., 1998. **120**(16): p. 4049-4050.

47. Small, B.L. and M. Brookhart, *Iron-Based Catalysts with Exceptionally High Activities and Selectivities for Oligomerization of Ethylene to Linear Î±-Olefins.* J. Am. Chem. Soc., 1998. **120**(28): p. 7143-7144.

48. Britovsek, G.J.P., V.C. Gibson, B.S. Kimberley, P.J. Maddox, S.J. McTavish, G.A. Solan, A.J.P. White, and D.J. Williams, *Novel olefin polymerization catalysts based on iron and cobalt.* Chem. Commun. (Cambridge), 1998(7): p. 849-850.

49. Xi, Z., H. Wang, Y. Sun, N. Zhou, G. Cao, and M. Li, *Direct epoxidation of olefins catalyzed by heteropolyoxometalates with molecular oxygen and recyclable reductant.* J. Mol. Catal. A: Chem., 2001. **168**(1-2): p. 299-301.

50. Mukaiyama, T. and T. Yamada, *Recent advances in aerobic oxygenation.* Bull. Chem. Soc. Jpn., 1995. **68**(1): p. 17-35.

51. Mastrorilli, P., C.F. Nobile, G.P. Suranna, and L. Lopez, *Aerobic oxidations of unsaturated substrates under Mukaiyama's conditions: the role of the metal and of the sacrificial aldehyde.* Tetrahedron, 1995. **51**(29): p. 7943-50.

52. Fernandez, I., J.R. Pedro, and l.S.R. de, *Aerobic catalytic epoxidation of unfunctionalized olefins using a new (salen)manganese (III) complex bearing a sesquiterpene salicylaldehyde derivative.* Tetrahedron, 1996. **52**(36): p. 12031-12038.

53. Ravikumar, K.S., F. Barbier, J. Begue, and D. Bonnet-Delpon, *Manganese(III) acetate dihydrate catalyzed aerobic epoxidation of unfunctionalized olefins in fluorous solvents.* Tetrahedron, 1998. **54**(26): p. 7457-7464.

54. Brunner, H. and C. Krumey, *Enantioselective catalysis. Part 124. Enantioselective Michael reaction catalyzed by optically active transition metal complexes.* J. Mol. Catal. A: Chem., 1999. **142**(1): p. 7-15.

55. Zhou, H., J. Cheng, S. Lu, H. Fu, and H. Wang, *Catalytic carbonylation of Î±-(6-methoxy-2-naphthyl)ethanol to methyl esters of naproxen using PdCl2-CuCl2-PPh3-acid catalyst system.* J. Organomet. Chem., 1998. **556**(1-2): p. 239-242.

56. Xie, B., C. Xia, S. Lu, K. Chen, Y. Kou, and Y. Yin, *The first asymmetric carbonylation of 1-(6-methoxy-2-naphthyl)ethanol to the methyl ester of (S)-naproxen.* Tetrahedron Lett., 1998. **39**(40): p. 7365-7368.

57. Jang, E.J., K.H. Lee, J.S. Lee, and Y.G. Kim, *Regioselective synthesis of ibuprofen via the palladium complex catalyzed hydrocarboxylation of 1-(4-isobutylphenyl)ethanol.* J. Mol. Catal. A: Chem., 1999. **138**(1): p. 25-36.

58. Jang, E.J., K.H. Lee, J.S. Lee, and Y.G. Kim, *Hydrocarboxylation of 1-(4-isobutylphenyl)ethanol catalyzed by heterogeneous palladium catalysts.* J. Mol. Catal. A: Chem., 1999. **144**(3): p. 431-440.

59. Beletskaya, I.P. and A.V. Cheprakov, *The Heck Reaction as a Sharpening Stone of Palladium Catalysis.* Chem. Rev., 2000. **100**(8): p. 3009-3066.

60. Cornils, B., W.A. Herrmann, and Editors, *Applied Homogeneous Catalysis with Organometallic Compounds, Volume 3: Developments, 2nd Edition*. 2002: Wiley-VCH. 416 pp.

61. Bhanage, B.M., S.-i. Fujita, and M. Arai, *Heck reactions with various types of palladium complex catalysts: application of multiphase catalysis and supercritical carbon dioxide.* J. Organomet. Chem., 2003. **687**(2): p. 211-218.

62. Brunel, J.M., A. Heumann, and G. Buono, *Highly efficient phosphapalladacyclic catalysts for the hydroarylation of norbornene.* Angew. Chem., Int. Ed., 2000. **39**(11): p. 1946-1949.

63. Muller, P. and P. Nury, *Desymmetrization of meso-N-sulfonylaziridines with chiral nonracemic nucleophiles and bases.* Helv. Chim. Acta, 2001. **84**(3): p. 662-677.

64. Mikami, K., M. Terada, and H. Matsuzawa, *"Asymmetric" catalysis by lanthanide complexes.* Angew. Chem., Int. Ed., 2002. **41**(19): p. 3554-3571.

65. Voet, D. and J.G. Voet, *Biochemistry: Second Edition*. 1995: Wiley. 1361 pp.

66. Cimerman, Z., R. Kiralj, and N. Galic, *The structure and tautomeric properties of 2-(3-pyridylmethyliminomethyl)phenol.* J. Mol. Struct., 1994. **323**(1-3): p. 7-14.

67. Elzahany, E.A., K.H. Hegab, S.K.H. Khalil, and N.S. Youssef, *Synthesis, characterization and biological activity of some transition metal complexes with Schiff bases derived from 2-formylindole, salicylaldehyde, and N-amino rhodanine.* Aust. J. Basic Appl. Sci., 2008. **2**(2): p. 210-220.

68. Vijey, A.M., S. George, and V. Vaidhyalingam, *Synthesis and antimicrobial activities of 1-(5-substituted-2-oxoindolin-3-ylidene)-4-(substituted pyridin-2-yl)thiosemicarbazide.* ARKIVOC, 2008(11): p. 187-194.

69. Mohamed, G.G., M.M. Omar, and A.M. Hindy, *Metal complexes of Schiff bases: preparation, characterization, and biological activity.* Turk. J. Chem., 2006. **30**(3): p. 361-382.

70. Chohan, Z.H. and S. Mushtaq, *Antibacterial cobalt(II) and zinc(II) complexes of pyrazine-derived NNO and NNN donor Schiff-bases.* Pak. J. Pharm. Sci., 2000. **13**(1): p. 21-7.

71. Nair, R., A. Shah, S. Baluja, and S. Chanda, *Synthesis and antibacterial activity of some Schiff base complexes.* J. Serb. Chem. Soc., 2006. **71**(7): p. 733-744.

72. Biyala, M.K., K. Sharma, M. Swami, N. Fahmi, and R.V. Singh, *Spectral and biocidal studies of palladium(II) and platinum(II) complexes with monobasic bidentate Schiff bases.* Transition Met. Chem. , 2008. **33**(3): p. 377-381.

73. Sinha, D., A.K. Tiwari, S. Singh, G. Shukla, P. Mishra, H. Chandra, and A. K. Mishra, *Synthesis, characterization and biological activity of Schiff base analogues of indole-3-carboxaldehyde.* Eur. J. Med. Chem., 2008. **43**(1): p. 160-165.

74. Bawa, S. and S. Kumar, *Synthesis of Schiff's bases of 8-methyl-tetrazolo[1,5-a]quinoline as potential anti-inflammatory and antimicrobial agents.* Indian J. Chem., Sect. B: Org. Chem. Incl. Med. Chem., 2009. **48B**(1): p. 142-145.

75. Jarrahpour, A., D. Khalili, C.E. De, C. Salmi, and J.M. Brunel, Jean Michel, *Synthesis, antibacterial, antifungal and antiviral activity evaluation of some new bis-Schiff bases of isatin and their derivatives.* Molecules, 2007. **12**(8): p. 1720-1730.

76. Shrivastava, H.Y., M. Kanthimathi, and B.U. Nair, *Interaction of Schiff Base with Bovine Serum Albumin: Site-Specific Photocleavage.* Biochem. Biophys. Res. Commun., 1999. **265**(2): p. 311-314.

77. Raman, N., J.D. Raja, and A. Sakthivel, *Synthesis, spectral characterization of Schiff base transition metal complexes: DNA cleavage and antimicrobial activity studies.* J. Chem. Sci., 2007. **119**(4): p. 303-310.

78. Yamada, S. and K. Yamanouchi, *Metal complexes of Schiff bases obtained from substituted salicylaldehydes and 2-aminopyridine derivatives.* Bull. Chem. Soc. Jap., 1969. **42**(9): p. 2562-6.

79. Kolawole, G.A., *Oxovanadium(IV) complexes of Schiff-bases derived from 2-aminopyridine and aromatic 2-hydroxyaldehydes.* J. Coord. Chem., 1987. **16**(1): p. 67-73.

80. Cimerman, Z., N. Galic, and B. Bosner, *The Schiff bases of salicylaldehyde and aminopyridines as highly sensitive analytical reagents.* Anal. Chim. Acta, 1997. **343**(1-2): p. 145-153.

81. Aggarwal, R.C., N.K. Singh, and R.P. Singh, *Magnetic and spectroscopic studies on N-(picolinamido)salicylaldimine complexes of some bivalent 3d metal ions.* Inorg. Chem., 1981. **20**(9): p. 2794-8.

82. Jalali-Heravi, M., A.A. Khandar, and I. Sheikshoaie, *Characterisation and theoretical investigation of the electronic properties and second-order nonlinearity of some three dentate salicylaldiminato Schiff base ligands.* Spectrochim. Acta, Part A, 2000. **56A**(8): p. 1575-1581.

83. Abdel-Latif, S.A., H.B. Hassib, and Y.M. Issa, *Studies on some salicylaldehyde Schiff base derivatives and their complexes with Cr(III), Mn(II), Fe(III), Ni(II) and Cu(II).* Spectrochim. Acta, Part A, 2007. **67A**(3-4): p. 950-957.

84. Kasumov, V.T., *Synthesis, spectroscopic and redox properties of nickel(II) salicylaldimine complexes containing sterically hindered phenols.* Transition Met. Chem. , 2002. **27**(2): p. 228-233.

85. Canpolat, E. and M. Kaya, *Studies on mononuclear chelates derived from substituted Schiff-base ligands (part 2): Synthesis and characterization of a new 5-bromosalicylidene-p-aminoacetophenoneoxime and its complexes with Co(II), Ni(II), Cu(II) and Zn(II).* J. Coord. Chem., 2004. **57**(14): p. 1217-1223.

86. Lehlinger, A.L., *Principles of biochemistry.* Worth Publishers, New York, 1975.

87. Salva, A., J. Donoso, J. Frau, and F. Munoz, *Theoretical studies on Schiff base formation of vitamin B6 analogues.* J. Mol. Struct.: Theochem., 2002. **577**(2-3): p. 229-238.

88. Dolphin, D., R. Poulson, and O. Avramovic, *Coenzymes and Cofactors, Vol. 1: Vitamin B6. Pyridoxal Phosphate. Chemical, Biochemical, and Medical Aspects, Pt. B*. 1986: John Wiley & Son). 792 pp.

89. Otto, P., J. Ladik, K. Laki, and A. Szent-Gyorgyi, *Internal charge transfer in proteins to the Schiff bases of their lysine side chains.* Proc. Natl. Acad. Sci. U. S. A., 1978. **75**(8): p. 3548-50.

90. McKee, T., and J. McKee, *Biochemistry.* Wm. C. Brown Publishers, Dubuque, 1996

91. Schmid, G.H., *Organic Chemistry.* William C Brown Pub., New York, 1996.

92. Carey, F.A., *Organic Chemistry.* McGraw-Hill, New York, 1986.

93. Arulmurugan, S., H.P. Kavitha, B.R. and Venkatraman, *Biological activities of of Schiff base and its complexes: A review.* Rasayan J. Chem., 2010. **3**(3): p. 385-410.

94. Basolo, F., and R. C. Johnson, *Coordination chemistry: The chemistry of metal complexes.* Benjamin 1964

95. Pfeiffer, P., E. Buchholz, and O. Bauer, *Inner complex salts from hydroxyaldimines and hydroxyketimines.* J. Prakt. Chem. , 1931. **129**: p. 163-77.

96. Calligaris, M., G. Nardin, and L. Randaccio, *Structural aspects of metal complexes with some tetradentate Schiff bases.* Coord. Chem. Rev., 1972. **7**(4): p. 385-403.

97. Yamada, S., *Recent aspects of the stereochemistry of Schiff base-metal complexes.* Coord. Chem. Rev., 1966. **1**(4): p. 415-37.

98. Cheeseman, T.P., D. Hall, and T.N. Waters, *The stereochemistry of copper in 2,2'-biphenylylenebis(2-iminomethylenephenolato)copper(II).* Proc. Chem. Soc.,, 1963: p. 379-80.

99. Lingafelter, E.C., G.L. Simmons, B. Morosin, C. Scheringer, and C. Freiburg, *The crystal structure of the α-form of bis(N-methylsalicylaldiminato)copper.* Acta Crystallogr., 1961. **14**: p. 1222-5.

100. Tumer, M., H. Koksal, S. Serin, and M. Digrak, *Antimicrobial activity studies of mononuclear and binuclear mixed-ligand copper(II) complexes derived from Schiff base ligands and 1,10-phenanthroline.* Transition Met. Chem. , 1999. **24**: p. 13-17.

101. Percy, G.C. and D.A. Thornton, *N-Aryl salicylaldimine complexes. Infrared and PMR spectra of the ligands and vibrational frequencies of their metal(II) chelates.* J. Inorg. Nucl. Chem., 1972. **34**: p. 3357-67.

102. Percy, G.C. and D.A. Thornton, *N-Alkyl salicylaldimine complexes. Infrared and PMR spectra of the ligands and vibrational frequencies of their metal(II) chelates.* J. Inorg. Nucl. Chem., 1972. **34**: p. 3369-76.

103. Newman, M.S., *Steric effects in organic chemistry.* John Wiley & Sons, Inc., New York, 1956: p. 710 pp.

104. Sacconi, L. and M. Ciampolini, *Pseudo-tetrahedral structure of some α-branched copper(II) chelates with Schiff bases.* J. Chem. Soc., 1964: p. 276-80.

105. Marvel, C.S., S.A. Aspey, and E.A. Dudley, *Quadridentate and sexadentate chelates. Some preliminary studies in their preparation and thermal stability.* J. Am. Chem. Soc., 1956. **78**: p. 4905-9.

106. Kaczmarek, M.T., R. Jastrzab, E. Holderna-Kedzia, and W. Radecka-Paryzek, *Self-assembled synthesis, characterization and antimicrobial activity of zinc(II) salicylaldimine complexes.* Inorg. Chim. Acta, 2009. **362**: p. 3127-3133.

107. Mahon, M.F., J. McGinley, R.A. Denise, J.M.D. Walsh, *Unusual copper(II) coordination mode from a potential Schiff-base reaction.* Inorg. Chim. Acta, 2009. **362**: p. 2353-2360.

108. Wang, Y., J. Liu, H. Xian, and G. Zhao, *Synthesis, crystal structure, and kinetics of the thermal decomposition of the nickel(II) complex of the Schiff base 2-[(4 methylphenylimino)methyl]-6-methoxyphenol.* Molecules, 2009. **14**: p. 2582-2593.

109. Dubey, R.K., U.K. Dubey, and C.M. Mishra, *Synthesis and physicochemical characterization of some Schiff base complexes of chromium(III).* Indian J. Chem., Sect. A: Inorg., Bio-inorg., Phys., Theor. Anal. Chem., 2008. **47A**: p. 1208-1212.

110. Valent, A., M. Melnik, D. Hudecova, B. Dudova, R. Kivekas, and M.R. Sundberg,, *Copper(II) salicylideneglycinate complexes as potential antimicrobial agents.* Inorg. Chim. Acta, 2002. **340**: p. 15-20.

111. Mashaly, M.M., Z.H. abd-Elwahab, and A.A. Faheim, *Preparation, spectral characterization and antimicrobial activities of Schiff base complexes derived from 4-aminoantipyrine. Mixed ligand complexes with 2-aminopyridine, 8-hydroxyquinoline and oxalic acid and their pyrolytical products.* J. Chin. Chem. Soc. , 2004. **51**: p. 901-915.

112. Suresh, M.S. and V. Prakash, *Preparation and characterization of Cr(III), Mn(II), Co(III), Ni(II), Cu(II), Zn(II) and Cd(II) chelates of Schiffs base derived from vanillin and 4-amino antipyrine.* Int. J. Phys. Sci., 2010. **5**: p. 2203-2211.

113. Sabaa, M.W., R.R. Mohamed, and E.H. Oraby, *Vanillin-Schiff's bases as organic thermal stabilizers and co-stabilizers for rigid poly(vinyl chloride).* European Polymer Journal, 2009. **45**(11): p. 3072-3080.

114. Nair, M.S. and D. Arish, *Synthesis, characterization and biological studies of Co(II), Ni(II), Cu(II) and Zn(II) complexes involving a potentially tetradentate Schiff base ligand.* Transactions of the Indian Institute of Metals, 2011. **64**(3): p. 287-292.

115. Rathore, K., R.K.R. Singh, and H.B. Singh, *Structural, Spectroscopic and Biological Aspects of O, N- Donor Schiff Base Ligand and its Cr(III),Co(II), Ni(II) and Cu(II)Complexes Synthesized through Green Chemical Approach.* E-Journal of Chemistry, 2010. **7**(S): p. 7.

116. Bhunora, S., J. Mugo, A. Bhaw-Luximon, S. Mapolie, J. Van Wyk, J. Darkwa, and E. Nordlander, *The use of Cu and Zn salicylaldimine complexes as catalyst precursors in ring opening polymerization of lactides: Ligand effects on polymer characteristics.* Applied Organometallic Chemistry, 2011. **25**(2): p. 133-145.

117. Al-Allaf, T.A.K. and A.Z.M. Sheet, *Platinum group metal Schiff-base complexes. Part II. Palladium and nickel complexes.* Asian J. Chem., 1996. **8**: p. 305-14.

118. Al-Allaf, T.A.K. and A.Z.M. Sheet, *Platinum group metal Schiff base complexes. I. Platinum complexes.* Polyhedron, 1995. **14**: p. 239-48.

119. Noro, S., M. Kondo, S. Kitagawa, T. Ishii, H. Matsuzaka, and M. Yamashita, *Synthesis and crystal structure of [Cu(N-salicylidene-3-aminopyridine)2]n constructed from*

unsymmetric bridging ligand with two dissimilar metal-binding sites. Mol. Cryst. Liq. Cryst. Sci. Technol., Sect. A, 2000. **342**: p. 231-236.

120. Al-Allaf, T.A.K., M.A. Al-Shama'a, and L.J. Rashan, *Diorganotin(IV) complexes of some Schiff bases with a potential biological activity.* Appl. Organomet. Chem., 1996. **10**: p. 545-548.

121. Ayad, M.I., S.A. Sallam, and H.E. Mabrouk, *Characterization and thermal behavior of copper(II) chelates of Schiff bases derived from aminopyridines.* Thermochim. Acta, 1991. **189**: p. 65-73.

122. Coppola, M., S. Catinella, P. Traldi, P. Guerriero, S. Tamburini, and P.A. Vigato, *Fast atom bombardment mass spectrometry of new polydentate Schiff bases. 2. The case of mono- and bisaldimines containing pyridine groups.* Org. Mass Spectrom., 1994. **29**: p. 566-70.

123. Datta, A., *Synthesis and Structural Characterization of N-(2-Pyridylmethyl)-3-Methoxysalicylaldiminato Copper(II) Chloride.* J. Chem. Crystallogr., 2009. **39**(9): p. 619-622.

124. Marzilli, L.G. and P.A. Marzilli, *Magnetic spin equilibriums in some new five-coordinate Schiff base complexes of cobalt(II).* Inorg. Chem., 1972. **11**: p. 457-661.

125. Tellez, F., H. Lopez-Sandoval, S.E. Castillo-Blum, and N. Barba-Behrens, *Coordination behavior of benzimidazole, 2-substituted benzimidazoles and benzothiazoles, towards transition metal ions.* ARKIVOC 2008: p. 245-275.

126. Güven, O.O., T. Erdoğan, H. Göker, and S. Yildiz, *Synthesis and antimicrobial activity of some novel phenyl and benzimidazole substituted benzyl ethers.* Bioorg. and Med. Chem. Lett., 2007. **17**(8): p. 2233-2236.

127. Mohamed, B.G., A.A.M. Abdel-Alim, and M.A. Hussein, *Synthesis of 1-acyl-2-alkylthio-1,2,4-triazolobenzimidazoles with antifungal, anti-inflammatory and analgesic effects.* Acta Pharmaceutica, 2006. **56**(1): p. 31-48.

128. Starčević, K., M. Kralj, K. Ester, I. Sabol, M. Grce, K. Pavelić, and G. Karminski-Zamola *Synthesis antiviral and antitumor activity of 2-substituted-5-amidino-benzimidazoles.* Bioorg. and Med. Chem., 2007. **15**(13): p. 4419-4426.

129. Ayhan-Kilcigil, G., C. Kuş, E.D. Özdamar, B. Can-Eke, and M. Içan, *Synthesis and antioxidant capacities of some new benzimidazole derivatives.* Archiv der Pharmazie, 2007. **340**(11): p. 607-611.

130. Mavrova, A.T., K.K. Anichina, D.I. Vuchev, J.A. Tsenov, P.S. Denkova, M.S. Kondeva, and M.K. Micheva *Antihelminthic activity of some newly synthesized 5(6)-(un)substituted-1H-benzimidazol-2-ylthioacetylpiperazine derivatives.* Eur. J. Med. Chem., 2006. **41**: p. 1412-1420.

131. Patil, A., S. Ganguly, and S. Surana, *A systematic review of benzimidazole derivatives as an antiulcer agent.* Rasayan J. Chem., 2008. **1**: p. 447-460.

132. Kuehler, T.C., J. Fryklund, N. Bergman, J. Weilitz, A. Lee, and H. Larsson, *Structure-Activity Relationship of Omeprazole and Analogs as Helicobacter pylori Urease Inhibitors.* J. Med. Chem., 1995. **38**: p. 4906-16.

133. Skeela, R., *Studies on some metal complexes of Biologically important ligands.* PhD Thesis, Cochin University of Science and Technology, Kerala, 1991.

134. Pujar, M.A., T.D. Dharmagouder, S.M. Gaddad, and Y.F. Neelgund, *Screening of Schiff base and benzamidazole derivatives for their antibacterial activity.* Indian J. Microbiol., 1987. **27**: p. 75-7.

135. Milanino, R., E. Concari, A. Conforti, M. Marrella, L. Franco, U. Moretti, G. Velo, K.D. Rainsford, and M. Bressan *Synthesis and anti-inflammatory effects of some bis(2-benzimidazolyl) thioethers and their copper(II) chelates, orally administered to rats.* Eur. J. Med. Chem., 1988. **23**: p. 217-24.

136. Drake, J.F. and R.J.P. Williams, *Uptake of molecular oxygen by ferrous complexes.* Nature 1958. **182**: p. 1084.

137. Corwin, A.H. and Z. Reyes, *Porphyrin studies. XIV. Preparation and properties of imidazole ferro- and ferriprotoporphyrin complexes.* J. Am. Chem. Soc., 1956. **78**: p. 2437-9.

138. Corwin, A.H. and S.D. Bruck, *Porphyrin studies. XV. Properties of proto- and mesoheme imidazole complexes.* J. Am. Chem. Soc., 1958. **80**: p. 4736-9.

139. Chang, C.K. and T.G. Traylor, *Neighboring group effect in heme-carbon monoxide bonding.* J. Amer. Chem. Soc., 1973. **95**: p. 8475.

140. Schrauzer, G.N., *Organocobalt chemistry of vitamin B12 model compounds (cobaloximes).* Accounts Chem. Res., 1968. **1**: p. 97-103.

141. Nicholls, D., in: J.C. Bailer, H.J. Emeleus, R. Nyholm and A.F. Trotman-Dickenson (eds.), *Comprehensive Inorganic Chemistry.* Pergamon Press. Oxford, 1973. **3**.

142. Ayhan, K.G. and N. Altanlar, *Synthesis and antifungal properties of some benzimidazole derivatives.* Turk. J. Chem., 2006. **30**: p. 223-228.

143. Shanmugapandiyan, P., K.S. Denshing, R. Ilavarasan, N. Anbalagan, and R. Nirmal, *Synthesis and biological activity of 2-[(thiazolidin-4-one)phenyl]-1H-phenylbenzimidazoles and 2-[4-(azetidin-2-one)-3-chloro-4-phenyl]-1H-phenylbenzimidazoles.* Int. J. Pharm. Sci. Drug Res., 2010. **2**: p. 115-119.

144. Hranjec, M., K. Starcevic, S.K. Pavelic, P. Lucin, K. Pavelic, Z.G. Karminski, *Synthesis, spectroscopic characterization and antiproliferative evaluation in vitro of novel Schiff bases related to benzimidazoles.* Eur. J. Med. Chem., 2011. **46**: p. 2274-2279.

145. Mohamed, G.G. and E.-W.Z.H. Abd, *Salicylidene-2-aminobenzimidazole Schiff base complexes of Fe(III), Co(II), Ni(II), Cu(II), Zn(II) and Cd(II).* J. Therm. Anal. Calorim., 2003. **73**: p. 347-359.

146. Liu, J., L. Chen, X. Song, H. Hong, Z. Chu, *Synthesis and crystal structure of a novel dinuclear copper(II) complex containing benzimidazole Schiff base ligand.* Chin. J. Struct. Chem., 2011. **30**: p. 764-767.

147. Chhonker, Y.S., B. Veenu, S.R. Hasim, N. Kaushik, D. Kumar, and P. Kumar *Synthesis and pharmacological evaluation of some new 2-phenyl benzimidazoles derivatives and their Schiff's bases.* E-Journal of Chemistry, 2009. **6**(SUPPL. 1): p. S342-S346.

148. Hatfield, W.E. and R. Whyman, *Copper complexes.* Transition Met. Chem., 1969. **5**: p. 47-179.

149. Ferguson, J., *Electronic absorption spectrum and structure of CuCl4.* J. Chem. Phys., 1964. **40**: p. 3406-10.

150. Lever, A.B.P., *Inorganic Electronic Specteroscopy, 2nd edition.* Elsevier, New York, 1978.

151. Ali, M.A. and S.E. Livingstone, *Metal complexes of sulfur-nitrogen chelating agents.* Coord. Chem. Rev., 1974. **13**: p. 101-32.

152. Battistoni, C., G. Mattogno, A. Monaci, and F. Tarli *Metal complexes of dithiocarbazic acid and its derivatives. I. Nickel(II) and zinc(II) complexes of N-substituted dithiocarbazic acids.* J. Inorg. Nucl. Chem., 1971. **33**: p. 3815-32.

153. Wikipedia, *Jahn-Teller.* F:\JahnTeller_files\jahnteller.gif, accessed date: 15-12-2011.

154. Harris, E.D., in: Rose J. (ed.), *Trace Elements in Health* Butterworths. London, 1983.

155. Danks, D.M., *Biological Roles of Copper.* Ciba Foundation Symposium 79 (new series). Excerpta Medica. Amsterdam., 1980.

156. Georgievskii, V.I., B.N. Annenkov, and Samokhin *Mineral Nutrition of Animals* Butterworths: London, 1982.

157. Frausto, J.J.R., and R.J.P. Williams, *The Biological Chemistry of the Elements, Second Edition*. 2001: Oxford University Press, Oxford. 650 pp.

158. Harris, E.D., J.K. Rayton, I.E. Balthrop, R.A. Di Silvestro, and M. Garcia-de-Quevedo, *Copper and the synthesis of elastin and collagen in "Biological Roles of Copper"* Ciba Foundation Symposium 79 (new series). Excerpta Medica, Amsterdam, 1980.

159. Guy, B., *Handbook of Metal-Ligand Interactions in Biological Fluids: Bioinorganic Chemistry, Volume 1*. 1995: Marcel Dekker Inc., New York. 724 pp.

160. Klevay, L.M., *Hypercholesterolemia in rats produced by an increase in the ratio of zinc to copper ingested.* Amer. J. Clin. Nutr., 1973. **26**: p. 1060-8.

161. Klevay, L.M., *Copper and ischemic heart disease.* Biol. Trace Elem. Res., 1983. **5**: p. 245-55.

162. Brown, D.H., W.W. Buchanan, A.F. el-Ghobarey, W.E. Smith, and J. Teape,, *Serum copper and its relationship to clinical symptoms in rheumatoid arthritis.* Ann Rheum Dis, 1979. **38**: p. 174-6.

163. Sorenson, J.R.J., *Copper complexes - a unique class of anti-arthritic drugs.* Prog. Med. Chem., 1978. **15**: p. 211-60.

164. Underwood, E.J., *Copper in: Trace Elements in Humans and Animals, 4th edition, Academic Press, New York, 1971.*

165. Vallee, B.L. and R.J.P. Williams, *Metalloenzymes. Entatic nature of their active sites.* Proc. Nat. Acad. Sci. U. S., 1968. **59**: p. 498-505.

166. Sigel, H. and D.B. McCormick, *Discriminating behavior of metal ions and ligands with regard to their biological significance.* Accounts Chem. Res., 1970. **3**: p. 201-8.

167. Sasaki, T. and F. Matsunaga, *Syntheses of vitamin B12 model compounds.* Bull. Chem. Soc. Jap., 1969. **42**(5): p. 1308-16.

168. Heeg, M.J. and S.S. Jurisson, *The Role of Inorganic Chemistry in the Development of Radiometal Agents for Cancer Therapy.* Acc. Chem. Res., 1999. **32**(12): p. 1053-1060.

169. Thompson, K.H. and C. Orvig, *Design of vanadium compounds as insulin enhancing agents.* Dalton, 2000(17): p. 2885-2892.

170. Zhang, C.X. and S.J. Lippard, *New metal complexes as potential therapeutics.* Curr. Opin. Chem. Biol., 2003. **7**(4): p. 481-489.

171. Grier, N., in: Block, S.S., (ed.), *Mercurials in: Inorganic and Organics (Disinfection, Sterilization and Preservation.).* Lea and Fabringer, Philadelphia, 1983.

172. Grier, N., in: Block, S.S., (ed.), *Silver and Its Compounds in: Inorganic and Organics (Disinfection, Sterilization and Preservation.).* Lea and Fabringer, Philadelphia, 1983.

173. Gupta, A., K. Matsui, J.F. Lo, and S. Silver, *Molecular basis for resistance to silver cations in Salmonella.* Nat Med, 1999. **5**: p. 183-8.

174. Clement, J.L. and P.S. Jarret, *Antibacterial silver.* Met.-Based Drugs, 1994. **1**: p. 467-82.

175. Briand, G.G. and N. Burford, *Bismuth Compounds and Preparations with Biological or Medicinal Relevance.* Chem. Rev. , 1999. **99**: p. 2601-2657.

176. Reglinski, J., *Chemistry of Arsenic, Antimony, and Bismuth.* Blackie Academic and Professional: London, 1988.

177. Briand, G.G. and N. Burford, *Coordination complexes of bismuth(III) involving organic ligands with pnictogen or chalcogen donors.* Adv. Inorg. Chem., 2000. **50**: p. 285-357.

178. Birch, N.J., in: Farell, Nicholas P., (ed.). *Uses of inorganic chemistry in medicine*. 1999: Royal Society of Chemistry, Cambridge.

179. Birch, N.J., *Inorganic pharmacology of lithium.* Chem. Rev. , 1999. **99**: p. 2659-2682.

180. Shaw, C.i.F., N. (ed.), *Shaw, C. Gold Complexes with Anti-arthritic, Anti-tumour and Anti-HIV Activity in: Uses of Inorganic Chemistry in Medicine.* The Royal Society of Chemistry: Cambridge, 1999.

181. Snyder, R.M., C.K. Mirabelli, and S.T. Crooke, *The cellular pharmacology of auranofin.* Semin. Arthritis Rheum., 1987. **17**: p. 71-80.

182. Rudkowski, R., G.G. Graham, G.D. Champion, and J.B. Ziegler *The activation of gold complexes by cyanide produced by polymorphonuclear leukocytes. I. The effects of aurocyanide on the oxidative burst of polymorphonuclear leukocytes.* Biochem. Pharmacol., 1990. **39**: p. 1687-95.

183. Hutchison, A.J., *Calcitriol, lanthanum carbonate, and other new phosphate binders in the management of renal osteodystrophy.* Perit Dial Int, 1999. **19 Suppl 2**: p. S408-12.

184. Hergesell, O. and E. Ritz, *Phosphate binders on iron basis: a new perspective?* Kidney Int., Suppl., 1999. **73**: p. S42-S45.

185. Lyonnet, B., X. Martz, and E. Martin, Presse. Med. , 1899. **1**.

186. Halberstam, M., N. Cohen, P. Shlimovich, L. Rossetti, and H. Shamoon *Oral Vanadyl sulfate improves insulin sensitivity in NIDDM but not in obese nondiabetic subjects.* Diabetes, 1996. **45**: p. 659-666.

187. Boden, G., X. Chen, J. Ruiz, D.V. G. van Rossum, and S. Turco *Effects of vanadyl sulfate on carbohydrate and lipid metabolism in patients with non-insulin-dependent diabetes mellitus.* Metab., Clin. Exp., 1996. **45**: p. 1130-1135.

188. Goldfine, A.B., et al., *In vivo and in vitro studies of vanadate in human and rodent diabetes mellitus.* Mol Cell Biochem, 1995. **153**(Copyright (C) 2011 U.S. National Library of Medicine.): p. 217-31.

189. Cohen, N., M. Halberstam, P. Shlimovich, C.J. Chang, H. Shamoon, and L. Rossetti,, *Oral vanadyl sulfate improves hepatic and peripheral insulin sensitivity in patients with non-insulin-dependent diabetes mellitus.* J. Clin. Invest., 1995. **95**: p. 2501-9.

190. Goldfine, A.B., D.C. Simonson, F. Folli, M. Patti, C.R. Kahn, *Metabolic effects of sodium metavanadate in humans with insulin-dependent and noninsulin-dependent diabetes mellitus in vivo and in vitro studies.* J. Clin. Endocrinol. Metab., 1995. **80**: p. 3311-20.

191. Goldfine, A.B., D.C. Simonson, F. Folli, M.E. Patti, and C .R. Kahn, *In vivo and in vitro studies of vanadate in human and rodent diabetes mellitus.* Mol. Cell. Biochem., 1995. **153**: p. 217-31.

192. Sakurai, H., K. Tsuchiya, M. Nukatsuka, J. Kawada, S. Ishikawa, H. Yoshida, and M. Komatsu, *Insulin-mimetic action of vanadyl complexes.* J. Clin. Biochem. Nutr., 1990. **8**: p. 193-200.

193. Sorenson, J.R.J., *Copper complexes in biochemistry and pharmacology.* Chem. Br., 1984. **20**: p. 1110-13.

194. Sorenson, J.R.J., *Copper chelates as possible active forms of the antiarthritic agents.* J. Med. Chem., 1976. **19**: p. 135-48.

195. Walker, W.R., S.J. Beveridge, and M.J. Whitehouse *Anti-inflammatory action of dermally applied copper salicylate preparations (Aleural and Dermeural) in "CSIRO*

Symposium on the Importance of Copper in Biology and Medicine" CSIRO Canberra, Australia, 1980.

196. Butler, A., and P. Rhodes, *Nitric Oxide in Physiology and Medicine; In Uses of Inorganic Chemistry in Medicine, Farrell, N., Ed.; The Royal Society of Chemistry: Cambridge.* Book, 1999.

197. Clarke, M.J. and J.B. Gaul, *Chemistry relevant to the biological effects of nitric oxide and metallonitrosyls.* Struct. Bonding (Berlin), 1993. **81**: p. 147-81.

198. Butler, A.R., and D.L.H. Williams, *The physiological role of nitric oxide.* Chem. Soc. Rev., 1993. **22**: p. 233-41.

199. Groves, J.T., *Peroxynitrite: reactive, invasive and enigmatic.* Curr. Opin. Chem. Biol., 1999. **3**: p. 226-235.

200. Kirschner, S., Y.K. Wei, D. Francis, and J. Bergman, *Anticancer and potential antiviral activity of complex inorganic compounds.* J. Med. Chem., 1966. **9**: p. 369-72.

201. Navarro, M., H. Perez, R.A. Sanchez-Delgado, *Toward a Novel Metal-Based Chemotherapy against Tropical Diseases. 3. Synthesis and Antimalarial Activity in Vitro and in Vivo of the New Gold-Chloroquine Complex [Au(PPh3)(CQ)]PF6.* J. Med. Chem., 1997. **40**: p. 1937-1939.

202. Navarro, M., E.J. Cisneros-Fajardo, T. Lehmann, R.A. Sanchez-Delgado, R. Atencio, P. Silva, R. Lira, and J.A. Urbina, *Toward a novel metal-based chemotherapy against tropical diseases. 6. Synthesis and characterization of new copper(II) and gold(I) clotrimazole and ketoconazole complexes and evaluation of their activity against Trypanosoma cruzi.* Inorg Chem, 2001. **40**: p. 6879-84.

203. Sanchez-Delgado, R.A., K. Lazardi, L. Rincon, J.A. Urbina, A.J. Hubert, and A.N. Noels, *Toward a novel metal-based chemotherapy against tropical diseases. 1. Enhancement of the efficacy of clotrimazole against Trypanosoma cruzi by complexation to ruthenium in RuCl2(clotrimazole)2.* J. Med. Chem., 1993. **36**: p. 2041-3.

204. Sanchez-Delgado, R.A., M. Navarro, H. Perez, and J.A. Urbina, *Toward a Novel Metal-Based Chemotherapy against Tropical Diseases. 2. Synthesis and Antimalarial Activity in Vitro and in Vivo of New Ruthenium- and Rhodium-Chloroquine Complexes.* J. Med. Chem., 1996. **39**: p. 1095-9.

205. Maity, D., M.G.B. Drew, J.F. Godsell, S. Roy, and G. Mukhopadhyay, *Synthesis and characterization of Cu(II) complexes of tetradentate and tridentate symmetrical Schiff base ligands involving o-phenylenediamine, salicylaldehyde and diacetyl monoxime.* Transition Met. Chem. , 2010. **35**(2): p. 197-204.

206. Unver, H., M. Yildiz, O. Ozgen, E. Kendi, B. Dulger, and T.N. Durlu, *Spectroscopic studies, antimicrobial activities and crystal structures of N-(2-hydroxy-3-methoxybenzalidene)1-aminonaphthalene.* J. Mol. Struct., 2005. **737**: p. 159-164.

207. Curtis, R.H., in: Nakamoto K., and P.S.J. McCarthy (eds.), *Visible and Ultraviolet spectroscopy in: spectroscopy and structure of metal chelate compounds.* John Wiley and sons, Inc. New York, 1968: p. 82.

208. Nakamoto, K., in: Nakamoto, K., and McCarthy, P.S.J. (eds.), *Infrared spectroscopy in: Spectroscopy and Structure of Metal Chelate Compounds, John Wiley & sons, Inc. Newy York*. 1968. 382 pp.

209. Bellamy, L.J. and R.F. Branch, *The infrared spectra of chelate compounds. II. Metal chelate compounds of β-diketones and of salicylaldehyde.* J. Chem. Soc., 1954: p. 4491-4.

210. Mellor, D.P. and L. Maley, *Stability constants of internal complexes.* Nature 1947. **159**: p. 370.

211. Sharma, V.S., H.B. Mathur, and A.B. Biswas, *Relation between the N-H stretching frequency and stability of metal complexes of β-alanine.* Spectrochim. Acta, 1961. **17**: p. 895-6.

212. Geary, W.J., *Use of conductivity measurements in organic solvents for the characterization of coordination compounds.* Coord. Chem. Rev., 1971. **7**: p. 81-122.

213. Yoshihiko, S., in: Nakamoto, K., and P.S.J. McCarthy, (eds.), *X-ray and neutron diffraction in: Spectroscopy and structure of metal chelate compounds.* John Wiley & Sons, Inc., New York, 1968: p. 1-71.

214. Hammett, L.P., *Some relations between reaction rates and equilibrium constants.* Chem. Rev., 1935. **17**: p. 125-36.

215. Hammett, L.P., *Effect of structure upon the reactions of organic compounds. Benzene derivatives.* J. Am. Chem. Soc., 1937. **59**: p. 96-103.

216. Williams, S.G. and F.E. Norrington, *Determination of positional weighting factors for the Swain and Lupton substituent constants f and r.* J. Am. Chem. Soc., 1976. **98**(2): p. 508-16.

217. Sung, K., *Substituent Effects on Stability and Isomerization Energies of Isocyanides and Nitriles.* J. Org. Chem., 1999. **64**(25): p. 8984-8989.

218. Taft, R.W., Jr., *The general nature of the proportionality of polar effects of substituent groups in organic chemistry.* J. Am. Chem. Soc., 1953. **75**: p. 4231-8.

219. McDaniel, D.S. and H.C. Brown, *Extended table of Hammett substituent constants based on the ionization of substituted benzoic acids.* J. Org. Chem., 1958. **23**: p. 420-7.

220. Taft, R.W., Jr. and I.C. Lewis, *The general applicability of a fixed scale of inductive effects. II. Inductive effects of dipolar substituents in the reactivities of m- and p-substituted derivatives of benzene.* J. Am. Chem. Soc., 1958. **80**: p. 2436-43.

221. Taft, R.W., Jr. and I.C. Lewis, *Evaluation of resonance effects on reactivity by application of the linear inductive energy relationship. V. Concerning a ÏfR scale of resonance effects.* J. Am. Chem. Soc., 1959. **81**: p. 5343-52.

222. Raman, N., A. Kulandaisamy, A. Shunmugasundaram, and K. Jeyasubramanian, *Synthesis, spectral, redox and antimicrobial activities of Schiff base complexes derived from 1-phenyl-2,3-dimethyl-4-aminopyrazol-5-one and acetoacetanilide.* Transition Met. Chem. , 2001. **26**(1-2): p. 131-135.

223. Garnovskii, A.D., A.L. Nivorozhkin, and V.I. Minkin, *Ligand environment and the structure of Schiff base adducts and tetracoordinated metal-chelates.* Coord. Chem. Rev., 1993. **126**: p. 1-69.

224. Shaibu, R.O., *A bioinorganic study of some cobalt(II) Schiff base complexes of variously substituted hydroxybenzaldimines.* PhD Thesis, Rhodes University, Grahamstown, 2007.

225. Tabei, K. and E. Saitou, *Nuclear magnetic resonance and infrared spectra of aromatic azomethines.* Bull. Chem. Soc. Jap., 1969. **42**(5): p. 1440-3.

226. Khoo, L.E., *Azomethine proton chemical shift of Schiff bases.* Spectrochim. Acta, Part A, 1979. **35A**(8): p. 993-5.

227. Ignoti, T., *Structure Determination of Organic Compounds by E. Pretsch, P. Buhlmann, and C. Affolter.* Chim. Ind. (Milan, Italy), 2001. **83**(10): p. 87.

228. Dudek, G.O. and E.P. Dudek, *Spectroscopic study of keto-enol tautomerization in phenol derivatives.* Chem. Commun. , 1965: p. 464-6.

229. Kamienski, B. and M. Paluch, *Influence of pyridine amino isomers on electric surface potential and surface tension in aqueous solutions.* Bull. Acad. Pol. Sci., Ser. Sci. Chim., 1967. **15**(8): p. 345-8.

230. Cimerman, Z. and Z. Stefanac, *Cyclic and open-chain tautomerism and complex formation behavior of the condensation product of 2-amino-3-aminomethyl-4-*

methoxymethyl-6-methylpyridine with salicylaldehyde. Polyhedron, 1985. **4**(10): p. 1755-60.

231. Cimerman, Z., N. Galesic, and B. Bosner, *Structure and spectroscopic characteristics of Schiff bases of salicylaldehyde with 2,3-diaminopyridine.* J. Mol. Struct., 1992. **274**: p. 131-44.

232. Zöke, G.V.S., *Vibrational spectra of benzene derivatives.* Academic press, New York, USA, 1969.

233. Preston, P.N., *Synthesis, reactions, and spectroscopic properties of benzimidazoles.* Chem. Rev., 1974. **74**(3): p. 279-314.

234. Tumer, M., C. Celik, H. Koksal, and S. Serin, *Transition metal complexes of bidentate Schiff base ligands.* Transition Met. Chem., 1999. **24**: p. 525-532.

235. Bowden, F.L. and D. Ferguson, *Redox reactions in the formation of titanium complexes with aromatic Schiff bases.* J. Chem. Soc., Dalton Trans., 1974(4): p. 460-2.

236. Syamal, A. and K.S. Kale, *New copper (II) complexes of tridentate dibasic ONO donor ligands derived from salicylaldehyde or substituted salicylaldehydes and o-hydroxybenzylamine.* Transition Met. Chem. , 1979. **4**: p. 298-300.

237. Sinn, E. and C.M. Harris, *Schiff base metal complexes as ligands.* Coord. Chem. Rev., 1969. **4**(4): p. 391-422.

238. Tokii, T., Y. Muto, M. Kato, K. Imai, and H.B. Jonassen, *Magnetic and spectral studies on copper(II) complexes with N-hydroxyalkylsalicylidenimines.* J. Inorg. Nucl. Chem., 1972. **34**(11): p. 3377-91.

239. Xie, M., L. Li, X. Yang, W. Liu, S. Yan, Y. Niu, and Z. Meng, *A new insulin-enhancing agent: [N,N'-bis(4-hydroxysalicylidene)-o-phenylenediamine]oxovanadium(IV) and its permeability and cytotoxicity.* Eur. J. Med. Chem., 2000. **45**(6): p. 2327-2335.

240. Percy, G.C. and D.A. Thornton, *Infrared spectra of N-aryl Schiff base complexes.* Inorg. Nucl. Chem. Lett., 1971. **7**(7): p. 599-604.

241. Percy, G.C. and D.A. Thornton, *Infrared spectra of N-arylsalicyaldimine complexes substituted in both aryl rings.* J. Inorg. Nucl. Chem., 1973. **35**: p. 2319-27.

242. Nakamoto, K., *Infrared and Raman Spectra of Inorganic and Coordination Compounds. 3rd Ed. John Wiley and Sons, New York.* 1978. 448 pp.

243. Dollish, F.R., W.G. Fateley, and F.F. Bentley, *Characteristic Raman Frequencies of Organic Compounds*. 1973: Wiley-Interscience, New York. 432 pp.

244. Yamanouchi, K. and S. Yamada, *Metal complexes with schiff bases obtained from salicylaldehyde derivatives and 2-aminoethylpyridine.* Inorg. Chim. Acta, 1975. **12**(1): p. 109-112.

245. Dubicki, L. and R.L. Martin, *The π system of binuclear copper(II) and chromium(II) acetates.* Inorg. Chem., 1966. **5**(12): p. 2203-9.

246. Barron-Garces, J.D., G. Mendoza-Diaz, F. Vilchez-Aguado, and S. Bernes, *Synthesis and characterization of bis[(2-ethyl-5-methyl-imidazol-4-yl)methyl]sulfide and its coordination behavior toward Cu(II) as a possible approach of a copper site type I.* Bioinorg. Chem. Appl., 2009.

247. Boyd, R.F., *General microbiology, 2nd edition.* Times Mirror/Mosby College Publishing St Louis, Missouri 63146, 1988. **2nd edittion**.

248. Wikipedia, *Penicillin.* http://en.wikipedia.org/wiki/Penicillin, accessed date: 08-02-2012.

249. Ryan, K.J., and C.G. Ray *Sherris Medical Microbiology (4th ed.).* McGraw Hill, New York, 2004.

250. Pathogen, *Staphylococcus aureus.* http://ppdictionary.com./, accessed date: 13/12/2011

251. Wikipedia, *Escherichia coli.* http://en.wikipedia.org/wiki/Escherichia_coli, Accessed date: 03-01-2012.

252. Wikipedia, *Fungus.* http://en.wikipedia.org/wiki/Fungus, accessed date-03-01-2012.

253. Wikipedia, *Candida albicans.* http://en.wikipedia.org/wiki/Candida_albicans, accessed date: 01-01-2012.

254. Healthscouth, *Candida albicans.* http://www.healthscout.com/ency/68/312/main.html, accessed date: 01-01-2012.

255. Jawetz, E., *in Katzung B.G. (Ed.); Basic and Clinical Pharmacology* Appleton and Lange, Norwalk, CT, 1989: p. 8.

256. Wanger, A., in: Schwalbe R., L. Steele-Moore and A.C. Goodwin (Eds.), *Antimicrobial Susceptibility Testing Protocols.* Taylor and Francis group, London, 2007: p. 6.

257. Foster, J.W. and H.B. Woodruff, *Microbiological aspects of penicillin. I. Methods of assay.* J. Bacteriol., 1943. **46**: p. 187-202.

258. Abraham, E.P., E. Chain, C.M. Fletcher, A.D. Gardner, N.G. Heatley, M.A. Jennings, and H.W. Florey, *Further observations on penicillin.* Lancet, 1941. **II**: p. 177-88.

259. Madigan, M.T., J.M. Martinko and J. Parker,, *Biology of microorganisms, 8th ed.* . 1998.

260. Wayne, P.A., *Methods for dilution antimicrobial susceptibility tests for bacteria that grow aerobically, 4th ed. Approved standard (M7-A4), National Committee for Clinical Laboratory Standards.* 1997.

261. N.C.C.L.S., *Methods for dilution antimicrobial susceptibility tests for bacteria that grow aerobically, 4th ed. Approved standard (M7-A4).* 1997.

262. Tweedy, B.G. and N. Turner, *Mechanism of sulfur reduction by conidia of Monilinia fructicola [Sclerotinia fructicola]*. Contrib. Boyce Thompson Inst., 1966. **23**: p. 255-65.

263. Ansari, K.F. and C. Lal, *Synthesis and evaluation of some new benzimidazole derivatives as potential antimicrobial agents.* Eur. J. Med. Chem., 2009. **44**(5): p. 2294-2299.